Reductive and oxidative dissociative electron transfers: transition between the concerted and stepwise mechanistic pathways

Jared Nathaniel Spencer

Dissertation submitted to the faculty of the Virginia Polytechnic Institute and State University in partial fulfillment of the requirements for the degree of

Doctor of Philosophy
in
Chemistry

James M. Tanko, Committee Chair
Paul R. Carlier
Richard D. Gandour
Diego Troya

March 23, 2016
Blacksburg, VA

Keywords: Dissociative electron transfer, Epoxyketones, Radical ions, Radical rearrangements

Reductive and oxidative dissociative electron transfers: transition between the concerted and stepwise mechanistic pathways

Jared N. Spencer

ABSTRACT

The dissociative electron transfer reactions of a series of α-epoxyketones and tetra-*n*-butylammonium acetate have been examined by electrochemical and computational techniques.

Results for both the direct electrochemical (linear sweep voltammetry and convolution voltammetry) and indirect electrochemical (homogeneous redox catalysis) reductions of the epoxyketones are presented. In cases where the ring-closed radical anion generated by reduction of the epoxyketones is resonance stabilized (aromatic epoxyketones) the mechanism proceeds in a stepwise fashion, where the electron transfer and bond breaking reactions occur in sequential, discrete steps. On the other hand, where there is no additional resonance stabilization afforded to the ring-closed epoxide radical anion (aliphatic epoxyketones) the reaction proceeds in a concerted fashion, where electron transfer and ring cleavage occur simultaneously. The presence (or absence) of resonance stabilization in the ring-opened distonic radical anion plays little role in the kinetics of these dissociative electron transfers. Computations with the Density Functional Theory (B3-LYP and BHandH-LYP) on α-epoxyketones are also presented, and are in good agreement with the electrochemical results.

The oxidative dissociative electron transfers of the acetate anion in "dry" and "wet" (0.5 M H_2O) acetonitrile were also characterized with direct and indirect electrochemical experiments, again utilizing linear sweep voltammetry, convolution voltammetry, and homogeneous redox catalysis. There is a significant change in the observed oxidation potential of the anion upon addition of water, as well as an apparent decrease in the intrinsic barrier to the electron transfer. The possible transition from a concerted to stepwise mechanism for the dissociative electron transfer of acetate upon addition of water is examined – the electrochemical data is compared to theoretical models for both the concerted and stepwise processes. It is determined that the indirect electrochemical experiments do not proceed through an outer sphere electron transfer. Additionally, it is shown that the difference between the direct oxidation of acetate in anhydrous and wet acetonitrile is unlikely to be the result of transition from a purely concerted mechanism to a purely stepwise mechanism based on thermodynamic considerations.

For Hope –
Light of my life, Heart of my heart, forever

For Luke, Jacob, and Molly –
All of my love, all of my life

For Adam, little brother –
Forever loved, always missed

Acknowledgements

Always first, I give my greatest thanks to my Lord and Savior, Jesus Christ. The farther we look and the deeper we dig, the more layers we peel back, the more deeply profound and startlingly beautiful we find this universe of yours to be. John 1:3

Without the support of my beautiful wife, Hope, I would have abandoned this pursuit years ago. Thank you for sticking with me, even when I didn't want to stick with this journey. Your gentle (and sometimes ungentle) prodding kept me going, even when it felt like this was forever away. I will always love you, and whatever the next chapter of our lives holds for us, I know that I can face it without fear as long as I do so with you. My heart is yours, forever.

I cannot thank my research advisor, Dr. James Tanko, enough. You are like my chemistry-father. Over the years our conversations, arguments, agreements, and sometimes shared confusion, as well as your admonishment, encouragement, and laughter have always made me feel that I could actually finish what I started. Without your guidance and instruction this would truly have been an impossible feat. I will always look back fondly on my (many) years in graduate school, in no small part due to your influence.

I owe a special debt of gratitude to the members of my research committee: Professors Paul Carlier, Richard Gandour, and Diego Troya. You could easily have abandoned me years ago as a lost cause; thank you for your unending patience with me as I finally completed this race. I must also give special thanks in remembrance of Professor Karen Brewer. In my very first year of graduate school I was nearly sure that I was intellectually incapable of obtaining an advanced degree in chemistry; Karen's encouragement in the beginning of my second year convinced me that I did have that ability, if only I would put the effort into the work as was required. Thank you, Karen; you will not be forgotten.

Of the many great teachers I have had over the years, my love of the sciences and mathematics was truly kindled under the tutelage of one man. David McCarty, thank you for your passion for understanding the world around us. We used to try to get you onto tangents in class, during which you would explain things well outside the purview of the subject at hand. I believe many of my fellow teenage students did so as a way of avoiding classwork; I was always more interested in learning something new about this place we call home. Thank you for fanning the flames of the fire that eventually led to this work and continues to burn within me.

Lastly, I don't even know where to begin in my thanks to my parents. Mom, Dad, you have made me everything I am today. You have never wavered in your support, care, and encouragement. If Mr. McCarty's teaching fanned the flames of my passion for the sciences, the World Books, the elementary school science fairs and projects, the competitions, and everything you sacrificed to allow me to do what I loved sparked that fire in the first place. This accomplishment is yours as much as mine. Thank you.

Table of Contents

List of abbreviations

A	Surface area of electrode
BDE	Bond dissociation energy (*D*)
C_M	Molar concentration of M
C_M^*	Bulk molar concentration of M
C_M^0	Electrode surface concentration of M
C_1 and C_2	Fitting parameter for mixed kinetic control in LSV
CV	Cyclic voltammetry
D	Bond dissociation energy (BDE)
D_M	Diffusion coefficient of M
DET	Dissociative electron transfer
cDET	Concerted dissociative electron transfer
sDET	Stepwise dissociative electron transfer
E	Electrode potential
$E_{O/R}^0$	Standard reduction potential of the redox couple R/O
$E_{R/O}^0$	Standard oxidation potential of the redox couple R/O
ET	Electron transfer
EC	EC mechanism; electron transfer followed by unimolecular rearrangement (a chemical step)
F	Faraday constant
i	Current
I	Convolutive current
I_{lim}	Limiting convolutive current
HRC	Homogeneous redox catalysis
k_n	Rate constant of reaction *n*
k_{het}	Heterogeneous electron transfer rate constant
k_{het}^0	Standard heterogeneous electron transfer rate

	constant (when $E = E^0_{O/R}$)
k_{obs}	Observed experimental rate constant
k^0_{et}	Standard rate constant for homogeneous electron transfer (when the standard potentials of the donor and acceptor redox couples are the same; i.e. – in HRC when the mediator and the substrate have the same reduction or oxidation potential)
LSV	Linear sweep voltammetry
n	Moles of electrons per mole of reaction, reactant consumed, or product formed
O/R	A redox couple where O is the oxidized species and R is the reduced species, e.g. – $O + e^- \rightarrow R$
R	Molar gas constant
T	Kelvin temperature
α	Transfer coefficient
λ, λ_i, λ_o	Total, inner, and outer (solvent) reorganization energies
λ_{ET}, λ_{CS}	Dimensionless rate constants for an electron transfer and chemical step, respectively
CCSD	Coupled cluster theory with single and double substitutions
DFT	Density functional theory
HF	Hartree-Fock theory

Chapter 1. Literature Review

1.1 Introduction

Electron transfers are fundamental and vital reactions that play important roles in all branches of chemistry. In the case of electron transfers involving organic species, these reactions typically result in unstable paramagnetic intermediates that undergo further reaction, such as bond breaking, bond formation, or additional electron transfers. Electron transfers are often initial steps in more complicated reactions schemes, and understanding the mechanisms of these reactions can lead to better understanding of the larger chemistries in which they play a significant role.

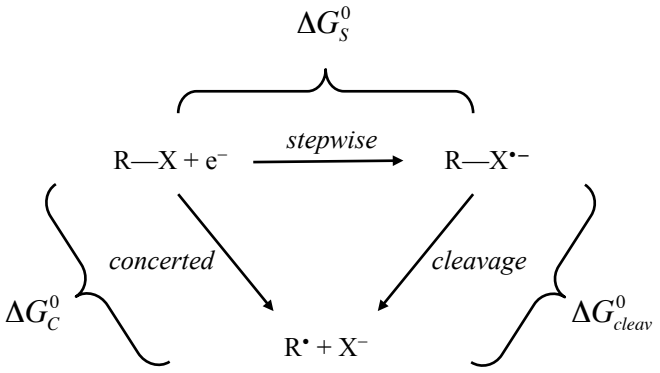

Scheme 1.1: Dissociative electron transfer reaction pathways.

It is often the case – particularly for organic molecules and ions – that electron transfer is followed by or occurs concurrently with bond breaking, as illustrated in **Scheme 1.1**. These dissociative electron transfer (DET) reactions have enjoyed much attention in the past several decades. The two possible modes of fragmentation – stepwise (sDET, wherein the electron transfer and bond breaking occur in two discreet steps) and concerted (cDET, wherein bond breaking occurs simultaneous with electron transfer) – and the balance between which mode is

favored is related to the lifetime of the intermediate radical anion. This is to say that the faster the parent radical anion decomposes, the more likely the mechanism is to follow the concerted pathway (*vide infra*).

$$\Delta G_S^{\ddagger} = \frac{(\lambda_o + \lambda_i)}{4}\left(1 + \frac{\Delta G_S^0}{(\lambda_o + \lambda_i)}\right)^2 \qquad \textbf{Eq. 1.1}$$

$$\Delta G_C^{\ddagger} = \frac{(\lambda_o + D)}{4}\left(1 + \frac{\Delta G_C^0}{(\lambda_o + D)}\right)^2 \qquad \textbf{Eq. 1.2}$$

Two dominant theories to describe the dynamics of DET have been proposed. The first, the Marcus model[1] (**Eq. 1.1),** describes the outer sphere electron transfer in the stepwise mechanism, leaving the bond breaking reaction to be explained by other models. The second, Savéant's DET theory[2-3] (**Eq. 1.2**), describes the concerted pathway. Both models arise from approximations of the Morse curves describing the reactants and products and the intersections thereof, and are thus similar treatments. The Marcus model describes the activation energy ($\Delta G_S^{\ddagger}$) for the initial electron transfer as a parabolic function of reaction thermodynamics (ΔG_S^0) and reorganization energy (λ), a term accounting for the structural reorganization both of the solvent cage around the reactants (λ_o) and any internal reorganization such as bond stretching or other geometric distortions within the reactants (λ_i). The Savéant model is visually very similar, with two exceptions: the driving force (ΔG_C^0) of the reaction is increased over that of the stepwise process by the bond dissociation energy (BDE, *D*) of the breaking bond, and the reorganization energy must account for breaking this bond. This means that the concerted process is thermodynamically more favorable than electron transfer in the stepwise process, however the intrinsic barrier for the concerted pathway will be much larger than that of the stepwise pathway, as typically $\lambda_o + D >> \lambda_o + \lambda_i$. There is a dynamic interplay between the two possible

mechanisms, and one focus of this chapter will be to explain the factors that drive the transition from one mechanistic pathway to the other.

This chapter will tackle the current state of DET reactions that arise from both reductive and oxidative processes. Section **1.2** will cover the reduction reactions, paying particular attention to the reductions of organic halides, whose chemistry led to the above models; cyclopropyl ketones, which are atypical examples of DET reactions in that the bond breaking reaction is enhanced via ring strain, and cleavage of the parent radical anion does not lead to two distinct products; and epoxy ketones, furthering the work of which is one of the primary objectives of this dissertation. Section **1.3** will cover oxidation reactions, paying particular attention to the Kolbe reaction – perhaps the most famous example of DET. Finally Section **1.4** will set forth the project goals of the research presented in this dissertation.

It should be noted that possibly the most common DET reaction is that where the leaving group is a proton. These proton coupled electron transfer reactions and their close cousins (such as hydrogen atom transfer) are enormously important in many areas of chemistry. This review will focus on DET reactions where the cleaved bond is between two heavy atoms, and will only mention reactions where an R—H bond is broken in passing; however, the reader is strongly encouraged to seek out any of the many reviews[4-7] dedicated to PCET reactions and its cousins.

1.2 Reductions

1.2.1 Organic halides and their derivatives

The reduction of organic halides was the first test of the electron transfer theory,[3,8] which led to verification of the models described previously. **Table 1.1** gives the pertinent structures, sorted by the mechanism they follow. Aryl and alkyl halides are the simplest to describe.

Reduction of the aromatic halides yields a stable radical anion intermediate (with the exception of some aromatic iodides, such as iodobenzene) which undergoes heterolytic cleavage, giving the neutral aryl radical and the halide ion. Conversely, alkyl halides follow a concerted mechanism, where both the electron transfer and bond breaking occur simultaneously, yielding an alkyl radical and the halide ion. The mechanistic preference in each of these cases can be rationalized as a function of the stability of the parent ion and the product radical. **Eq. 1.3** describes the driving force for cleavage of the radical intermediate as a function of the BDE (*D*), the oxidability of the leaving group, the reduction potential of the neutral parent, and the entropy effects associated with cleaving the parent species.[8]

$$\Delta G^0_{cleav} = -E^0_{RX/R^{\cdot}+X^-} + E^0_{RX/RX^{\cdot-}} = D - E^0_{X^{\cdot}/X^-} + E^0_{RX/RX^{\cdot-}} - T\Delta S_{RX\rightarrow R^{\cdot}+X^{\cdot}} \qquad \textbf{Eq. 1.3}$$

As driving force for cleavage of the ion radical increases, a passage from the stepwise to the concerted mechanism is expected, and thus a weak RX bond, a negative value of $E^0_{RX/RX^{\cdot-}}$, and positive value of $E^0_{X^{\cdot}/X^-}$ should favor the concerted mechanism over the stepwise mechanism. In the case of the aryl halides, $E^0_{RX/RX^{\cdot-}}$ is a relatively positive value, as the low-lying π^* orbital is easily accessible relative to the σ^* orbital of the alkyl halides. Furthermore, *D* is a larger value in aryl halide bonds than in alkyl halide bonds, as cleavage of the bond gives the less stable aryl radical. As such driving force for cleavage of the aryl halide radical anion is less than that of the alkyl halide radical anion, and following the stepwise mechanism in this case is a reasonable result.

Table 1.1
Organic halides that undergo DET. Adapted from reference 8.

Stepwise	Concerted
Examples of the prevailing role of $E^0_{RX/RX^{\cdot-}}$	
Aryl halides, except some iodides	Alkyl halides
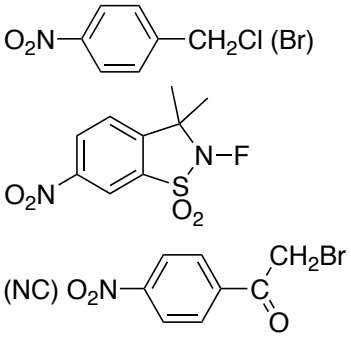	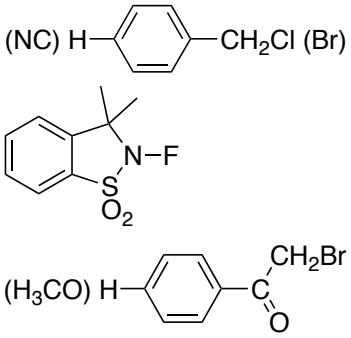
Examples of the prevailing role of the bond dissociation energy (D)	
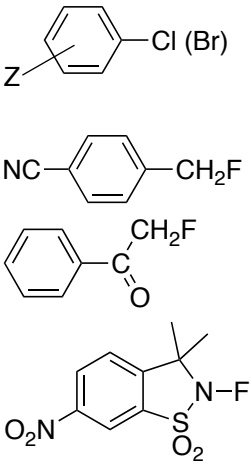	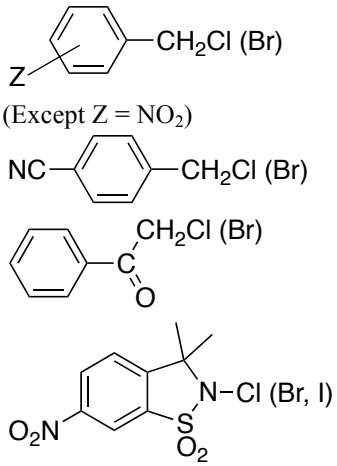 (Except Z = NO_2)
Examples of the prevailing role of $E^0_{X^{\cdot}/X^-}$	
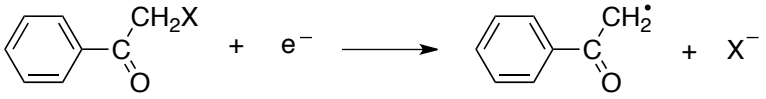	
X = OPh, OCH_3, OC_2H_5, SPh, SC_2H_5, $N(C_2H_5)_2$	X = Br, Cl

Although each of the terms in **Eq. 1.3** is important for any given reaction, families of organic halides can be identified where the passage from the concerted to stepwise pathway is mostly dependent on one of the terms, as given in **Table 1.1**.[8] The aforementioned aryl and alkyl halides undergo transition from a stepwise to a concerted mechanism mostly due to change in $E^0_{RX/RX^{\cdot-}}$. Allyl halides also fall into this family, where benzyl chloride(bromide) and 4-cyanobenzyl chloride(bromide) undergo concerted DET and 4-nitrobenzyl chloride(bromide) undergoes a stepwise mechanism, again due to the effect of the *para*-substituent group on $E^0_{RX/RX^{\cdot-}}$.

The BDE, *D*, of the breaking bond is the dominant factor when comparing 4-cyanobenzyl fluoride (stepwise) to 4-cyanobenzyl chloride(bromide).[9-10] Here, the C—F bond is much stronger than the C—Cl or C—Br bonds, and from **Eq. 1.3** this means that the driving force for cleavage of the radical anion will be less, considering $E^0_{RX/RX^{\cdot-}}$ and $E^0_{X^{\cdot}/X^-}$ will be approximately the same in each case. Similarly, 2-fluoro-1-phenylethanone follows a stepwise pathway, while 2-chloro(bromo)-1-phenylethanone follow a concerted pathway.[11]

$E^0_{X^{\cdot}/X^-}$, the oxidability of the leaving group, is one way of measuring the stability of the leaving group. A more positive oxidation potential of X^- is indicative of the stability of that ion in a given system. Therefore when X^- = Br^- or Cl^-, each of which have very positive oxidation potentials, the mechanism is more likely to be concerted. This is illustrated at the bottom of **Table 1.1**, where a concerted mechanism is followed when X = Br or Cl, and a stepwise mechanism is followed when X = OPh, OCH_3, OC_2H_5, and so forth.[11]

1.2.2 DET reactions involving cleavage of R—S, R—O, and R—C bonds

A common misconception is that the existence of a concerted DET mechanism implies that the parent radical anion does not "exist". This is not necessarily the case; rather, a concerted DET mechanism is followed when the intersection of the reactant and product potential curves occurs at a lower energy than that of the reactants and stepwise intermediates as illustrated in **Figure 1.1**. At very low electron potential the intermediate potential energy surface is

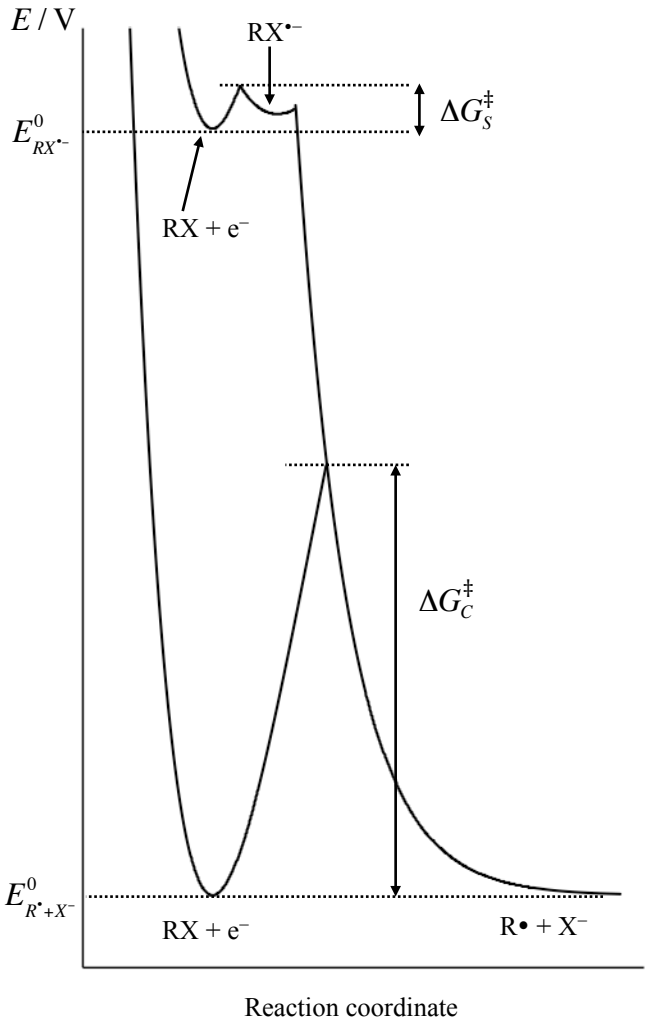

Figure 1.1: Morse potential curves showing the intersections between the potential wells corresponding to the parent molecule, intermediate radical anion, and cleaved products, demonstrating the difference in activation barrier for a concerted vs. a stepwise DET. The vertical access corresponds to the potential of the working electrode. Adapted from Reference 8.

inaccessible and the reaction must follow a concerted pathway. As driving force increases by increasing the electron potential, this intermediate well becomes accessible and the stepwise mechanism is preferred (for a more thorough discussion of the concerted-to-stepwise transition see **3.2.1** and **3.2.2**). It is thus possible that "borderline" cases, where the mechanism passes from the concerted pathway at lower driving forces to the stepwise pathway at larger driving forces, may be observed. A family of sulfonium cations[12] (**Scheme 1.2**), which undergo DET, illustrates this nicely. As expected from **Eq. 1.1** and **Eq. 1.2**, the intrinsic barrier is much larger in the concerted case than in the stepwise case. Electrochemically, in order to force a cDET transfer process to occur, a large overpotential must be applied. The effect is that of raising the energy well of the reactants, and as such the transfer coefficient, α, which measures the location of the transition state, is expected to be small (typically around 0.3). In contrast, the intrinsic barrier for the stepwise electron transfer is much smaller, meaning less overpotential must be applied to drive the reaction, and α is expected to be larger, around 0.5. Thus, measurement of α is usually a good diagnostic tool for determining the mechanism of the overall reaction.[8]

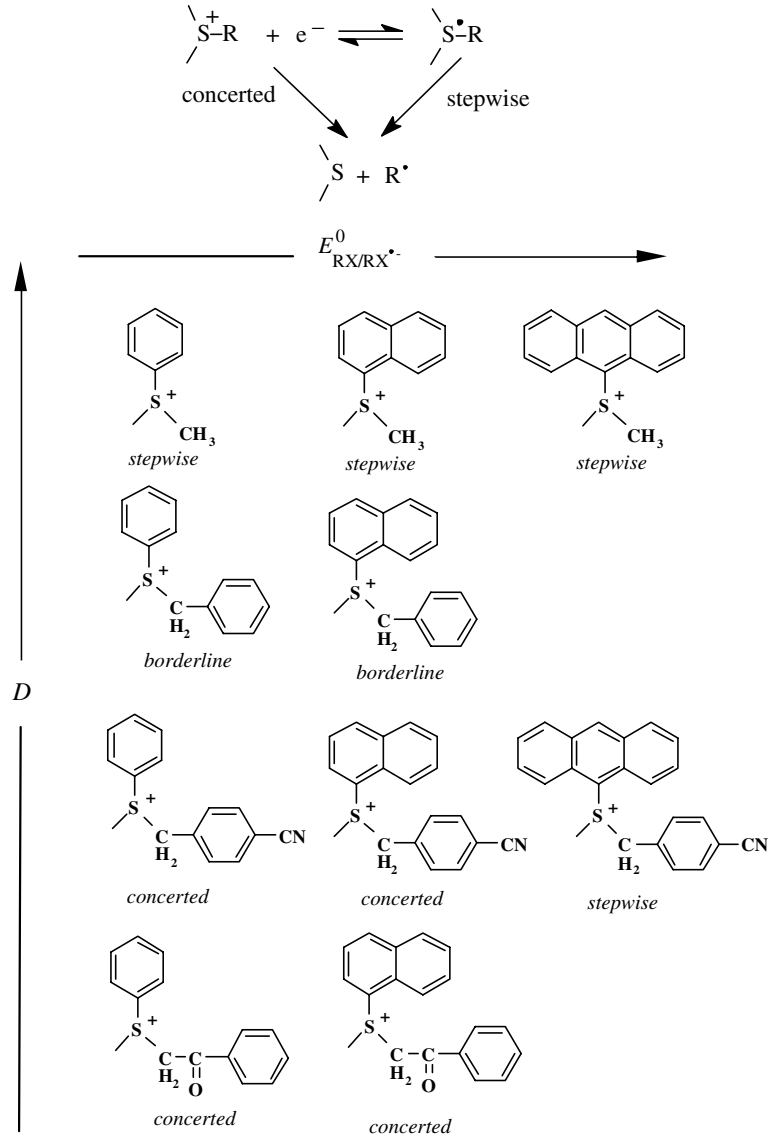

Scheme 1.2: A family of sulfonium ions that undergo DET reactions. Adapted from reference 8.

Scheme 1.2 is arranged by increasing $E^0_{RX/RX^{\cdot-}}$ and decreasing *D*. As with the organic halides discussed previously, these two terms contribute to which pathway the electron transfer mechanism follows. However, in the middle of the table, there are examples of "borderline" cases. In these cases, lower driving force leads to a concerted mechanism and higher driving force leads to a stepwise mechanism. This is accomplished by varying the sweep rate (ν, the rate at which the electrode potential is changed per unit time) in the cyclic voltammetry experiment.

At faster sweep rates, greater driving force is applied to the system and the mechanism moves from concerted to stepwise, as illustrated by the measured α values in **Figure 1.2**. This can be explained upon close inspection of **Figure 1.1**. At slow sweep rates, the driving force applied to the system is small, and the energy well of the reactants (RX and $e^{\bullet -}$) intersects with the overall reaction products without crossing the intermediate's well, leading to a concerted mechanism. There is still a large intrinsic barrier, a large overpotential must be applied, and α is small. As sweep rate is increased, the reactant energy well is raised and begins to intersect the intermediate's well; this leads to a stepwise mechanism and an α approaching 0.5. This clearly demonstrates that the radical anion intermediate does exist in this case; it is however inaccessible at low driving force (slow sweep rates) and when this is the case the concerted mechanism is followed.

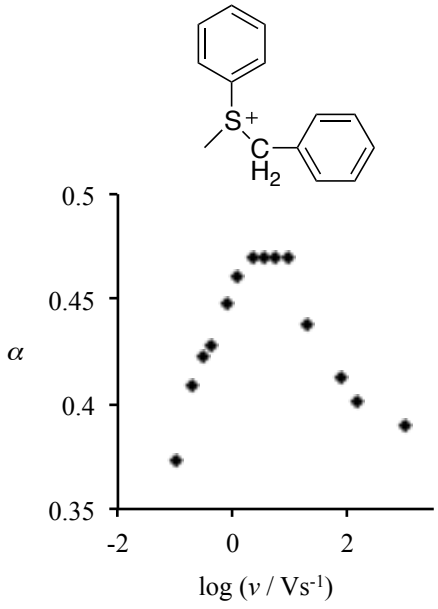

Figure 1.2: Variation of the transfer coefficient with sweep rate for the sulfonium ion shown, demonstrating a change in mechanism from concerted to stepwise with increasing driving force.[12]

Maran and co-workers have shown[13-16] that organic peroxides, peresters, and disulfides also in many cases undergo DET reactions, with cleavage of the O—O and S—S bonds, respectively. The peresters and peroxides are given in **Table 1.2**, and the disulfides in **Scheme 1.3**. Of the peroxides, di-*tert*-butyl peroxide (DTBP) provided a particularly interesting case. Initially Maran reported[16] that DTBP undergoes a concerted DET that did not fit Savéant's published model – the kinetics for the cDET process were many orders of magnitude different than those predicted by the Savéant model. This discrepancy was partially explained on Maran's use of bond dissociation free energy for the breaking bond as opposed to the appropriate bond dissociation energy.[17] However, this error only accounted for part of the theoretical/experimental discrepancy. Consequently, the Savéant model was modified.[18] In the original model, the products of the electron transfer reaction were presumed to be purely repulsive. In some cases, however, a residual interaction may occur between the cleaved moieties, and this has an effect on the kinetics of the electron transfer process. The mathematics are beyond the scope of this review, but **Figure 1.3** gives a physical representation of this effect, showing how a small interaction between the cleaved moieties can lead to a large reduction of the activation barrier for the cDET process.

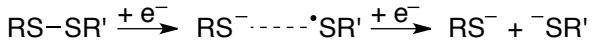

(1-4) R = R' = H, CH_3, tBu, Ph
(5) R = CH_3 R' = Ph
(6) R = tBu R' = Ph

Scheme 1.3: DET of disulfides reported by Maran.[14]

Table 1.2
Peroxides and peresters studied by Maran and co-workers.[13,19]

Structure	Mechanism
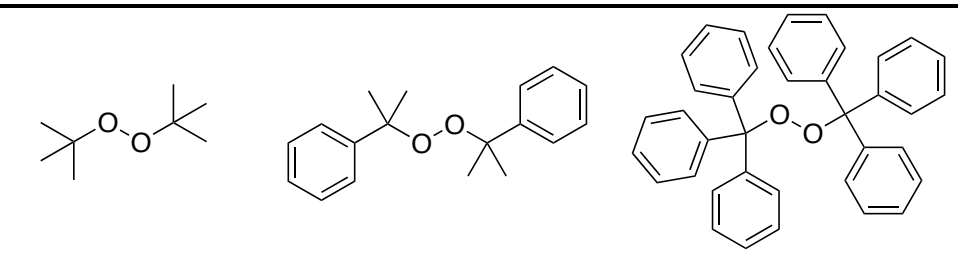	Concerted
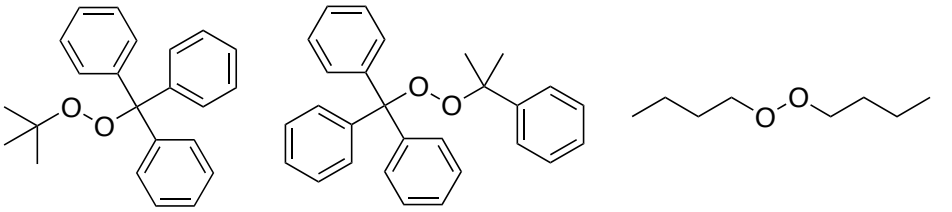	Concerted
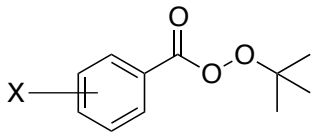 X = H(a), 4-OCOMe(b), 4-OCMe(c), 4-CN(d), 3-NO_2(e), 4-NO_2(f)	(a) Concerted (b-e) Borderline (f) Stepwise
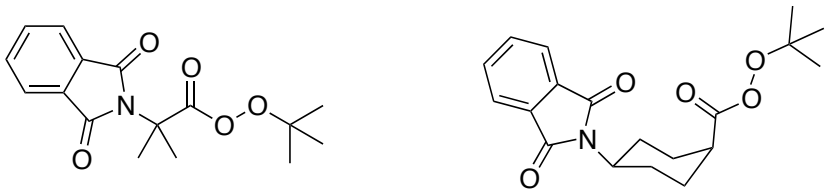	Borderline
	Concerted

The disulfides in **Scheme 1.3** presented another problem.[14] The DET reduction of many of these disulfides was shown to proceed through a stepwise process, however the internal reorganization component was much larger than expected, approaching the values usually obtained in a concerted process. These results were rationalized by realization that the radical

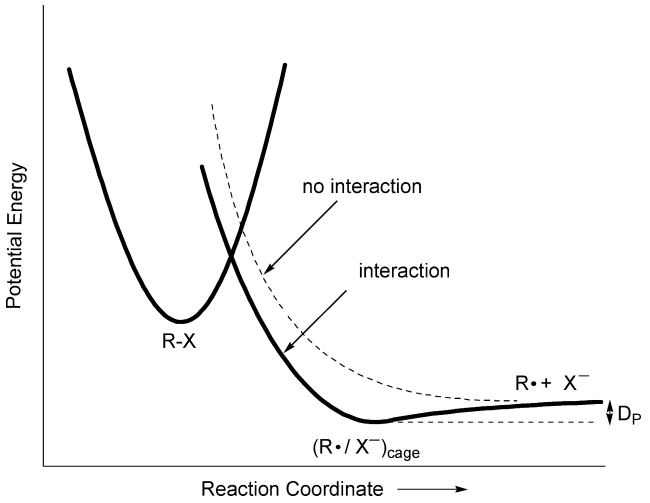

Figure 1.3: Illustration of the effect of residual interactions between the cleaved species while still in the solvent cage. This interaction, though weak, leads to large changes in the intrinsic barrier for cDET, as shown. Reprinted with permission from reference 20. Copyright 2007 American Chemical Society.

generated was a σ^*-type radical, where the SOMO of the radical ion was located mostly within the σ-framework of the S—S bond. This led to a significant stretching of this bond in the electron transfer transition state structure, which Maran termed a loose radical anion. This stretching contributes to the internal reorganization energy, making it much larger than typically seen for a stepwise process. The loose radical anion DET mechanism is simply a stepwise electron transfer reaction, following the Marcus model, where the internal reorganization component is unusually large.

Table 1.3
Cyclopropyl ketones studied by Tanko and co-workers.[20-31]

Structure **(a)**	k_{ro} (s^{-1})[a]	Structure **(b)**	k_{ro} (s^{-1})[a]
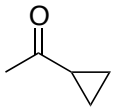	$>10^7$	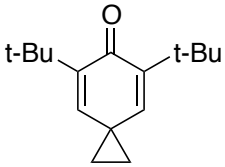	$>3 \times 10^8$
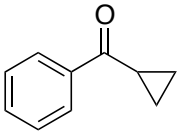	<10	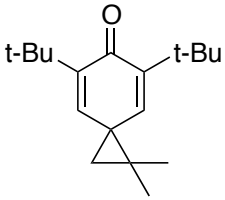	$>3 \times 10^8$
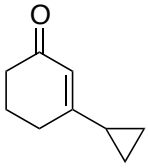	1.6×10^6	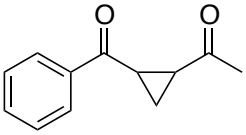	1.0×10^5
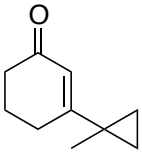	2.5×10^6	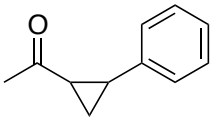	$>10^8$
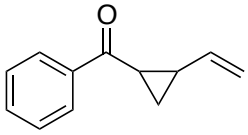	2.4×10^5	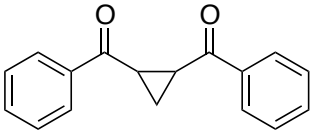	7.14×10^5
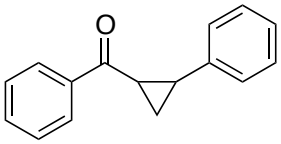	9.6×10^6	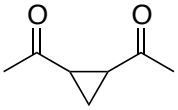	cDET

(*a*) Ring-opening rate constant of radical anion produced by reduction of the respective structure

Cyclopropanes have often been used as free radical clocks in reactions probing for electron transfer versus polar pathways. It has been assumed, often erroneously, that the radical anion analogue of the neutral cyclopropylcarbinyl radical would exhibit the same characteristics of this neutral radical rearrangement – namely, that the rate constants in both the neutral radical rearrangement and in the radical anion rearrangement would be similar. In testing this, Tanko and co-workers determined the rate constant for ring opening of the cyclopropyl ketones given in **Table 1.3a**.[21-30] In these examples, relief of ring strain provides much of the driving force for the

bond-breaking reaction. However, the kinetics of the ring opening reaction depend as heavily (if not more so) on resonance energy in the reactants and products as depicted in **Scheme 1.4**. Loss of resonance stabilization in the products leads to a dramatic slowing of the rate constants. In the context of **Eq. 1.3** this is unsurprising, as the $E^0_{RX/RX^{\cdot-}}$ is relatively positive due to the presence of the stabilizing resonance afforded by the phenyl group. Other cyclopropyl derivatives (**Table 1.3b**) were examined,[31-32] where resonance energy in the products alleviated much of this problem, and the rate constants found in these cases were much larger. This can be interpreted in the context of **Eq. 1.3** as a decrease in the BDE, *D*, because the resulting radical is resonance stabilized; this is analogous to how an allylic C—H bond is weaker than an aliphatic C—H bond.

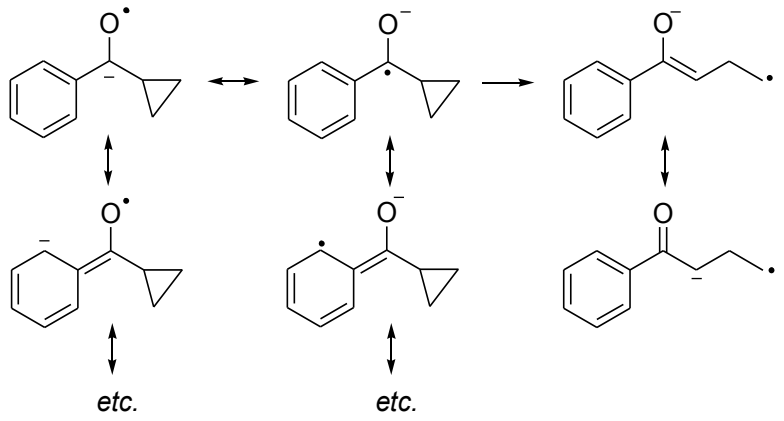

Scheme 1.4: Resonance effects in the ring opening reaction of phenylcyclopropylketone radical anion.

A particularly interesting example is 1,2-diacetylcyclopropane. This is the first reported concerted DET process where the cleaved bond is a C—C bond,[20] and consequently deserves additional attention. This example is particularly illustrative of the utility of quantum mechanical computations in these electron transfer reactions. As pointed out previously, non-existence of the radical ion parent is not a requirement for concerted DET to be a viable pathway, however, if the parent radical does not exist then the electron transfer must of necessity proceed through a

concerted pathway. Results for electrochemical experiments with 1,2-diacetylcyclopropane were inconclusive: α values were found to be moderate, in the range of 0.4-0.46, depending on how they were obtained, and estimates of the total reorganization energy for the electron transfer were not that far different from those of other cyclopropyl ketones which were confirmed to undergo a stepwise mechanism. Furthermore, fitting of the heterogeneous rate constant data to the concerted model was unsuccessful; the heterogeneous rate constants proved to be larger than those predicted by the concerted model. However, computations attempting to optimize the ring closed radical anion failed and instead led to a ring-opened distonic radical anion, the product of ring opening (**Figure 1.4**). These computations suggested that the ring closed radical anion did not exist as a discrete intermediate.

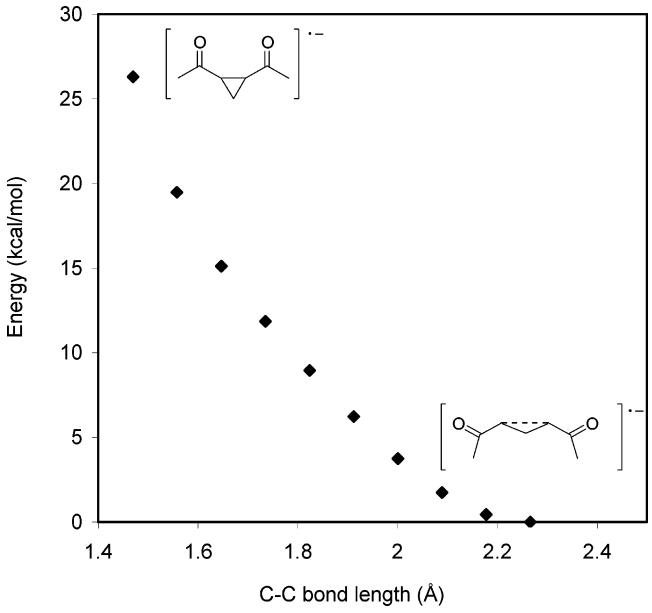

Figure 1.4: Energy profile of 1,2-diacetylcyclopropane radical anion, showing purely repulsive characteristics between the two C-atoms, indicating that the radical anion does not exist as a discrete intermediate. Calculated with the UHF/6-31+G* theory and basis set. Reprinted with permission from reference 20. Copyright 2007 American Chemical Society.

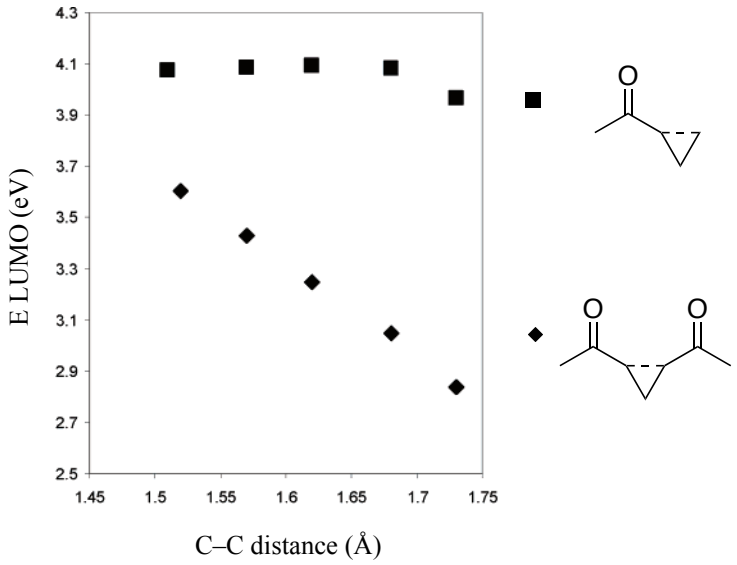

Figure 1.5: LUMO energies as a function of C—C (indicated with dotted bond) bond length for 1,2-diacetylcyclopropane and methylcyclopropylketone, indicating that the LUMO energy of 1,2-diacetylcyclopropane is more sensitive to stretching of the carbon-carbon bond than that of methylcyclopropylketone. Calculated with the HF/6-311G* theory and basis set. Adapted with permission from reference 20. Copyright 2007 American Chemical Society.

These results were consolidated by computations on the parent ketone, and in particular, by looking at the LUMO energy as a function of C—C bond length (see **Figure 1.5**). It was found that stretching of the bond resulted in a large decrease in the calculated LUMO energy of 1,2-diacetylcyclopropane. This, combined with rationalization of the electronic structure of the cyclopropane where the orbitals of both the paramagnetic and ionic portions of the cleaved radical are π-type orbitals as opposed to the π- and σ-type orbitals used to develop the concerted model, led to the diagnosis that 1,2-diacetylcyclopropane does in fact undergo concerted DET.

The DET reactions of α-epoxyketones have also been reported.[33-37] These reductions have been induced photolytically and via homogeneous electron donors. Quantitative diagnosis of the reaction mechanisms including the determination of the ring opening rate constants, the reduction potentials of the parent ketones, and the preferred DET pathway (concerted versus stepwise) have not been reported. A significant potion of the results presented in this dissertation

will be dedicated to elucidating these details. It should be noted, however, that in all cases (whether the ET reactions were photoinduced or induced via reaction with a homogeneous electron donor) the products resulting from C—O bond cleavage have been observed exclusively.

1.3 Oxidations

Oxidative DET reactions where the cleaved bond is between two heavy atoms have not enjoyed as much attention as their reductive counterparts; however, a few examples exist. In most cases the work is qualitative in nature, and examples where the full mechanism has been resolved are lacking. For organic species, this is due in part to oxidations potentials being largely more positive than corresponding reduction potentials, making them in many cases inaccessible to electrochemical techniques, the most useful tool in diagnosing electron transfer reactions. Furthermore, the radical cations generated in many cases are potent acids, and therefore dissociative reactions often occur with cleavage of an R—H bond, as opposed to a heavy atom—heavy atom bond.

1.3.1 Oxidation of carboxylates

Since its discovery more than 100 years ago,[38] the Kolbe reaction has been of huge importance in organic electrochemistry.[39-49] In many ways, the Kolbe reaction (**Scheme 1.5**) is the best-known DET reaction. A Kolbe type rearrangement can arise from oxidation of a carboxylate anion, hydrogen abstraction from a carboxylic acid, intramolecular electron transfers in esters, among other possible modes.

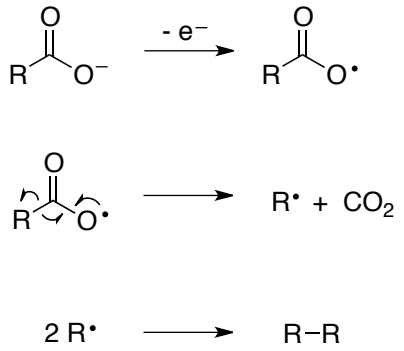

Scheme 1.5: Kolbe reaction.

Oxidation of carboxylates have been carried out by Savéant[50] as well as others to probe the mechanism of the electron transfer as well as the general electrochemical response of these anions. Galicia and Gonzalez published a report in 2002[51] pertaining to the oxidations of a series of linear aliphatic carboxylates (acetate to hexanoate), wherein they reported that all of the carboxylates studied followed a stepwise mechanism. This result was obtained via measuring the peak widths of the cyclic voltammograms as well as the variation of the peak potential with scan rates, both of which produced α values near 0.5. Both diagnostic criteria pointed to an electron transfer controlled mechanism, where the initial electron transfer step is fast; that is, a stepwise DET mechanism was followed. They also reported a further electrode oxidation of the alkyl radical product to a carbocation which underwent additional reactions with the carboxylate, in agreement with work done via Savéant on a series of benzoates (**Scheme 1.6**).[50] The result of this mechanism is an overall one electron oxidation, where half of the electron mole is used to oxidize half of the surface carboxylate, and the other used to oxidize the resulting alkylic radical. The resulting carbocation then reacted with the other half of the surface carboxylate, yielding an overall 1:1 stoichiometry of acetate to electrons in the reaction mechanism. Savéant's work with a series of *para*-substituted benzoates showed similar results;[50] the mechanism was a stepwise DET where electron transfer was rate limiting. It should be noted that in each of these cases direct measurement of the oxidation potential of the carboxylate was not made; instead, average

peak potentials from the voltammograms were used to estimate the oxidation potentials of the carboxylates.

$$R{-}CO_2^- - 2\,e^- \rightarrow R^+ + CO_2$$
$$R^+ + CH_3CN + H_2O \rightarrow RNHCOCH_3 + H^+$$
$$R{-}CO_2^- + H^+ \rightarrow R{-}CO_2H$$

$$R{-}CO_2^- - e^- \rightarrow CO_2 + 1/2\,RNHCOCH_3 + 1/2\,R{-}CO_2H$$

Scheme 1.6: Mechanism for the one electron reduction of carboxylates.[51]

Astudillo et al. also performed mediated homogeneous redox catalysis of acetate with the ferrocene/ferrocenium redox couple as mediator.[52] The advantage of this scheme is that electrode potentials are kept much more negative than in the direct electrochemical case, avoiding oxidation of the alkyl radical products of the electron transfer reaction. Instead, these neutral radicals grafted to the electrode surface, and it was shown that after 11 successive scans

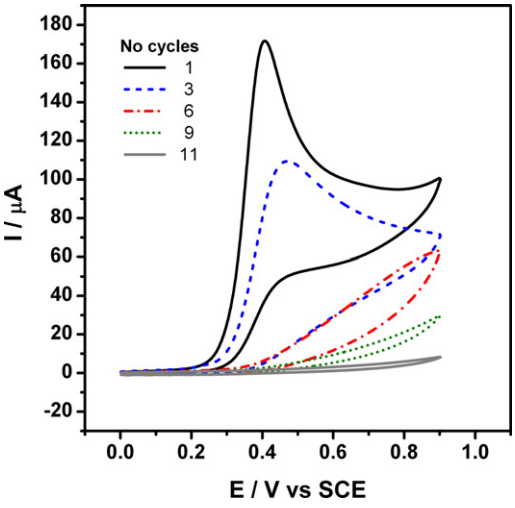

Figure 1.6: Homogeneous redox catalysis of acetate with ferrocene as mediator. After multiple successive scans, electrode activity was significantly decreased until complete electrode inactivation occurred. Reprinted from reference 52, with permission from Elsevier.

complete inactivation of the electrode surface occurred (**Figure 1.6**).

1.3.2 Oxidations of amines and anilines

As previously stated many organic compounds are difficult to oxidize. Exceptions to this are amines and anilines, where the lone pair of electrons located on the nitrogen atom is usually relatively accessible by normal techniques. Unsurprisingly, much of the oxidative DET work in the literature has focused on these compounds.

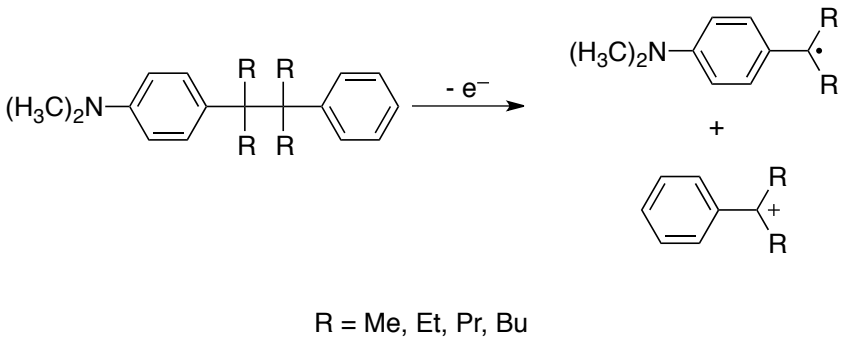

R = Me, Et, Pr, Bu

Scheme 1.7: DET reactions of anilines studied by Maslak et al.[53]

A series of anilines (**Scheme 1.7**) were studied by Maslak et al.;[53] the radical cations were generated via homogenous oxidation, electrochemically, and photolytically. Decay of the resultant radical cation was monitored via electron paramagnetic resonance spectroscopy, UV/visible spectroscopy, and cyclic voltammetry. Each of the anilines followed a stepwise DET mechanism, and the rate constants for C—C bond cleavage was reported to be on the order of 10^5 s^{-1}.

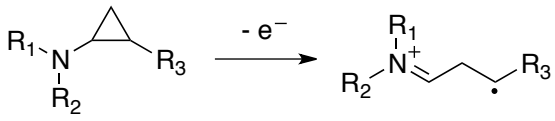

Scheme 1.8: DET reaction of amine/aniline cyclopropanes.

Cyclopropyl amines and anilines can be oxidized, and as in the case of their ketyl radical anion analogues, the resultant radical ion quickly undergoes fragmentation of the cyclopropyl ring, as shown in **Scheme 1.8**. This type of rearrangement is of significant importance biologically, as cyclopropyl amines and anilines are often used in enzymatic studies to probe the mechanistic pathway that enzymatic action follows. As was the case with cyclopropyl ketones, the rate of ring opening of the radical cations was expected to be similar to that of the cyclopropylcarbinyl rearrangement; upon further examination, this was found to not always be true.

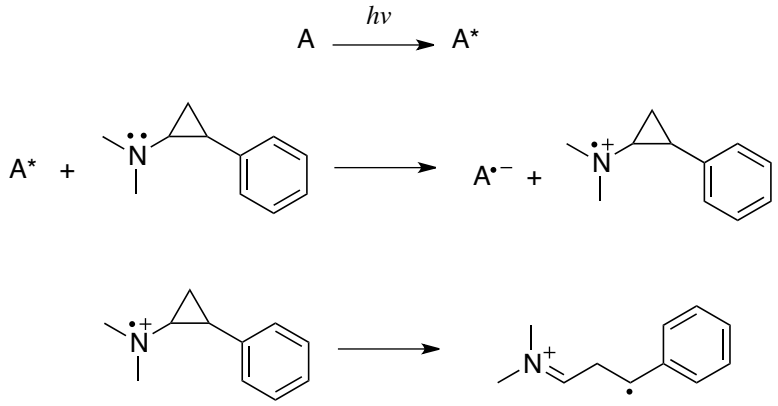

Scheme 1.9: Photoinitiated DET reaction of *N,N*-dimethyl-2-phenylcyclopropanamine, where **A** is a photoinitiated acceptor molecule.[54]

The reaction in **Scheme 1.9** was studied by Wang et al.[54] and is particularly interesting in that cleavage of the ion radical can lead back to the ring-closed neutral parent. Photoactivation of the acceptor molecule (**A**) makes it an excellent oxidizing agent. Wang showed that the bond cleavage pathway had a negligible barrier for ring opening, and ergo the rate of ET followed by

bond cleavage is very facile. As such, the bond cleavage occurs within the solvent cage of the electron transfer products, leading to two possible outcomes as shown in **Figure 1.7**. The first was simple bond cleavage of the cyclopropane ring, giving the radical cation product and radical anion acceptor (path *a* in **Figure 1.7**). However, the reaction coordinates for this dissociative pathway intersect with the reaction coordinate for the dark oxidation reaction (path *a* to *c* in **Figure 1.7**), and thus a second relaxation pathway is opened, wherein the cyclopropane bond is reformed concurrently with back electron transfer to the radical anion of the acceptor, leading to the starting products. This process was dubbed associative return electron transfer, and is one of the few examples of a concerted associative electron transfer reaction, wherein electron transfer occurs concertedly with bond formation.

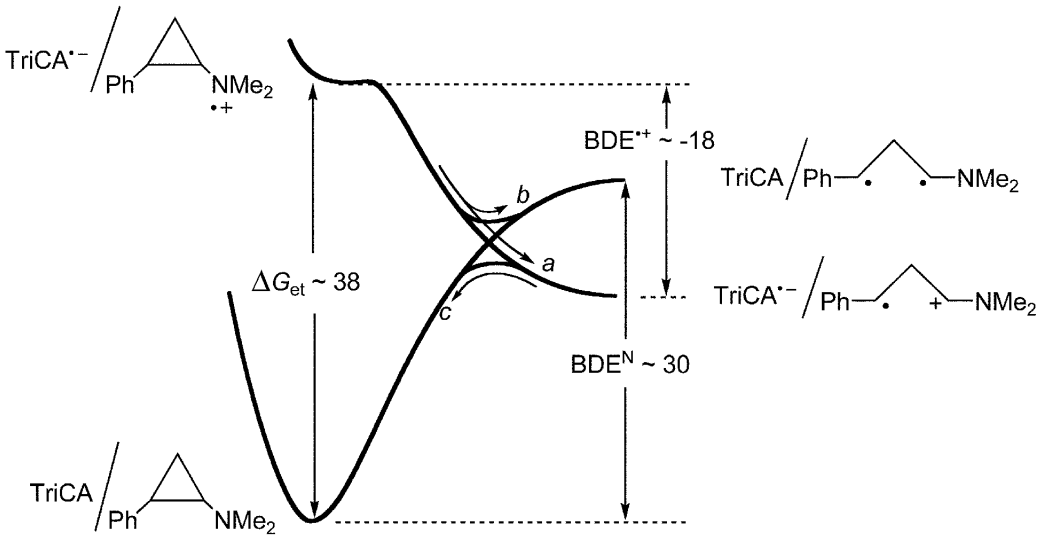

Figure 1.7: Associative return electron transfer. 2,9,10-tricyanoanthracene (TriCA) is used as a photoinitiated acceptor molecule, oxidizing 1-dimethylamino-2-phenylcyclopropane to its radical cation, which should then undergo ring opening to the distonic radical cation (path *a*). However, a crossing of product and reactant potential curves (*b*) leads to reformation of the cyclopropane C—C bond (*c*) and a return to reactants. BDE = bond dissociation energy for the C—C bond of the cyclopropane in the radical cation (≈ –18 kcal/mol) and the neutral cyclopropane (≈ 30 kcal/mol). Reprinted from reference 54 with permission of the Royal Society of Chemistry.

Grimm et al studied a series of cyclopropanamines computationally,[55] including those utilized in the above study. These computations were in agreement with Wang's findings that the barrier for ring opening of the 1-dimethylamino-2-phenylcyclopropyl radical cation was very small, to the point that the ring opening reactions of the radical anions could be considered barrier-less at room temperature at the UHF/6-31G* and UMP2/6-31G* levels of theory and basis set. The same result was obtained for the 1-amino-2-phenylcyclopropyl radical cation. However, it was found that in the case of the *N,N*-dimethyl-*N*-cyclopropanamine radical cation the barrier to ring opening was approximately 4.7 kcal/mol at the UHF/6-31G* level of theory. Additionally, the ring-opening reaction of the 1-dimethylamino-2-phenylcyclopropyl radical cation was found to be exothermic by approximately 27 kcal/mol, qualitatively consistent with Wang's estimation of the BDE for these radical cations.

Table 1.4
Cylclopropyl amines and anilines studied by Tanko and co-workers.[55-57]

Structure	k_{ro} (s^{-1})[a]	$E^0_{RX/RX^{\cdot+}}$ (V, vs. $Ag/AgNO_3$)
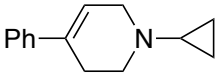	10^9	-
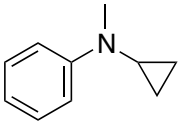	4.1×10^4	0.528
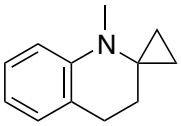	3.5×10^2	0.300
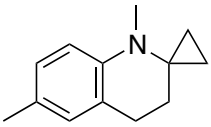	4.1×10^2	0.366

(*a*) Ring-opening rate constant of the radical cation produced by the oxidation of the respective structure

Tanko also studied the ring-opening reactions of a series of *N*-cyclopropylanilines, as given in **Table 1.4**, via electrochemistry and laser flash photolysis.[55-57] In contrast to their amine counterparts, these anilines exhibited a much slower ring opening rate. This can be explained in the context of **Eq. 1.3b** (rewritten for the case of oxidations for clarity) as follows. The oxidation potential, $E^0_{RX/RX^{\cdot+}}$, is much more negative for anilines than for amines, due to resonance stabilization. When compared to the 2-phenylcyclopropanamines discussed above, the BDE is expected to be much larger – that is, the C—C bond of the cyclopropane is stronger when neither of the carbons is allylic. It can be expected that the driving force for cleavage of the radical anion is much less in the cyclopropylanilines than in the cyclopropanamines, and consequently the rate of ring opening is much smaller.

$$\Delta G^0_{cleav} = D - E^0_{X^{-}/X^{\cdot}} + E^0_{RX/RX^{\cdot+}} - T\Delta S_{RX \rightarrow R^{\cdot}+X^{\cdot}} \qquad \textbf{Eq. 1.3b}$$

It was assumed that part of the slowing of the ring-opening reaction could be attributed to a conformational bias of the neutral anilines. That is, the lowest energy conformer was shown computationally to be one where the cyclopropane ring was orthogonal to the orbital in which the unpaired electron is located. This implies that an unfavorable conformational change would be required before ring opening could occur, as depicted in **Figure 1.8**, with a value of approximately 3.6 kcal/mol as predicted computationally. To alleviate this requirement, a new series of cyclic anilines were synthesized with the thought that locking the cyclopropane in the

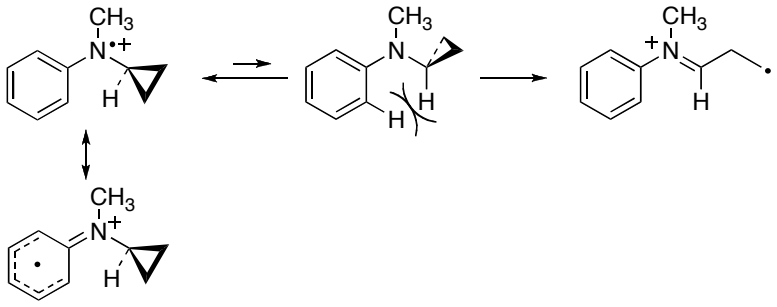

Figure 1.8: Conformation bias in cyclopropylanilines. The conformation required for ring opening is approximately 3.6 kcal/mol higher energetically than the optimized radical cation. Reprinted from reference 56.

correct conformation for ring opening would speed the ring opening reaction (examples 3 and 4 in **Table 1.4**). These compounds were examined electrochemically and found to undergo ring opening at an even more retarded rate relative to their acyclic counterparts, contrary to expectations.[56]

In retrospect these results are explicable by application of intramolecular dissociative electron transfer. Savéant's model can be applied to cleavage of primary radical ions, wherein an intramolecular electron transfer occurs concurrently with bond cleavage giving the radical and ionic fragment products. The conformational change required in the case of acyclic cyclopropylanilines costs about 3.6 kcal/mol, of which only one fourth contributes to the

activation barrier, according to Savéant's model. This means that the conformational change only counts at most 1 kcal/mol in the standard activation energy for the ring opening reaction, an amount most likely swamped by the contributions of bond breaking and solvent reorganization. Reorganization energy only accounts for one parameter of the model, the other parameter being the driving force for bond cleavage as given by **Eq. 1.3b**. The BDE of the cyclopropyl C—C bond is not expected to be significantly different in the acyclic and cyclic cyclopropylanilines; the same can be said for reduciblity of the leaving group ($E^0_{X^-/X^\cdot}$). The final parameter is then $E^0_{RX/RX^{\cdot+}}$; this value will be made more negative due to inductive affects by addition of an alkyl substituent at the *meta*- position, a direct consequence of cyclization. The difference in oxidation potentials of *N*-cyclopropyl-*N*-methylaniline and its cyclized analogue was found to be 0.228 eV (approximately 5 kcal/mol), a reasonable value when compared to their *N,N*-dimethylaniline cousins. When applied to **Eq. 1.3b** and then to the intermolecular dissociative electron transfer model, it is unsurprising that the rates for the ring-opening reaction of the cyclized cyclopropylanilines are less than the reaction rates of their acyclized brethren.

1.3.3 Other examples

Few other examples of oxidative DET reactions involving breaking of heavy atom—heavy atom bonds exist in the literature where the dynamics of the electron transfer have been quantified. By far the largest example is that of so-called free electron transfer (FET) reactions.[58] Using an approach similar to that of Wang discussed previously, photolysis or radiolysis of an organic solvent generates a triplet species, which then undergoes electron transfer with other solvent molecules, yielding the radical cation and anion of the solvent. Often alkyl chlorides are chosen as solvents in such cases, because the initial electron transfer is a concerted DET electron transfer yielding the solvent radical cation, a neutral alkyl radical, and a chloride anion (**Scheme 1.10,** first two steps). The radical cation then acts as a powerful oxidant, rapidly oxidizing any substrate in its vicinity, which is the basis of the technique (**Scheme 1.10,** third and fourth steps). Electron transfers from donor substrates in such reactions are usually remarkably fast, as the electron transfer process is endowed with large driving force due to how potent of an oxidant the solvent radical cation is. Brede and Naumov have shown that this FET can lead to surprising products.[58] The DET is simultaneously stepwise and concerted in some cases, as there is no time for conformational changes to occur in the solvent cage upon approach of the donor and acceptor species. Ergo, some conformations of the donor lead to stable radical cations and some do not, and the product ratio at the instant of electron transfer as measured by UV/visible spectroscopy

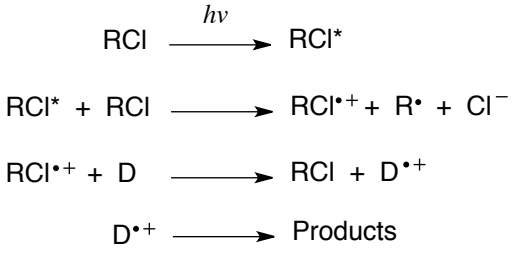

Scheme 1.10: Free electron transfer (FET).[58]

reflects this. Using this technique, the DET of many compounds have been shown, where the broken bonds include O—H, S—H, Se—H, N—H, C—C, C—O, C—S, and C—N bonds.[58] This technique is also synthetically popular, as the resulting neutral radical upon bond cleavage can lead to useful products.[58]

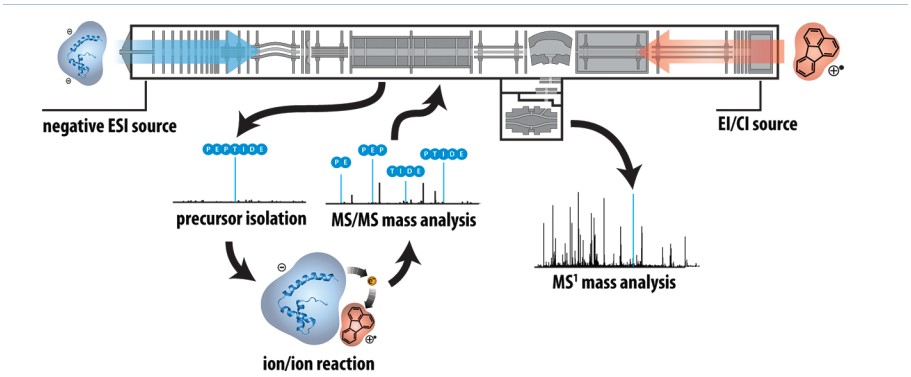

Figure 1.9: Negative electron transfer dissociation mass spectroscopy. Reprinted with permission from reference 59. Copyright 2012 American Chemical Society.

Finally, a very interesting and useful oxidative DET has been applied to mass spectroscopy of peptides.[59] This negative electron transfer dissociation (NETD) method involves generating the fluoranthene radical cation and then introducing it to a deprotonated peptide chain. The radical anion oxidizes the peptide chain, which leads to cleavage of the C—C backbone of the chain, producing ion and ion radical subunits that are then analyzed via mass spectroscopy. The apparatus is given in **Figure 1.9**. Using NETD mass spectroscopy in 2012, McAlister et al. were able to identify more than 2000 peptides from yeast,[59] which they claimed to be the most from any form of tandem mass spectroscopy up to that time.

1.4 Project definition

Previous work in the group has focused on the reductive DET reactions of cyclopropylketones. A logical extension of this work is the reductions of α-epoxyketones.

Substitution of oxygen in the cyclopropane ring leads to many interesting questions. Most obviously, ring opening may now proceed via two distinct pathways: C—C bond cleavage and C—O bond cleavage (**Scheme 1.11**). Which pathway is preferred and why? Secondly, this substitution could have an effect on the rate of ring opening: if so, what is it? Finally, what role do substituents (R_1 and R_2, **Scheme 1.11**) play in the ring opening dynamics? Do they influence which bond is broken? Do they have an effect on which DET pathway (stepwise or concerted) is observed?

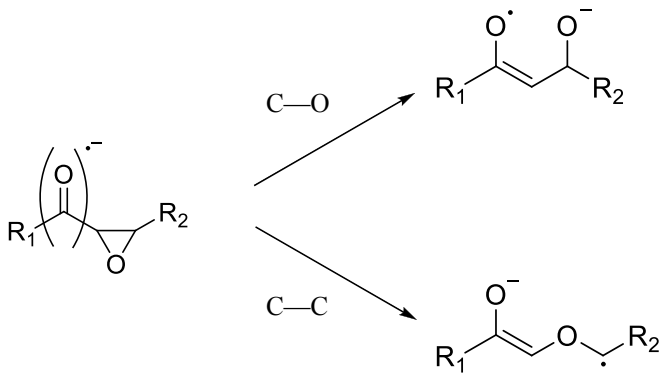

Scheme 1.11: DET reactions of epoxyketones, illustrating bond cleavage pathways.

To answer these questions, the series of α-epoxyketones given in **Chart 1.1** have been chosen for further examination. These species were chosen because they offer the full complement of possibilities with regards to question 3 – namely, reduction of **1** and **2** would yield resonance stabilized parent radical anions and **3** and **4** would not; and C—C bond cleavage of **1** and **3** would yield resonance stabilized product radicals, lending additional facility to the C—C bond cleavage pathway, leading possibly to mixed cleavage products (**Scheme 1.11**). These species were examined electrochemically by direct and indirect methods to characterize the mechanism, their reduction potentials, and their ring opening rate constants, where possible. Results of these studies are presented in **Chapter 2** of this document.

These electrochemical studies were supplemented with quantum mechanical computations. As shown earlier in this review, computational chemistry can often help elucidate mechanistic questions that remain ambiguous from the electrochemical experiments. Computational modeling of **1** – **4** (or close analogues thereof) was performed. The results of these simulations are included in **Chapter 2**.

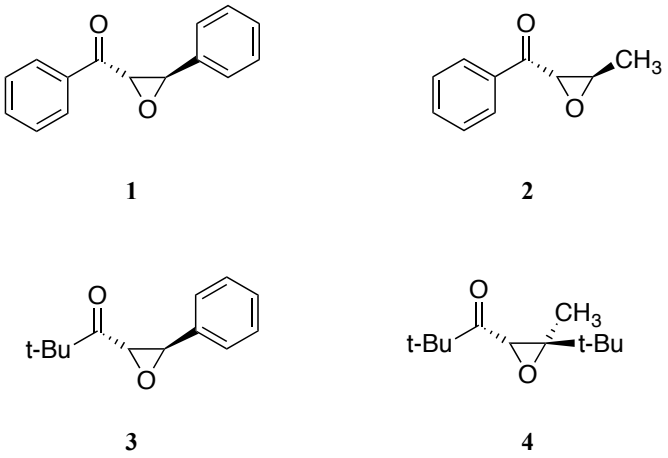

1 **2**

3 **4**

Chart 1.1

Oxidative DET reactions have not enjoyed as much quantitative attention as their reductive cousins; however, our group has recently been very interested in the oxidative reactions of a series of amines and anilines. It has been widely accepted[60-62] that the reaction of the *N,N*-dimethylaniline radical cation with acetate proceeds via acid/base chemistry, yielding a neutral aniline radical and acetic acid (**Scheme 1.12**). However, previous results in our group

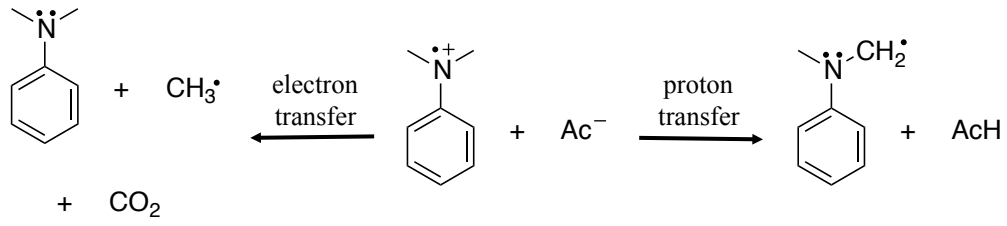

Scheme 1.12: Two possible pathways for reaction between dimethylaniline radical cation and acetate.

suggest that this is not the case, and that this reaction proceeds through a homogeneous electron transfer, yielding the parent aniline and the acetoxyl radical, which then undergoes rapid decarboxylation, as given in **Scheme 1.12**. Although the electrochemistry of carboxylates has been examined in the past (*vide ante*), a thorough examination of the indirect electrochemistry of acetate is lacking. Thus, the homogeneous redox catalysis reactions of acetate with a series of ferrocene derivatives was examined. Additionally, no experimental value of the oxidation potential of acetate has been published; convolution voltammetry of the direct electrochemistry of the acetate anion has been used to establish this value. Furthermore, the effect of water in these oxidative reactions has been examined. The combined results of the direct and indirect electrochemistry of acetate are the topic of **Chapter 3**.

Chapter 2. Reductions: The dissociative electron transfer reactions of a series of α-epoxyketones

2.1 Introduction

Electron transfer reactions are fundamental chemical processes and often lead to bond cleavage. Electron transfers that are followed by or occur concurrently with bond cleavage are termed dissociative electron transfers and are described by one of two theories: the Marcus-Hush model (**Eq. 2.1**, *vide infra*) of outer sphere electron transfer[1] for stepwise mechanisms and the Savéant model (**Eq. 2.10**, *vide infra*) of concerted dissociative electron transfers[2] for concerted mechanisms. Both theories are similar treatments based on approximations derived from intersections of the Morse potential energy functions of the reactants and products, the most significant difference between the two being that the Savéant model incorporates the bond dissociation energy of the bond being broken in the concerted process. Both theories will be described in more detail later in this document.

Examples of dissociative electron transfer reactions are very common in the literature; full application of the Marcus and Savéant models is less so. However, many examples have been shown for reductive dissociative electron transfers involving, among others, cleavage of carbon-halogen[3], carbon-sulfur[12], sulfur-sulfur[14], and even carbon-carbon[20] bonds (see **Chapter 1**). There has been noticeably less reported with respect to carbon-oxygen bonds; particularly lacking is any full treatment of electron transfer reactions involving carbon-oxygen bond cleavage with the Marcus and Savéant models, in part because it is rare that electron transfer leads immediately to cleavage of a carbon-oxygen bond. One possible exception may be for structures containing small rings such as epoxide, where relief of ring strain can provide driving

force to facilitate the cleavage of the carbon-oxygen bond in a radical species. The present work attempts to explore this idea, particularly with respect to a series of α-epoxyketones as described shortly.

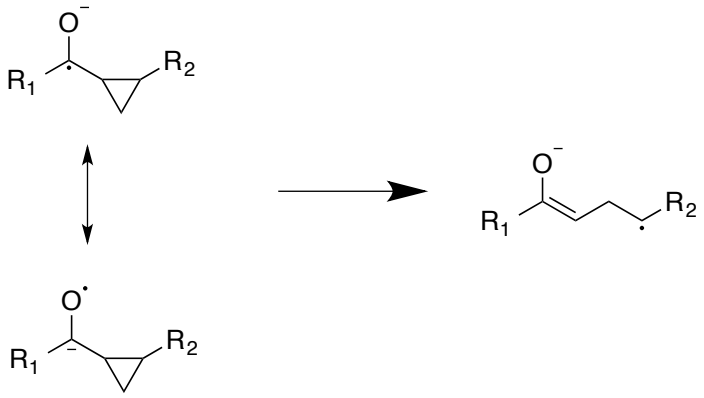

Scheme 2.1: Ring opening of cyclopropylketyl radical anions. R_1 may provide resonance stabilization of charge *and* spin in the ring closed radical anion and R_2 may provide resonance stabilization of spin in the ring opened radical anion.

There are two families of compounds that have been thoroughly examined with respect to electron transfer theory that are of particular relevance to the work presented here. The first is the dissociative electron transfers of cyclopropane-containing ketones that have been extensively characterized by Tanko and co-workers (**Scheme 2.1**).[20,23,25-32,57,63-64] They have shown that the bond-breaking reactions following (and concurrent with) the reduction of these ketones to their radical anions are in large part the result of the structural functionalization of the parent compound. The rate of ring opening (the bond-breaking rate) is heavily influenced by the structural composition of the species, particularly with respect to charge *and* spin stabilization in both the parent and ring-opened radical anions (**Scheme 2.1**). **Table 2.1** demonstrates the transition from very slow cleavage reactions to very fast ones. Notice how the general trend is such that slow reactions correspond to parent structures that exhibit large resonance stabilization

Table 2.1
Cyclopropylketylradical anion rearrangement as reported by Tanko and co-workers.[20,23,25-32,57,63-64]

Structure[a]		k_{ro} (s^{-1})	$E^0_{RC/RC^{\bullet-}}$
$RC^{\bullet-}$	$RO^{\bullet-}$		(V, vs. $Ag/AgNO_3$)
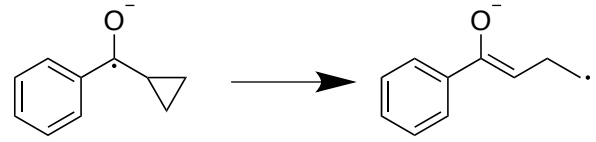		<10	-2.42
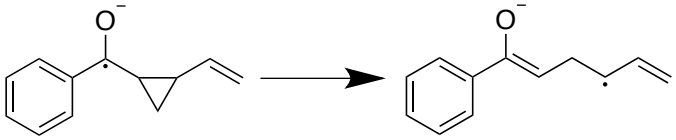		2.5×10^5	-2.40
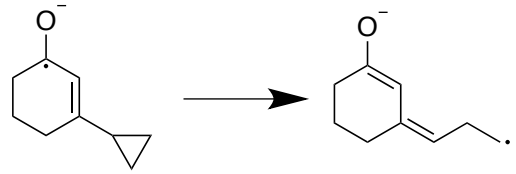		1.6×10^6	-2.80
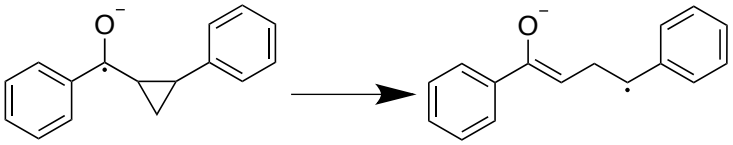		9.6×10^6	-2.44
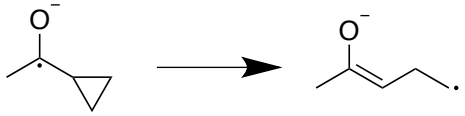		$>10^7$	-3.22
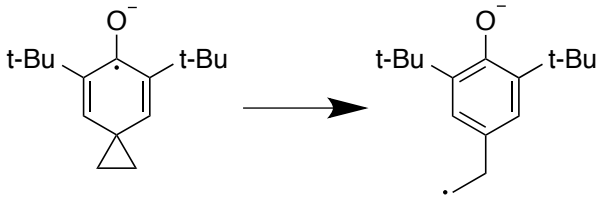		$>3 \times 10^8$	-2.60
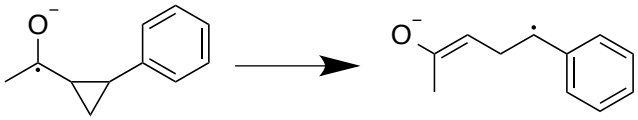		$>10^8$	-2.98
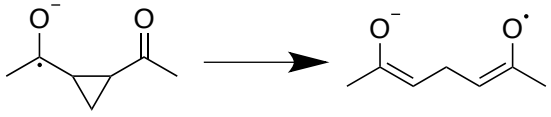		cDET	-2.55

(*a*) RC = ring closed, RO = ring opened

of charge and spin and cleaved structures where this stabilization has been destroyed. Very fast reactions tend to either exhibit the opposite trend or involve some additional driving force (such as formation of an aromatic ring in the 6th entry in the table) enabling the cleavage process. Thus electron transfer induced cleavage of carbon-carbon bonds is facilitated by weak bonds (as in the cyclopropyl moiety), by unstable parent radical ions, by resonance stabilized cleavage products, and by additional driving force provided by other considerations such as formation of an aromatic ring in the product structure.

Although the classic demonstration of the validity of the electron transfer theory is the reduction of organic halides (see **Chapter 1** for many specific examples), their relevance in comparison with the epoxides examined in this work is more than merely historical. A carbon-oxygen single bond is in many ways similar to an inactive carbon-halogen bond. A carbon-oxygen bond can often be made to undergo chemistry similar to organic halide chemistry by activating the oxygen, usually via protonation. A classic example is activation of an alcohol as a leaving group in nucleophilic substitution reactions by using a strong acid to protonate the oxygen, making the leaving group a more favorable water molecule as opposed to the poor-leaving hydroxide anion. An additional way to "activate" a carbon-oxygen single bond is by placing it in small ring, such as an epoxide. The carbon-oxygen bond is weakened by ring strain; its reactivity is increased and it may behave more like the carbon-halogen bonds such as those in the organic halides described below.

In general, carbon-halogen bonds undergo stepwise dissociative electron transfer in aryl halides and concerted dissociative electron transfer in alkyl halides.[2-3,65] This is mainly a function of the reduction potential of the neutral species/parent radical anion couple. Aryl halides have a much lower reduction potential than alkyl halides and their radical anions are thus more stable

intermediates than those of their alkyl halide brethren because the added electron is accommodated in the π-system of the aromatic ring. The greater the stability of the uncleaved intermediate, the less likely the dissociative electron transfer will follow a concerted mechanism and vice versa. Additionally, aryl halides have a LUMO with π^* character – this tends to stabilize the radical anion by delocalization of the spin and charge. Structurally, the π* LUMO does not overlap with the σ C—X bond of the aryl halide bond that is broken in the subsequent cleavage step, making it quite natural that the reduction and bond breaking are distinct and consecutive mechanistic steps.

Contrast this with the cyclopropylketones discussed previously, where moving from aryl to alkyl substituents in general only affected rate of bond cleavage and not the mechanistic pathway itself; it remains to be determined if the carbon-oxygen bond in an epoxide ring will behave more like the carbon-carbon bond of the cyclopropyl ketones or the carbon halogen bond of the organic halides.

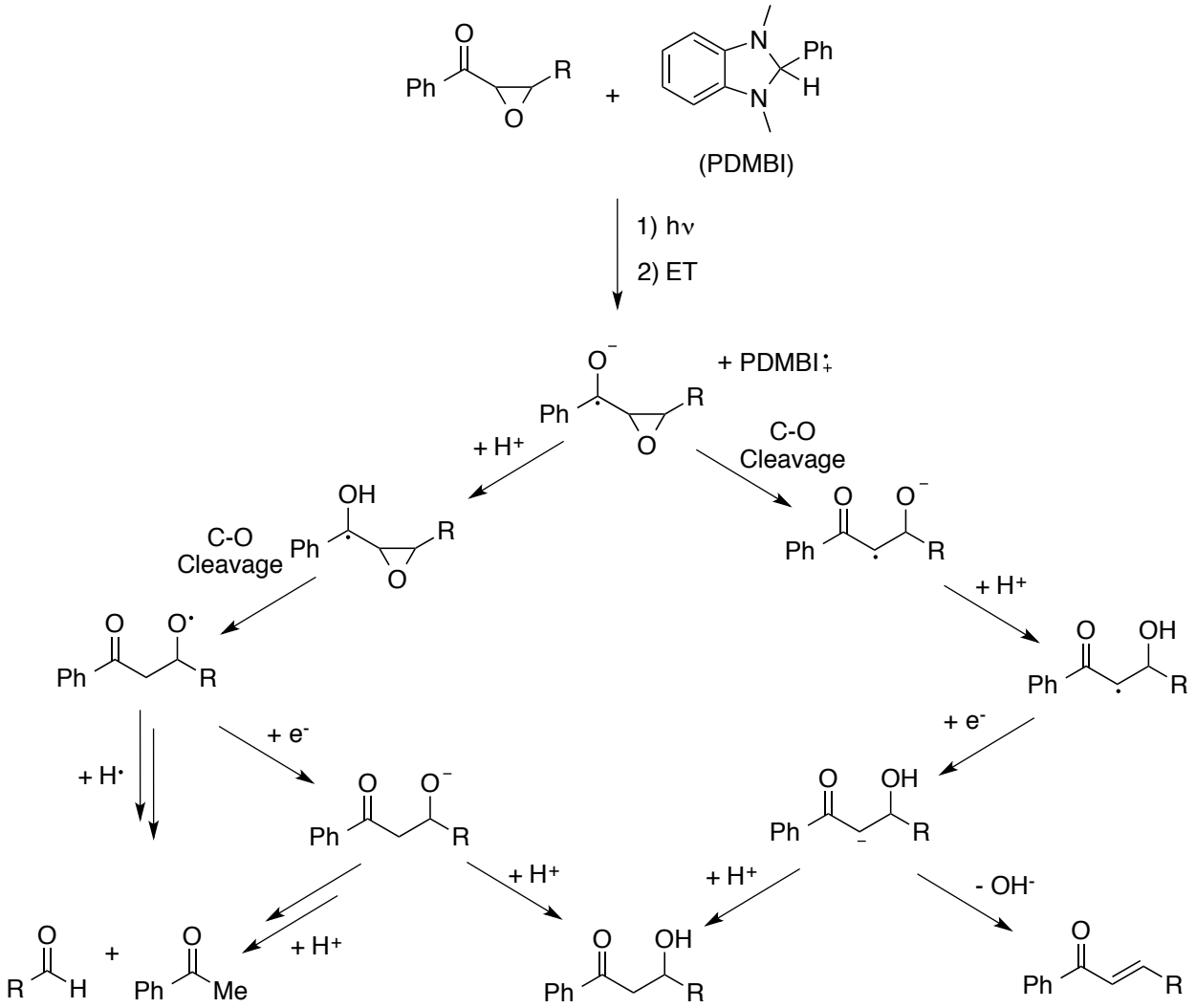

Scheme 2.2: Hasegawa's proposed mechanism for photoinduced reduction of α-epoxyketones in the presence of PMDBI showing how cleavage of the carbon-oxygen bond can give an aldol and retro-aldol addition products in the presence of available protons and electrons. Adapted from reference 66.

Hasegawa has reported[33-37,66-68] reductions of α-epoxyketones in the literature. These reductions are typically achieved with photoinduced irradiation of the ketone, which then undergoes electron transfer with a donor molecule such as 2-phenyl-N,N-dimethybenzimidazoline (PDMBI, **Scheme 2.2**). Hasegawa reported products that were consistent with carbon-oxygen bond cleavage, particularly the alcohol formed from epoxide cleavage as shown in **Scheme 2.2,** as well as organic acids and aldehydes arising from retro-aldol condensation of this alcohol, depending on the specific conditions of the photosynthesis.

Recently, reductive bond cleavage of α-epoxyketones via visible light activated photocatalysis has also been reported.[69-70] As with the Hasegawa work, products consistent with carbon-oxygen bond cleavage were observed and no rate data was reported for the bond cleavage process itself. Reduction potentials for the α-epoxyketones also remain unknown. Additionally, although several mechanisms were proposed for the reductive bond cleavage, there was no attempt made to determine the specific mechanistic pathway, particularly with respect to the stepwise/concerted nature of the electron-transfer-and-bond-cleavage process. Furthermore, no attempt has been made to identify what role the structure of the ketones would play on the overall reaction rates as well as on the stepwise-concerted dichotomy.

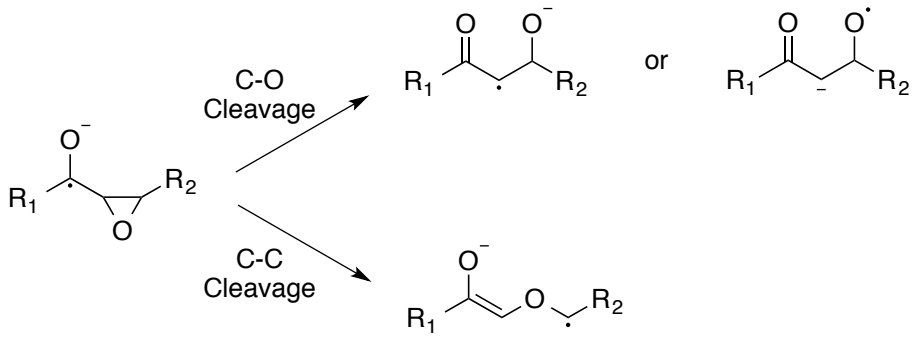

Scheme 2.3: Possible cleavage pathways for ring opening of α-epoxyketones.

The goal of this work is to elucidate the mechanism of reductive cleavage of α-epoxyketones, and in particular to answer the following questions. Does reduction of the ketones lead to cleavage of the epoxide moiety? If ring opening does occur is it via carbon-oxygen or carbon-carbon bond cleavage? Does the bond cleavage occur concurrently with or subsequently to the electron transfer? What role does structure, if any, play in the rate of bond cleavage and in the stepwise-concerted dichotomy discussed previously? To investigate these questions a series of α-epoxyketones were chosen (**Chart 2.1**) which should provide a solid answer to the last question. Compound **1** could potentially exhibit large resonance stabilization of both the parent

and cleaved radical anions (if the carbon-carbon bond is cleaved); **2** would only give stabilization in the parent radical anion; **3** would potentially only give stabilization in the cleaved radical anion (again, should the carbon-carbon bond break); and **4** would exhibit no additional stabilization (other than that inherent in the α-epoxyketyl motif itself). **Scheme 2.3** shows the possible cleavage pathways and the possible products that may arise directly from cleavage of the epoxide ring via either carbon-carbon or carbon-oxygen bond breaking.

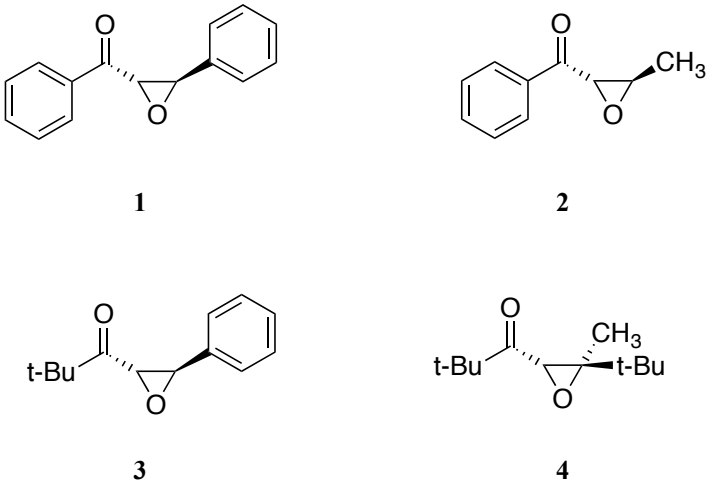

Chart 2.1

*Note: Special thanks to Michelle Grimm who synthesized compound **3** for this study*

2.2 Results

The study of radical ions requires a method or combination of methods that generates the species of interest and monitors their lifetimes while simultaneously providing analytical measurements of the observables of these reactions, such as reduction and oxidation potentials, rate constants, and so forth. Electrochemistry thus emerges as an ideal tool for initiating and monitoring these charge transfer reactions for three reasons: 1) The species are generated by the method, 2) the driving force of the reactions is controlled by and related to the (known) potential

of the electrode, and 3) the rate of reaction is directly related to the current drawn by the electrochemical cell and measured by the potentiostat. Thus electrochemical techniques give quantitative information about the thermodynamics as well as the kinetics of the reaction of interest while simultaneously generating the species in a controlled manner, without the need for a separate monitoring technique, such as spectroscopy.

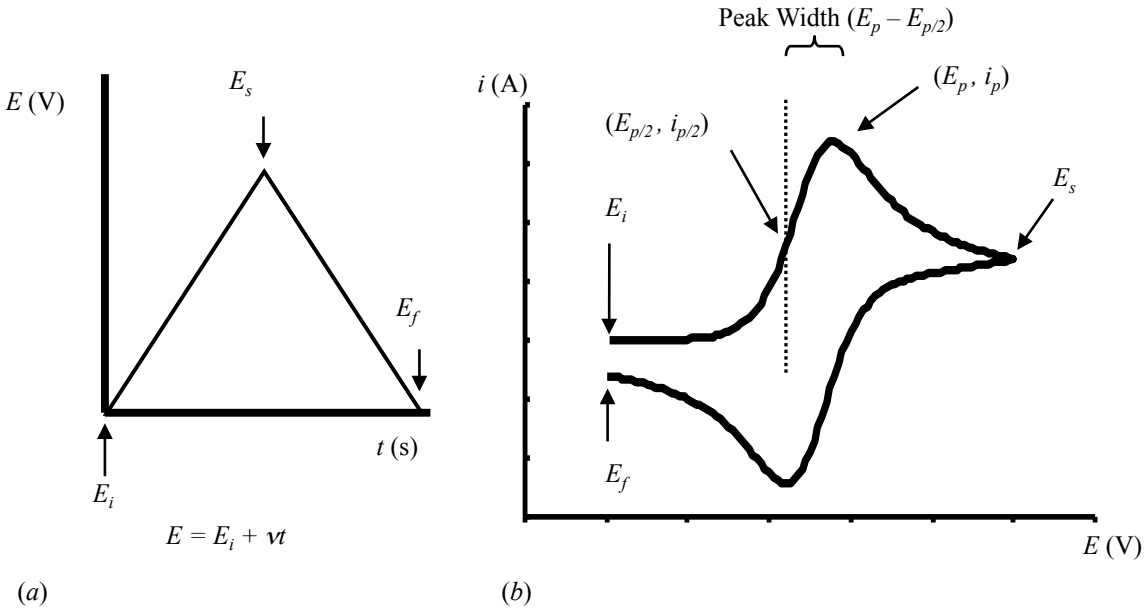

Figure 2.1: Cyclic voltammetry. (*a*) Potential waveform. (*b*) Voltammogram. Important potentials and currents marked. ν = sweep rate (typically in V/s).

The two quantitative methods presented here encompass both direct (where electron transfer to the species of interest happens at the electrode surface) and indirect (where electron transfer to the species of interest happens in the solution, away from the electrode surface) techniques. Both methods are linear potential sweep chronoamperometric techniques, wherein the electrode potential is swept in a linear fashion from one potential to another, and the resultant current is measured. A typical waveform for the electrode potential versus time is given in

Figure 2.1. In practice, all of the experiments are cyclic voltammetry experiments, where the potential is swept at a certain volts per second (sweep rate, ν) from an initial potential to a switching potential, whereupon the potential is returned back to its starting value at the same rate. Where there is no discernable faradaic current drawn on the reverse sweep, the technique is analyzed as linear sweep voltammetry and the reverse sweep is ignored.

Preparative (sometimes called bulk) electrolysis is often a useful way to identify the products of electrochemical experiments. Although the techniques discussed previously sometimes allow precise measurement of rate, rate constants, reduction or oxidations potentials, and the like, they cannot in and of themselves inform the identity of the process they are measuring. That is to say, they may point to what the rate limiting step of the mechanism is, perhaps even what the mechanism type is, but they cannot elucidate what the specific mechanism is, only the class type. For instance, the chemical step in an EC mechanism may be carbon-oxygen bond cleavage; it may also be carbon-carbon bond cleavage, or perhaps some other chemical transformation that has heretofore not been considered. The actual mechanistic pathway must be obtained from another technique, product studies, or computational chemistry, and often the observer must intuitively interpret the electrochemical data based on familiarity with the possible reaction pathways. Preparative electrolysis can help with this, as it should yield products similar to those obtained in the electrochemical techniques discussed previously.

Finally, quantum mechanical computations offer significant advantages when applied to unimolecular rearrangements of the nature described here. Particularly, these calculations can focus on the radical anion intermediates and give insight into the rearrangement reactions that are impossible to observe with the electrochemical experiments described above.

2.2.1 Direct electrochemistry

2.2.1.1 Resonance stabilized epoxyketyl radical anions 1 and 2

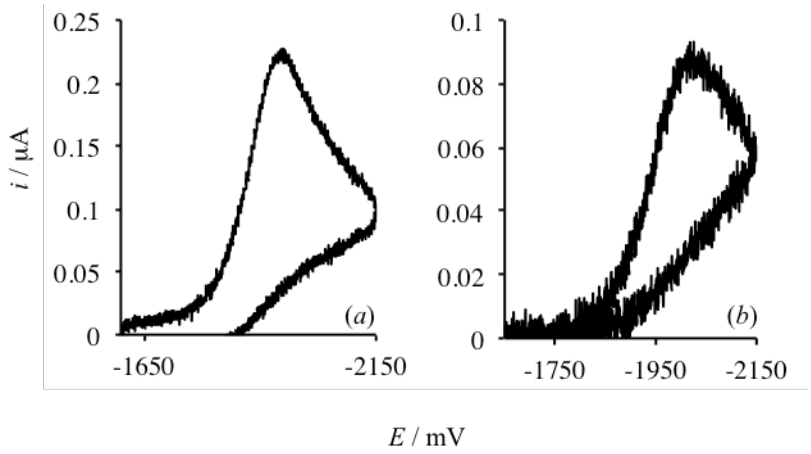

Figure 2.2: Example voltammograms of **1** (*a*, 0.0030 M) and **2** (*b*, 0.0026 M, with a smaller electrode) in DMF. ν = 800 mV/s, 0.5 M supporting electrolyte.

Typical voltammograms resulting from cyclic voltammetry of **1** and **2** are given in **Figure 2.2**. The immediate characteristic of the waves that should be noted is their irreversibility; there is no oxidative wave in the voltammograms which would correspond to an oxidation of the reduction product generated in the forward sweep. This implies that the immediate reduction product (e.g., $\mathbf{1}^{\bullet-}$) has a short lifetime relative to the timeframe of the experiment, and undergoes further reaction (bond breaking or dimerization, for example) quickly enough such that there is little or none remaining to be oxidized back to the parent species as the electrode potential sweeps back to more positive values. This further suggests that the reduction is following an *EC*-type mechanism, the simplest of which is given in **Scheme 2.4**, where the first step is a heterogeneous (from the electrode phase to the solution phase) electron transfer to the substrate (step *E*) followed by some chemical transformation (step *C*).

$$A + e^{\bullet -} \underset{k_{-het}}{\overset{k_{het}}{\rightleftharpoons}} A^{\bullet -} \qquad (E)$$

$$A^{\bullet -} \xrightarrow{k_{cs}} \text{Products} \qquad (C)$$

Scheme 2.4: EC mechanism.

The mechanism type has a large effect on the shape of the waves as well as how the shape changes when the sweep rate is changed. In particular, the location of the peak as well as the peak width (defined in **Figure 2.1**) depends on both the mechanism type and the rate-limiting step of the mechanism. These data can be used as diagnostic criteria for establishing the rate-limiting step of the mechanism and in some cases the overall mechanism itself. Three common cases (rate-limiting electron transfer followed by a first order chemical step, electron transfer followed by a rate-limiting first order chemical step, and electron transfer followed by a rate-limiting second order dimerization) are shown in **Table 2.2**.[71] Note that if the heterogeneous electron transfer step is rate limiting, the identity of the rest of the mechanism cannot be established. This means that if the reaction is under electron transfer control, no information on further steps can be determined (e.g., if the following step is an unimolecular rearrangement, a bimolecular dimerization, and so forth.). Likewise, no information on the kinetics of any

Table 2.2
Mechanism diagnosis from voltammogram response. Bolded letters indicate the rate-limiting step of the mechanism.[71]

	EC[a]	E**C**[b]	E**C**$_{\mathbf{dim}}$[b]
$\partial E_p / \partial \log \nu$	-59.1	-29.6	-19.7
$\lvert E_p - E_{p/2} \rvert$	95.1	47.5	38.8
$\partial E_p / \partial \log C_A^*$	0	0	19.7

(a) in millivolts, for T = 25° C, $\alpha = 0.5$ and $n = 1$ *(b)* in millivolts, for T = 25° C and $n = 1$

following steps may be obtained, such as the rate constant for a possible bond-breaking step like (in this case) cleavage of the epoxide ring.

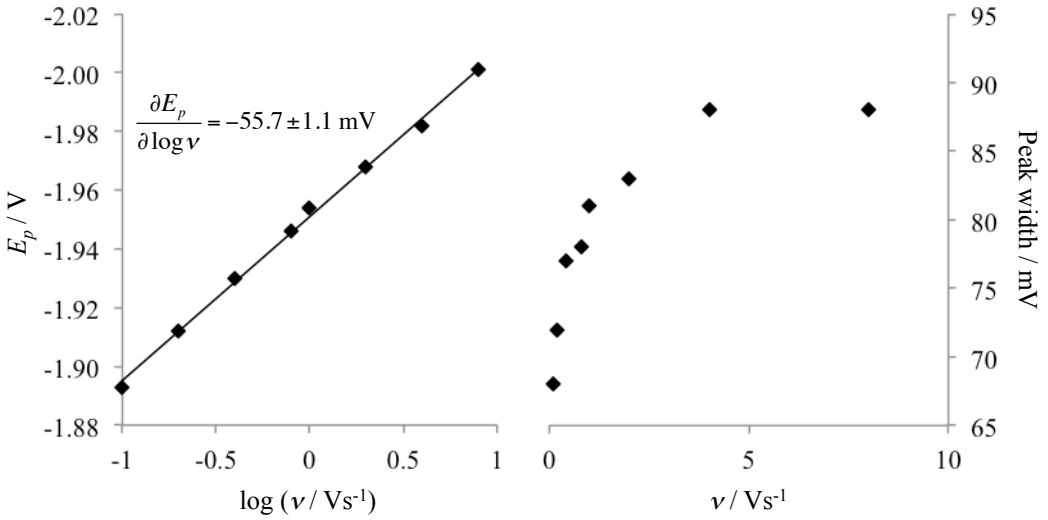

Figure 2.3: Variation of peak potential (*left*) and $|E_p - E_{p/2}|$ (peak width, *right*) as a function of sweep rate for **1** in DMF. C_1 = = 0.003 M, 0.5 M supporting electrolyte, ν = 100, 200, 400, 800, 1000, 2000, 4000, and 8000 mV/s.

The direct electrochemistry of **1** was shown to give a variation of peak potential per decade change in sweep rate of -55.7 ± 1.1 mV; simultaneously, the peak width rose from a value of ca. 65 mV at low sweep rates to a value of ca. 90 mV at faster sweep rates (**Figure 2.3**).

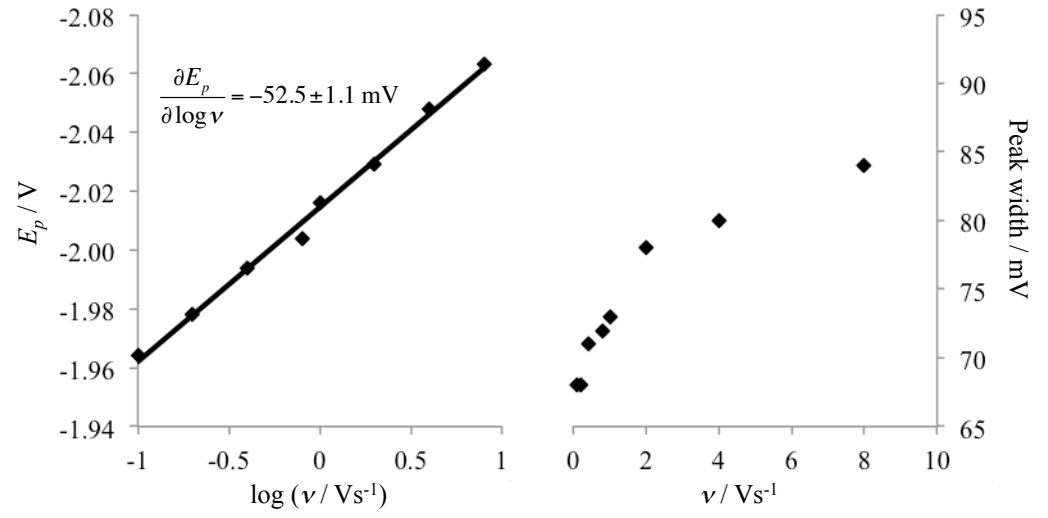

Figure 2.4: Variation of peak potential (*left*) and $|E_p - E_{p/2}|$ (peak width, *right*) as a function of sweep rate for **2** in DMF. C_2 = 0.003 M, 0.5 M supporting electrolyte, ν = 100, 200, 400, 800, 1000, 2000, 4000, and 8000 mV/s.

Comparing this data to the diagnostic criteria given in **Table 2.2** shows no clear match for immediate mechanism diagnosis. **2** showed similar results, as detailed in **Figure 2.4**. The peak potential varied as a function of sweep rate by -52.5 ± 1.1 mV per decade, and the peak widths were again not constant, generally increasing at faster sweep rates.

Each of the above results lead to some ambiguity about the reaction mechanism, particularly with respect to diagnosis of the rate-limiting step. Peak widths are principally interesting. Clearly, at faster sweep rates the reaction appears to be under electron transfer control, but at slower sweep rates the waves are narrower and look more like the expected result for a mechanism where the chemical step is rate limiting. The significance of these results will be discussed later in **2.3.1.1**.

2.2.1.2 Epoxyketyl radical anions 3 and 4 with no resonance stabilization

As with the aromatic species discussed in the previous section, cyclic voltammetry was used to analyze the reactions of aliphatic ketones **3** and **4.** Typical voltammograms resulting from these experiments are illustrated in **Figure 2.5**. As with the previous examples, the main

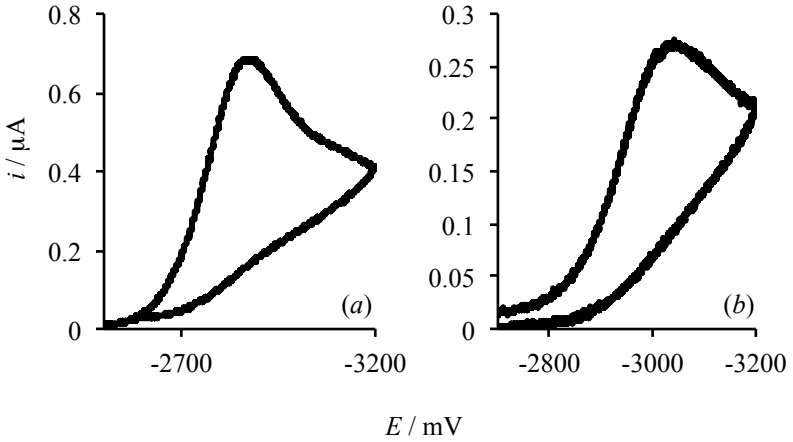

Figure 2.5: Example voltammograms of **3** (*a*, 0.0030 M) and **4** (*b*, 0.0013 M) in DMF. ν = 400 mV/s, 0.5 M supporting electrolyte.

characteristic of these voltammograms is their irreversibility, however, upon closer inspection, some key differences between these compounds and their aromatic cousins arise.

The peak potential variation with changing sweep rate is given for **3** in **Figure 2.6** as well as the peak width data. In contrast with the aromatic radical anions discussed earlier, peak widths did not vary as a function of scan rate and were found to be large, larger than typical for "standard" electron transfer reactions. It should be noted that for reactions dominated by the electron transfer step, the peak widths are a function of the transfer coefficient, α. This coefficient is a measurement for location of the transition state structure in the reaction coordinate diagram, and its value has a significant impact on the shape of the potential-current response (*vide infra*).

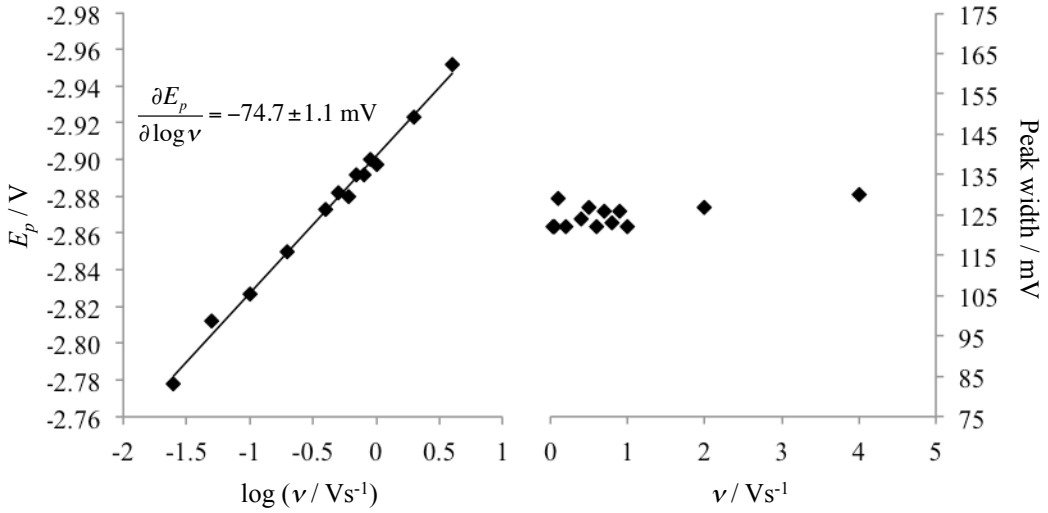

Figure 2.6: Variation of peak potential (*left*) and $|E_p - E_{p/2}|$ (peak width, *right*) as a function of sweep rate for **3** in DMF. $C_3 = 0.003$ M, 0.5 M supporting electrolyte, $\nu = 25$, 50, 100, 200, 400, 500 - 1000, 2000, and 4000 mV/s.

According to Marcus theory, the activation energy for an electron transfer reaction (and thus the corresponding rate constant) depends heavily on 2 parameters: the driving force for the electron transfer and the reorganization energy, λ (**Eq. 2.1**).

$$\Delta G^{\ddagger} = \frac{\lambda_o + \lambda_i}{4}\left(1 + \frac{\Delta G^0}{\lambda_o + \lambda_i}\right)^2 \qquad \textbf{Eq. 2.1}$$

In a direct reduction process, the driving force of the reaction is controlled by the potential of the working electrode, and can be adjusted as determined by the user. The reorganization energy, which is composed of both an internal component (the internal reorganization energy, λ_i, accounting for things like bond stretching or other structural changes required for the electron transfer to occur) and an external component (the outer reorganization energy, λ_o, accounting for solvent reorganization that accompanies the charge transfer process), is system dependent and cannot be controlled by the user. Systems that have a large value of λ are kinetically slow reactions and will have a small standard heterogeneous electron transfer rate constant. In order to make these reactions "go", a large overpotential must be applied, making the reaction thermodynamically more favorable and thus increasing the rate of reaction in accordance with Marcus theory. One effect of increasing this thermodynamic parameter is that the location of the transition state structure is moved from a location equidistant between the reactants and products (at the standard state) towards the reactants. The transfer coefficient, α, is a measurement of this transition state structure location and ranges from a value of 0 (transition state structure resembles reactants) to 1 (transition state structure resembles products). For typical electrode reactions involving small organic compounds this value tends to fall around 0.5, as there is usually only a small amount of reorganization required for the electron transfer process to occur. Peak widths for these "typical" electron transfer reactions tend to be around 95 mV at room temperature.[71]

However, when there is a significant amount of reorganization required for the reaction to proceed, such as would be the case in a concerted dissociative electron transfer where bond-breaking occurs concurrently with the electron transfer process, there must be a large overpotential applied to overcome the kinetic drawback of this large reorganization energy, and this results in an α value smaller than expected, as described above. Because α is small, peak widths tend to become large. Therefore peak widths larger than 95 mV indicate a reaction where electron transfer is rate limiting and that a larger than normal structural reorganization is required. **4** gave similar results, and overall results for **3** and **4** are detailed in **Table 2.3**.

Table 2.3
Linear sweep voltammetry results of compounds **3** and **4**. Values in parenthesis indicate standard error.

	$\partial E_p / \partial \log \nu$ (mV)	$\lvert E_p - E_{p/2} \rvert$ (mV)	$\alpha_{avg}{}^{a}$	$\alpha_{avg}{}^{b}$
3	-74.7(1.1)	124(3)	0.400(0.010)	0.381(0.009)
4	-76(5)	123(3)	0.39(0.03)	0.390(0.010)

(a) average value calculated from variation of peak potential with sweep rate *(b)* average value obtained from peak widths

In contrast to the aromatic species discussed earlier, both **3** and **4** are clearly under electron transfer control, and both clearly have a larger than typical reorganization energy. One of the defining features in systems where a concerted dissociative mechanism is followed are peak widths that give an α value of around 0.3. Using the peak widths obtained from the voltammograms, the average $\alpha_{peak\ width}$ value for **3** and **4** are 0.38 and 0.39 respectively.

Convolution voltammetry is a useful tool for electron transfer reactions where the ET step is clearly rate limiting. Although often referred to as an experimental method, convolution is actually a mathematical analysis of LSV data that allows more points of the voltammogram to be analyzed, rather than a separate technique unto itself. Current is directly related to the rate of the

electrochemical reaction, and when analyzing a typical linear sweep or cyclic voltammogram, a few things should be noted (see **Figure 2.7**). As the potential of the electrode begins to approach the reduction potential of the species of interest, electron transfer begins to occur, converting the oxidized form of the couple to the reduced form. As this potential passes through the reduction potential and moves toward more negative potentials, this process becomes more favorable and faster (see the previous discussion on Marcus theory), and current increases. At some point, however, the amount of oxidized substrate in the vicinity of the electrode is depleted to a point where there is very little remaining, and more must diffuse in toward the electrode before it can be reduced. Eventually this process begins to compete with the kinetics of the electron transfer until they are balanced, at which point the current reaches its peak. After this the kinetics of diffusion become dominant (i.e. rate limiting), and current begins to decreases as it takes longer and longer for substrate to diffuse from the bulk of the solution to the electrode in order to be reduced. Thus the kinetics of mass transport has a major effect on the shape of the voltammograms, as well as the mathematics that describe that shape.

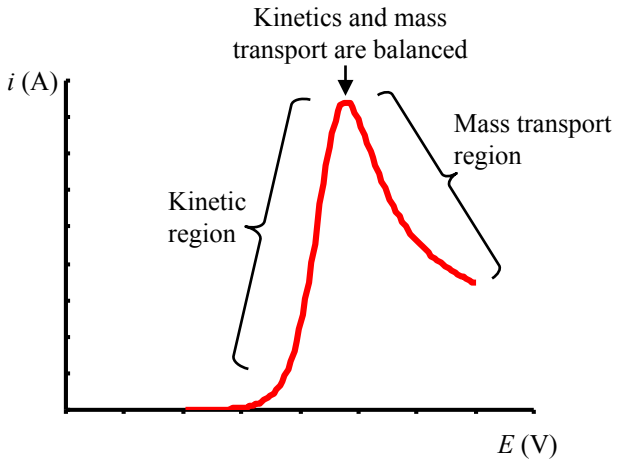

Figure 2.7: Linear sweep voltammogram showing the three regions of rate control: kinetic (current limited by electrode kinetics), balanced (electrode kinetics and diffusion balanced), and mass transport control.

Diffusion in a cyclic voltammetry experiment using an electrode of typical size is called semi-infinite linear diffusion. This means that the electrode is so large relative to the size of the diffuse layer that diffusion can be considered to be a linear process (see **Figure 2.8**), and mathematically the rate of diffusion is related to the inverse square root of the time. Because of the diffusion component of the observed current, mathematical analysis of each point on the voltammogram is difficult, and in practice only two points of the voltammograms are analyzed: the peak potential and the half-peak potential (where $i = i_p/2$), the latter value only being used to calculate peak width.

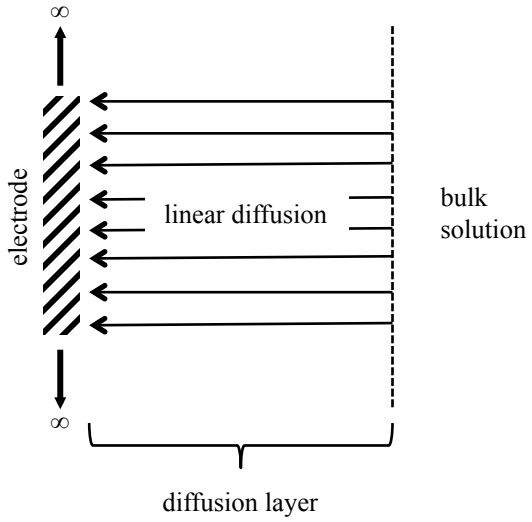

Figure 2.8: Semi-infinite linear diffusion.

Convolution voltammograms are obtained via semi-integration[72-74] of the LSV voltammograms using **Eq. 2.2**; this method effectively integrates the voltammetric data with respect to the inverse square root of time, and mathematically removes the effect of mass transport. In principle, the method is akin to using an infinitely slow sweep rate or conversely to "speeding up" the diffusion process, such that diffusion no longer effects the experimental results, and the current observed is due solely to the electron transfer kinetics. This results in a limiting

current which is defined in **Eq. 2.3**, where *n* is the number of moles of electrons consumed per mole of reaction, *A* is the electrode surface area, D_A is the diffusion coefficient of species A, and C_A^* is the bulk concentration of A (note that the real current is always defined with a lowercase *i* and the convolution current with an uppercase *I*). From this equation the diffusion coefficient of the reactive species can be determined.

$$I(t) = \frac{1}{\pi^{1/2}} \int_0^t \frac{i(u)}{(t-u)^{1/2}} du \qquad \textbf{Eq. 2.2}$$

$$I_{lim} = nFAD_A^{1/2} C_A^* \qquad \textbf{Eq. 2.3}$$

The LSV data for **3** and **4** at sweep rates of 500, 600, 700, 800, 900, and 1000 mV/s were subjected to convolution analysis and examples of the resultant convoluted voltammograms are

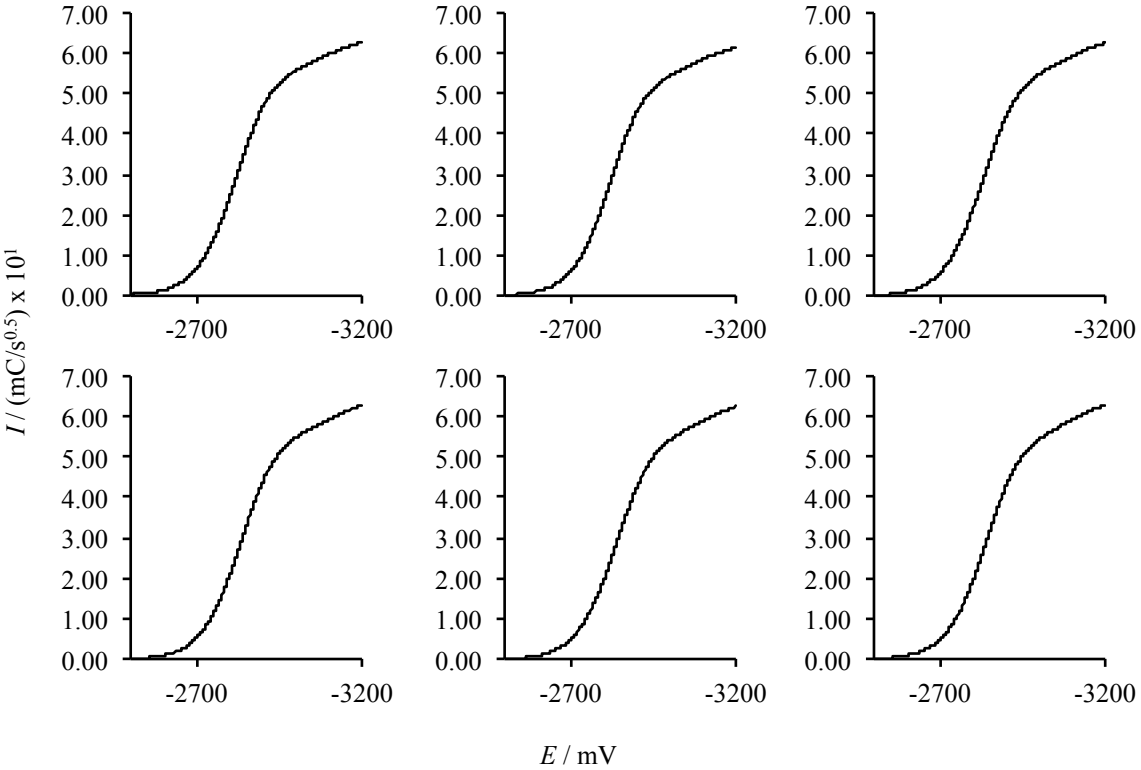

Figure 2.9: Convolution voltammograms of **3** in DMF. $\boldsymbol{C_3}$ = 0.0030 M, 0.5 M supporting electrolyte, ν = 500 (upper left), 600, 700, 800, 9000, and 1000 mV/s (lower right).

given in **Figure 2.9** for **3**. It should be noted that the convolutive current (*I(t)*) is independent of scan rate; therefore, voltammograms obtained at different scan rates only differ within experimental error and by a small change in the potential of the curve with increasing scan rate (analogous to the change in peak potential with increasing scan rate observed in LSV). Further analysis of these convolution voltammograms will be presented in **2.3.2.1**.

2.2.2 Indirect electrochemistry

The information obtained from simple cyclic and linear sweep voltammetry – particularly when there is no discernable reversibility in the voltammograms – is limited at best, and simply does not give enough information to "solve" the system, i.e. – to obtain the pertinent rate constants and reduction potentials of interest. Even in the best-case scenario, when the reaction is clearly under chemical step control, the equation (**Eq. 2.4**)[71] that describes the mechanism contains two unknowns: the reduction potential of the parent compound and the rate constant (k_{cs}) for the subsequent chemical step.

$$E_p = E^0_{A/A^{\cdot-}} - 0.78\frac{RT}{nF} + \frac{RT}{2nF}\ln\frac{k_{cs}RT}{\nu nF} \qquad \textbf{Eq. 2.4}$$

Armed with only this information, these important quantities cannot be resolved. It is often required that another experiment must be attempted to obtain one of these two unknowns independently. If, for example, the reduction potential of the parent compound were able to be determined from another experiment, then **Eq. 2.4** could be solved and the rate constant for the chemical step obtained. Indirect methods like homogeneous redox catalysis are therefore a valuable tool, often times yielding information that can be used concurrently with the data given by the direct electrochemical experiments to give a complete picture of the reaction of interest.

Indirect electrochemical methods remove the reduction or oxidation of the intended species from the electrode surface, and instead involve some means of producing these reactive intermediates in the solution phase. Homogeneous redox catalysis[75-80] (HRC) replaces the electrode as the source of electrons with a carrier molecule, the "mediator" (**M**, see **Scheme 2.5**), which shuttles electrons from the electrode into the solution before transferring the electron to the substrate of interest. The experiment works as follows: The mediator is reduced or oxidized at the electrode surface; from there it diffuses into the solution phase where it eventually encounters the species of interest. A homogenous electron transfer ensues, generating the reactive species of interest and catalytically regenerating the passive form of the mediator. Finally the substrate of interest undergoes further chemical reaction(s), for example bond-breaking or dimerization.

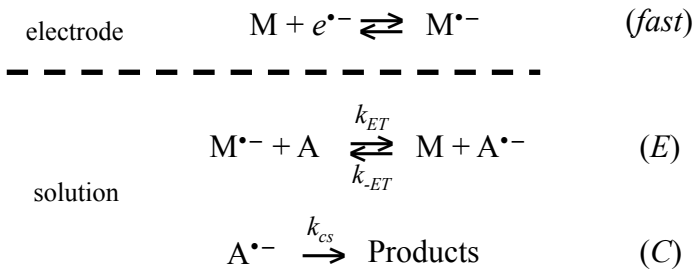

Scheme 2.5: EC mechanism in the case of homogeneous redox catalysis. **M** is chosen such that its heterogeneous kinetics are fast and play no role in the overall reaction kinetics.

In order for HRC to be successful, some requirements must be met:

- The mediator itself must exhibit Nernstian (reversible) behavior over the timeframe of the experiment, meaning that its heterogeneous electrode kinetics are extremely fast and play no role in the rate of the subsequent reactions and that there are no further reactions that the active form of the mediator would undergo in the absence of the substrate of interest. Fulfilling this requirement eliminates the further

complications that would ensue should the kinetics of the mechanism be muddled by a slow heterogeneous electron transfer or by competitive reactions in which the mediator would partake coincident with the reaction of interest. In this respect, the mediator must behave as an electrode proxy, and its own independent chemistry should not affect the reaction of interest.

- The mediator must be reduced (or oxidized) at a potential positive (or negative) to that of the substrate itself, that is, $E^0_{M/M^{\cdot -}} > E^0_{A/A^{\cdot -}}$. This requirement is obvious: if the mediator is reduced at potentials negative to that of the substrate, the substrate would be reduced at the electrode *first*, and therefore the substrate would not be available to react with the activated mediator, defeating the entire purpose of the experiment.
- The reduction potential of the mediator must be more negative than that of the overall reaction of interest, meaning $E^0_{A/Products} > E^0_{M/M^{\cdot -}}$. This is not so straightforward. The previous requirement means that the homogeneous electron transfer is by definition an unfavorable process. The equilibrium would favor the reactants of this step, and no or very little reaction would be observed. It is thus required that the subsequent chemical step be a favorable process to give the necessary driving force for the overall reaction to proceed. This requirement highlights why HRC is a good technique to monitor dissociative electron transfers: bond-breaking for these kinds of reactive intermediates is typically a thermodynamically favorable and irreversible process, and lends sufficient driving force to the overall reaction to make HRC a viable technique.

Cyclic voltammograms for the mediator in the absence of substrate are obtained over a series of sweep rates; this establishes the "baseline" behavior of the mediator in the absence of any

concurrent chemical reactions. The substrate of interest is then added to the solution (the substrate to mediator concentration ratio, γ, is known as the excess factor and defined as C_A^*/C_M^*, and typically ranges from 1 – 10.0 at the experimenter's discretion) and cyclic voltammograms at the same sweep rates are obtained.

At slower sweep rates, more time is allowed for the active form of the mediator to react with the substrate of interest. This electron transfer regenerates the passive form of the mediator. However, the mediator is by requirement Nernstian, which means that the concentration ratio at the electrode surface $C_M^0/C_{M^{\cdot-}}^0$ is not determined by the reactions that **M** undergoes but instead by the rigorously controlled potential of the electrode. When this concentration ratio is thrown off by the catalytic reaction the system attempts to "balance" itself by generating more of the activated mediator. This results in an increase in current relative to that obtained in the absence of substrate (**Figure 2.10**). This excess current is known as the catalytic current.

At faster sweep rates, there is less time allowed for the homogeneous electron transfer to take place, and thus there is a decrease in catalytic current, until the sweep rate reaches a large

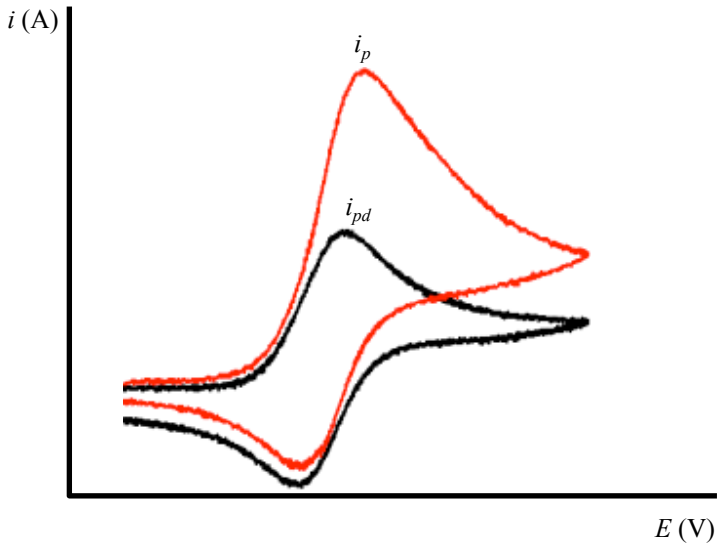

Figure 2.10: Homogeneous redox catalysis. Mediator in the presence (i_p) and absence (i_{pd}) of substrate.

enough value that there is no discernable difference between the voltammograms with and without the substrate present. The peak current in the presence of substrate (i_p) and in the absence of substrate (i_{pd}) is collected at each sweep rate. The ratio of the catalytic current to diffusion only current ($i_p/\gamma i_{pd}$) can then be used to determine the rate-limiting step of the reaction and sometimes the pertinent rate constants (*vide infra*).

Experimental results for **1** via mediated catalysis with azobenzene, 9-fluorenone, and 4-nitro-*o*-xylene respectively are given in **Figure 2.11**. The peak current ratio is plotted as a function of sweep rate, $i_p/\gamma i_{pd}$ versus log $(1/\nu)$ and log (C_M^*/ν). Plotting the data allows a quick determination on any mediator concentration dependency that might exist in the system. This is important as it allows the determination of the rate-limiting step for the reaction mechanism as described below.

Electrochemical experiments by their nature are more complicated than typical solution phase reactions. At their core, electrochemical experiments involve two phases: the electrode itself and the solution phase. Thus electrode material, size, and shape play a role in the experiments. Further complicating matters, the solution phase is not homogenous. Over the course of the experiment the concentration profile of the solution in the general vicinity of the electrode changes dramatically relative to the bulk solution, and these changes are in turn related to the chosen parameters of the experiment, namely the sweep rate and the initial and vertex potentials chosen. These concentration changes mean that diffusion plays a key role in the experiments, moving substrate from the bulk solution toward the electrode and electrode reaction products away from the electrode. Direct elucidation of pertinent constants becomes very difficult, even beyond the normal problems of comparing, for example, a first order rate constant to a second order rate constant.

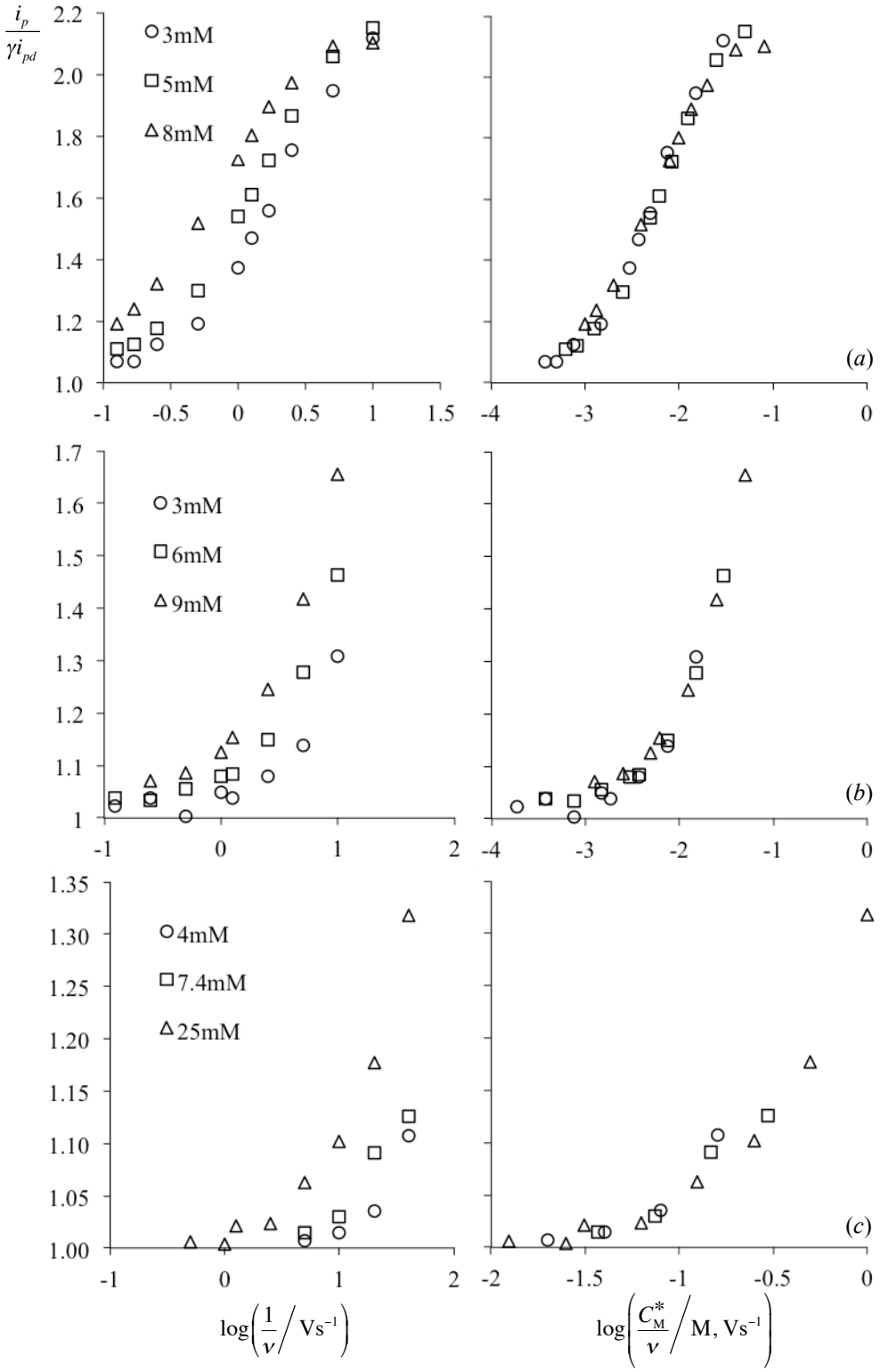

Figure 2.11: Variation of $i_p/\gamma i_{pd}$ as a function of sweep rate and mediator concentration for **1** clearly demonstrating electron transfer control in each case. (*a*) azobenzene, (*b*) 9-fluorenone, (*c*) 4-nitro-*o*-xylene.

These complications are accounted for by changing the important parameters into dimensionless quantities, removing the complicating factors of concentration, time, electrode area, and so forth. This is accomplished by multiplying the rate constants of interest by the appropriate constants, concentrations, and experimental parameters in order to obtain a dimensionless quantity. **Scheme 2.5** gives the typical *EC* mechanism for an HRC experiment. The dimensionless form of the pertinent rate constants are given as follows:[80]

$$\lambda_{ET} = \left(\frac{RT}{nF}\right)\left(k_{ET}\frac{C_M^*}{\nu}\right)$$

$$\lambda_{-ET} = \left(\frac{RT}{nF}\right)\left(k_{-ET}\frac{C_M^*}{\nu}\right)$$

$$\lambda_{cs} = \left(\frac{RT}{nF}\right)\left(k_{cs}\frac{1}{\nu}\right)$$

The measurable quantity $i_p/\gamma i_{pd}$ is a function of these dimensionless rate constants as long as γ is held constant for all experiments. It is important to note that *for a given mechanism* the dimensionless response of any system is exact, regardless of the specific rate constants and experimental parameters of that system. This fact is what allows the determination of the rate constants from the experimental data.

Should the chemical step (*C*, **Scheme 2.5**) be rate limiting, the homogeneous electron transfer is an equilibrium process and the concentration of the mediator plays no role. The rate is controlled by the composite dimensionless rate constant $\frac{\lambda_{et}}{\lambda_{-et}}\lambda_{cs}$. Substitution of the above equations into this dimensionless constant yields $\frac{k_{et}}{k_{-et}}\left(\frac{RT}{nF}\right)\left(k_{cs}\frac{1}{\nu}\right) = K_{et}\left(\frac{RT}{nF}\right)\left(k_{cs}\frac{1}{\nu}\right)$. The mediator concentration is thus removed. If there were no concentration dependency on the mediator, then there would be no difference in the data obtained for experiments of different mediator concentrations, and the peak current versus log ($1/\nu$) plot would "converge", that is, the

data would be one continuous set of data. If, however, the electron transfer (*E*) is rate limiting, the rate is controlled by $\lambda_{et} = \left(\frac{RT}{nF}\right)\left(k_{et}\frac{C_M^*}{\nu}\right)$, which is mediator-concentration dependent and the peak current versus log (C_M^*/ν) plot would "converge". Generating these two plots (**Figure 2.11a** as an example) from the data allows easy determination of the rate-limiting step for this reaction. From **Figure 2.11** it is obvious that electron transfer is rate limiting for each of the mediators used in these experiments. It should be noted that just as in LSV if the rate-limiting step is electron transfer, the identity and the rate constants for any following chemical steps cannot be obtained from this data.

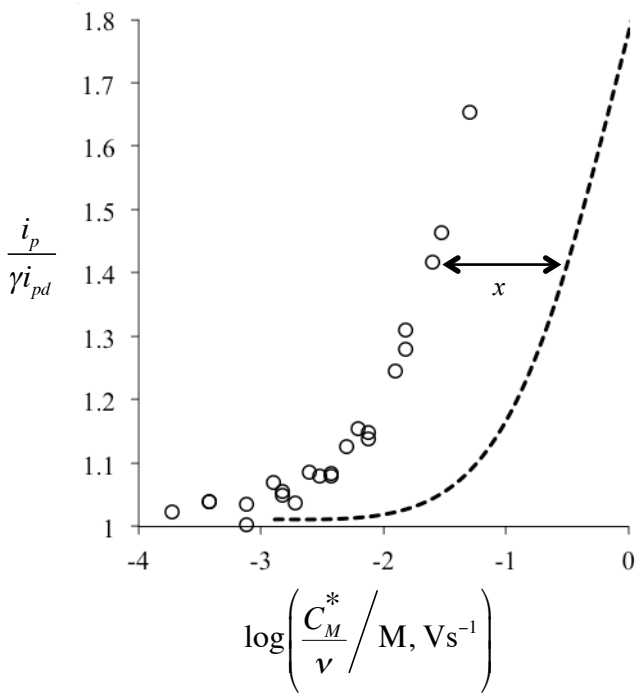

Figure 2.12: Demonstration of fitting HRC data for **1** (mediated by 9-fluorenone) to working curves. (– – –, simulated working curve; o, experimental data, $x = \log [(RT/nF)*k_{ET}]$).

Further analysis of this data is obtained by fitting to "working curves",[80] which are obtained via digital simulation. Again, *for a given mechanism*, the dimensionless response of any system will be identical. Plots of peak current ratio versus log (λ_{et}) for any system following a

given mechanism are the same, and theoretical working curves can be obtained for that mechanism which model these results. Note that $\log(\lambda_{et}) = \log\left\{\left(\frac{RT}{nF}\right)\left(k_{et}\frac{C_M^*}{\nu}\right)\right\} = \log\left(\frac{RT}{nF}k_{et}\right) + \log\left(\frac{C_M^*}{\nu}\right)$. Therefore, a plot of $i_p/\gamma i_{pd}$ versus $\log\left(\frac{C_M^*}{\nu}\right)$ will be offset from the theoretical working curves by a value equal to $\log\left(\frac{RT}{nF}k_{et}\right)$, and k_{et} can be determined. **Figure 2.12** shows how this can be accomplished. In practice, the data for each of the mediators was fit against a library of working curves corresponding to a range of possible mechanisms using TableCurve 2D,[81] yielding the homogeneous electron transfer rate constants summarized in **Table 2.4**. Plots of all fit data are available in **Chapter 5.1.1** and **5.1.2**.

Table 2.4
Homogeneous electron transfer rate constants for HRC experiments of **1** and **2**. Values in parenthesis indicate standard error.

Mediator	log k_{et}[a]	
	1	**2**
1,4-diacetylbenzene	-	5.23(0.07)
azobenzene	3.682(0.016)	2.746(0.020)
9-fluorenone	2.705(0.012)	1.80(0.03)
4-nitro-*o*-xylene	1.174(0.018)	-

(*a*) k_{et} in units of M^{-1} s^{-1}

Experimental results for **2** via mediated catalysis with 1,4-diacetylbenzene, azobenzene, and 9-fluorenone respectively are given in **Figure 2.13**. Again, each of these mediators shows electron transfer control of the reaction rate. These data were treated identically as those just described for **1**, and the resultant rate constants are included in **Table 2.4.**

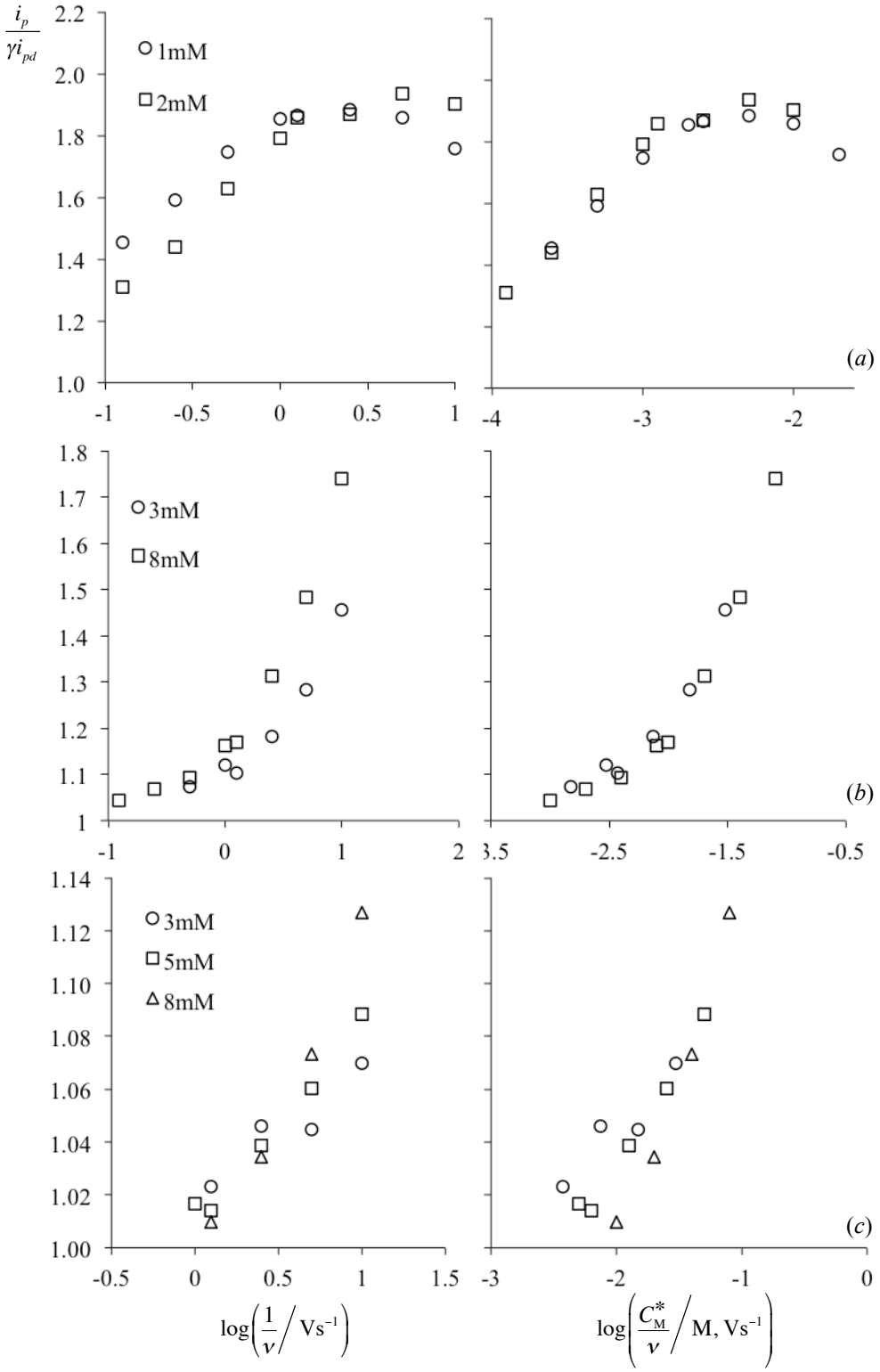

Figure 2.13: Variation of $i_p/\gamma i_{pd}$ as a function of sweep rate and mediator concentration for **2** demonstrating electron transfer control in each case. (*a*) 1,4-diacetylbenzene, (*b*) azobenzene, (*c*) 9-fluorenone.

In summary, HRC of **1** and **2** resulted in both cases with electron transfer control – the homogeneous electron transfer from the mediator to the substrate limits the rate. Thus no information for the subsequent chemical step (cleavage of the C—O or C—C bond) can be obtained directly from the HRC experiments. Further analysis of the data will be discussed in **2.3.1.1**.

2.2.3 Preparative electrolysis

Linear sweep voltammetry, cyclic voltammetry, homogeneous redox catalysis and the like are considered non-destructive techniques. That is to say that there is so little turnover of reactant to product in each experiment that no measurable amount of products relative to the bulk concentration of reactants is produced and can therefore not be identified post-experiment. Conversely, preparative electrolysis is a destructive technique where a significant number of electrons are passed from the electrode into the solution, generating copious amounts of product. Although typically cell conditions in a preparative electrolysis are chosen to as closely match those of the quantitative experiments as possible, in practice conditions during preparative electrolysis are usually much more harsh than those in a typical quantitative experiment, as will be explained shortly.

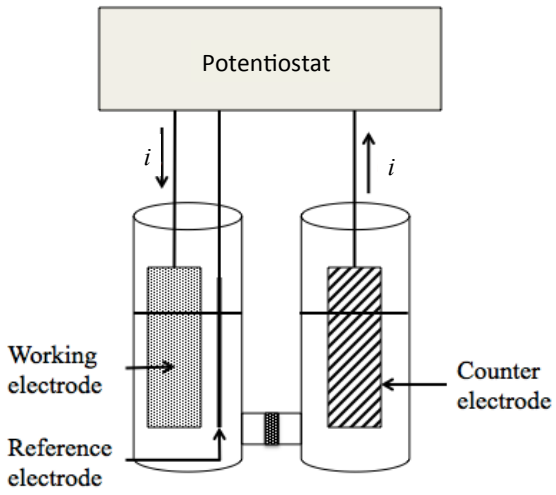

Figure 2.14: Diagram of a typical bulk electrolysis cell.

A typical preparative electrolysis cell is shown in **Figure 2.14**. Preparative electrolysis is generally conducted in one of two ways: constant potential electrolysis (where the working electrode is held at a potential where the substrate of interest is reduced over the course of a predetermined timeframe) and constant current electrolysis (where a constant current is passed for a set length of time). Although the two techniques sound similar, they behave fundamentally different in practice.

Constant potential electrolysis is the "softer" of the two techniques. This arises from the electrode not being forced to pass electrons, only to maintain a set potential for the duration of the electrolysis. For well-behaved systems this works phenomenally well. Unfortunately, generating a solution filled with radical anions typically does not result in a well-behaved system. Particularly of nuisance is fouling of the electrode surface. This can lead to inactivation of the electrode because the electrode is "coated" with insulating material, which prematurely ends the electrolysis as reduction at the electrode surface ceases.

Conversely, constant current electrolysis is a much harsher technique that has the advantage of overcoming electrode fouling to an extent. In a constant current electrolysis the

instrument applies whatever potential is necessary (within the limits of the instrument's power supply) to maintain the set current through the cell. Although this overcomes the electrode-fouling problem, further problems arise because the electrode potential can typically increase to the point where many electrode reactions that are not of interest can begin to occur, such as reduction of the supporting electrolyte or solvent and/or further reduction of product species. Products generated from these side reactions are often very reactive themselves and may interact with the intended reactant in unwanted ways. However, for systems where electrode fouling is a problem constant current electrolysis is often the only viable technique to attempt to identify reaction products.

Furthermore, both techniques suffer from long timeframes. Quantitative experiments (like a cyclic voltammetry experiment) last from tens of seconds to fractions of a second. Preparative electrolysis lasts thousands of seconds. Because the timeframe of the experiments is much longer, slow reactions that are not observed on the quantitative timeframe become important on the preparative scale and can have a major impact on the types of products observed in the electrolysis. Nevertheless, bulk electrolysis is one of the few ways to produce identifiable products from electrode reactions.

Each of compounds **1 – 4** were subjected to constant current preparative electrolysis. In spite of its harsher nature, constant current electrolysis was necessary, because of copious electrode fouling, to generate enough products for identification. In order to attempt to make the electrolysis as benign as possible, only ½ equivalent of electrons was passed in each case. Analysis of the product mixture was made via gas chromatography with flame ionization detection as well as gas chromatography with a mass spectrometer as the detector.

Workup of the product solutions was problematic. In order to as closely emulate conditions in the quantitative experiments as possible the solvent/supporting electrolyte combination in each case was chosen to be *N*,*N*-dimethylformamide (DMF) and tetrabutylammonium perchlorate (TBAP), the same as was used in the quantitative experiments. In the case of the bulk electrolysis a lower concentration of electrolyte was used to attempt to make product extraction easier. Removal of TBAP is difficult and tedious as it is insoluble in water, thus making a typical liquid-liquid extraction unfeasible. Instead, a series of liquid-liquid extractions and back extractions (as described in **Chapter 4**) were necessary to remove the electrolyte. Unfortunately this series of back extractions led to loss of some product, as evidenced by the changing of peak ratios in the gas chromatograms before and after the workup.

Chlorobenzene was added quantitatively to each solution upon completion of electrolysis to act as an internal standard in gas chromatography, and each solution was then immediately quenched with a drop of saturated ammonium chloride, which resulted in a fast color change from a dark purple to a pale yellow. A small sample was immediately analyzed by gas chromatography. This was necessary (although usually unadvisable as the initial product solution contained large quantities of TBAP and was solvated in DMF, each of which are not good for column health) in order to obtain correct peak areas for products in the chromatogram.

Each of the chromatograms obtained after the series of liquid-liquid extractions to remove the supporting electrolyte and DMF from the products were obviously different than those obtained before the extraction workup, with many of the post-electrolysis products entirely gone and the ratios of peak areas for others altered significantly. Although dramatically changing the product compositions of the electrolysis, the back extractions were necessary in order to obtain a “clean” enough solution for analysis via GC/MS, which then could be used for product

identification but, unfortunately, not for quantifying product yields. The latter could only be attempted with the chromatograms obtained directly after quenching of the product solution before the series of liquid-liquid extractions.

In general the preparative electrolysis of **1-4** was untidy, yielding many products in each case. Product species that had the same retention time under the same GC conditions in all 4 cases were assumed to be products of reduction of TBAP at the electrode surface or reaction of TBAP with the products of the desired reaction and were ignored. In most of these cases these peaks disappeared after the extraction workup and were unable to be analyzed via GC/MS. Products that were present both before and after the extraction workup were identified with a combination of GC/MS and verification with authentic samples when possible. When the electrolysis experiments were repeated, the products obtained from one experiment to the next were the same (as determined by GC retention time), but were never obtained in exactly the same product ratios.

Table 2.5
Products arising from the preparative reductions of epoxides **1** – **4**.

	Initial[a]	Recovered[b]	Electrons passed[c]	Ketone[d]	Aldehyde[d]	Aldol[e]	Aldol condensate[e]
1	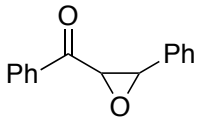			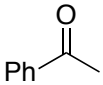		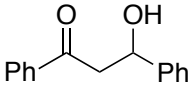	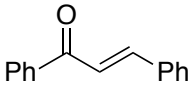
	0.30	0.05	0.15	0.02	0.07	observed	not observed
2	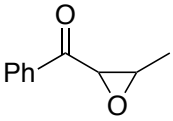			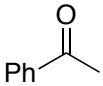		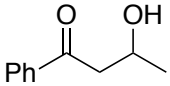	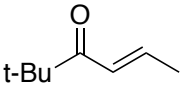
	0.30	0.02	0.15	0.02	not observed[f]	not observed	not observed
3	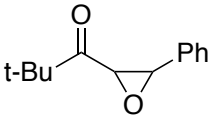			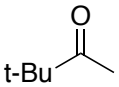		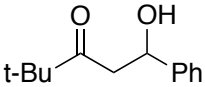	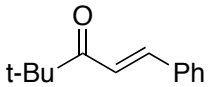
	0.30	0.22	0.15	observed[g]	0.07	not observed	not observed
4	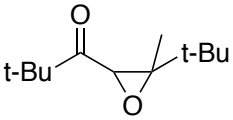			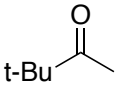	NA	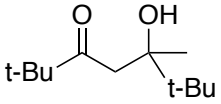	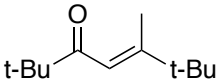
	0.40	0.21	0.19	observed[g]		not observed	not observed

All numbers reported are millimoles. (*a*) Obtained from solution preparation (*b*) Obtained via internal standard (see text) (*c*) Obtained from potentiostat (*d*) Retro-aldol addition products, obtained via internal standard (see text) (*e*) The aldol alcohol was identified via mass spectrometry where indicated; however, it was not verified via authentic samples or quantified via the internal standard (*f*) Eluted with solvent (*g*) Identified with authentic samples but unable to be quantified (see text).

The main products identified for electrolysis of **1-4** were those that could be obtained from retro-aldol condensation of the alcohol that would results from ring opening of the parent alcohol, and are given in **Table 2.5**. Mass balance was not good, as far less of the starting material was recovered than would be expected based on the number of equivalents of electrons (0.5 eq.) used for the electrolysis, although the amount of retro-aldol condensation products are reasonable as will be discussed in **2.3.3**.

2.2.4 Computational results

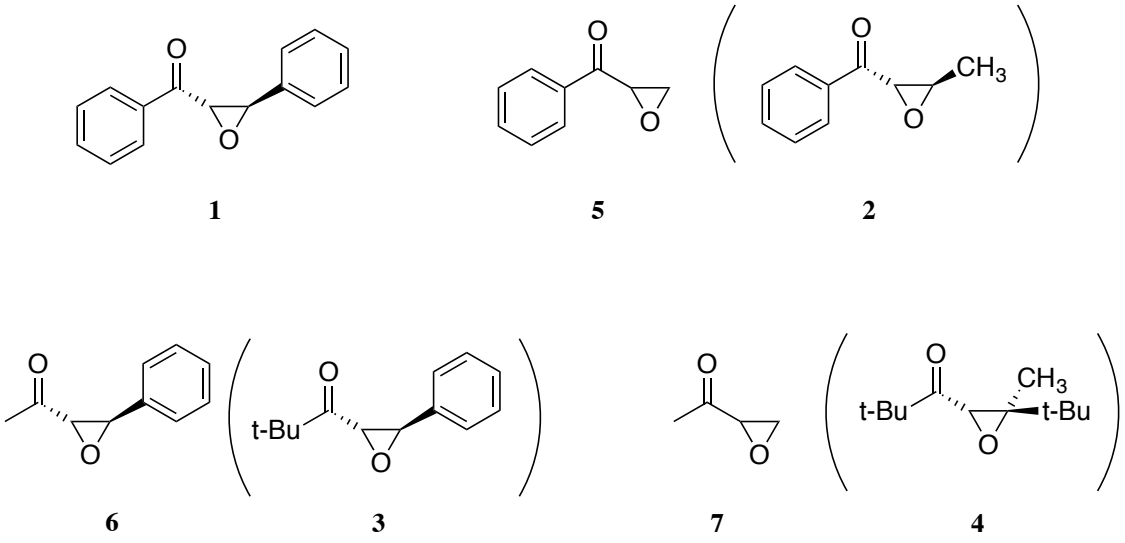

1 **5** **2**

6 **3** **7** **4**

Chart 2.2

The structures given **Chart 2.2**, where analogues used in electrochemical experiments are given in parenthesis, have been chosen as computational models. These structures were chosen to be electronically similar to the compounds examined electrochemically in this work, but to reduce computation time as much as possible. The majority of the computational work presented herein was performed with the Gaussian 09[82] computational package utilizing the density functional theory, specifically the B3-LYP[83] and BHandH-LYP[84] correlation-exchange functionals. These methods were chosen both because they are relatively inexpensive as well as because they have been successfully used to describe radical and radical ion reactivity in the past.[85] For closed shell species the restricted methods were used; to avoid issues of spin contamination in the case of open shell species the restricted open shell methods were used. In all cases a Pople type 6-31+G* basis set was used. In most cases the computations were also performed using a PCM solvent model to simulate the solvent effects of the electrochemical cell. In some cases where more accurate energies were required, single point energies were computed

using the coupled-cluster CCSD[86-89] method with the 6-31+G* basis set. Please see **Chapter 4** for a more detailed description of the computational procedures.

2.2.4.1 Aromatic radical anions

1 and **5** were optimized using the DFT methods described previously; the resultant geometries were then optimized as radical anions using the described method to verify the "existence" of the ring closed radical anion. In both cases computations yielded a ring-closed minimum, indicating that these ring-closed radical anions do exist at a potential energy minimum in keeping with the electrochemical experiments. Frequency calculations on each of the optimized radical anion structures confirmed their existence.

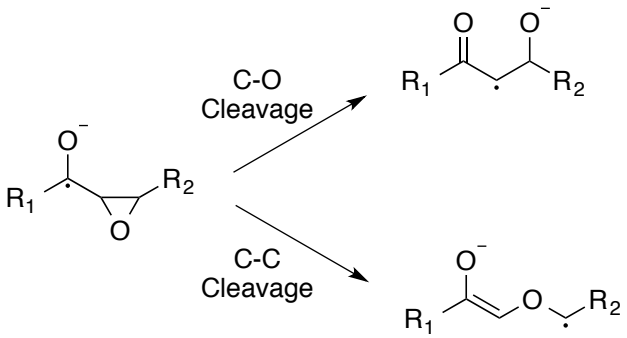

Scheme 2.3: Possible cleavage pathways for ring opening of α-epoxyketones.

It is possible for the ketyl radical anions discussed here to undergo fragmentation via two possible pathways: C—C bond cleavage and C—O bond cleavage (**Scheme 2.3)**. C—O cleavage leads to a product that would likely isolate negative charge on the electronegative oxygen atom and would allow some resonance stabilization of the unpaired spin by the carbonyl structure. This would come at the cost of any major resonance contribution of either R group shown in **Scheme 2.3**. In contrast, C—C cleavage would lead to a product where spin may be resonance

stabilized by R_2. In the case of cyclopropylketones this resonance stabilization had a major effect on the rate of ring opening.

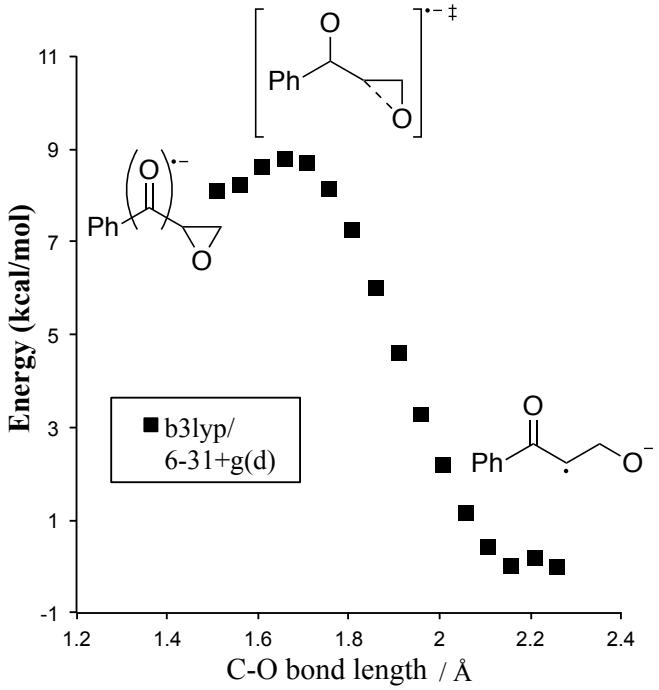

Figure 2.15: C—O ring-opening profile of **5** showing ring closed radical anion, transition state structure, and ring-opened radical anion. The geometry corresponding to the highest point on this potential energy surface was used as a starting point for a transition state optimization. Activation energies were taken to be the difference in electronic energy between the optimized transition state structure and the parent radical anion. Ring-opening profiles for **1** and with the BHandH-LYP theory are similar.

In order to study this dichotomy, the optimized radical anion structures were used as starting points for energy profile computations of the bond-breaking processes (as an example, **Figure 2.15**). In each case the bond in question was stretched at 0.05 Å increments from its optimized bond length to a length approximately 1 Å larger. The resulting structure was then itself optimized with no constraints; this structure was taken as the ring-opened distonic radical anion. The structure in the energy profile that gave the largest energy was then used as a base structure in an attempt to computationally obtain the transition state structure of the bond breaking process. The difference in electronic energy between the optimized transition state

structure and the parent radical anion (both corrected for zero-point vibrations) was taken to be approximately the activation barrier for ring opening. In this way energetics of the ring opening processes could be obtained and compared. The results are summarized in **Table 2.6**.

Table 2.6
Difference in electronic energies at 0 K[a] between the optimized transition states for C—C and C—O bond cleavage and their ring-closed radical parents.

	C—C cleavage		C—O cleavage	
	B3LYP	BHandHLYP	B3LYP	BHandHLYP
	CCSD[b]	**CCSD**	**CCSD**	**CCSD**
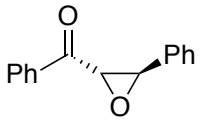	11.6[c] **18.4**	15.1 **18.3**	1.0 **2.4**	3.3 **2.3**
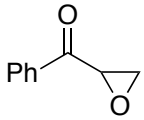	22.8 **25.4**	24.6 **25.7**	0.7 **2.3**	3.1 **2.3**

All calculations performed with the 6-31+G* basis set (*a*) All electronic energies are corrected for zero-point vibrations by factors obtained from frequency calculations using the indicated DFT theory. The same correction factors were used for the CCSD single point energies. (*b*) Obtained from single point CCSD simulations performed on the optimized geometries generated by the respective DFT method. (*c*) kcal/mol

2.2.4.2 Aliphatic radical anions

As with the aromatic ketones, **6** and **7** were optimized and the resultant structures were again subjected to optimization as radical anions with the described methods. The most obvious feature of the computations is the lack of existence of a discrete ring-closed radical anion intermediate. In contrast to the aromatic radical anions, where definite ring-closed structures were observed computationally, the aliphatic anions fell apart into a distontic, ring-opened radical anion. Importantly, in every case it was the C—O bond that was cleaved in the optimization process.

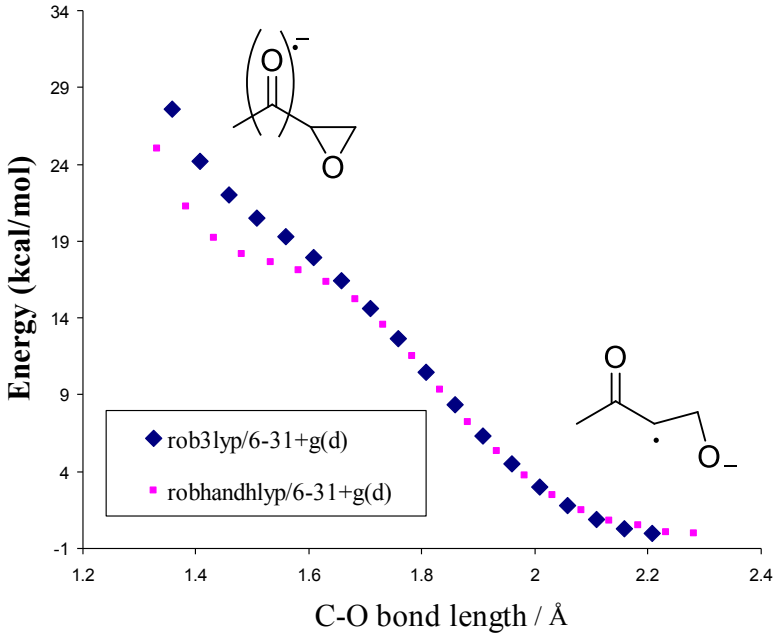

Figure 2.16: Attempted ring-closing profile of **7** showing that no stable ring closed radical anion exists at these levels of theory and basis sets. Similar attempts yielded like results for **6**.

To verify that the radical anion parent does not exist as a discrete intermediate, C—O ring closing profiles were generated by using the optimized, ring-opened structure as a starting point and systematically shortening the C—O bond length by 0.05 Å until the interatomic distance was much shorter that a typical bond length (**Figure 2.16**). The resulting energy profile was then examined in an attempt to find anything that resembled a stable, ring-closed intermediate. In all cases no such intermediate was seen, and it was determined computationally that the ring-closed radical anion does not exist as a discreet, stable structure.

2.3 Discussion

2.3.1 Aromatic radical anions

The previous section covered the results of the analytical electrochemical experiments (LSV and HRC), the products obtained from preparative electrolysis, and the results of computations of these epoxyketones. When used conjunctively, these data can give a better idea

as to the overall reaction mechanisms and the pertinent physical constants for each of the substrates of interest, as well as paint a clear picture on how these reactions fit into the theoretical models for dissociative electron transfers.

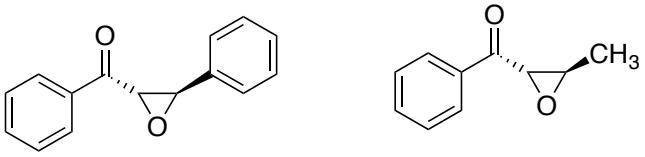

1 **2**

Chart 2.3

The LSV data for **1** and **2** (**Chart 2.3**) indicate a change in rate-limiting step from the chemical step to the heterogeneous electron transfer. This is particularly illustrated by the peak width data, which moves from a value indicating chemical step control (~65 mV) to one that indicates electron transfer control (~90 mV, see **Figure 2.3** and **Figure 2.4**) with increasing sweep rate. This is indicative of mixed kinetic control, where the system is moving from the rate being determined by the chemical step at slow sweep rates to the rate being under electron transfer control at faster sweep rates. This phenomenon arises from the heterogeneous kinetics: at slow sweep rates enough time is allowed for the heterogeneous electron transfer reaction to "catch up" with the changing potential of the electrode, and the chemical step is rate limiting. At faster sweep rates, less time is allowed for the electrode reaction to occur, the peak potentials are shifted negatively, the back-electron transfer becomes much slower, and the electron transfer step becomes rate limiting.

Savéant has published[90] an analysis for this mixed kinetic control case, and by fitting the LSV data to his published working curves one can elucidate an equation which contains two unknowns: the reduction potential of the substrate of interest and the rate constant for the consequent chemical reaction. The treatment involves fitting the peak width data and the

variation of peak potential to these working curves to obtain the parameters C_1 and C_2. (note: here C_1 and C_2 are not concentrations; they are experimentally determined reaction parameters)

$$C_1 = \log\left(\frac{nF}{2RT}\frac{k_{cs}{D_A}^2}{{k_{het}}^4}\right)$$

$$C_2 = E^0_{A/A^{\cdot-}} + \left(\frac{RT}{nF}\ln 10\right)\log\left(\frac{k_{cs}D_A}{{k_{het}}^2}\right)$$

Working curves are shown in **Figure 2.17**, and the data is fit first by plotting peak width versus log ν to find C_1 and then plotting E_p versus log $\nu + C_1$ to obtain C_2. These two equations are then combined, yielding **Eq. 2.5**, which only contains two unknowns: the reduction potential of **A**, $E^0_{A/A^{\cdot-}}$, and the rate constant for the chemical step, k_{cs}.

$$E^0_{A/A^{\cdot-}} + \left(\frac{RT}{2nF}\ln 10\right)\log k_{cs} = C_2 - \left(\frac{RT}{2nF}\ln 10\right)\left[C_1 - \log\left(\frac{nF}{2RT}\right)\right] \qquad \textbf{Eq. 2.5}$$

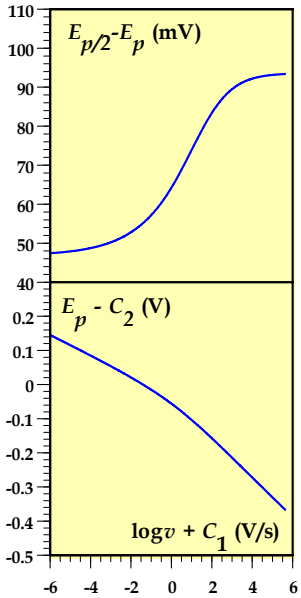

Figure 2.17: Working curves to determine C_1 and C_2 for LSV in the mixed kinetic control case. Reprinted with permission from reference 90. Copyright 1997 American Chemical Society.

The LSV data of **1** and **2** was subjected to this treatment, and the pertinent values obtained for each of these species is summarized in **Table 2.7** on page 80.

As noted previously, very often direct methods in and of themselves cannot give enough information to completely determine the variables of interest for the reaction, in this case the rate constant for ring opening of the epoxide and the reduction potential of the parent ketone. Either the rate constant of the chemical step or the reduction potential of the substrate must be determined via some other method to "solve" the system, or a second equation containing these two unknowns must be obtained.

As presented earlier, the HRC experiments provide the rate constants for electron transfer from the mediator to the substrate, as well as the mediator reduction potentials. Because the rate-limiting step was determined to be electron transfer in these reactions, there is no information to be gained from the data regarding the rate constant for ring opening of the epoxide. However, from this data it is possible to construct a Marcus plot, which relates the driving force of the electron transfer reaction to the rate constant of said reaction, and from this plot it is possible to determine the reduction potential of the substrate.

$$\mathrm{D} + \mathrm{A} \underset{k_d}{\overset{k_d}{\rightleftarrows}} (\mathrm{D}//\mathrm{A}) \qquad (1)$$

$$(\mathrm{D}//\mathrm{A}) \underset{k_{-ET}}{\overset{k_{ET}}{\rightleftarrows}} (\mathrm{D}^{\bullet+}//\mathrm{A}^{\bullet-}) \qquad (2)$$

$$(\mathrm{D}^{\bullet+}//\mathrm{A}^{\bullet-}) \underset{k_d}{\overset{k_d}{\rightleftarrows}} \mathrm{D}^{\bullet+} + \mathrm{A}^{\bullet-} \qquad (3)$$

$$\mathrm{A}^{\bullet-} \xrightarrow{k_{cs}} \text{Products} \qquad (4)$$

Scheme 2.6: Elementary steps of a homogeneous electron transfer reaction followed by an irreversible chemical step, such as bond breaking.

A Marcus plot is developed based on the elementary steps of an electron transfer process. Although often referred to as a single step, there are actually three individual steps in a homogeneous electron transfer, any one of which could be the rate-limiting step (**Scheme 2.6**). The donor and acceptor species must first diffuse together (*1*), whereupon the electron transfer occurs (*2*), followed by the two products diffusing apart, often called counter-diffusion (*3*). For the case where this electron transfer is followed by a fast chemical step, a treatment of the overall kinetics of the mechanism(s) has been described. For the simplest case, where the chemical step occurs after counter-diffusion of the electron transfer products, **Eq. 2.6**[91] can be used to describe the overall kinetics of the electron transfer process: k_D is the diffusion limited rate constant, k_{ET}^S is the electron transfer rate constant for a reaction at zero driving force, α is the transfer coefficient, and all other values have their usual meaning.

$$\frac{1}{k_{obs}} = \frac{1}{k_D} + \frac{1}{k_{ET}^S \exp\{(-\alpha nF/RT)(E^0_{M/M^{\cdot-}} - E^0_{A/A^{\cdot-}})\}} + \frac{1}{k_D \exp\{(-nF/RT)(E^0_{M/M^{\cdot-}} - E^0_{A/A^{\cdot-}})\}} \qquad \textbf{Eq. 2.6}$$

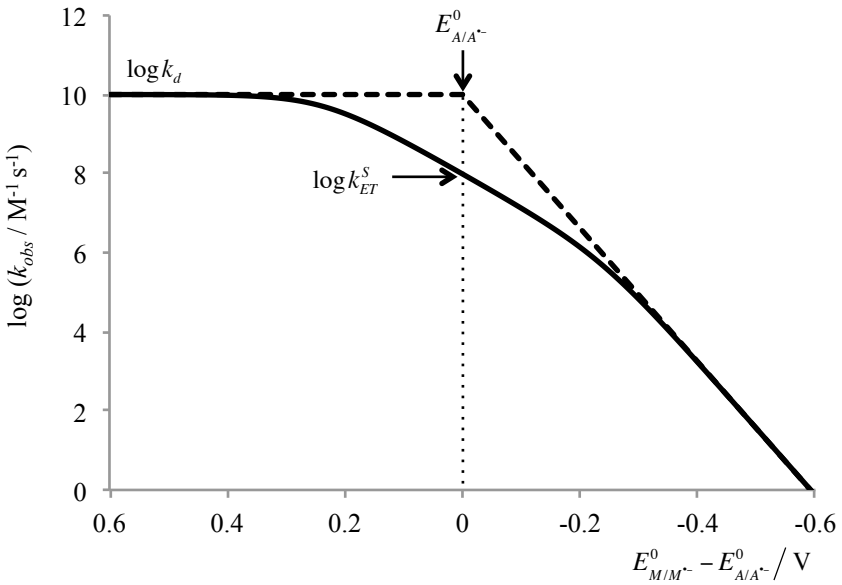

Figure 2.18: Theoretical Marcus plot demonstrating how to obtain $E^0_{A/A^{\bullet-}}$ from the HRC data. Adapted from reference 91.

Figure 2.18 is an example Marcus plot of this equation. Note that there are three distinct regions in this equation: diffusion control, where the rate is limited only by diffusion of the donor and acceptor together; activation control, where the rate is limited by the electron transfer itself, and counter-diffusion control, where the rate is limited by counter-diffusion of species in the product cage. When $E^0_{M/M^{\bullet-}} \gg E^0_{A/A^{\bullet-}}$ the forward-electron transfer rate constant k_{ET} is small, and conversely, the back-electron transfer rate constant k_{-ET} is large. Therefore, the rate is determined by counter-diffusion of the product species apart. When $E^0_{M/M^{\bullet-}} \approx E^0_{A/A^{\bullet-}}$, forward-electron transfer is faster, and thus back-electron transfer slower, leading to activation control. In the final case, $E^0_{M/M^{\bullet-}} \ll E^0_{A/A^{\bullet-}}$, forward-electron transfer is very fast, back-electron transfer very slow, and the rate is limited only by diffusion of the donor and acceptor species together. Reaction coordinate diagrams giving examples of each of these possibilities are given in **Figure 2.19**.

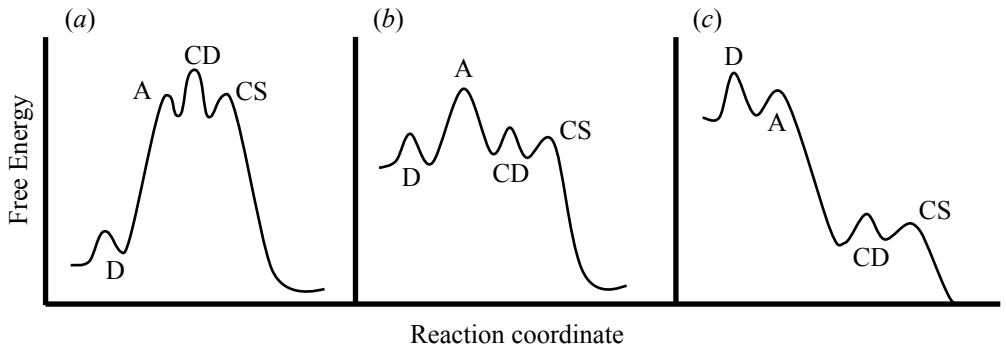

Figure 2.19: Example homogeneous electron transfer reaction coordinate diagrams demonstrating (*a*) counter-diffusion control (CD), (*b*) activation control (A), and (*c*) diffusion control (D) as the rate limiting step in the overall electron transfer process. The chemical step (CS) is also demonstrated as a "fast" follow-up mechanistic step.

In HRC experiments, of necessity $E^0_{M/M^{\bullet-}} > E^0_{A/A^{\bullet-}}$, and thus the data obtained from the experiments are expected to fall in the activation or counter-diffusion regions of the graph. For data falling clearly under counter-diffusion control, the diffusion and activation terms in **Eq. 2.6** are insignificant and can be ignored, giving:

$$\frac{1}{k_{obs}} = \frac{1}{k_D \exp\{(nF/RT)(E^0_{A/A^{\cdot-}} - E^0_{M/M^{\cdot-}})\}}$$

Inverting and taking the log:

$$\log k_{obs} = \log k_D + \log[\exp\{(nF/RT)(E^0_{A/A^{\cdot-}} - E^0_{M/M^{\cdot-}})\}]$$

And then linearizing to give:

$$\log k_{obs} = \log k_D + \frac{nF}{2.303RT}(E^0_{A/A^{\cdot-}} - E^0_{M/M^{\cdot-}}) = \log k_D - 17.08\ \mathrm{V}^{-1}(E^0_{M/M^{\cdot-}})$$

Similarly, in the activation controlled portion the diffusion and counter-diffusion terms can be ignored, and following the same treatment yields:

$$\log k_{obs} = \log k^S_{ET} + \frac{\alpha nF}{2.303RT}(E^0_{A/A^{\cdot-}} - E^0_{M/M^{\cdot-}}) = \log k^S_{ET} - 8.54\ \mathrm{V}^{-1}(E^0_{M/M^{\cdot-}})$$

Therefore a plot of $E^0_{M/M^{\cdot-}}$ versus log k_{obs} can be made and the slope analyzed to determine which region (activation or counter-diffusion) the data fits.

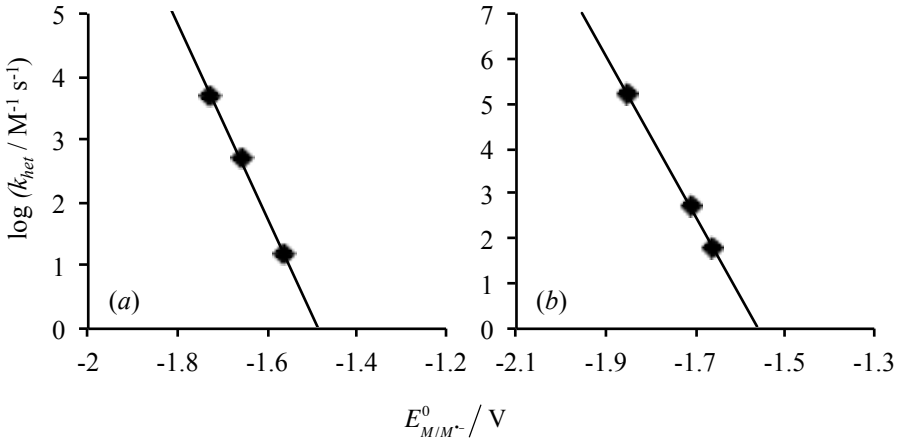

Figure 2.20: Marcus plots for **1** (*a*) and **2** (*b*).

Marcus plots for **1** and **2** derived from the HRC data are given in **Figure 2.20**. Each of the points on both graphs appear to fall in the "counter-diffusion" control regime, as indicated by slope values of -15.4 ± 0.5 V^{-1} and -17.8 ± 0.3 V^{-1} respectively. Theoretically, the slope can be projected back to the diffusion limited rate constant for the solvent used and the reduction potential of the substrate can thus be obtained. In practice, small errors in the slope in the region where the data is located project to large errors in the obtained $E^0_{A/A^{\cdot-}}$, and instead each mediator is independently analyzed using the theoretically correct slope (17.08 V^{-1}). The results are summarized in **Table 2.7**.

Table 2.7
Final analysis of quantitative electrochemistry of **1** and **2** including measured reduction potentials and ring-opening rate constants. Values in parenthesis indicate standard error.

	C_1 [a]	C_2 [a]	$E^0_{R/RX^{\cdot-}}$ [b]	k_{ro} [c]
1	1.38(0.07)	-1.8293(0.0011) V	-2.09(0.01) V	4(3) x 10^8 s^{-1}
2	1.14(0.05)	-1.9077(0.0013) V	-2.14(0.01) V	8(6) x 10^7 s^{-1}

(*a*) Obtained from fitting to published working curves (*b*) Obtained from HRC analysis (*c*) Obtained from application of Eq. 2.5

From this analysis the reduction potentials of **1** and **2** were found to be -2.09 ± 0.01 V and -2.14 ± 0.01 V respectively (vs. $Ag/AgNO_3$), and good agreement between the values

obtained for each mediator justifies the treatment of the data as if it were under purely counter-diffusion control.

It is now possible with the reduction potential of each compound determined from the HRC data to apply these results to that obtained from the mixed kinetic control analysis of the CV data and solve for the rate constant of the epoxide ring opening. It is thus determined that k_{ro} of **1** is (4 ± 3) x 10^8 s^{-1} and k_{ro} of **2** is (8 ± 6) x 10^7 s^{-1}. A summarization of these findings is presented in **Table 2.7**.

2.3.2 Aliphatic radical anions

The LSV data of the aliphatic radical anions (**Chart 2.4**) reveal two important clues to the reaction mechanism: 1) The rate is limited by the heterogeneous electron transfer reaction, and 2) the electrode reaction requires an unusually large overpotential to drive the chemistry forward. This second observation most often occurs because of an unusually large internal reorganization energy in the electron transfer process, and is often indicative of bond breaking occurring in the transition state – that is, a concerted dissociative electron transfer process. Direct elucidation of the reaction mechanism is difficult from the LSV data alone.

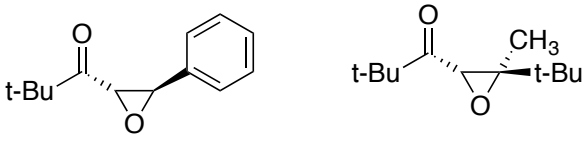

3 **4**

Chart 2.4

Convolution voltammetry is useful because it allows many more points of data from the voltammograms to be analyzed. The typical LSV voltammogram can only be analyzed at 2 points on the graph (the peak potential and the half-peak potential). Removing the mass transport

component of the voltammograms allows nearly every point on the graph to be analyzed, increasing the total number of meaningful data points by two to three orders of magnitude. The pertinent equations are as follows:[72-74]

$$I_{lim} = nFAD_A^{\frac{1}{2}}C_A^* \qquad \textbf{Eq. 2.3}$$

$$E_{applied} = E^0_{A/A^{\cdot-}} - \frac{RT}{\alpha nF}\ln\left(\frac{D_A^{\frac{1}{2}}}{k_{het}}\right) + \frac{RT}{\alpha nF}\ln\left(\frac{I_{lim} - I_t}{i_t}\right) \qquad \textbf{Eq. 2.7}$$

$$\ln k_{het} = \ln D_A^{\frac{1}{2}} - \ln\left(\frac{I_{lim} - I_t}{i_t}\right) \qquad \textbf{Eq. 2.8}$$

$$\alpha = \frac{\partial \Delta G^{\neq}}{d\Delta G^0} = -\left(\frac{RT}{nF}\right)\frac{\partial \ln k_{het}}{\partial E} = \frac{nF\left(E - E^0_{A/A^{\cdot-}}\right)}{2\lambda} + \frac{1}{2} \qquad \textbf{Eq. 2.9}$$

Eq. 2.3 defines the limiting current, and from it the diffusion coefficient, D_A can be obtained. **Eq. 2.7** is a linear relationship (assuming a constant value of α) describing the applied potential as a function of the *current function*, $\ln\left(\frac{I_{lim}-I_t}{i_t}\right)$. It is important to note that as I_t approaches I_{lim} and as i_t approaches 0 the current function is undefined, and at the extremes of the voltammogram results become too noisy for analysis. Typically, therefore, only the middle 60 – 80% of each convolution voltammogram is analyzed. **Eq. 2.8** relates the standard heterogeneous rate constant to the current function, and thus to the electrode potential. From this analysis then one is able to calculate the heterogeneous rate constant as a function of potential.

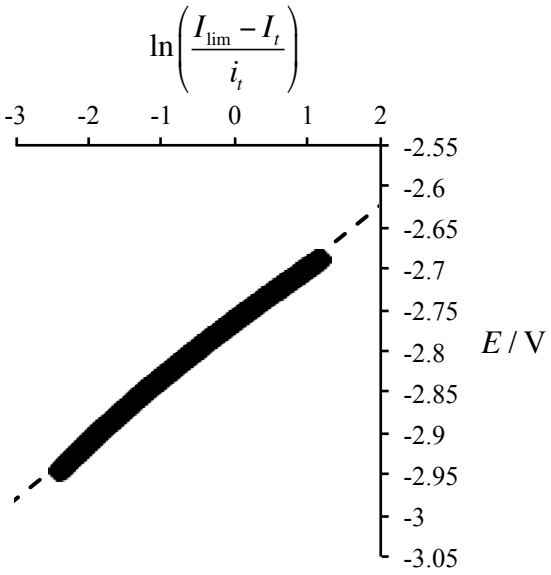

Figure 2.21: Current function vs. potential, demonstrating the non-linearity due to α not being constant. An average α is obtained from the slope via linear regression. **3**, ν = 500 mV/s, C_3 = 0.0030 M in DMF, 0.5 M supporting electrolyte (TBAP).

The assumption that **Eq. 2.7** is linear is based on a constant value of the transfer coefficient, α. In fact, α is not a constant and varies slightly as a function of electrode potential. A plot of the current function versus potential can be made, and the resultant data will typically have a gentle curve (see **Figure 2.21**). The slope obtained when treating this data as linear is equal to $\frac{RT}{\alpha nF}$, and an average value for the transfer coefficient may be obtained. However, it is much more useful to know the value of α as a function of potential: α at zero driving force (i.e.: $E - E^0_{A/A^{\bullet-}} = 0$) by definition is 0.5, and a plot of α versus E can be used to obtain $E^0_{A/A^{\bullet-}}$ via extrapolation to α = 0.5. Non-linear regression software such as TableCurve can be used to fit the ln k_{het} versus E data to a generic form of the Marcus equation, and the derivative of this fit gives α as a function of potential (**Eq. 2.9**, where α is the partial derivative of the activation free energy with respect to the driving force, i.e. – the derivative of the Marcus equation with respect to driving force).

Convolution voltammetry is thus a powerful tool allowing the elucidation of the reduction potential of the substrate, the standard heterogeneous electron transfer rate constant, α as a function of potential, and the value of the heterogeneous electron transfer rate constant as a function of potential, none of which is possible from typical analysis of LSV data.

The convolution voltammograms for **3** and **4** were subjected to this treatment, and the results are summarized in **Table 2.8** on page 90. **Figure 2.21** gives an example of fitting the voltammetric data to **6**; **Figure 2.22** gives an example of the ln k_{het} versus E data used to fit to the Marcus equation, and **Figure 2.23** gives the collected α versus E for each sweep rate, which demonstrates how the reduction potential of the species is determined. From this data the process of fitting these results to known theoretical models to better understand the chemistry at play in these reactions begins.

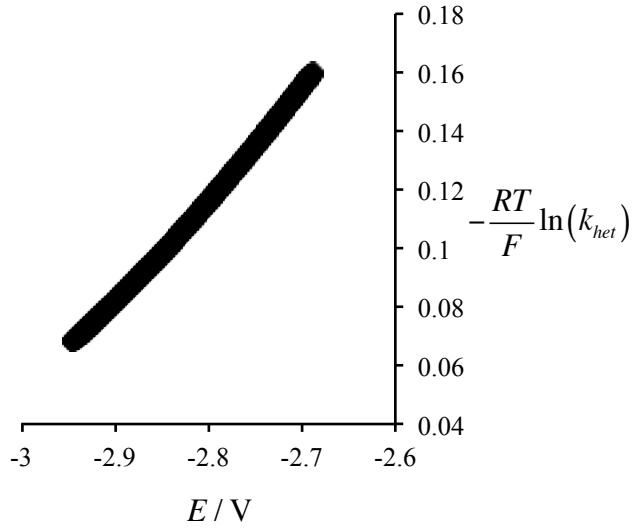

Figure 2.22: ln (k_{het}) as a function of potential. **3**, ν = 500 mV/s, C_3 = 0.0030 M in DMF, 0.5 M supporting electrolyte (TBAP).

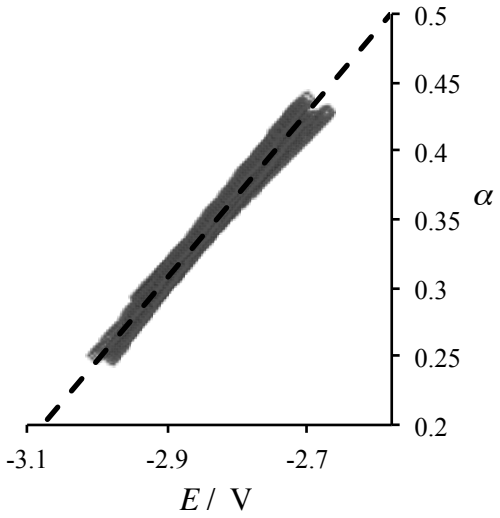

Figure 2.23: α as a function of potential. **3**, C_3 = 0.0030 M in DMF, ν = 500-1000 mV/s. Extrapolation to α = 0.5 gives the standard reduction potential of **3**.

Average values of α for concerted dissociative electron transfers typically fall around 0.3. The average α values for **3** and **4** are given in **Table 2.8**, calculated three ways: from the variation of E_p with ν, from the peak widths, and from the convolution voltammograms via **Eq. 2.7**. These values range from approximately 0.35 – 0.4, smaller than 0.5, the typical value for a stepwise mechanism, and slightly large than that expected for a concerted mechanism. The appropriate approach to resolving this difference is to fit the heterogenous rate constant data to both the Marcus model for electron transfer as well as the concerted dissociative electron transfer model proposed by Savéant[2] (**Eq. 2.1** and **Eq. 2.10** respectively, where D is the bond dissociation energy of the cleaved bond; note that λ_i is considered to be small relative to D and is usually ignored in the Savéant model, although this is not necessary).

$$\Delta G^{\ddagger} = \frac{D + \lambda_o}{4}\left(1 + \frac{\Delta G^0}{D + \lambda_o}\right)^2 \qquad \textbf{Eq. 2.10}$$

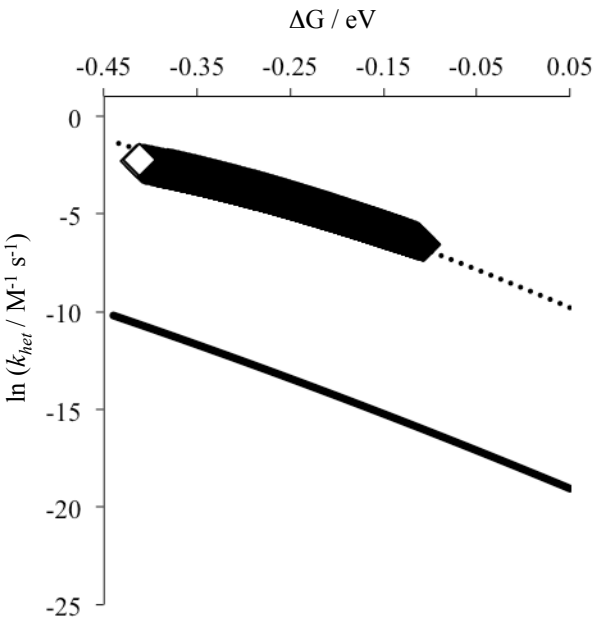

Figure 2.24: Fitting of heterogeneous rate constant data vs. driving force for **3**. Solid line indicates predicted cDET theory, dashed line indicates fit Marcus parameters (see text).

These fits are given in **Figure 2.24**. Fitting to the Marcus theory requires a total reorganization energy of 1.77 eV and 2.09 eV for **3** and **4**; these values are rather large. In dimethylformamide, the solvent reorganization energy component of λ can be estimated from the radius of the neutral parent ketone, as obtained via quantum calculations, by the empirically derived relationship $\lambda_o = \frac{3.15}{a}\ (eV)$, where *a* is the radius. In the case of **3** this value is 0.63 eV, leaving 1.14 eV as the internal reorganization energy component. This value is much larger than typical values, too large to account for things like bond stretching or other similar geometric distortions. Conversely, the data does not fit the Savéant cDET model where *D* = the bond strength of the bond being broken. The bond strength of the C—O bond in the case of **3** was estimated to be 2.13 eV from thermodynamic cycles (*vide infra)*, and following the cDET model gives the solid dark line in **Figure 2.24**.

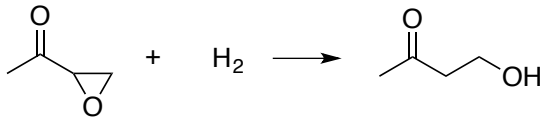

$$D_{C-O} = \Delta H^0_{rxn} - D_{H_2} + D_{C-H} + D_{O-H}$$

Scheme 2.7: The hydrogenation reaction used to determine the bond energy of C—O in the epoxide. ΔH^0_{rxn} obtained from quantum mechanical calculations (MP2/AUG-CC-PVTZ).

The C—O bond energies were estimated based on the computationally obtained thermodynamic values for the hydrogenation reaction depicted in **Scheme 2.7**. The equations presented in Scheme 2.7 were then used to determine the bond energy using known bond dissociation energies for the other bonds broken and formed in the reaction sequence. All species in the hydrogenation reaction were optimized at the MP2[92]/AUG-CC-PVTZ[93] theory and basis set and enthalpy corrections to the electronic energy were obtained from frequency calculations at the same level of theory and were used to calculate ΔH^0_{rxn}. This resulted in an estimated bond dissociation energy of 49.1 kcal/mol (2.13 eV). This number is reasonable, considering the bond energy of the C—O bond in dimethyl ether is 84.11 kcal/mol.[94] Assuming a recently reported ring strain of 26.68 kcal/mol[95] and a radical stabilization energy of 5.81 kcal/mol due to the presence of the carbonyl moiety, group additivity predicts a bond dissociation energy of 51.62 kcal/mol (2.24 eV), in keeping with the computational results.

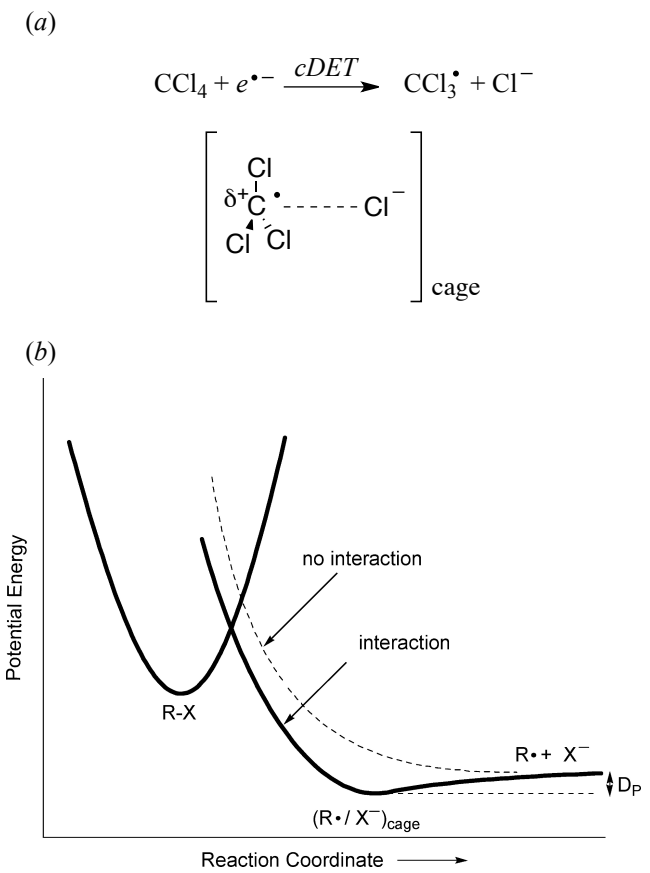

Figure 2.25: (*a*) The reduction of carbon tetrachloride, an example of the "residual" interaction between the cleaved fragments of a cDET that follows the "sticky" mechanism. (*b*) Reaction coordinate diagram for the "sticky" model of cDET demonstrating the effect of the residual interaction on the intrinsic barrier. (*b*) Reprinted with permission from reference 20. Copyright 2007 American Chemical Society.

It is clear from these results that the electron transfer reactions of these compounds fit neither the Marcus model for electron transfer nor the concerted dissociative electron transfer theory. A third possible model for these electron transfers requires a residual interaction between the cleaved fragments of the parent species. This model, an extension of cDET theory, is known as "sticky" cDET[18] and an example to illustrate the idea is given in **Figure 2.25**. This "sticky" model is formulated after the cDET theory, but allows for some residual interaction (usually electrostatic) between the cleaved portions of the parent ion. The effect is illustrated in **Figure 2.25** and follows the equations:

$$\Delta G^{\ddagger} = \frac{\left(\sqrt{D} - \sqrt{D_p}\right)^2 + \lambda_o}{4}\left(1 + \frac{\Delta G^0 - \Delta G^0_{sp}}{\left(\sqrt{D} - \sqrt{D_p}\right)^2 + \lambda_o}\right)^2 \qquad \textbf{Eq. 2.11}$$

$$\Delta G^0_{sp} = D_p - T\Delta S_{sp} \qquad \textbf{Eq. 2.12}$$

where D is the bond dissociation energy, D_p is the value of the residual interaction between the cleaved moieties, and ΔG^0_{sp} is a free energy correction factor due to this residual energy where ΔS_{sp} is a factor related to entropy effects (in the case of ring opening these entropic effects were considered to be negligible and ΔS_{sp} was approximated to be zero). In essence this model is a middle ground between Marcus theory and the pure cDET transfer theory. At the limits (as $D_p \rightarrow D$ and as $D_p \rightarrow 0$) **Eq. 2.11** simplifies to give the Marcus equation and the Savéant cDET equation respectively.

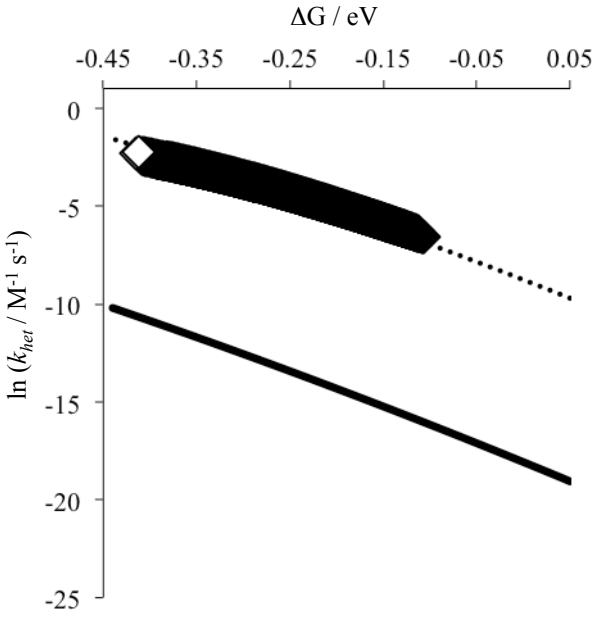

Figure 2.26: Fitting of heterogeneous rate constant data vs. driving force for **3**. Solid line indicates predicted cDET theory, dashed line indicates fit "sticky" parameters (see text).

The previous data for **3** was fit to the "sticky" cDET theory with λ_o = 0.63 eV and D = 2.13 eV, as determined previously. The fit was made via varying the value of D_p until the theoretical line fit the experimental data as demonstrated in **Figure 2.26**. The best fit gives a value of 0.096 eV for D_p, approximately 4.5% of the total bond strength. This corresponds to a residual interaction approximately 2.2 kcal/mol in value, which may be explained as an interaction of an anion (the oxygen originating in the epoxide) and the carbonyl dipole, **Figure 2.27**.

Table 2.8
Results of convolution analysis of LSV experiments for **3** and **4** and fitting to the "sticky" cDET model to obtain the residual interaction, D_p.

	$\alpha_{avg}{}^{a}$	$\alpha_{avg}{}^{b}$	$\alpha_{avg}{}^{c}$	$E^0_{RX/RX\cdot-}$	k^0_{het}	D_p
3	0.400(0.010)	0.381(0.009)	0.35(0.01)	-2.57(0.05) V	(1.6 ± 0.5) x 10^{-4} cm s^{-1}	0.096 eV
4	0.39(0.03)	0.390(0.010)	0.33(0.01)	-2.78(0.01) V	(7 ± 4) x 10^{-6} cm s^{-1}	0.075 eV

(*a*) From $\partial E_p/\partial \log \nu$ (*b*) From peak widths (*c*) From application of Eq. 2.7

Data for **4** was treated likewise and a similar analysis followed. The total results for **3** and **4** are given in **Table 2.8**.

In conclusion, the results from the LSV experiments and the subsequent convolution analysis point to the "sticky" cDET mechanism as the observed mechanism for reduction of these aliphatic ketones. In order for this model to fit, a residual interaction of approximately 2 kcal/mol must be present between the cleaved moieties of the parent ion. The existence of this interaction will be further explored and analyzed in the following section.

2.3.3 Preparative electrolysis

The proposed mechanism for reduction of the ketones during electrolysis is given in

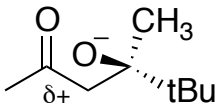

Figure 2.27: Possible residual interaction in ring-opened radical anion.

Scheme 2.8. The ketones are reduced at the electrode surface. Subsequent to (or concurrent with) this electron transfer the epoxide undergoes ring opening via carbon-oxygen bond cleavage, yielding a distonic radical anion. This radical anion is ripe for further reduction at the potentials of the electrolysis, which would yield the strongly basic dianion. This would then act as a base in a Hoffman elimination reaction involving the cation (tetrabutylammonium) of the supporting electrolyte, yielding tributylamine, but-1-ene, and an anion that would undergo further decomposition to the ketone and aldehyde products observed in the product analysis of the electrolysis. These products (acetophenone and benzaldehyde in the case of **1**, acetophenone in the case of **2**, benzaldehyde and pinacolone in the case of **3**, and pinacolone in the case of **4**) were all observed and verified via mass spectrometry and matched retention times with authentic samples in gas chromatography. Particularly low weight products (such as formaldehyde in the case of **2**) would have eluted with or before the solvent and thus were not observed.

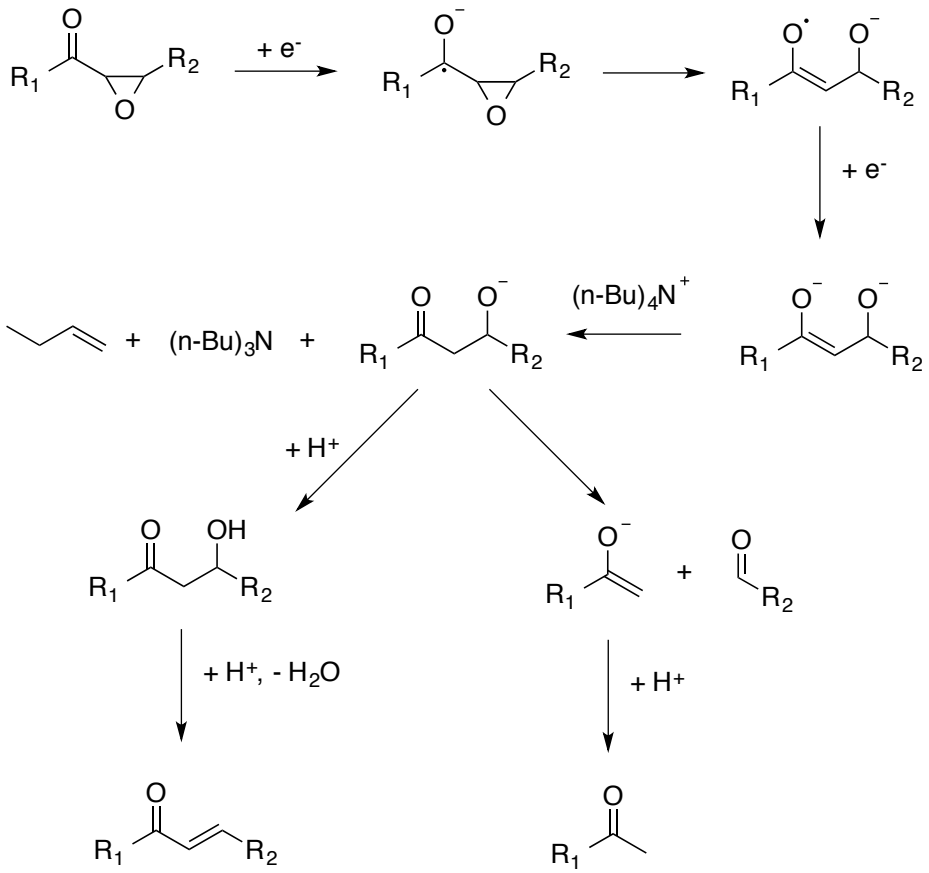

Scheme 2.8: Possible mechanism for reduction of α-epoxyketones under electrolysis conditions.

Both benzaldehyde and acetophenone were cleanly separated from other products via GC in the post electrolysis chromatograms, and their amounts in the product mixture were able to be quantified via obtaining response factors for these compounds relative to the internal standard added after electrolysis, chlorobenzene. Pinacolone was too low weight to be separated from the solvent mixture via GC before the DMF was removed by the extraction workup – that is pinacolone's peak was obscured by other peaks of low weight products in the chromatogram. Although pinacolone was identified by matching retention times with an authentic sample after this workup, data based on its peak area could not be obtained and its concentration in the product mixture could not be quantified.

Table 2.5
Preparative electrolysis results.

	Initial[a]	Recovered[b]	Electrons passed[c]	Ketone[d]	Aldehyde[d]	Aldol[e]	Aldol condensate[e]
1	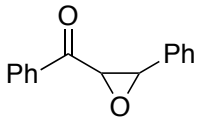			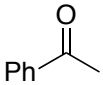		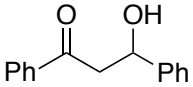	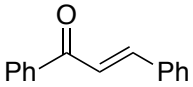
	0.30	0.05	0.15	0.02	0.07	observed	not observed
2	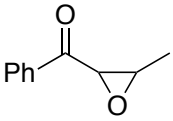			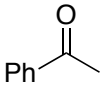		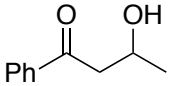	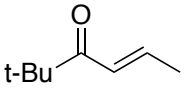
	0.30	0.02	0.15	0.02	not observed[f]	not observed	not observed
3	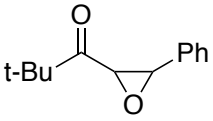			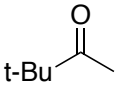		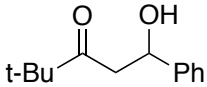	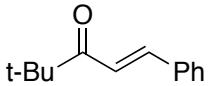
	0.30	0.22	0.15	observed[g]	0.07	not observed	not observed
4	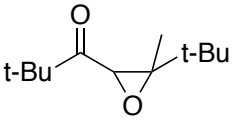			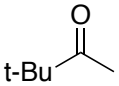	NA	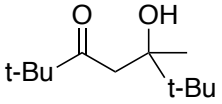	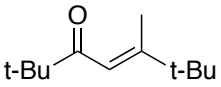
	0.40	0.21	0.19	observed[g]		not observed	not observed

All numbers reported are millimoles. (*a*) Obtained from solution preparation (*b*) Obtained via internal standard (see text) (*c*) Obtained from potentiostat (*d*) Retro-aldol addition products, obtained via internal standard (see text) (*e*) Both the aldol alcohol and the corresponding aldol condensation product were identified via mass spectrometry where indicated; however, they were not verified via authentic samples or quantified via the internal standard (*f*) eluted with solvent (*g*) identified with authentic samples but unable to be quantified (see text)

In all cases the quantity of the recovered starting material was also obtained via using the internal standard and measured response factors. These data, along with the data obtained from the ketone and aldehyde products discussed above, are presented in **Table 2.5**. Unfortunately the results are not ideal. The aldehydes are the best case for support of the proposed mechanism. They appear in quantities that would be expected based on a two-electron process. The ketones, on the other hand, appear to be present in amounts less than would be expected; particularly in the case of **1**, where there is a clear discrepancy between the amount of ketone and aldehyde product present in the product solution (the same could be assumed of **2**, although the aldehyde in this case is not available for quantitative analysis). This may be explained readily enough; the direct products of the retro-aldol condensation are the neutral aldehyde and a presumably

reactive enolate anion, whose concentration could conceivably be lowered by further reaction during the course of the electrolysis.

The amount of recovered starting material, on the other hand, does not directly match with the mechanism proposed previously, as far more of the starting material has been consumed than predicted for a two electron process. However, it should be noted that the conditions of the electrolysis are particularly harsh and last for an extended time (usually about 40 minutes). The solution is very basic and it is feasible that the α-epoxyketones cannot survive these kinds of conditions and may participate in reactions unrelated to the electrode process – for example, reaction with the aforementioned enolate anion of the retro-aldol process. However, there are no positively identified peaks in the GC/MS chromatograms that would entirely account for products obtained from these possible side reactions. It should be noted however, that the single largest product by peak area in each chromatogram had an identical retention time (approximately 7 minutes for the program used for analysis) for all 4 epoxides. This product, however, is completely removed by the extraction workup and could not be identified via mass spectrometry and is presumed to be a product of reaction with the supporting electrolyte. It may be that whatever side reaction generates this product consumes the missing unrecovered starting material.

The best than can be said of the electrolysis products is that they do not disagree with a mechanism where reduction of the ketone is followed by cleavage of the carbon-oxygen bond. Indeed, the major products identified for each epoxyketone are consistent with this mechanism. Mass balance is, however, unable to be established and the number of electrons transferred does not agree with the amount of ketone consumed. It should be noted, however, that the products obtained are the same as those reported in the literature by Hasegawa[33-34,68] for photo-induced

reductive cleavage of α-epoxyketones. Although these studies cannot completely rule out the possibility that ring opening may occur through cleavage of the carbon-carbon bond, it appears much more likely that it is the carbon-oxygen bond that is cleaved. Certainly, there are no products identified in the electrolysis results that can only be obtained via carbon-carbon bond cleavage. Furthermore, there is no precedent in the literature for carbon-carbon bond cleavage based on the products of reduction of α-epoxyketones. Further circumstantial evidence for carbon-oxygen bond cleavage may be obtained by comparison of the ring-opening rate data with that of analogous cyclopropylketones (*vide infra*) and by computational chemistry.

2.3.4 Computational results

Comparing the computational analysis with the electrochemical data presented previously gives good agreement between theory and experiment, particularly when comparing the C—O bond cleavage computational results with those obtained electrochemically.

Most importantly, the activation barrier for C—C bond cleavage is much larger (between 10 – 23 kcal/mol) than that obtained for C—O bond cleavage by the same method, as described previously (**Table 2.6**). This is overwhelmingly large, and even in the absence of direct evidence from electrochemistry for the preferred cleavage pathway, this result can be taken as strong evidence that these epoxyketones undergo C—O bond cleavage. It is clear that taken together the electrochemical experimental results and computations provide strong evidence that these aromatic α-epoxyketones undergo stepwise dissociative electron transfer cleavage of the C—O bond of the epoxide ring.

Pertaining to the aliphatic epoxyketones, quantum mechanical calculations could prove to play an essential role in understanding the results obtained in the previous section; particularly,

they may confirm or deny the existence of the residual interaction between the cleaved fragments of the parent ketone required for the "sticky" cDET theory to be applicable in their case. Computational experiments are particularly suited to this kind probing as they allow the isolation of the distonic radical anion, something unachievable in laboratory practice. Furthermore, they can estimate the location of charge in the radical anion, which could give credence to an electrostatic interaction between the cleaved portions of the radical anion.

The most obvious feature of the computations to note is the non-existence of a discrete ring-closed radical anion intermediate (see **Figure 2.16** and the relevant discussion in Section **2.2.4.2**). In principle this gives good agreement with the electrochemical results, as these calculations indicate that the dissociative electron transfer must be of a concerted type (the parent radical anion does not exist as a discrete intermediate). It should be noted that even if the parent radical anion "exists" as an intermediate with a finite lifetime at room temperature, the reaction mechanism can still proceed via a concerted pathway. It may be that the potential surface wherein the radical anion resides is at higher energies than those obtained in the electrochemical experimental conditions (i.e – more negative working electrode potentials). However, if the parent radical anion does not exist as a discrete intermediate then the reaction mechanism must by necessity proceed via a concerted pathway. At this level of theory it appears that the computations suggest the latter case to be true for these aliphatic epoxyketones.

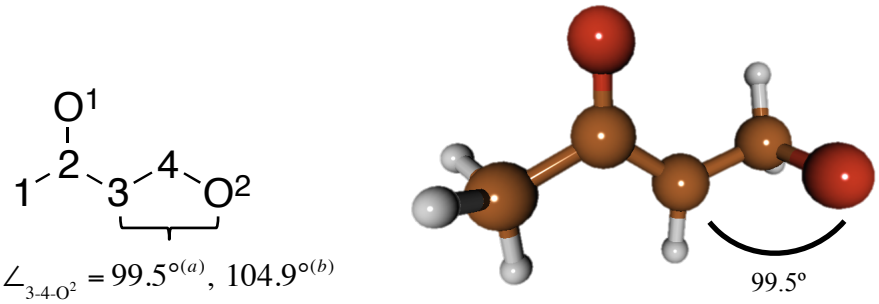

Figure 2.28: (*left*) Identification of atoms and the "unusual" bond angle found via (*a*) B3LYP and (*b*) BHandHLYP. (*right*) Ball and stick model obtained from B3LYP optimization of **7**.

When the optimized, ring-opened radical anion is closely examined an interesting feature emerges with respect to the geometry of the species, in particular, the C_3—C_4—O_2 bond angle shown in **Figure 2.28**. C_4 is a sp^3-hybridized carbon, and the expected bond angle should be approximately 109°. The optimized structure gives bond angles of 99.5° and 104.9° from B3LYP and BHandHLYP simulations, respectively. This result indicates the possibility of the existence of an interaction between the oxygen which had been a member of the epoxide ring in the parent species and the carbonyl moiety of the radical anion. As explained in section **2.3.2**, the Savéant "sticky" concerted dissociative electron transfer model requires just such an interaction between the cleaved parts of the radical anion (of ca. 2 kcal/mol, in this particular case) in order to be applicable. This bond angle distortion may be the result of exactly this kind of "sticky" interaction.

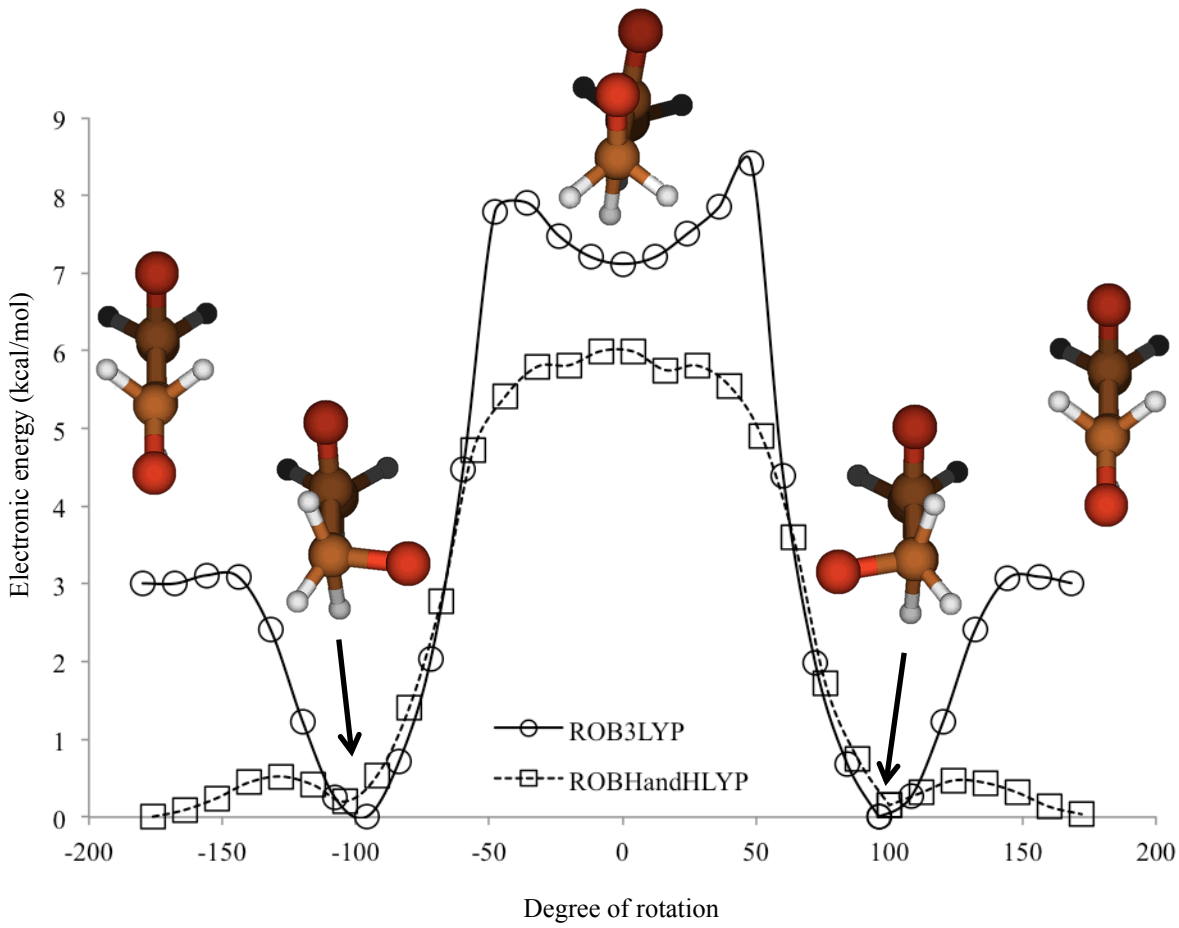

Figure 2.29: Energy profile for rotation of the 2-3-4-O^2 dihedral at the roB3LYP and roBHandHLYP levels. All electronic energies are relative to the lowest energy point found in each method.

To test this, an experiment was performed to generate an energy profile for rotation around the dihedral composed of C_2—C_3—C_4—O_2. The energy profile was obtained with the same method described earlier for the radical anions, and the results are shown in **Figure 2.29**. The methods both agree that the geometry arrived at via optimization of the ring-closed radical anion is located in an energy minimum; unfortunately, the energies obtained from these methods are not in good agreement. The two levels of theory (B3-LYP and BHandH-LYP) do not agree either on the lowest energy conformer or on the relative energies between various dihedral angles. Furthermore, DFT methods are not comparable; there is no "best" method, and (unlike for something like configuration interaction theory) the method cannot be progressively increased until an apparent lowest energy structure is found for the species in question. When such a

disagreement between the two methods occurs it is best to go to a different method in order to better understand the computational results.

To address these discrepancies single point energy calculations were preformed on the geometries obtained at each point on the energy profile using the CCSD method and the same basis set and solvent model as before. The results are given in **Figure 2.30**. It can be seen from these results that the structure located at the global minima for this rotational energy profile is the same that arises from optimization of the ring closed radical anion. There appears to be an interaction between the oxygen that originated in the epoxide ring and the carbonyl dipole (see **Figure 2.31**) Although no exact value for this interaction may be established, it is satisfying to note that rotation away from this possible interaction and around the C—C bond costs somewhere between 1 and 6 kcal/mol, which falls nicely into the energy range that the "sticky" model requires to fit (approximately 2 kcal/mol).

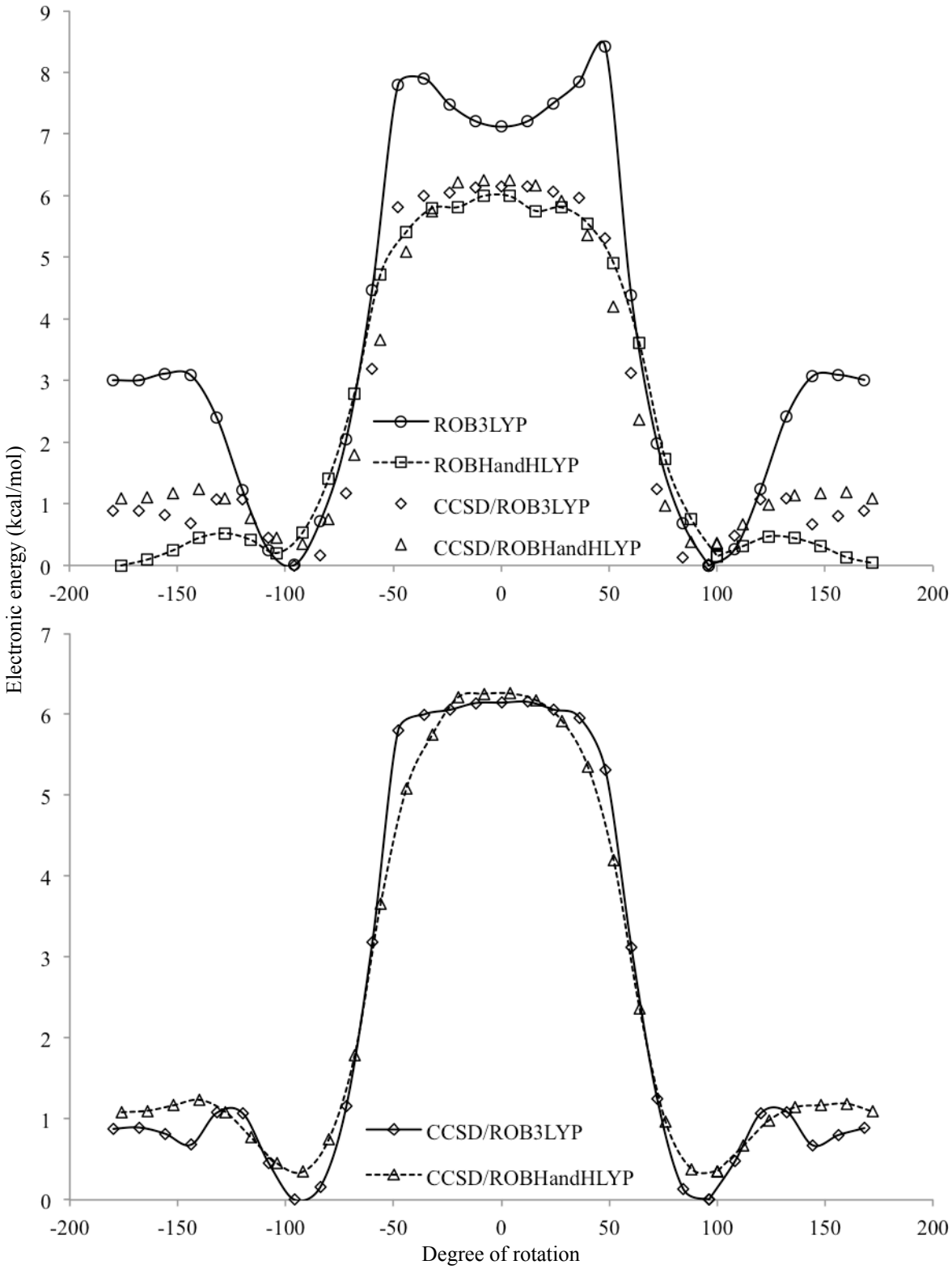

Figure 2.30: (*above*) Results of CCSD single point energy calculation on the geometries obtained from B3LYP and BHandHLYP optimizations. (*below*) Isolated CCSD single point electronic energies. All electronic energies are relative to the lowest energy point found in each method.

Finally, electrostatic potential maps may be generated from the computational data (**Figure 2.31**). The maps show that significant negative charge is located on both oxygen atoms in the ring-closed and ring-opened radical anions. The maps also show that, expectedly, resonance stabilization of negative charge by the phenyl ring in $\mathbf{5}^{\bullet-}$ is greatly reduced upon ring opening. Additionally, both ring-opened radicals demonstrate a significant charge imbalance in the carbonyl, with large positive charge on the carbon. The electrostatic attraction between the oxygen that was originally in the epoxide ring and this carbon atom is the most likely explanation for the effect described in the preceding pages, and the source of the residual interaction that must be present in order for the Savéant "sticky" model for concerted dissociative electron transfer to be the appropriate description of the reduction of these aliphatic epoxyketones.

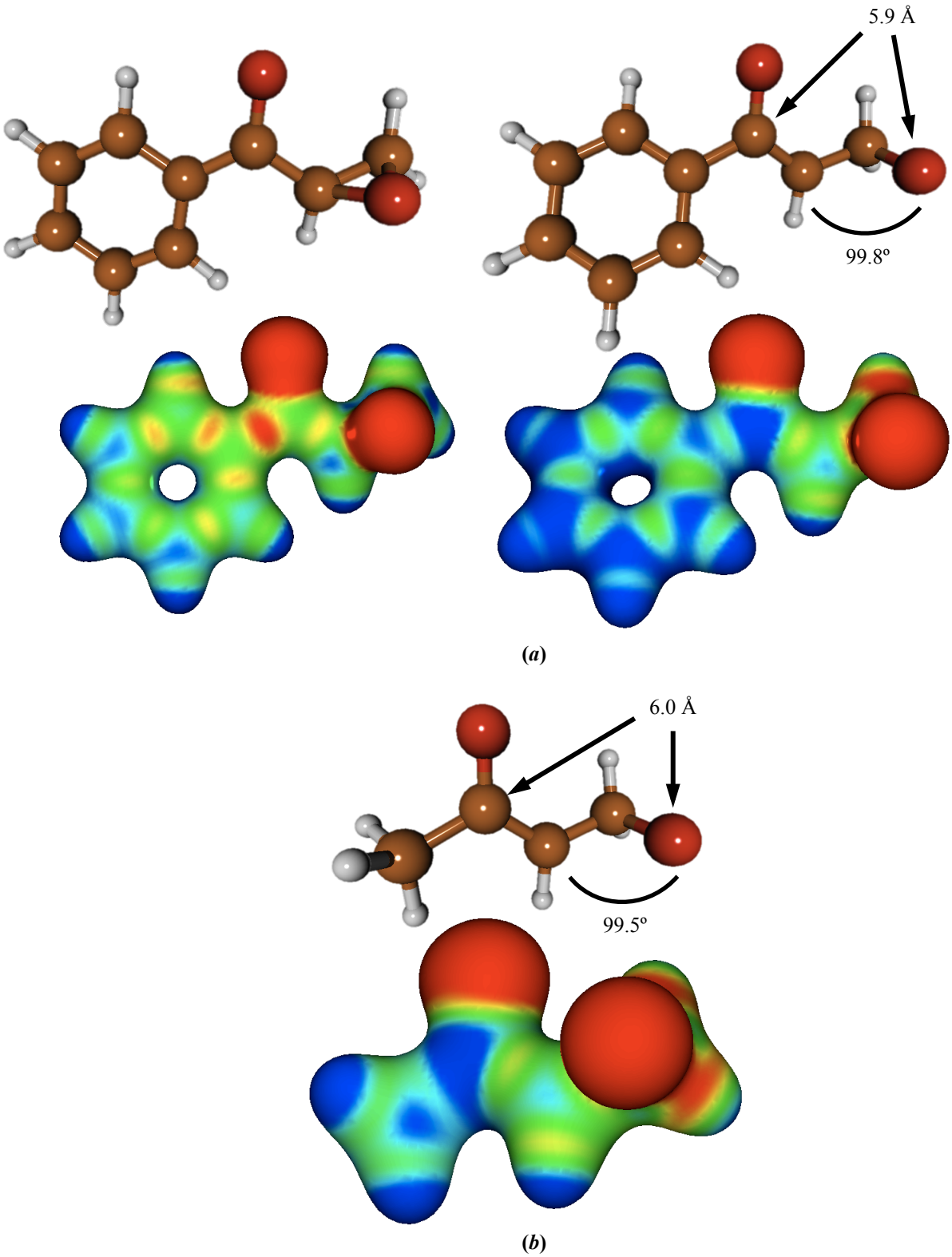

Figure 2.31: Electrostatic potential maps for (*a*) $\mathbf{5}^{\bullet-}$ and its ring opened product and (*b*) the ring opened product of $\mathbf{7}^{\bullet-}$. Maps were generated from CCSD/6-31+G* single point energy jobs from B3LYP optimized geometries at an electron density contour value of 0.05. Bond angles and atomic distances that may indicate a residual electrostatic interaction within the structures are shown.

2.3.5 Summary

In conclusion, it has been shown that α-epoxyketones undergo dissociative electron transfer of the C—O bond in the epoxide ring. The mechanism of these reactions depends on the structure of the ketone.

Aromatic ketones, where the charge and spin of the radical anion produced by the electron transfer are resonance stabilized, undergo a stepwise mechanism. The rate constant associated with the unimolecular ring opening reaction is quite large, on the order of 10^7 s^{-1}. The computational simulations overwhelmingly prefer ring opening via the C—O bond cleavage. Although the preparative electrolysis experiments were not able to conclusively determine the pathway of bond cleavage, the products of the experiments were in keeping with C—O bond cleavage; coupled with the computations and with literature precedent it is safe to conclude that the reaction proceeds via C—O bond cleavage.

Aliphatic α-epoxyketones undergo concerted dissociative electron transfers, as evidenced by both electrochemical experiments as well as computational chemistry. More specifically, these ketones fit the "sticky" concerted model for dissociative electron transfer, where a residual electrostatic interaction within the distonic radical anion leads to a lowering of the activation barrier for the electron transfer and thus to slightly larger values of the transfer coefficient α for these reactions. Computational simulations support the existence of this residual interaction. Again, preparative electrolysis cannot conclusively rule out C—C bond cleavage, however the electrolysis results are consistent with C—O bond cleavage, and considering there is only one

example of concerted dissociative electron transfer of a C—C bond in the literature, it is safe to conclude that the C—O bond is cleaved.

2.4 Comparison to literature

Now that good working models for the reductions of these species has been determined, comparisons to similar species previously reported in the literature can be made, particularly with respect to the cyclopropyl and organic halides mentioned in the introduction to this chapter.

Table 2.9 compares and contrasts both the cyclopropyl aromatic ketones and the epoxide aromatic ketones covered in this work. It is interesting to note how the results differ from the former to the later, particularly when considering the effect of resonance on the reaction rates. For the cyclopropylketones changing the structure of the R-groups allows for fine-tuning of the rate of ring opening *after* the electron transfer. The reaction follows a stepwise mechanism, and the following chemical step may either be very slow as in the case of entry 2 or extremely fast as in the case of entries 3 and 4.

In contrast, the R_2 identity of the α-epoxyketones seems to play only a small role in the ring opening process, as may be predicted if ring opening occurs through carbon-oxygen bond cleavage. The R_2 group is more or less electronically isolated from the epoxyketone moiety by the sp^3-hybridized carbon of the epoxide ring and cannot play a dramatic role in the stabilization of carbon-epoxide cleavage products. Instead, the mechanistic pathway is determined by the identity of R_1. If this group allows for large resonance stabilization of charge and spin (i.e. the aromatic ring of **1** and **2**) then the mechanism follows a stepwise pathway, and the rate of ring opening is only slightly changed by the identity of the R_2 group. If, instead, R_1 is an alkyl group affording no resonance stabilization of charge or spin, then the mechanism follows a concerted

pathway, where R_2 only has a slight effect on the reduction potential of the process. Circumstantially, this also provides evidence for carbon-oxygen bond cleavage of the epoxide ring. If the carbon-carbon bond were broken, the identity of R_2 would be expected to play a dramatic role in the rate of ring opening. Furthermore, there should be no reason for carbon-carbon bond cleavage to be a concerted process in any case, as an epoxide undergoing ring opening via carbon-carbon bond cleavage would be expected to follow the same mechanistic pathway at very similar rates to the cyclopropylketones listed in **Table 2.9**.

A perhaps more valid precedent to the reduction of these α-epoxyketones was set by the reduction of organic halides; in fact, the comparison is nearly exact. Aryl halides undergo stepwise dissociative electron transfers, just as **1** and **2** do. Alkyl halides undergo a concerted mechanism, as does **3** and **4**. The major difference in the latter being that the alkyl halides adhere to the strict Savéant model for concerted dissociative electron transfer, and the epoxyketones appears to follow the so-called "sticky" model. This may be easily rationalized by recognizing that the simple alkyl radical formed from the alkyl halide bond cleavage is non-polar and does not interact significantly with the leaving halide. However, the ketyl radical formed from ring opening of the epoxide is polar in nature and some interaction between the cleaved portions of the distonic radical anion may be expected, leading to adherence to the "sticky" model for concerted dissociative electron transfer.

Table 2.9
Cyclopropylketones vs. α-epoxyketones. Comparision of reaction mechanism and rate.

Cyclopropylketone		α-epoxyketone	
Structure	k_{ro} (s^{-1})[a]	Structure	k_{ro} (s^{-1})[a]
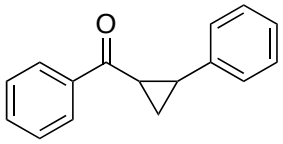	9.6 x 10^6	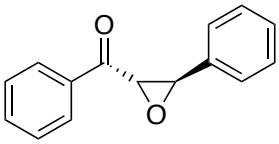 **1**	5 x 10^7
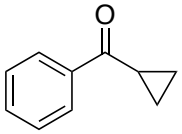	<10	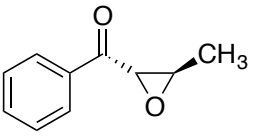 **2**	3 x 10^6
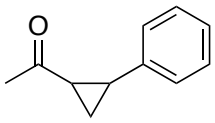	>10^8	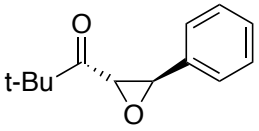 **3**	cDET
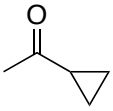	>10^7	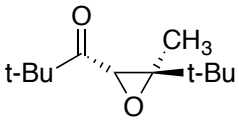 **4**	cDET

(*a*) Ring-opening rate constant of radical anion produced by reduction of the respective structure

2.5 Conclusion

The reductive dissociative electron transfer reactions of this series of α-epoxyketones have been analyzed and fit to known electron transfer models. Passage from a stepwise mechanism to a concerted mechanism is controlled by resonance stabilization of the parent radical anion – large stabilization allows for a stepwise process, and small or no stabilization

allows for a concerted process. Resonance stabilization in the product distonic radical anion appears to play no role in determining the mechanistic pathway and only a small role in determining the rate of ring opening and the reduction potential of the parent molecule. This points to a ring-opening process where the carbon-oxygen bond of the epoxide ring is cleaved either subsequent to or concurrent with electron transfer for the neutral parent molecule.

These results fit neatly into the framework of literature precedent for these kinds of reactions. The carbon-oxygen bond in the epoxide ring appears to behave more like a carbon-halogen bond than the carbon-carbon bond of the cyclopropane ring in cyclopropylketones, as may be expected. In fact, results of the electrochemical reduction of these α-epoxyketones effectively mimic those of similar alkyl and aryl halides. Although the results of preparative electrolysis are not entirely satisfactory, products formed from electrolysis are consistent with those reported in the literature for other reductive processes involving epoxyketones, and are indicative of if not proof of carbon-oxygen bond cleavage as the main pathway for ring opening of these α-epoxyketones.

Chapter 3. Oxidations – The electron transfer reactions of tetra-*n*-butylammonium acetate in dry and "wet" acetonitrile

3.1 Introduction

Cyclopropylamines have been used in the past to probe the mechanistic pathways of enzymes, particularly to test the hypothesis that these enzymatic mechanisms involve electron transfers. It was thought that upon oxidation by the enzyme these cyclopropylamines would undergo ring-opening reactions at rates comparable to the neutral cyclopropylcarbinyl radical rearrangement ($> 10^8$ s^{-1}). Addition of these cyclopropylamines can lead to deactivation of the enzymes (**Scheme 3.1**), presumably due to generation of a distonic radical cation upon ring opening which binds to the enzyme, rendering it inert.

The assumption that these cyclopropylamines undergo rapid unimolecular rearrangement has been shown to be incorrect in some cases,[56-57] and work has been completed focusing on why these reactions may be much slower than anticipated. As part of these studies, competition experiments were used to compare the rate of ring opening for cyclopropylaniline radical cations with deprotonation of the radical cations via a weak base such as tetra-*n*-butylammonium acetate. In the process of these experiments, it was discovered that the acetate anion unexpectedly undergoes apparent electron transfer reactions with both ferrocenium radicals as well as dimethylaniline cation radicals.[96] This unexpected result was confirmed in 2007, when Gonzalez and coworkers published[52] results showing deactivation of electrode surfaces via homogeneous redox catalysis of acetate with ferrocene as mediator.

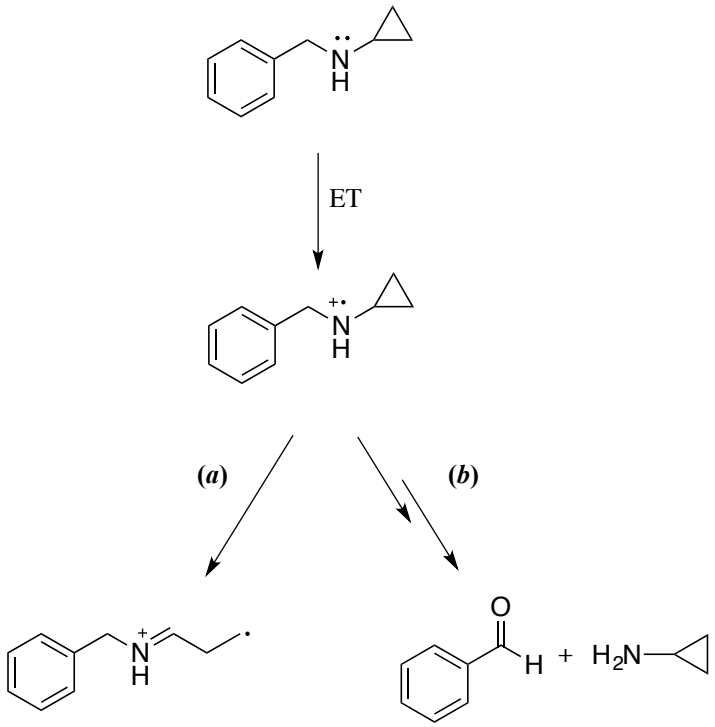

Scheme 3.1: Possible mechanistic pathway for enzyme deactivation by cyclopropyl containing nitrogen centered radical cations. (*a*) After electron transfer to the enzyme the radical cation undergoes (presumably) rapid ring opening, giving a distonic radical cation where spin is localized on a primary carbon atom that then may bind the active site of the enzyme, rendering it inert. (*b*) Pathway to normal enzymatic products. If the rate of (*a*) is not large enough relative to the rate of the forward path (*b*), the cyclopropylamine will not be a good probe to determine if there is an initial electron transfer step in the enzymatic mechanism.

Because an experimental value for the electrochemical oxidation potential of acetate has not been published, and because the homogeneous electrochemistry of the acetate anion is relatively unknown, it was determined that a comprehensive study of the electrochemical behavior of acetate would be beneficial, particularly with respect to determining the correct method of analysis for the competition experiments involving aniline and cyclopropylaniline radical cations.

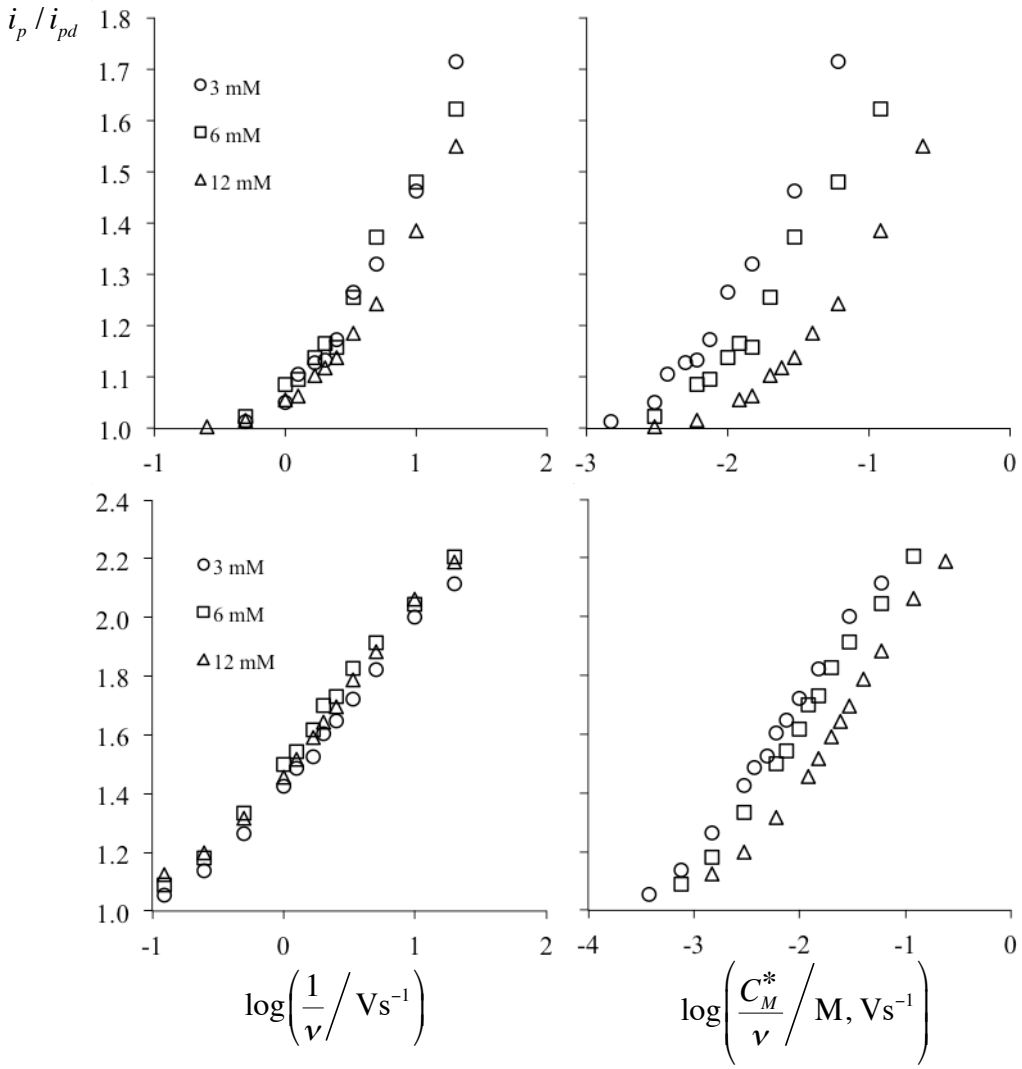

Figure 3.1: Initial mediated homogeneous redox catalysis results with ferrocene (top) and vinylferrocene (bottom) as mediators for electron transfer, as obtained by Hayati Çelik, 2007. 0.5 M H_2O/acetonitrile, 0.5 M supporting electrolyte, $\gamma = 5$. Surprisingly, these results indicate that the chemical step, decarboxylation of the acetoxyl radical, is rate limiting, however, repetition of the experiment did not yield the same results – or any reproducible results.

Struggles ensued. It became apparent that systems involving the oxidation of acetate behave poorly. As an example, **Figure 3.1** gives the results of mediated homogenous redox catalysis with ferrocene and vinylferrocene mediators. In both cases it appears that these reactions exhibit kinetic control by the post electron transfer chemical step – presumably decarboxylation of the acetoxyl radical, a reaction that is known to be exceedingly fast. In general, results were not reproducible; oft-repeated experiments did not yield consistent data.

3.2 Results

The electrochemistry of the acetate anion as detailed above has proven to be particularly challenging to study systematically and achieve reproducible results. It is apparent that day-to-day variations in laboratory environments (e.g. – temperature and humidity) as well as small variations in experimental procedures (e.g. – small differences in concentration from one sample preparation to the next) and the normally ignorable aging of chemicals (e.g. – distilled solvents and/or supporting electrolyte absorbing trace water even over the course of just 24 hours) can lead to large discrepancies in the analysis of the experimental results – even as much as to obscure determination of the rate limiting step of a homogeneous electron transfer process, something normally taken for granted as being straightforward for better behaved systems. As such, extreme care must be taken to perform the experiments in a way that leads to the acquisition of useful data, and this involves unusual methods such as: all sets of experiments must be performed within a 24 hour timeframe; each experiment must be carefully performed using stock solutions and an exacting dilution program to prepare the samples for analysis; all glassware and associated lab equipment must be consistently cleaned and dried to exacting standards to avoid contamination from water vapor; all samples must be prepared quickly to limit exposure to the atmosphere and exactly to minimize possible concentration variations in the samples that lead to data which cannot be appropriately interpreted via normal electrochemical analysis. Additionally, the oxidation of the acetate anion inevitably leads to large electrode fouling, meaning that the electrode must be polished between each experiment – greatly increasing the likelihood of introducing contaminants (e.g. – water) that will ruin the analysis. Finally, the solvent in use is acetonitrile, which evaporates rapidly at room temperature, particularly when purging the solution of oxygen by bubbling argon through the solution. This

evaporation leads to large changes in the concentration of the electrolyte, again ruining the experiment.

3.2.1 Neat acetonitrile

3.2.1.1 Direct electrochemistry

A sample voltammogram for the oxidation of tetra-*n*-butylammonium acetate in neat acetonitrile is given in **Figure 3.2**. The main characteristics of the voltammograms are that they are irreversible (no faradaic current drawn on the reverse sweep) and quite broad with an average peak width of 134 ± 4 mV. Peak widths for composite heterogeneous electrode reactions (for example, reactions where an electron transfer is followed by a chemical step) are dependent on the rate-limiting step of the reaction mechanism. Peak widths around 48 mV at room temperature are typically indicative of an electron transfer followed by a rate-limiting chemical step. Broader peaks indicate that the electron transfer is rate limiting. Peak widths of ca. 95 mV at room temperature are observed for normal rate-limiting outer sphere electron transfer reactions. When

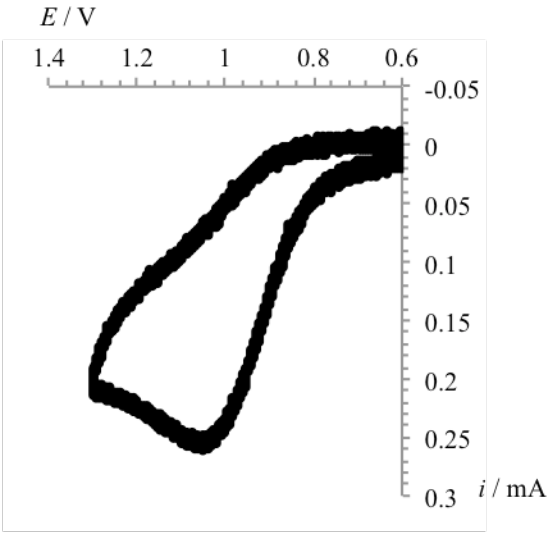

Figure 3.2: Cyclic voltammogram of tetra-*n*-butylammonium acetate (3.0 mM) in neat acetonitrile. $\nu = 411$ mV/s, 0.1 M supporting electrolyte

the electron transfer step is rate limiting, the transfer coefficient α plays a major role in the observed peak widths, where (in the case of an oxidation at the electrode surface) $E_p - E_{p/2} = 1.86\frac{RT}{\alpha nF}$. This means that when electron transfer is rate limiting, peak width is a tool to measure α for the reaction. An average peak width of 134 mV for the acetate anion in acetonitrile requires a value of α = 0.35 ± 0.01.

The transfer coefficient is a measure of transition state symmetry; that is, an α of 0.5 indicates a transition state that is centered between the reactant and products states. An α > 0.5 indicates a transition state that is product like; an α < 0.5 indicates a transition state that is reactant like. For small organic molecules and ions, electrode kinetics tend to be fast and therefore the surface concentrations of the redox couple follow the Nernst equation, **Eq. 3.1** (in the case of the oxidative electrode reaction $\mathrm{R} \rightleftarrows \mathrm{O} + n\mathrm{e}$ where E is the electrode potential, $E^{0\prime}$ is the formal potential of the redox couple and is approximately E^0 in the chosen solvent, C_M is the molar concentration of M, n is the number of electrons transferred per mole of reactant, and R, T, and F have their usual meanings).

$$E = E'^{0}_{\mathrm{R/O}} + \frac{RT}{nF}\ln\frac{C_\mathrm{O}}{C_\mathrm{R}} \qquad \textbf{Eq. 3.1}$$

$$\Delta G^{\ddagger} = \frac{(\lambda_i + \lambda_o)}{4}\left(1 + \frac{\Delta G^0}{\lambda_i + \lambda_o}\right)^2 = \frac{(\lambda_i + \lambda_o)}{4}\left(1 + \frac{nF\left(E^0_{\mathrm{R/O}} - E\right)}{\lambda_i + \lambda_o}\right)^2 \qquad \textbf{Eq. 3.2}$$

$$\alpha = \frac{\partial \Delta G^{\ddagger}}{\partial \Delta G^0} = \frac{1}{2} + \frac{\Delta G^0}{2(\lambda_i + \lambda_o)} = \frac{1}{2} + \frac{nF\left(E^0_{\mathrm{R/O}} - E\right)}{2(\lambda_i + \lambda_o)} \qquad \textbf{Eq. 3.3}$$

In such cases small variations in the electrode potential, E, result in large changes in the concentration ratio $\frac{C_O}{C_R}$. Working potentials of the electrode for these reactions hover near the standard potential $E^0_{R/O}$ where $\alpha = 0.5$ (**Eq. 3.3**). For this reason electron transfer reactions featuring fast electrode kinetics are approximated to have a constant value of $\alpha = 0.5$ and peak widths in the voltammograms will be approximately 95 mV. When reactions exhibit slow electrode kinetics according to the Marcus Hush model[1] of electron transfers (**Eq. 3.2**, where $\Delta G^{\ddagger}$ is the electron transfer activation free energy and λ_i and λ_o correspond to the inner and outer reorganization energies) they must have some large intrinsic barrier for the electron transfer reaction, called the reorganization energy. This barrier may be due to some internal component (λ_i, bond stretching, conformational requirements, and so forth.) or an external component (λ_o, reorganization of the solvent shell). These reactions require a large applied overpotential to

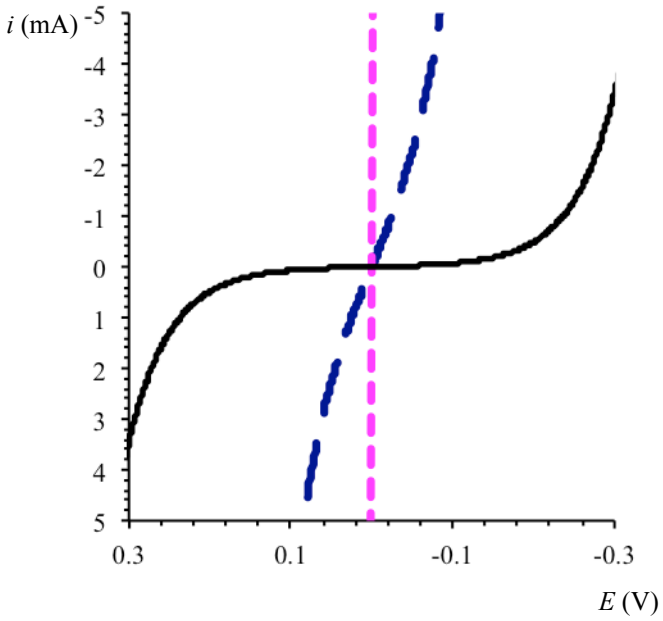

Figure 3.3: Current vs. overpotential plot, where $E = 0$ V at the standard oxidation potential of the analyte. Electron transfer reactions with large intrinsic barriers (solid line, $\alpha << 0.5$) require large overpotentials to draw significant current. Electron transfers with moderate intrinsic barriers require less overpotential (long-dashed line, $\alpha < 0.5$), and Nernstian electron transfers (where electrode kinetics are so fast they are ignored) require infinitesimal overpotentials to draw significant current (short-dashed line, $\alpha = 0.5$). Mass transport effects have here been ignored. Adapted from reference 74.

overcome this intrinsic barrier and do not strictly adhere to the Nernst equation. To achieve significant electrode oxidation the electrode potential *E* must be much greater than the oxidation potential E^0. This in turn means that α will be less than 0.5 (see **Figure 3.3**). An α = 0.35 as observed in the case of acetate in neat acetonitrile means that the reaction has an abnormally large intrinsic barrier, which may be accounted for by a large internal reorganization energy such as that associated with bond breaking in the transition state.

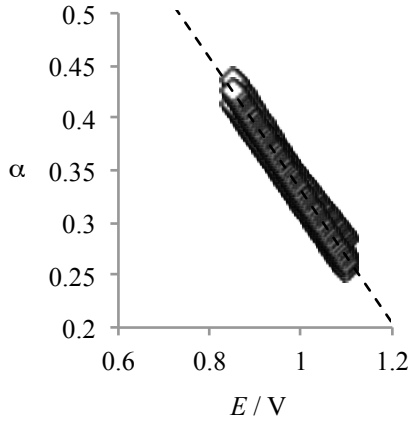

Figure 3.4: α vs. *E* for the oxidation of tetra-*n*-butylammonium acetate in neat acetonitrile (0.1 M supporting electrolyte, ν = 0.1, 0.2, 0.3, and 0.4 V/s). Extrapolation of the data back to α = 0.5 yields E^o_{ox} of the acetate anion.

In the case of an electrode mechanism where electron transfer is rate limiting, the voltammograms can be subjected to convolution analysis.[72-74] Convolution of the voltammograms effectively removes the mass transport component of the current response and allows for analysis of many more data points in the voltammogram than can typically be used in cyclic voltammetry. The convolution voltammograms can be used to obtain α as a function of potential (see **Chaper 2.3.2** for a complete description of this process). As noted earlier, at α = 0.5, $E = E^0$; linear regression analysis of the α versus *E* data can be used to determine E^0 (**Figure 3.4**). The formal reduction potential (vs. $Ag/AgNO_3$) in neat acetonitrile and 0.5 M tetra-*n*-butylammonium perchlorate is thus determined to be 0.730 ± 0.025 V.

3.2.1.2 Indirect electrochemistry

As described in **3.1** the acetate anion is known to undergo oxidation via a mediated electron transfer mechanism (**Scheme 3.2**). Although it is clear that there is a reaction between the acetate anion and the ferrocenium radical cation, the presence of a catalytic current does not necessarily inform the exact nature of the electron transfer mechanism. Indirect electrochemical experiments are required to attempt to unravel this mechanism.

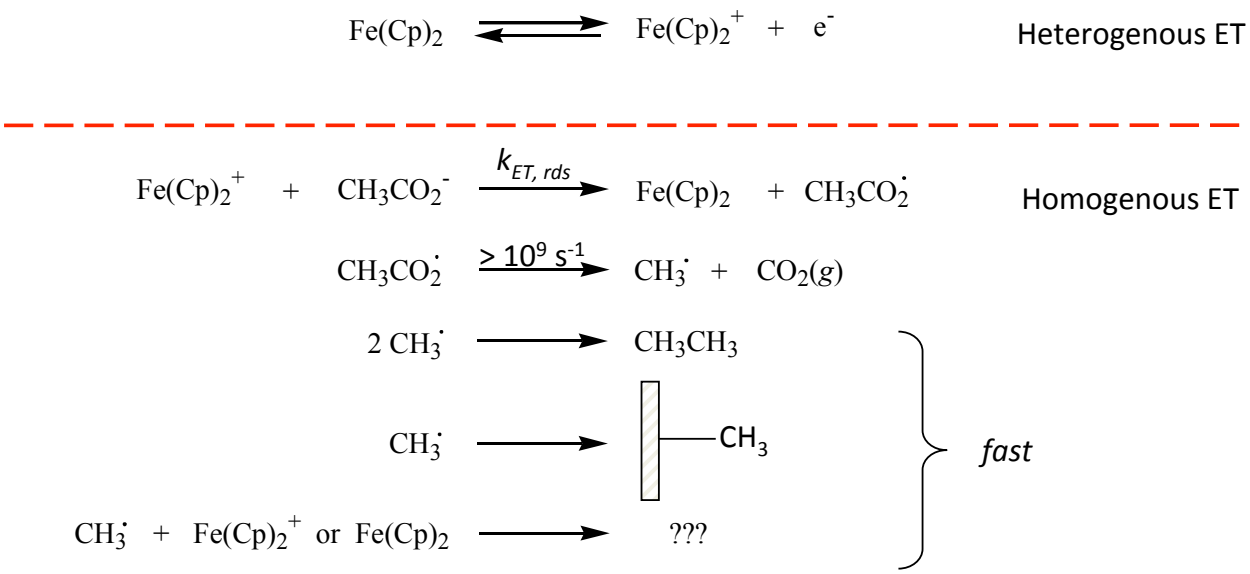

Scheme 3.2: Possible mechanisms for mediated indirect electrochemistry of acetate.

Unfortunately, homogeneous redox catalysis (HRC)[75-80] experiments proved to be extremely difficult for this system. As detailed previously, day-to-day variations in laboratory conditions (usually small enough to ignore for HRC experiments) had significant impact on experimental error, rendering normal HRC experiments (which are typically performed over the course of 3 to 5 days) ineffective for this system. The only way to obtain meaningful data was to perform all of the experiments consecutively in one 24-hour period. Additionally, each sample had to be prepared via dilution from the previous example. Small variation in the excess factor γ,

defined as the bulk concentration of the substrate relative to mediator ($\gamma = \frac{C_A^*}{C_M^*}$), render analysis of the data impossible in the case of acetate. Normally each sample for a set of HRC experiments is prepared individually and γ is only approximately constant over the set of experiments. This was not adequate for this system, and all samples had to be prepared via dilution of the previous sample to maintain a constant γ. This is not ideal as any error in sample preparation is manifested in all subsequent samples rendering the results unusable.

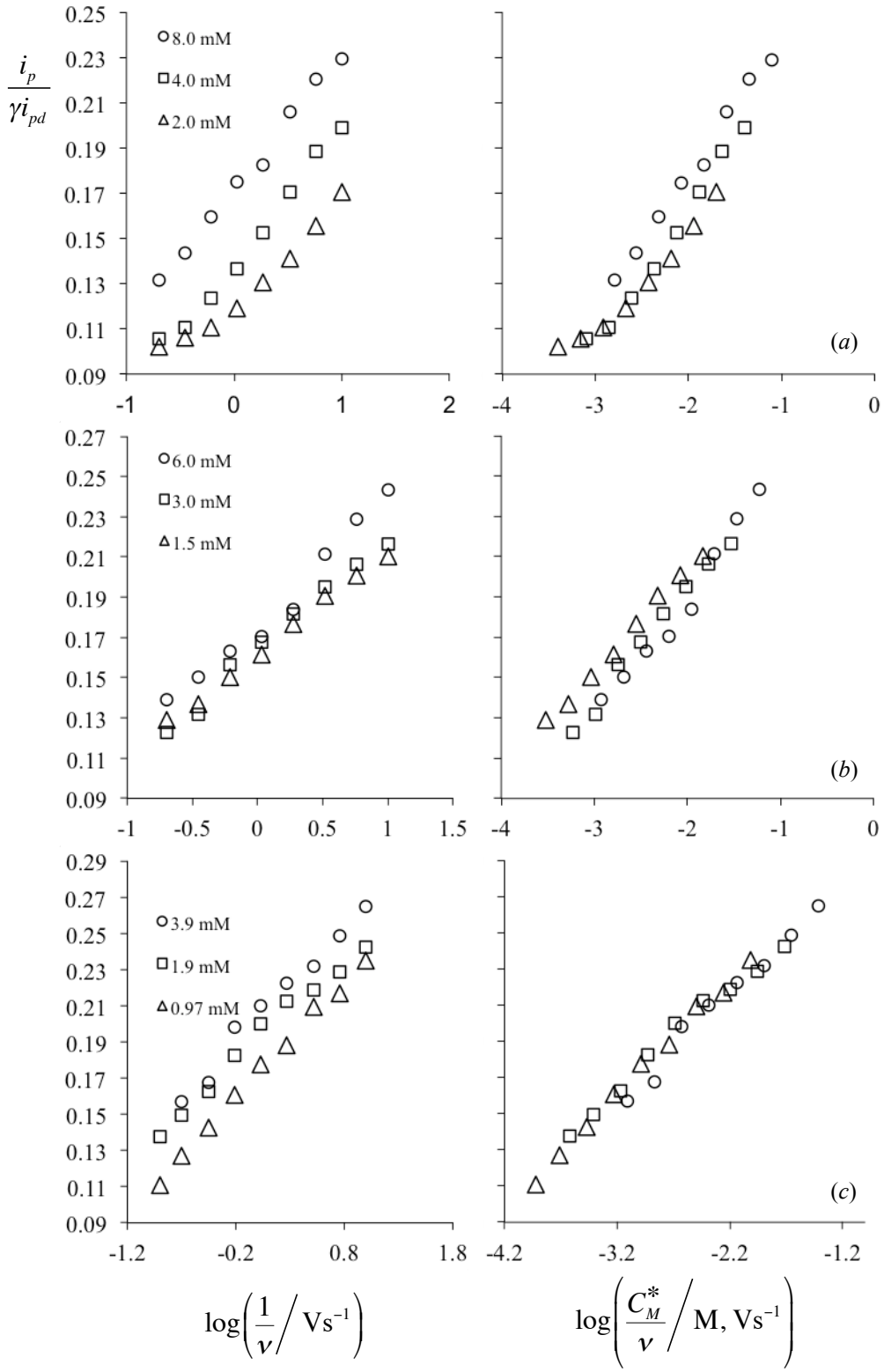

Figure 3.5: Mediated oxidation of tetra-*n*-butylammonium acetate in dry acetonitrile (0.5 M supporting electrolyte, γ = 10). (*a*) Ferrocene, (*b*) Vinylferrocene, (*c*) *p*-Bromophenylferrocene. Catalysis measured as the ratio of catalytic current (i_p) to diffusion current (i_{pd}) as a function of changing scan rate. Dependence of catalysis on mediator concentration indicates kinetic control by the homogeneous electron transfer.

The results of HRC experiments of tetra-*n*-butylammonium acetate using ferrocene, vinylferrocene, and *p*-bromophenylferrocene are presented in **Figure 3.5**. The most obvious feature of the data is that it is dependent on C_M. This is indicative of homogeneous electron transfer control (as described previously in **Chapter 2.2.2**).

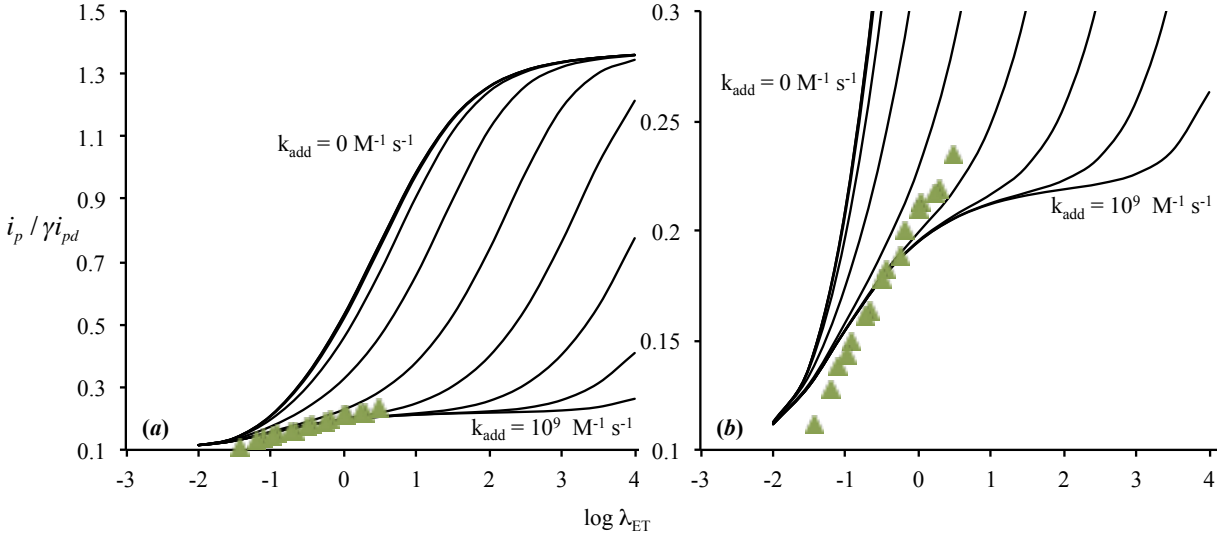

Figure 3.6: Simulated working curves (solid lines) and fit *p*-bromophenylferrocene HRC data (triangles) demonstrating fitting of mediated electrochemical data to the theoretical curves. (*a*) Full working curves where the top leftmost curve corresponds to no addition of products to the activated mediator (k_{add} = 0 M^{-1} s^{-1}) and the bottom rightmost curve corresponds to significant addition of products to the activated mediator (k_{add} = 10^9 M^{-1} s^{-1} (*b*) Same working curves with the y-axis scaled appropriately to better show demonstration of data fitting

The HRC data can be fit to dimensionless working curves obtained via digital simulation. In this case two potential mechanisms (**Scheme 3.3**, last step – where the first possible mechanism involves electron transfer from the activated mediator to generate the methyl cation and the second possible mechanism involves the activated mediator forming a bonded complex with the methyl radical) were simulated and the data fit to each. The redox catalysis data best fit the curves generated for addition of the methyl radical to the mediator. The chief feature of these working curves is that for fast addition to the catalyst, mediated catalysis plateaus over a large range of driving force (see right-most bottom curve in **Figure 3.6a**). In order for the experimental data to be successfully fit to these working curves, an experimentally accessible

range of sweep rates must be available such that the amount of catalysis changes over the course of the experiments significantly (i.e. – the data cannot fall into the plateau portion of the working curves, as the data is fit horizontally on the x axis, and if there is no slope in the data it cannot be fit to the working curves). Fortunately, this was possible in the case of each set of experimental data and an example of the fit data is given in **Figure 3.6**. Existence of this "plateau" region has since been verified with other mediators.[97]

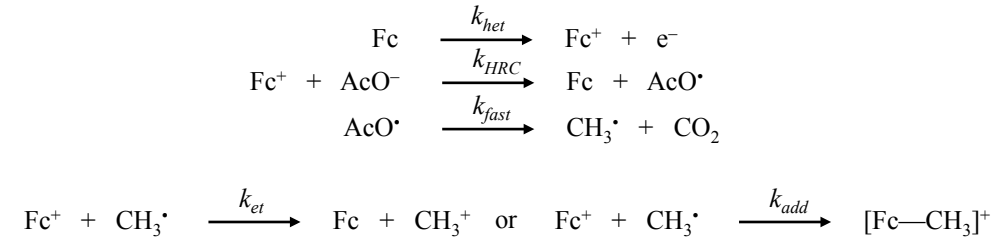

Scheme 3.3: Simulated mechanism for homogeneous redox catalysis used to generate working curves presented in Figure 3.6. The specific working curves shown in Figure 3.6 were generated for the addition mechanism (bottom right) as these are the curves that best fit the experimental data.

As described previously (**2.2.2**) the experimental data is offset from the dimensionless data by a quantity related to the rate constant for the electron transfer (**Eq. 3.4**), where λ_{ET} is the dimensionless rate constant for the forward electron transfer, C_M^* is the mediator concentration in the bulk solution, ν is the sweep rate in units of V/s, and all other symbols have their normal meaning.

$$\log \lambda_{ET} = \log\left\{\frac{RT}{nF} k_{ET} \frac{C_M^*}{\nu}\right\} = \chi + \log \frac{C_M^*}{\nu} \qquad \textbf{Eq. 3.4}$$

$$\text{where } \chi = \log\left\{k_{ET} \frac{RT}{nF}\right\}$$

The fitting parameter χ of the experimental data then only depends on the magnitude of the forward electron rate constant k_{ET}. The data is plotted alongside the theoretical working curves as in **Figure 3.6** and the fitting parameter χ is obtained, from which the value of k_{ET} may be

extracted. It should be noted that were the chemical step of the reaction rate limiting, a similar treatment could be used to obtain the composite rate constant for the reaction, $K_{ET}k_{CS} = exp\left\{\frac{nF}{RT}\left(E^0_{M/M^{\cdot-}} - E^0_{A^-/A^{\cdot}}\right)\right\}k_{CS}$. When subjected to this treatment the rate constants for the mediated electron transfer reactions were obtained and the results are given in **Table 3.1**.

Table 3.1
Oxidation of tetra-*n*-butylammonium acetate in dry and wet acetonitrile (0.5 M H_2O/acetonitrile) via homogeneous redox catalysis.

	Mediator	$E^0_{M/M^{\cdot+}}$ [a]	k_{et} [b]
Neat acetonitrile	Ferrocene	0.0281(0.0020)	$5.80(0.10)\times10^2$
	Vinylferrocene	0.0468(0.0016)	$2.7(0.6)\times10^3$
	p-Bromophenylferrocene	0.0926(0.0010)	$1.21(0.26)\times10^4$
Wet acetonitrile	Ferrocene	0.0245(0.0011)	9.3 (0.7)
	Vinylferrocene	0.0493(0.0021)	$1.63\ (0.17)\times10^2$
	p-Bromophenylferrocene	0.0894(0.0022)	$7.2\ (1.2)\times10^3$

(*a*) V, vs. $Ag/AgNO_3$ (*b*) $M^{-1}s^{-1}$

3.2.2 0.5 M H_2O/acetonitrile

3.2.2.1 Direct electrochemistry

In contrast with those produced under anhydrous conditions, the voltammograms produced via CV of tetra-*n*-butylammonium acetate in 0.5 M H_2O in acetonitrile were typical of normal electron transfer reactions of small organic structures where bond breaking does not occur concurrently with electron transfer. The voltammograms exhibited a peak width of ca. 95 mV, a typical value for most small organic electrolytes. These peak widths indicate that the value of the transfer coefficient α is approximately 0.5, indicative of a small reorganization energy.

These values are not unusual for a standard electron transfer reaction, which may then be followed by a chemical step involving bond breaking or formation. It then appears that addition of water to the acetonitrile leads to a significant change in the intrinsic barrier of the electron transfer. This often indicates a change in reaction mechanism (*vide infra*).

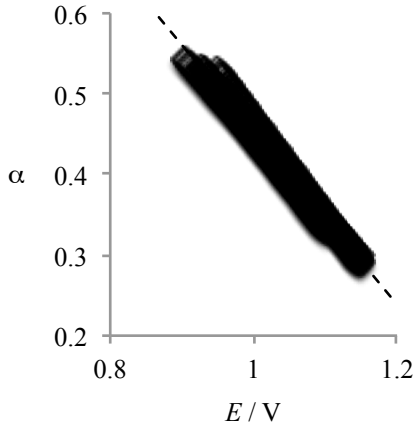

Figure 3.7: α vs. *E* for the oxidation of tetra-*n*-butylammonium acetate in 0.5 M H_2O/acetonitrile (0.5 M supporting electrolyte, ν = 0.1, 0.2, 0.3, and 0.4 V/s). Linear regression analysis allowed for determination of E^o_{ox} of the acetate anion at α = 0.5.

As with those produced in neat acetonitrile, the voltammograms were subjected to convolution analysis. The value of the transfer coefficient as a function of potential was determined via fitting to the Marcus equation (α vs *E* given in **Figure 3.7**). At α = 0.5 the formal oxidation potential of tetra-*n*-butylammonium acetate in 0.5 M H_2O/acetonitrile can be obtained and is found to be 0.959 ± 0.011 V (vs. $Ag/AgNO_3$).

3.2.2.2 Indirect electrochemistry

Addition of water to the solvent dramatically slows catalysis in the indirect electrochemistry of the acetate anion. This is demonstrated qualitatively in **Figure 3.8**, where the voltammogram presented in **Figure 3.8a** was obtained in neat acetonitrile and that presented in

Figure 3.8b was obtained after addition of one drop of deionized water to the solution. It is apparent that water plays a major role, by either contributing to the magnitude of the intrinsic barrier for electron transfer or by altering the thermodynamic parameters of the electron transfer (i.e. – the oxidation potential).

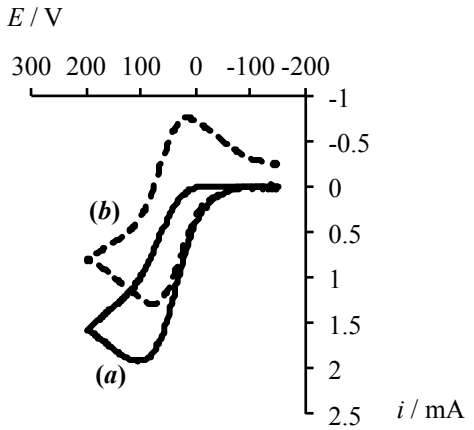

Figure 3.8: HRC voltammogram for tetra-*n*-butylammonium acetate in (*a*) neat acetonitrile and (*b*) after addition of one drop of water. (0.5 M supporting electrolyte).

HRC experiments were performed in the water/acetonitrile solvent and the resulting $i_p/\gamma i_{pd}$ versus $\log\left(\frac{1}{\nu}\right)$ plots are presented in **Figure 3.9**. The most obvious feature of the data when contrasted with that obtained from experiments in neat acetonitrile is that the catalysis has been significantly decreased; as a result the sweep rate had to be decreased in the HRC experiments in order to obtain a large enough catalytic current to make analysis of the data possible. The data can be fit to simulated working curves as described previously and the results are given in **Table 3.1**. (Plots of all the fit data are available in **5.2**.)

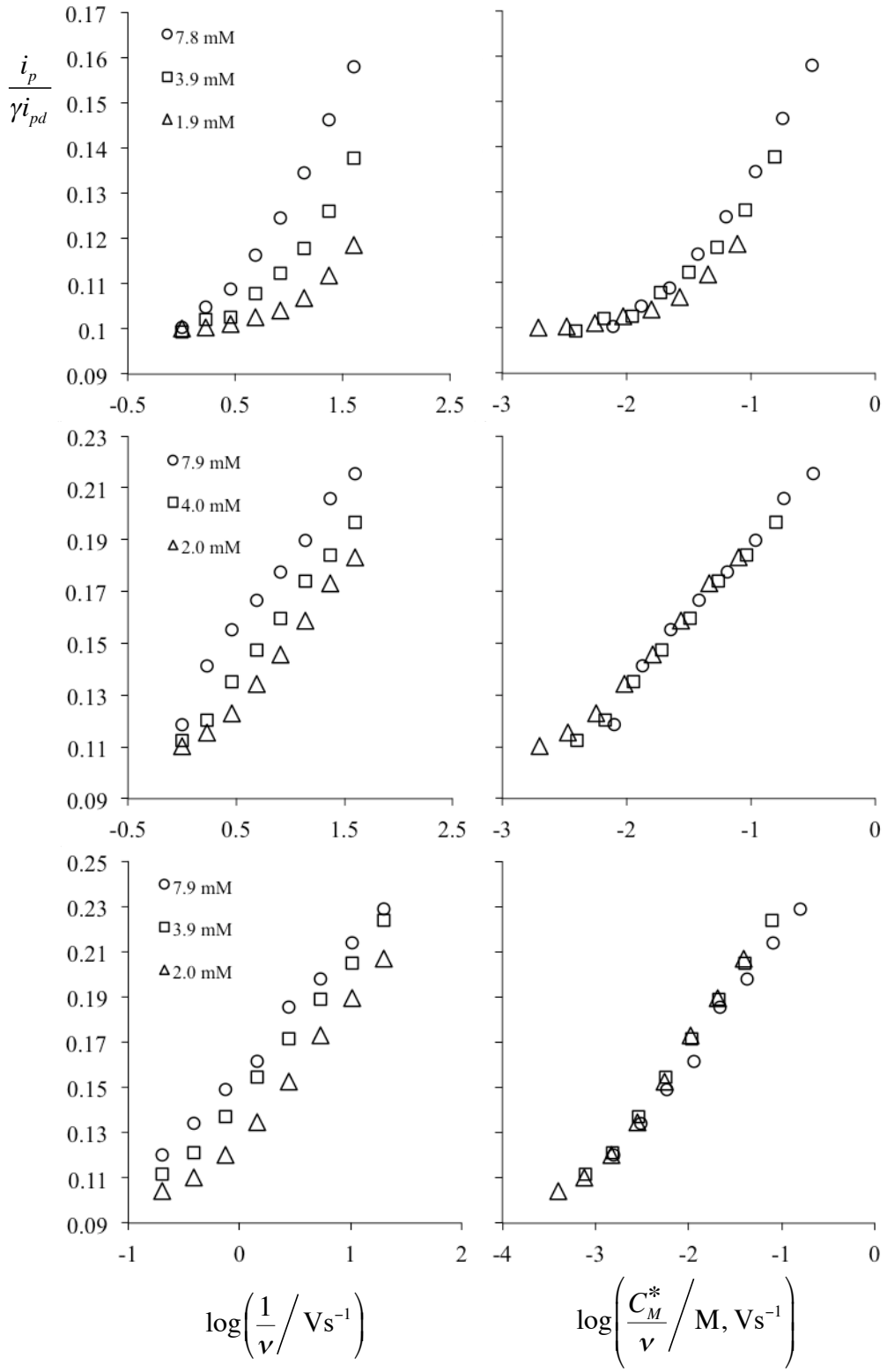

Figure 3.9: Mediated oxidation of tetra-*n*-butylammonium acetate in 0.5 M H_2O/acetonitrile (0.5 M supporting electrolyte, γ = 10). (*a*) Ferrocene, (*b*) Vinylferrocene, (*c*) *p*-Bromophenylferrocene. Dependence of catalysis on mediator concentration indicates kinetic control by the homogeneous electron transfer.

3.3 Discussion

Based on the indirect and direct electrochemical data presented above it is clear that addition of water to the system entails a major change in, if not the overall reaction mechanism, then the parameters that govern the electron transfer reaction – i.e. the kinetic parameters (inner and outer reorganization energy) and the thermodynamic parameter (the apparent oxidation potential of tetra-*n*-butylammonium acetate). Of course, the difference between the neat and wet acetonitrile systems could indicate that the mechanism has changed (perhaps from a concerted to a stepwise reaction, **Scheme 3.4**) or even that the oxidized species may in fact not be the acetate anion in both cases. To answer these questions the results of both direct and indirect electrochemistry are examined for each case below and then the systems are compared with one another.

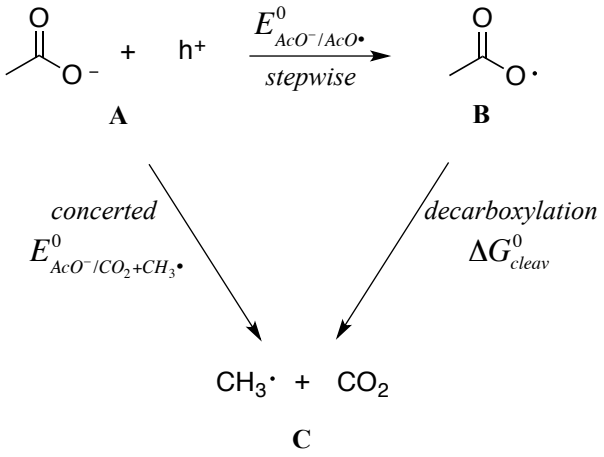

Scheme 3.4: Stepwise vs. concerted oxidation and decarboxylation of the acetate anion. $\Delta G^0_{cleav} = -nF\left(E^0_{AcO^-/AcO\cdot} - E^0_{AcO^-/CO_2+CH_3\cdot}\right)$.

3.3.1 Neat acetonitrile

The direct oxidation of the acetate anion at the electrode surface in neat acetonitrile is an electron transfer controlled reaction with a large intrinsic activation barrier. As previously described, the value of the transfer coefficient α is indicative of the size of the intrinsic barrier. For an observed $\alpha \approx 0.3$ under normal cyclic voltammetry experiments, the intrinsic barrier must be quite large, larger than typical for the usual electron transfer reactions of small organic structures. The most common interpretation of these results is that the electron transfer and decarboxylation occur simultaneously – that the reaction follows a concerted dissociative electron transfer mechanism (**Scheme 3.4**). The Marcus Hush model for outer sphere electron transfer does not upon first inspection appear to apply to electron transfers that occur concurrently with bond breaking. Savéant[2] extended the model to include this concerted case as given in **Eq. 3.5**, where the intrinsic barrier includes a contribution equal to one quarter of the bond dissociation energy of the cleaved bond (*D*).

$$\Delta G^{\ddagger} = \frac{(D + \lambda_o)}{4}\left(1 + \frac{\Delta G^0}{D + \lambda_o}\right)^2 \qquad \textbf{Eq. 3.5}$$

Bond dissociation energies are very large relative to typical internal reorganization energies and thus the intrinsic barrier for concerted dissociative electron transfers are much larger than in the case of a stepwise reaction. This results in large measured values of the transfer coefficient in a cyclic voltammetry experiment, as the potential of the electrode must be much larger than the oxidation potential of the electrolyte to overcome this large intrinsic barrier.

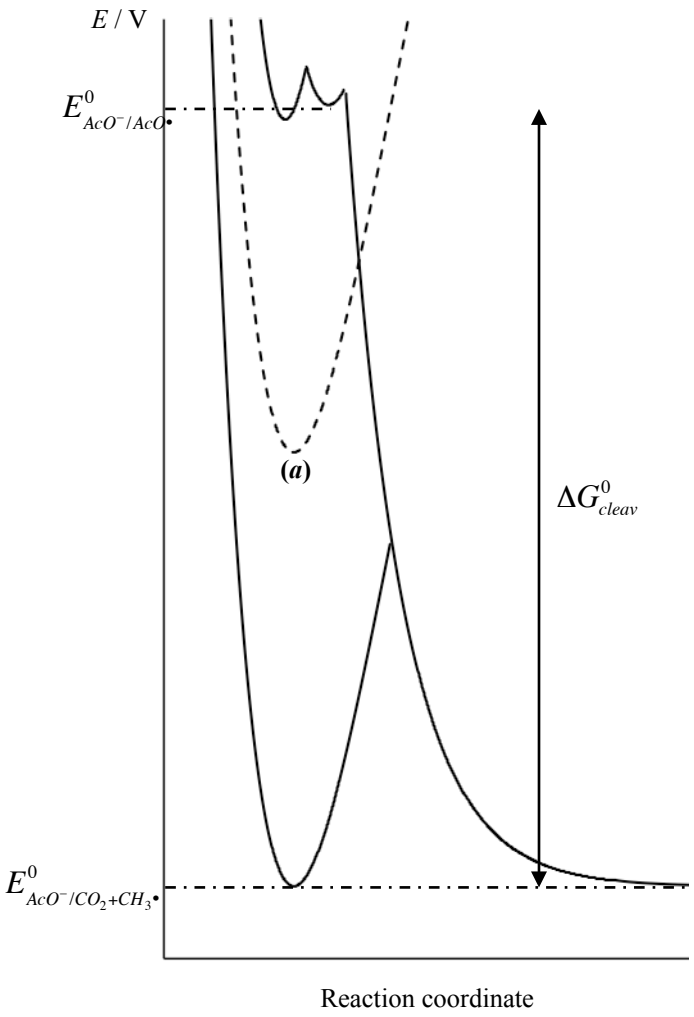

Figure 3.10: Reaction coordinate diagram showing a possible concerted-to-stepwise transition of the mechanism for oxidation of acetate and relevant potentials and Gibb's energies. (*a*) Potential well corresponding to an observed concerted DET process. Increasing driving force increases (*a*) until it crosses the potential well corresponding to the stepwise intermediate, where the observed mechanism transitions from concerted to stepwise. The potential *E* can represent either the potential of the working electrode in direct oxidation or the potential of the mediator relative to E^o_{ox} in redox catalysis. Adapted from reference 8.

Figure 3.10 shows the oxidation at the electrode surface in both the concerted and stepwise dissociative electron transfer cases. Attention should be paid to the different redox couples and the subtle differences between them (**Scheme 3.4**). In the concerted case the measured oxidation potential is for the couple corresponding to the parent anion and the cleaved product composite, $E^0_{AcO^-/CO_2+CH_3^{\cdot}}$; this potential includes a contribution from the potential associated with the decarboxylation.

$$\Delta G^{\ddagger} = \frac{(D + \lambda_o)}{4}\left(1 + \frac{nF\left(E^0_{AcO^-/CO_2+CH_3^{\cdot}} - E\right)}{D + \lambda_o}\right)^2 \qquad \textbf{Eq. 3.6}$$

The Savéant equation can be written in terms of a heterogeneous oxidative electrode reaction (**Eq. 3.6**), where *E* is the potential of the electrode. Recall that $\alpha = \frac{\partial \Delta G^{\ddagger}}{\partial \Delta G^0}$, then, in terms of electrode potential:

$$\alpha = \frac{\partial \Delta G^{\ddagger}}{-nF\partial E} = \frac{1}{2} + \frac{nF\left(E^0_{AcO^-/CO_2+CH_3^{\cdot}} - E\right)}{2(D + \lambda_o)}$$

So then at $\alpha = 0.5, E = E^0_{AcO^-/CO_2+CH_3^{\cdot}}$. In this treatment the standard oxidation potential obtained from the convolution of the cyclic voltammetry data is the oxidation potential of the concerted dissociative electron transfer process, $E^0_{AcO^-/CO_2+CH_3^{\cdot}} = 0.730 \pm 0.025$ V.

The oxidation potential may be obtained via a second method, using the HRC data. The rate constants for the homogeneous electron transfers can be expressed as a function of the driving force $nF\left(E^0_{M/M^{\cdot+}} - E^0_{AcO^-}\right)$, **Eq. 3.7,** where k_D is the diffusion controlled rate constant and k^S_{ET} is the electron transfer rate constant when $E^0_{AcO^-} = E^0_{M/M^{\cdot+}}$. It is not immediately clear if the oxidation potential of acetate here is that associated with the concerted or stepwise dissociative electron transfer processes. A plot of log k_{obs} versus $E^0_{M/M^{\cdot+}}$ is called a Marcus plot[91] (**2.3.1**), and exhibits three distinct regions as each term in **Eq. 3.7** comes to dominate the value of k_{obs}.

$$\frac{1}{k_{obs}} = \frac{1}{k_D} + \frac{1}{k^S_{ET}\exp\left\{\left(\frac{\alpha nF}{RT}\right)\left(E^0_{M/M^{\cdot+}} - E^0_{AcO^-}\right)\right\}} + \frac{1}{k_D\exp\left\{\left(\frac{nF}{RT}\right)\left(E^0_{M/M^{\cdot+}} - E^0_{AcO^-}\right)\right\}} \qquad \textbf{Eq. 3.7}$$

These three regions are named the diffusion controlled $\left(\frac{1}{k_D}\text{ dominates}\right)$, activation controlled $\left(\frac{1}{k_{ET}^{S}\exp\left\{\left(\frac{\alpha nF}{RT}\right)\left(E^{0}_{M/M^{\cdot+}}-E^{0}_{AcO^{-}}\right)\right\}}\text{ dominates}\right)$, and counter-diffusion controlled $\left(\frac{1}{k_D\exp\left\{\left(\frac{nF}{RT}\right)\left(E^{0}_{M/M^{\cdot+}}-E^{0}_{AcO^{-}}\right)\right\}}\text{ dominates}\right)$ regimes, respectively. Each regime corresponds to a linear region of the plot that exhibits a different slope ($m_{diff} = 0$, $m_{act} = 8.54\ V^{-1}$, and $m_{cnt\text{-}diff} = 17.08\ V^{-1}$, see **2.3.1**) than the other regions. Plotting log k_{obs} against the oxidation potential of the mediators given in **Table 3.1** and subsequent linear regression analysis of the data gives the slope (in this case $19 \pm 5\ V^{-1}$). The value of the slope indicates which regime of control is exhibited in the data. For the HRC experiments performed with this set of mediators, it appears that the counter-diffusion step is rate limiting ($19 \pm 5\ V^{-1} \approx 17.08\ V^{-1}$).

As implied above, global stepwise dissociative electron transfer is actually a series of three elementary steps followed by bond cleavage. These are diffusion of the mediator and substrate together, electron transfer, and counter diffusion of the product species apart. Each of the regimes described previously corresponds to one of these steps being rate limiting. In the case of the mediators given above, the counter-diffusion step appears to be the rate-limiting step. In such cases the theoretical slope can be used to extrapolate back to the point where log k_{obs} = log k_D. At this point $E^{0}_{AcO^{-}} = E^{0}_{M/M^{\cdot+}}$ and the oxidation potential $E^{0}_{AcO^{-}}$ is obtained. In this system the oxidation potential is found to be 0.43 ± 0.08 V (vs. $Ag/AgNO_3$).

This value of the oxidation potential is incompatible with that obtained from the direct electrochemistry experiments (0.730 ± 0.025 V). It is well outside the possible experimental error. It may be that the two oxidation potentials obtained, E^{0}_{conv} and E^{0}_{HRC} are not measures of the oxidation potential for the same process; perhaps one corresponds to a stepwise electron transfer process and the other to a concerted process.

This hypothesis can immediately be discarded intuitively on the grounds of **Figure 3.10**. The oxidation potential for a stepwise process should be much more positive than that measured for a concerted process; this would only make the discrepancy between the direct and indirect electrochemistry larger. Nevertheless, it is instructive to look at how the Marcus plot would be different in the case of a different reaction mechanism (concerted versus stepwise dissociative electron transfer).

The standard Marcus plot derived from **Eq. 3.7** assumes that the product of electron transfer is long lived enough to survive the time required for diffusion away from the mediator after electron transfer. In the case of a concerted dissociative electron transfer this is obviously incorrect, as the product of the electron transfer *is* the cleaved product ensemble. Furthermore, if the rate of decomposition of the *stepwise* electron transfer is large enough the electron transfer product will decay previous to or concurrent with counter-diffusion of the product ensemble away from the mediator.

In the case of a concerted dissociative electron transfer the Marcus plot still contains three regions: diffusion control, activation control, and counter-diffusion control. The form of the equation governing the reaction is exactly that of **Eq. 3.7**, only the oxidation potential is clearly the oxidation potential of the concerted process, $E^0_{AcO^-} = E^0_{AcO^-/CO_2+CH_3\cdot}$. The slopes of the three regions correspond exactly to the slopes presented above. In practice, the third region corresponds to values of $E^0_{M/M^{\cdot -}} - E^0_{AcO^-/CO_2+CH_3\cdot}$ so small that the resulting rate constants are below the lower limit of detection for HRC experiments, and no data from HRC experiments should give a slope smaller than ≈ 17 V^{-1} within experimental error.

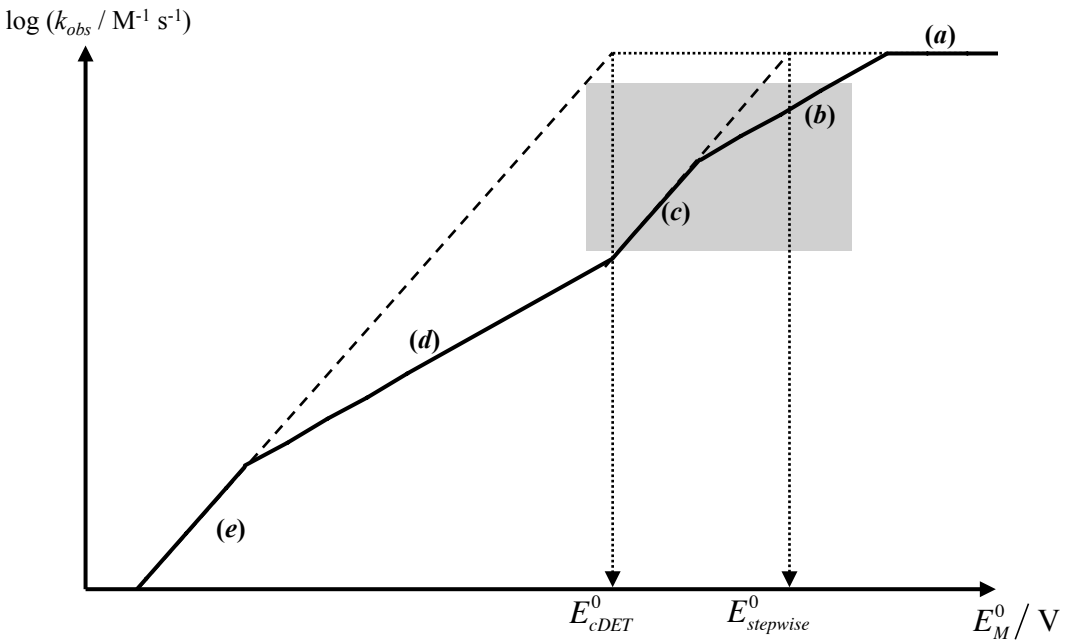

Figure 3.11: Schematic representation of a Marcus plot in the case of competing concerted and stepwise pathways. The shaded area is the typical area accessible in the homogeneous redox catalysis method (*a*) Diffusion control (*b*) Activation by stepwise electron transfer (*c*) Counter-diffusion control in the stepwise case (*d*) Activation by concerted dissociative electron transfer (*e*) Counter-diffusion control in the concerted case. Extrapolation of (*c*) and (*e*) to the diffusion controlled rate yields the oxidation potentials for the stepwise and concerted pathways, respectively.

However, the second possibility is more intriguing. If the following chemical step is very fast, as decarboxylation is expected to be, the Marcus plot may potentially exhibit five possible regions (**Figure 3.11**).[91] The reasons for this expected behavior are not intuitively obvious, and should be explored further.

Of particular interest to this discussion is how the mechanism for a dissociative electron transfer reaction transitions from a concerted to a stepwise pathway. It first must be made clear that the existence of a concerted mechanism does not imply that the uncleaved intermediate does not exist. Indeed, the uncleaved intermediate may exist, but only at potentials much higher than the cleaved product ensemble[8] (this follows from the idea that most fast bond-breaking reactions are thermodynamically very favorable), see **Figure 3.10**. At low driving force (curve (*a*), **Figure 3.10**) the concerted pathway is not only preferred; it is the only accessible pathway. One should

also note that the activation barrier for such concerted reactions at low driving force are very large, as predicted by the Savéant model.

As driving force is increased (by increasing the oxidation potential of the mediator) the global electron transfer rate constant increases (the intrinsic barrier decreases, in keeping again with Marcus and Savéant). At some point, however, the potential energy surface of the uncleaved electron transfer product becomes accessible. At this transition point the mechanism changes from a concerted dissociative electron transfer to a stepwise dissociative electron transfer. Although not shown explicitly in **Figure 3.10**, this stepwise mechanism can be further reduced to the normal electron transfer elementary steps (diffusion, activation, and counter-diffusion) described previously. Working in the reverse direction (from large driving force to small driving force), the regimes of kinetic control would be as follows (right to left in **Figure 3.11**): diffusion of the HRC couple together (m = 0 V^{-1}), activation of the stepwise electron transfer reaction (m = 8.54 V^{-1}), counter-diffusion of the electron transfer products apart from one another (m = 17.08 V^{-1}), activation of the concerted dissociative electron transfer reaction (after the transition of the mechanism from a stepwise pathway to a concerted pathway with decreasing driving force, m = 8.54 V^{-1}), and finally to counter-diffusion of the concerted dissociative electron transfer product ensemble apart from one another at very small driving force (m = 17.08 V^{-1}). In principle all 5 of these regimes are possible. The size and even existence of some of these potential rate-controlling regions depend on the specifics of each system (does the uncleaved electron transfer product "exist" at k_BT, what is the magnitude of the cleavage rate constant in the stepwise pathway, what potential does the uncleaved electron transfer product exist at relative to the cleaved product ensemble, and so forth.). As with the purely concerted case, the fifth possible region (counter-diffusion of the concerted dissociative

electron transfer product ensemble) is not observable on the timescale of typical HRC experiments and can be ignored.

One interesting feature of the above system is that in the case where the following chemical step is very fast – that is, fast enough to occur before diffusion outside of the solvent sphere of the mediator but not quite so fast as to occur concurrently with the electron transfer (i.e. – not a concerted mechanism) – the effect is to push the counter-diffusion control region of the plot to smaller driving force. This could potentially result in an underestimation of the substrate oxidation potential if the procedure for fitting to a standard Marcus plot were used – as shown previously for the acetate anion to obtain the oxidation potential of the anion in neat acetonitrile as $E^0_{AcO^-}$ = 0.429 ± 0.08 V. If this were the situation with tetra-*n*-butylammonium acetate then perhaps the discrepancy between the two pieces of electrochemical data could be explained. (i.e. – that E^0_{conv} = 730 mV and E^0_{HRC} = 429 mV is an artifact of underestimation of the E^0_{HRC} value by ignoring a possible transition at lower driving force into a concerted mechanism).

Unfortunately, it has been shown[91] that the maximal error introduced by ignoring the possible concerted pathway (at 29 ºC) is 83 mV for typical systems such as this. At worst, (including experimental error) the potential may be underestimated by ca. 160 mV, which still does not account for the difference in measured potential between E^0_{conv} and E^0_{HRC}. It is thus determined that the two experimental results are simply not compatible, and a new, entirely different, explanation must be proposed to explain these results (*vide infra*).

3.3.2 0.5 M H_2O/acetonitrile

Unlike in neat acetonitrile, the voltammetry of tetra-*n*-butylammonium acetate in 0.5 M H_2O in acetonitrile is very typical for a "normal" oxidation of a small organic molecule. The

peak widths are the common 95 mV $\left(E_p - E_{p/2} = 1.86\frac{RT}{\alpha nF} = \frac{47.8}{\alpha}mV\right)$ at room temperature expected for a one-electron oxidation without a large reorganization energy ($\alpha \approx 0.5$). Convolution of the voltammetry data and subsequent fitting of the α versus E data leads to a measured value of $E^0_{AcO^-} = 0.959 \pm 0.012$ V (**3.2.2.1**).

It is interesting that the oxidation potential of the anion increases by ca. 240 mV upon addition of water. It should be noted that although the apparent addition of water is small, it is still present in ≈ 150x the analyte concentration ($C^*_{AcO^-} = 0.001 - 0.004$ M). It is not unreasonable to assume that because of the large excess of water and likely hydrogen bonding with the acetate the oxidation could be considered to be that of an acetate/water complex as opposed to oxidation of a "normal" acetate anion in acetonitrile

The most obvious explanation of the differences between the anhydrous and wet electrochemistry is that the mechanism has changed upon addition of the water, in this case from a concerted mechanism in neat acetonitrile to a stepwise mechanism in the wet acetonitrile. Although this interpretation agrees qualitatively with the data, it should be examined more closely to determine if it is sensible.

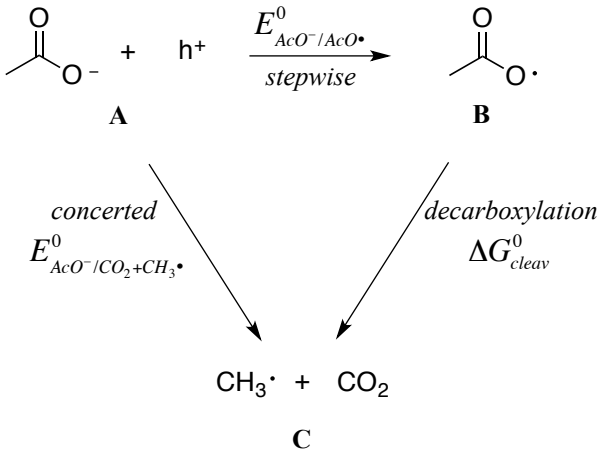

Scheme 3.4: Stepwise vs. concerted oxidation and decarboxylation of the acetate anion.
$\Delta G^0_{cleav} = -nF\left(E^0_{AcO^-/Ac\cdot} - E^0_{AcO^-/CO_2+CH_3\cdot}\right)$

Scheme 3.4 is presented again here for convenience. As stated before, the reaction mechanism may be driven from a concerted mechanism to a stepwise mechanism in two fashions. The first is to increase driving force (typically accomplished by increasing the scan rate, ν), and the second is to lower the potential well of the uncleaved intermediate to make it accessible in the experimental conditions.

To understand how changing sweep rate can lead to a change in the observed mechanism, it is simplest to first imagine a potential step experiment. The electrode potential may be stepped instantaneously (within experimental means) from some potential $E < E^0_{AcO^-/CO_2+CH_3\cdot}$ to a potential where the stepwise mechanism is observed. Since a potential step experiment is essentially a linear sweep voltammetry experiment where the sweep rate, ν, approaches infinity, it is straightforward to see that increasing sweep rate eventually leads to a change in observed mechanism from a concerted to a stepwise pathway. Although this is by far the most common way to observe a change in mechanism from concerted to stepwise in the literature, it is not the case here as comparable sweep rates have been used in both the dry and wet systems.

The second possible way to change the mechanism is to change the potential of the stepwise intermediate **B** in such a way as to make it accessible within the experiment potentials.

This can be rationalized in one of two (equivalent) ways. First, the concerted dissociative pathway consists of the acetate anion and an electron "hole" (h^+) as reactants. This hole represents the Fermi level of the working electrode to which the electron from acetate will transfer and is directly controlled by the potential of the electrode. It is not unreasonable to assume that the electrochemical potential of the anion will be lowered in solution significantly by addition of water, much more so than the products of the cleavage reaction (the methyl radical and carbon dioxide). Since by definition the oxidation potential is the electrode potential where the concentrations of the redox couple ($AcO^-/CO_2 + CH_3\cdot$) are equal, the potential of the hole, h^+, must increase by an amount equal in magnitude to the stabilization of the anion by addition of water. The net effect is an apparent increase of the potential of the product ensemble (**Figure 3.12**). The same idea can be applied to the stepwise electron transfer, however, it can be expected that the addition of water would also have some effect on lowering the electrochemical potential of the stepwise intermediate, **B**. The net effect would be to lower the potential well of the intermediate to the product ensemble (**Figure 3.12**). An equivalent line of reasoning would be that the addition of water would lower the potential of **B** relative to the product ensemble, decreasing driving force for bond cleavage and making the stepwise pathway more accessible. (Although this second explanation is qualitatively correct it is not as convenient as it fails to clarify why the oxidation of the decarboxylation product ensemble is expected to have a higher oxidation potential upon addition of water.)

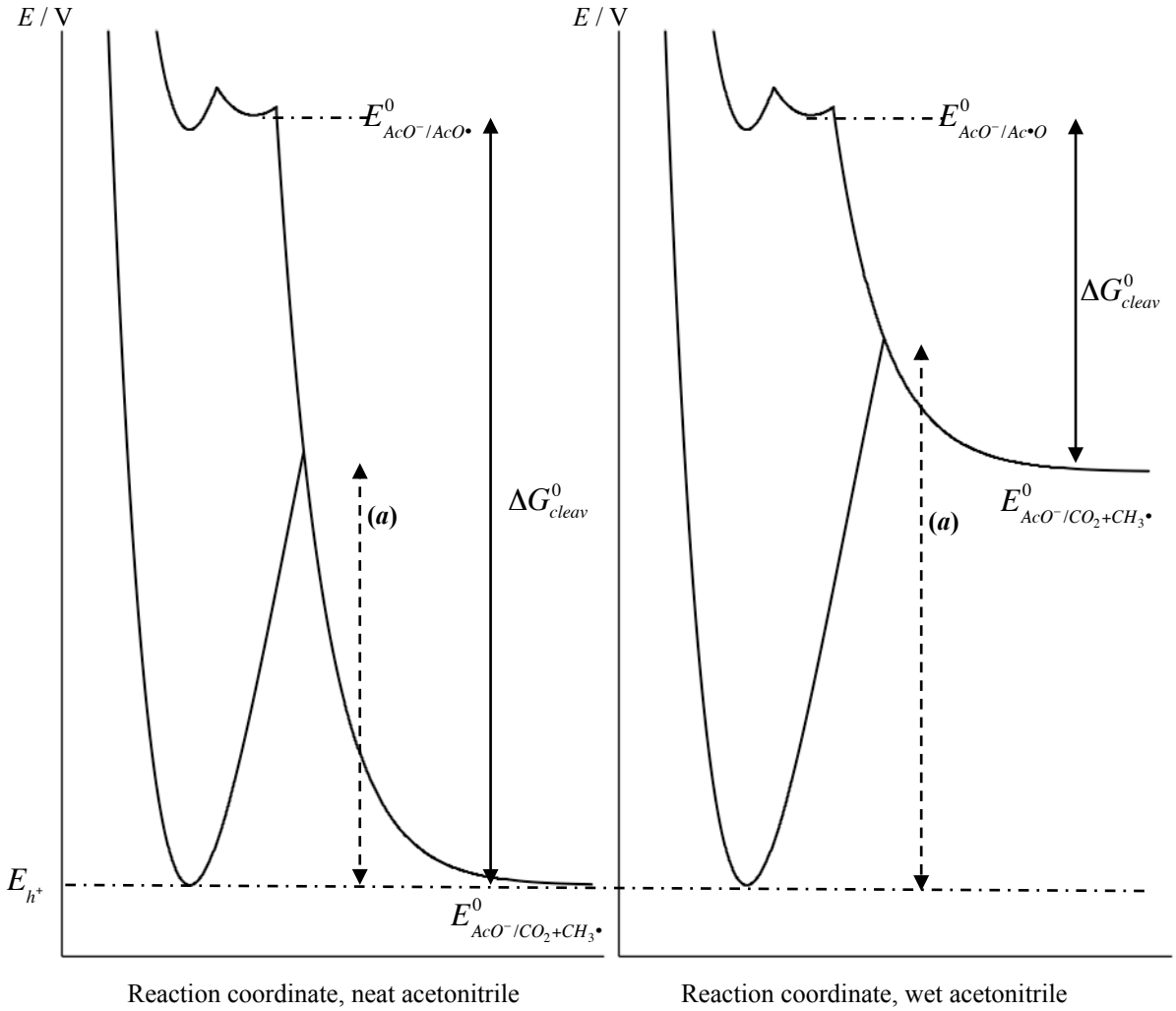

Figure 3.12: Reaction coordinate diagram showing possible concerted-to-stepwise transition of the mechanism upon addition of water for oxidation of acetate and relevant potentials and Gibb's energies. If addition of water stabilizes the stepwise intermediate relative to the cleaved product ensemble, the Gibb's energy for decarboxylation will decrease at the cost of an increase in the concerted electron transfer activation barrier (*a*) for any given potential of the electrode E_{h^+}.

It is reasonable that the preceding explains the difference in observed α and $E^0_{AcO^-}$ for the wet and dry acetonitrile systems. In the case of neat acetonitrile, the observed α corresponds to the transfer coefficient observed for a concerted process where the intrinsic barrier is increased because of the contribution of the bond breaking process as in the Savéant model, and $E^0_{AcO^-} = E^0_{AcO^-/CO_2+CH_3}$. In the wet system, the observed α corresponds to a stepwise electron transfer with small intrinsic barrier and $E^0_{AcO^-} = E^0_{AcO^-/AcO}$. as in the Marcus Hush model.

One potential problem with the above analysis concerns the difference in potential between the two electron transfer steps, $\Delta E_{B/C} = E^0_{AcO^-} - E^0_{AcO^-/CO_2+CH_3\cdot}$, where **B** and **C** correspond to the cleavage reactants and products as labeled in **Scheme 3.4**. It can be shown that this quantity corresponds roughly to the Gibb's free energy for decarboxylation of the acetoxyl radical. The free energy of reaction for the concerted and stepwise electron transfers can be written as, respectively:

$$\Delta G_{cDET} = -nF\left(E - E^0_{AcO^-/CO_2+CH_3\cdot}\right)$$

$$\Delta G_{stepwise} = -nF\left(E - E^0_{AcO^-/AcO\cdot}\right)$$

Where *E* is the electrode potential. The difference of these Gibb's energies gives the free energy for cleavage of the stepwise intermediate:

$$\Delta G_{cDET} - \Delta G_{stepwise} = \Delta G_{cleav}$$

$$\Delta G_{cleav} = -nF\left(E - E^0_{AcO^-/CO_2+CH_3\cdot}\right) + nF\left(E - E^0_{AcO^-/AcO\cdot}\right)$$

$$\Delta G^0_{cleav} = -nF\left(E - E^0_{AcO^-/CO_2+CH_3\cdot} - E + E^0_{AcO^-/AcO\cdot}\right)$$

$$\Delta G^0_{cleav} = -nF\left(E^0_{AcO^-/AcO\cdot} - E^0_{AcO^-/CO_2+CH_3\cdot}\right)$$

From the experimental data then an approximation of the cleavage driving force, ΔG^0_{cleav}, may be obtained as –5.3 ± 0.6 kcal/mol. It should be noted that $E^0_{AcO^-/AcO\cdot}$ was obtained in the presence of water and $E^0_{AcO^-/CO_2+CH_3\cdot}$ was not, and the influence on the thermodynamics of the system by addition of water has here been ignored.

$$CH_3COO^-/H_2O \longrightarrow CH_3COO^{\cdot}/H_2O + e^- \qquad \Delta G_{stepwise} = -nF\left(E - E^0_{stepwise}\right)$$

$$CH_3COO^- + H_2O \longrightarrow CH_3COO^-/H_2O \qquad \Delta G_2$$

$$CH_3COO^{\cdot}/H_2O \longrightarrow CH_3COO^{\cdot} + H_2O \qquad \Delta G_3$$

$$CH_3COO^{\cdot} \longrightarrow CH_3^{\cdot} + CO_2 \qquad \Delta G_{cleav}$$

$$CH_3COO^- \longrightarrow CH_3^{\cdot} + CO_2 + e^- \qquad \Delta G_{cDET} = -nF\left(E - E^0_{cDET}\right)$$

Scheme 3.5: Thermodynamic cycle for the concerted-to-stepwise dissociative electron transfer mechanism upon addition of water to the system

A more detailed treatment of the data can be obtained via the thermodynamic cycle given in **Scheme 3.5**, which includes the effect of water in the system. A value of $\Delta G_{cleav} = -34.0$ kcal/mol was obtained from frequency calculations on the gas-phase decarboxylation of the acetoxyl radical at 300 K (optimizations and frequency calculations performed with MP2[92] theory and the AUG-CC-PVTZ Dunning basis set[93]). It can be seen that the difference between the oxidation potentials obtained in wet and dry acetonitrile gives the sum $\Delta G_2 + \Delta G_3 + \Delta G_{cleav} = -nF\left(E^0_{stepwise} - E^0_{cDET}\right)$. Under the assumption that the dry system follows a concerted path and the wet a stepwise path, then $\Delta G_2 + \Delta G_3 = -nF\left(E^0_{AcO^-/AcO\cdot} - E^0_{AcO^-/CO_2+CH_3\cdot}\right) - \Delta G_{cleav} = -5.3\,\text{kcal/mol} + 34.0\,\text{kcal/mol}$, (see **Scheme 3.6**). This hugely endergonic value would need to correspond to exchange of a water molecule from the neutral acetoxyl radical to the acetate anion – an absurd result. Given this, it is apparent that the change in the voltammetric behavior in the system upon addition of water does not correspond to a change in mechanism from a concerted to stepwise dissociative electron transfer pathway.

$$CH_3COO^- + H_2O \longrightarrow CH_3COO^-/H_2O \qquad \Delta G_2$$

$$CH_3COO^{\cdot}/H_2O \longrightarrow CH_3COO^{\cdot} + H_2O \qquad \Delta G_3$$

$$CH_3COO^- + CH_3COO^{\cdot}/H_2O \longrightarrow CH_3COO^-/H_2O + CH_3COO^{\cdot} \qquad \Delta G_{H_2O\ exchange}$$

Scheme 3.6: Gibb's energy for exchange of a water molecule from the acetoxyl radical to the acetate anion. For the hypothesis that the reaction follows a concerted pathway in dry acetonitrile and a stepwise reaction in wet acetonitrile to hold $\Delta G_{H_2O\ exchange}$ must be ca. 30 kcal/mol.

The indirect electrochemistry for the wet acetonitrile parallels the dry case. **Figure 3.13** gives the Marcus plot. What should be first noted is the slope of the experimental data is larger than theoretically possible at 28 ± 9 V^{-1}. This may just be an artifact of the difficulty of HRC with this experiment and only being able to use three mediators in the analysis. Nevertheless, the slope of the curve only matches counter-diffusion control as the activation and diffusion regimes have even lower slopes (*vide ante*). When treated as previously to obtain an oxidation potential for acetate in the HRC experiments, the oxidation potential was once again found to be much less than that obtained directly, with $E^0_{AcO^-} = 0.51 \pm 0.09$ V (vs. Ag/NO_3) (where $E^0_{AcO^-} = 0.959 \pm 0.012$ V from convolution voltammetry in wet acetonitrile). Again, even when considering the possible errors arising from ignoring in-cage decarboxylation in a fast chemical step (maximum underestimation of oxidation potential by 83 mV) the direct and indirect electrochemical results are simply incompatible.

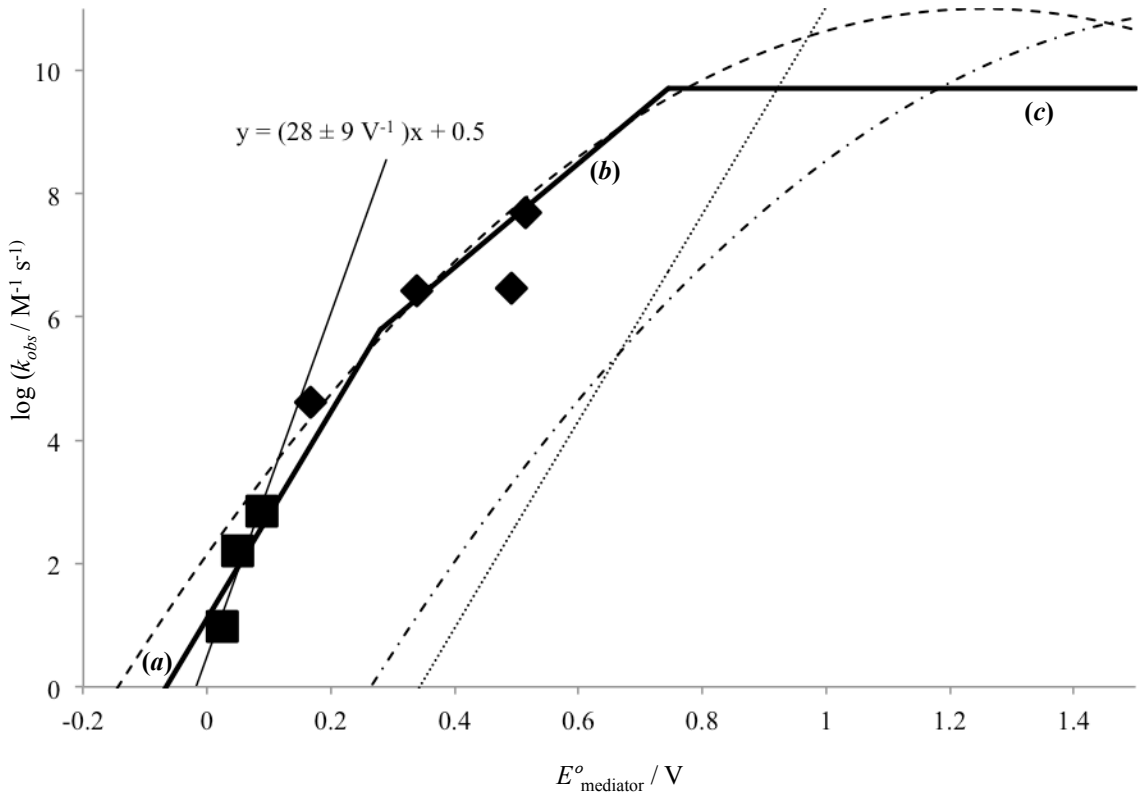

Figure 3.13: Marcus plot of tetra-*n*-butylammonium acetate. Heavy line segments (*a*), (*b*), and (*c*) correspond to the three regions of electron transfer control with slopes of 17.08 V^{-1} (counter-diffusion control), 8.54 V^{-1} (activation control), and 0 V^{-1} (diffusion control) respectively. Squares (■) correspond to the ferrocene derivative mediators presented in the text (trend line and regression equation shown) and diamonds (◆) correspond to N,N-dimethylaniline derivatives (see text). The dashed curve is the Marcus curve for electron transfer generated from the HRC data. The dashed-dotted curve is the Marcus curve for electron transfer generated from the convolution voltammetry data. The dotted line is the line for the counter-diffusion control region expected from the convolution voltammetry data. The HRC data is too large (above the dotted line) by ca. 6 orders of magnitude.

Homogeneous redox catalysis experiments have been performed previously with the tetra-*n*-butylammonium acetate anion using dimethyaniline and a series of dimethylaniline derivatives as mediators.[96] It was shown that the acetate underwent electron transfer with the activated dimethylanaline radical anion in a redox catalysis process. As such, the data from these experiments should fit on a Marcus plot with the data gathered from the ferrocene derivative redox catalysis experiments presented here. In fact, the data fits remarkably well (**Figure 3.13**, diamond markers). The fitting parameters to obtain this Marcus plot are $E^0_{AcO^-} = 0.510$ V, $k^S_{ET} =$ 5.5 x 10^7 M^{-1} s^{-1}, and $k_D = 5$ x 10^9 M^{-1} s^{-1}. The fit is appealing, with one glaring exception: the

oxidation potential of acetate is 400 mV below that obtained from direct electrochemistry of the anion.

3.3.3 Final analysis

The indirect electrochemistry of the acetate anion should be addressed first. It is obvious that an interpretation of the HRC data via Marcus analysis is quantitatively incorrect. The oxidation potentials thus obtained simply cannot belong to anything in solution. If there were something (acetate anion or else) in solution with an oxidation potential of ca. 400 – 500 mV there would be an oxidative current drawn in the direct cyclic voltammetry of the systems near these potentials. Even in the case of an electron transfer with a very large intrinsic barrier (larger even than commonly seen in, for example, a typical concerted dissociative electron transfer), the observed wave, though shifted anodically, would be extremely broad, and convolution analysis would point towards an oxidation potential in the 400-500 mV range. Were HRC possible for such a system, the oxidation potential of the mediators would need to be very positive relative to that of the substrate to even drive such a reaction. In the case of the acetate system presented above, the oxidation potentials of the mediator are actually well negative of that obtained for acetate from the data. If this were the case, redox catalysis for this series of mediators should be so slow as to be unobservable with this technique (i.e. – the half life of the homogeneous electron transfer reactants would be significantly longer than the longest possible cyclic voltammetry experiment). Regardless, the oxidative wave in the case of the 0.5 M H_2O/acetonitrile mix is unexceptionally narrow, at ca. 95 mV; this example is simply incompatible with having an oxidation potential remotely near that required by the Marcus analysis of the HRC data.

A different mechanism must therefore be at play in the HRC experiments. The Marcus model, as well as the Savéant model, is intended to model outer sphere electron transfer, meaning that there is no meaningful bond formed in the transition state structure of the electron transfer process. In the case of an inner sphere electron transfer, where substantial bonding is found in the transition state structure, the rate of reaction is typically much larger than that for an outer sphere electron transfer, usually several orders of magnitude faster.[98] Very often a Marcus-like plot can be built from inner sphere electron transfers, and assuming every mediator in the series undergoes a similar inner sphere process the log k_{obs} versus E data can appear to follow a Marcus curve; however, the Marcus Hush model is not applicable in these cases. Any oxidation potential or other parameter obtained via Marcus analysis in such cases are not applicable, as they are measurements of a potential associated with an inner sphere process and not the true outer sphere electron transfer, where things like an oxidation potential are applicable.

Ferrocenium, the activated form of the ferrocene mediator, appears on first glance to be a poor candidate for an inner sphere electron transfer reaction. However, due to spin polarization, it has been shown that a significant amount of spin is located on the cyclopentadiene ligands.[99] This opens many possible mechanistic pathways for bond formation to the cyclopentadiene ligand, and it is apparent that one of these pathways is being followed in the HRC experiments. As with outer sphere electron transfer reactions, the inner sphere electron transfer would consume the activated mediator, and, as discussed previously, cause an increase in the production of ferrocenium at the electrode surface in an attempt to maintain Nernstian behavior – an apparent catalytic current will be drawn, as seen in the HRC experiments.

Further work is being planned to study this possible reaction pathway; particularly, product studies are being planned which will attempt to isolate and characterize any products that

may result from an inner sphere electron transfer from homoegeneous redox catalysis. Results of this study should eliminate any remaining doubt as to the nature of the reaction observed in HRC and justify dismissal of the HRC obtained oxidation potentials as a true measure of the oxidation potential of tetra-*n*-butylammonium acetate in acetonitrile.

Interpretation of the direct electrochemistry is more straightforward, if not absolutely conclusive. It is apparent that the oxidation of tetra-*n*-butylammonium acetate in neat acetonitrile is stunted by a large intrinsic barrier, as evidenced by the peak widths of the voltammograms. Addition of water to the system results in major narrowing of the voltammograms, indicating that the barrier has decreased significantly. This narrowing is accompanied by an anodic shift of the oxidation potential of tetra-*n*-butylammonium acetate to a more positive potential. Both are potentially explained by a change of mechanism from a concerted dissociative electron transfer to a stepwise dissociative electron transfer. It should be noted that this transition has been further examined recently via scaled addition of water to acetonitrile and measurement of the oxidation potentials and peak widths with increasing water, this time in a glove box where control over the concentration of water in the experiments was more readily attained.[100] It was found that slowly increasing the water concentration led to a smooth gradual change between the two limiting behaviors presented here. The difference in oxidation potential between the two systems is significant (≈ 250 mV), however, it does not appear to be large enough to substantiate the hypothesis that the change in mechanism via addition of water is the change from a concerted to a stepwise pathway. It appears that there in fact may simply be an abnormally large internal reorganization energy in a stepwise pathway that is relieved via addition of water.

If the acetate anion undergoes stepwise electron transfer in both the neat and wet acetonitrile two questions must be answered: 1) Why does the oxidation potential increase so

significantly upon addition of water? and 2) Why does the activation barrier to electron transfer decrease significantly upon addition of water?

If the mechanism is a stepwise mechanism, then given the electron transfer reaction:

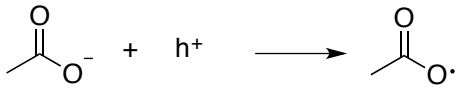

water must stabilize the acetate anion relative to the acetoxyl radical by 5.3 ± 0.6 kcal/mol $\left(-nF\left(E^0_{AcO^-,wet} - E^0_{AcO^-,dry}\right)\right)$. This is a large, although not unreasonable, value, and may be evidence that in 0.5 M H_2O/acetonitrile the acetate anion exists as a bound complex with one or more molecules of water. Loss of this stabilization energy after the electron transfer could account for the difference in measured oxidation potentials.

Finally, if addition of water does not lead to a change in mechanism it must instead lead to a decrease in the Marcus reorganization energy, λ. Although no immediate candidates for such a change are obvious, it is possible to determine the value of the reorganization energy from the convolution data presented previously. Recalling from **Eq. 3.3** the definition of the transfer coefficient α:

$$\alpha = -\frac{RT}{nF}\frac{\partial \ln k_{het}}{\partial E} = \frac{1}{2} - \frac{nF\left(E + E^0_{AcO^-/CO_2+CH_3^{\cdot}}\right)}{2\lambda}$$

then a plot of α versus E (**Figure 3.4** and **Figure 3.7**) has a slope $m = \frac{-nF}{2\lambda}$. Linear regression analysis of this data yields reorganization energies of 18.2 kcal/mol and 10.7 kcal/mol in the dry and wet cases respectively. For thermoneutral oxidations at the electrode surface the intrinsic barrier is one-fourth the reorganization energy; the barrier decreases by ca. 2 kcal/mol upon addition of water. Given transition state theory:

$$k_{het} = Z_{echem} \exp\left(\frac{-\Delta G^{\ddagger}}{RT}\right)$$

and taking the pre-exponential factor to be the collision frequency with the electrode $\left(Z_{echem} = \left(\frac{RT}{2\pi M}\right)^{\frac{1}{2}}\right.$ where M is the molar mass$\left.\right)$, the standard heterogeneous rate constant $\left(\right.$where $\left(E = E^{0}_{AcO^{-}/AcO^{\cdot}}\right)\left.\right)$ may be estimated as:

$$k^{0}_{het} = \left(\frac{RT}{2\pi M}\right)^{\frac{1}{2}} \exp\left(\frac{-\lambda}{4RT}\right)$$

For dry acetonitrile $k^{0}_{het} = 3.7$ cm s^{-1} and for wet acetonitrile $k^{0}_{het} = 87.8$ cm s^{-1}. This analysis fits nicely with a qualitative analysis of the cyclic voltammetry of tetra-*n*-butylammonium acetate. A significant increase in heterogenous rate constant upon addition of water to the system corresponds to narrower peak widths and more moderate values of α.

It remains to be seen what could be the cause of this decrease in the intrinsic barrier of the electron transfer upon addition of water. A possibly interesting explanation for the larger than normal activation barrier in the dry case arises upon examination of the optimized structures of the acetate anion and the acetoxyl radical (**Figure 3.14**). The highest occupied molecular orbital in acetate is a π orbital orthogonal to the symmetry plane of the anion (this plane is, in fact, a node of the orbital). However, the highest occupied orbital of the neutral radical appears to arise from a p-orbital on oxygen that is parallel with this plane. It should be noted that the lone electron is required to be in just such an orbital in order for decarboxylation of the radical to occur. It may be that there is an unusually large reorganization energy associated with oxidation of acetate to facilitate this change in the location of the HOMO from the reduced to the oxidized structures. These structures were obtained in the gas phase; presumably acetonitrile plays little

role in this process. However, addition of water (particularly if acetate exists as a bound structure with water in 0.5 M H_2O/acetonitrile) may facilitate to relax this process and lead to lower activation energies for the oxidation. Further work is in process to fetter out these possible explanations for the unusual change in reorganization energy upon addition of water to the system.

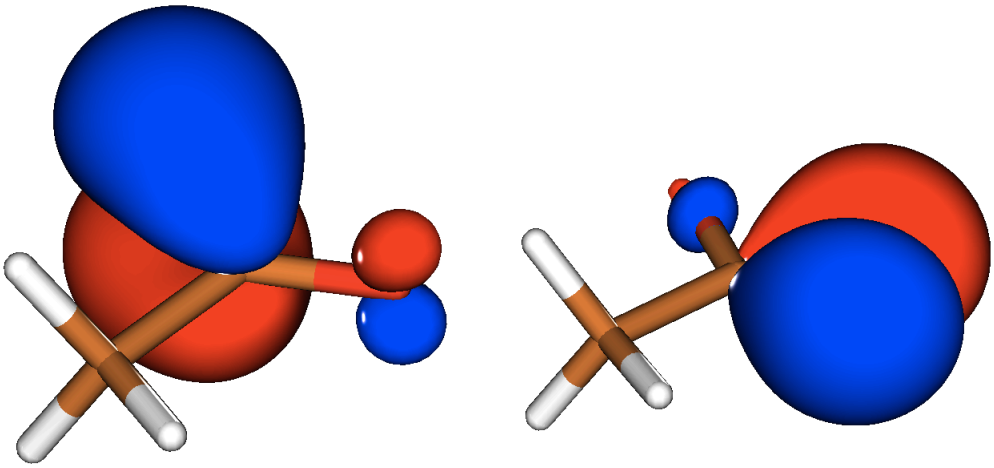

(*a*) (*b*)

Figure 3.14: Highest occupied natural localized molecular orbital of the (*a*) acetate anion and the (*b*) acetoxyl radical. Generated from optimized structures (CCSD/AUG-CC-PVTZ, Natural Bond Orbital analysis). The HOMO of acetate is a π orbital orthogonal to the molecular plane, and the radical HOMO corresponds to a p-like orbital localized on an oxygen atom parallel with the molecular plane.

3.4 Summary

The direct and indirect electrochemistry of tetra-*n*-butylammonium acetate has been examined using cyclic voltammetry, convolution voltammetry, and homogeneous redox catalysis in both neat and wet acetonitrile (0.5 M H_2O). Although initial analysis of the experimental data is promising, upon further examination confusion abounds.

It is apparent that the indirect electrochemistry of the acetate anion leads to an inner sphere electron transfer. As such, no information pertaining to the mechanism of oxidation of acetate can be gained from the HRC experiments, including the oxidation potential of acetate itself, the rate constant of the decarboxylation reaction, or indeed what pathway the electron transfer follows.

Table 3.2
Values obtained from cyclic voltammetry and convolution voltammetry of tetra-*n*-butylammonium acetate. Values in parenthesis indicate standard error.

Solvent	$E_p - E_{p/2}{}^a$	α	λ^b	$k_{het}^0{}^c$	E^{od}
CH_3CN	134(4)	0.354(0.015)	18.22(0.07)	87.8(est)	0.730(0.025)
0.5 M H_2O CH_3CN	96(5)	0.497(0.027)	10.75(0.17)	3.74(est)	0.959(0.011)

(*a*) V (*b*) kcal mol^{-1} (*c*) cm s^{-1} (*d*) V, vs. $Ag/AgNO_3$

In contrast, the direct electrochemistry of acetate was successful in revealing the oxidation potential of acetate in both neat and wet acetonitrile. Also, values for the reorganization energy and standard heterogeneous rate constant were obtained (**Table 3.2**). There is a large change in both the oxidation potential and the reorganization energy upon addition of water to the system. On first inspection this change seems to indicate a change from concerted dissociative electron transfer to stepwise dissociation electron transfer with addition of water; this can however be discarded based on thermodynamic considerations. Instead, it is apparent that oxidation of acetate in dry acetonitrile has an uncharacteristically large activation barrier and addition of water relieves that barrier in addition to stabilizing the acetate anion and lowering its electrochemical potential which results in an increase in the measured oxidation potential for the stepwise process.

Further work on the electrochemical reactions of carboxylates is ongoing. In the indirect case, product studies are planned to attempt to verify that HRC is not a reliable tool for measuring the outer sphere electron transfer reactions of acetate and other carboxylates as well as

to study these potentially interesting inner sphere reactions. As for the outer sphere electron transfer reactions, possible explanations for the change in activation energy going from dry to wet acetonitrile are being explored computationally and via the electrochemistry of other carboxylate anions.

Chapter 4. Experimental

4.1 Instrumentation

Electrochemical experiments were performed on a Princeton Applied Research (EG&G) model 273 potentiostat controlled by a MS-DOS PC. Preparative electrolysis products were characterized by gas chromatography (GC) performed on a Hewlett-Packard HP 5890A with FID detector and HP3398A integrator utilizing a DB-5 column (~ 30 m x 0.32 mm) and GC with mass spectrometry detector performed on a Hewlett-Packard MSD. α-epoxyketones **1** – **4** were characterized by NMR with a Varian Inova 400 NMR spectrometer. Computational simulations were performed with Gaussian 09[82] on HokieOne, an interdepartmental shared memory SGI UV server with 492 2.66 GHz Intel Xeon cores and 2.62 TB memory. Experiments were typically performed on one node (6 core processors) and utilizing 30 GB of memory. Structures were created in Spartan[101], WebMO[102], or Molden[103]. Molden was used to visualize all results and generate graphical representations of orbitals and electronic densities.

4.2 Materials and purification

Unless otherwise noted all substances were obtained from Aldrich. Solvents used in electrochemical experiments were distilled prior to use. DMF was distilled over copper(II) oxide (CuO) and activated neutral aluminum oxide under reduced pressure using an aspirator valve. Acetonitrile was fractionally distilled over calcium hydride (CaH_2) with the first and last 20-30% of distillate being discarded. Tetra-*n*-butylammonium perchlorate (TBAP) was prepared by the method of House[104] from tetra-*n*-butylammonium bromide and perchloric acid and recrystallized by dissolving in ethyl acetate and hexanes. Tetra-*n*-butylammonium acetate was purchased from

Aldrich and recrystallized from ethyl acetate prior to use. Ferrocene derivatives were purchased except for *p*-bromophenylferrocene, which was prepared by a procedure previously described.[56] α-epoxyketones **1** – **4** were prepared by modification of existing procedures[105-108] and characterized by NMR. All chemical shifts and splitting patterns matched those reported in the literature. (**1**, **2**, and **4** synthesized by the author, **3** synthesized with thanks by Michelle Grimm)

4.3 Electrochemical measurements

4.3.1 Reductions

Cyclic voltammetry and homogeneous redox catalysis experiments were performed in a typical three electrode cell with a glassy carbon working electrode (GCE) which was polished to a mirror finish with a series of fine abrasives, a platinum counter electrode, and a $Ag/AgNO_3$ reference electrode isolated from the rest of the cell by a porous Vycor glass rod acting as a porous bridge. All cell components were cleaned then dried in an oven generally 6 hours to overnight and cooled in a desiccator prior to use. A typical experiment involved preparation of a 10 mL sample by placing 1.71 g (5.00 mmol) TBAP in a clean and dry volumetric flask and dissolving with fresh solvent. This solution was used to obtain background voltammograms for later subtraction from the sample voltammograms. Sample was then weighed onto a piece of weigh paper and transferred to the solution to obtain the voltammogram. In the case of HRC experiments the mediator was added first to obtain mediator only voltammograms, then sample added to obtain the catalyzed voltammograms. Before each experiment the solution was degassed by bubbling argon through it for ≈ 10 minutes. Between all direct electrochemical experiments the GCE was polished to remove potential surface contaminants and voltammograms were collected in triplicate. For indirect electrochemical experiments typically

the electrode was only polished after addition of substrate and usually only after a set of voltammograms at one scan rate had been collected in triplicate. After each polishing of the electrode the solution was again degassed with argon to remove any oxygen that may have been introduced in the polishing process.

4.3.2 Oxidations

Direct electrochemistry was performed essentially as described above in the case of the reductions with the exception that degassing was performed with argon that had previously been passed through an acetonitrile solution in an attempt to saturate the argon gas and lessen the evaporation of the solution over the course of the experiment.

Homogeneous redox catalysis experiments failed under the method described in the case of reductions. A more rigorous approach had to be made as follows. 100 mL of solvent and supporting electrolyte stock solutions were made similarly to the sample preparation described previously. These were used to obtain background voltammograms. 25 mL stock solutions of mediator at high concentration (e.g. 8 mM) were made from the stock electrolyte/solvent solutions. Of this, 10 mL samples were used to generate voltammograms at the stock concentration. When completed, 5 mL of the solution were removed from the cell via glass pipet and transferred to a clean and dry 10 mL volumetric flask and diluted with the stock elecetrolyte solvent solution to produce a new mediator solution half the concentration of the first (e.g. 4 mM). This process was repeated once more to produce a third set of mediator voltammograms. At this point the sample was discarded and all glassware cleaned and quickly dried in a 100 ºC oven. The stock mediator solution was used to produce a new 10 mL solution, this time including substrate. This solution was then used to produce catalyzed voltammograms at the highest

concentration (e.g. 8 mM) and the dilution procedure was repeated twice to obtain three sets of mediated voltammograms at three concentrations (e.g. 8m mM, 4 mM, and 2 mM). Electrode fouling required polishing of the GCE after every experiment. Because day to day variations appeared to have a major effect on the results of the HRC experiments for tetra-*n*-butylammonium acetate, all three sets of mediated experiments had to be performed sequentially, so the above set of experiments were required to be performed back-to-back-to-back, a process which takes 22 – 24 hours.

4.3.3 Preparative electrolysis

Preparative electrolysis was performed in a conventional H-cell as described previously. 50 mL 0.2 M TBAP solutions were divided evenly between the anodic and cathodic compartments of the cell and substrate (0.30 mmol) was added to the cathodic compartment. Solutions were both stirred by magnetic stir bar and agitated by degassing with argon during the course of the electrolysis. 0.5 equivalents of electrons were passed in a constant current electrolysis, typically over the course of 45 minutes. Upon completion of electrolysis 1 drop of saturated aqueous ammonium chloride was added to the solution to quench the reaction and an appropriate amount of internal standard (chlorobenzene) was added for quantification of product yields. Because workup yielded significant product loss, the raw electrolysis solution was analyzed by GC with FID detection to obtain product retention times and yields. The product solution was then subjected to a series of back-extractions, where 5 successive liquid-liquid extractions with diethyl ether and water were utilized to remove any trace of DMF and TBAP[109]. The final ether solutions were then subjected to GC/MS analysis to help identify products that survived the reaction workup.

4.4 Computations

Initial structures were typically assembled using Spartan[101] or WebMO[102] and optimized at either AM1 or HF/6-31G levels of theory. These structures were then uploaded to the HokieOne server and Molden[103] used to generate files that could be edited into appropriate input files for the Gaussian 09 computation software package. These structures were then optimized at the indicated level of theory and basis set, typically HF/6-311G*, B3-LYP[83]/6-31+G*, or BHandH-LYP[84]/6-31+G* using the PCM solvent model. Some care was taken to obtain the lowest energy conformation utilizing potential energy surface scans around dihedrals, and so forth. In most cases this optimized structure was used as the input geometry for the radical generated by removal or addition of an electron. In the cases of **1** and **5**, optimization of the radical lead to a stable, ring-closed intermediate. In the cases of **6** and **7** optimization led to ring opening of the epoxide ring. All optimized structures were confirmed to be stationary points by frequency calculations.

For species $\mathbf{1}^{\bullet-}$ and $\mathbf{5}^{\bullet-}$, the two possible cleavage pathways were explored by stretching the carbon-carbon bond and the carbon-oxygen bond respectively and the resulting ring-opened radical anions were optimized as described above. Transition state structures were obtained either by direct optimization of the highest energy structure in the bond stretching profile (utilizing the Gaussian Opt(TS) keyword), or in cases where this failed by using the QST3 method (Gaussian keyword Opt(QST3)) where the optimized reactant and product structures and a guessed transition state structure are provided as input to obtain the optimized transition state structure.

In cases where a more accurate value of the energy was desirable, single point energy calculations were performed at the CCSD[86-89]/6-31+G* theory and basis set on structures

obtained from the DFT methods. For example, optimized transition state structures and reactant structures were used for the single point CCSD energy calculations to obtain a better estimation of the activation energy for the ring-opening reactions.

4.4.1 Optimized structures

1

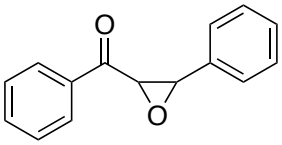

HF/6-311G* Geometry

C	4.284309	0.569181	1.427
C	5.108296	0.003252	0.467789
C	4.5497	-0.656558	-0.613518
C	3.173627	-0.748165	-0.74181
C	2.346161	-0.177647	0.213969
C	2.909725	0.475199	1.301981
C	0.859549	-0.249944	0.094231
O	0.323195	-1.004302	-0.950231
C	0.133256	0.379448	-1.014716
C	-1.221881	1.014721	-0.821779
O	-1.298105	2.167202	-1.111907
C	-2.394954	0.291373	-0.232507
H	0.707078	0.881387	-1.772596
H	0.3293	-0.366897	1.024937
H	2.274841	0.913153	2.052966
H	2.740315	-1.270052	-1.574108
H	5.184281	-1.104802	-1.3569
H	4.710607	1.079805	2.271732
H	6.176803	0.072573	0.565328
C	-3.409253	1.080607	0.30956
C	-4.537084	0.499752	0.851272
C	-4.675363	-0.881261	0.842465
C	-3.682877	-1.67171	0.294139
C	-2.541106	-1.091875	-0.238191
H	-3.299288	2.147633	0.295874
H	-5.308771	1.117554	1.273571
H	-5.556343	-1.335944	1.259357
H	-3.79168	-2.741001	0.277506
H	-1.780506	-1.714844	-0.659878

1$^{\bullet-}$ 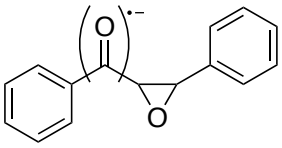

ROB3-LYP/6-31+G* Geometry

C	-4.321452	-0.994709	-1.266377
C	-5.159239	-0.288327	-0.395253
C	-4.601803	0.416146	0.67945
C	-3.218652	0.419878	0.880089
C	-2.37097	-0.283099	0.00696
C	-2.938185	-0.99531	-1.063191
C	-0.891808	-0.276946	0.174206
O	-0.362191	0.004048	1.484776
C	-0.102552	0.970697	0.421638
C	1.269986	1.288364	-0.0869
O	1.361243	2.462783	-0.639992
C	2.395249	0.382869	-0.046255
H	-0.70348	1.877499	0.531771
H	-0.373172	-1.087565	-0.343043
H	-2.290662	-1.555114	-1.739561
H	-2.792906	0.962758	1.722483
H	-5.247494	0.963171	1.366436
H	-4.745155	-1.552589	-2.101334
H	-6.238017	-0.290829	-0.548844
C	3.631694	0.791984	-0.644633
C	4.755518	-0.027896	-0.64005
C	4.722508	-1.301535	-0.044507
C	3.520618	-1.725488	0.553552
C	2.389183	-0.915265	0.559727
H	3.67508	1.772295	-1.112019
H	5.674996	0.326578	-1.108975
H	5.603648	-1.941533	-0.042539
H	3.469947	-2.70612	1.029244
H	1.494229	-1.271362	1.057384

1$^{\bullet-}$ 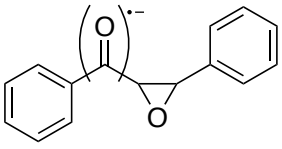

ROBHandH-LYP/6-31+G* Geometry

C	-4.301621	-0.947002	-1.273337
C	-5.12544	-0.27844	-0.37654
C	-4.563574	0.38467	0.708632
C	-3.18819	0.384456	0.893981
C	-2.356145	-0.280373	-0.005011
C	-2.925889	-0.951073	-1.085105
C	-0.881231	-0.275111	0.150874
O	-0.357622	-0.0152	1.445744
C	-0.106537	0.954863	0.419675
C	1.262038	1.278651	-0.07474
O	1.35587	2.446108	-0.613534
C	2.379138	0.379086	-0.038958
H	-0.699663	1.853264	0.544945
H	-0.369628	-1.072054	-0.374642
H	-2.289173	-1.480801	-1.78141
H	-2.758078	0.894794	1.74314
H	-5.198602	0.901653	1.414409
H	-4.729287	-1.471196	-2.116429
H	-6.196859	-0.277847	-0.51857
C	3.605905	0.793237	-0.624534
C	4.723101	-0.020167	-0.625585
C	4.69008	-1.289817	-0.049114
C	3.496445	-1.718189	0.535113
C	2.371364	-0.915704	0.547336
H	3.64983	1.770397	-1.077158
H	5.635859	0.337698	-1.084052
H	5.564635	-1.923844	-0.051637
H	3.445727	-2.696436	0.994978
H	1.482599	-1.277405	1.032625

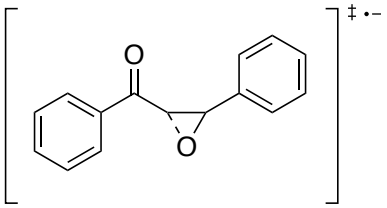

$1^{\bullet-}_{C—O\ TS}$

ROB3-LYP/6-31+G* Geometry

C	-4.566178	-0.425019	-1.217455
C	-4.977755	0.84875	-0.809878
C	-4.193265	1.570033	0.097763
C	-3.003732	1.024461	0.589915
C	-2.581059	-0.249984	0.183301

C	-3.379138	-0.970492	-0.718556
C	-1.294438	-0.847137	0.684754
O	-0.767813	-0.351538	1.905044
C	0.001919	-0.207025	0.402963
C	1.231912	-0.943949	0.189147
O	1.237155	-2.235062	0.204423
C	2.482478	-0.19734	-0.038249
H	-0.039222	0.849659	0.165273
H	-1.286375	-1.938988	0.610333
H	-3.069476	-1.966389	-1.030131
H	-2.39847	1.580249	1.300854
H	-4.509682	2.557934	0.424303
H	-5.172233	-0.996766	-1.916127
H	-5.903282	1.272861	-1.191207
C	3.639044	-0.905464	-0.457416
C	4.848471	-0.253644	-0.69492
C	4.961489	1.132537	-0.518056
C	3.834132	1.851006	-0.090519
C	2.622928	1.203738	0.148582
H	3.559414	-1.979261	-0.595508
H	5.712216	-0.830415	-1.020785
H	5.905076	1.640534	-0.700425
H	3.903261	2.925474	0.067503
H	1.783185	1.795083	0.501919

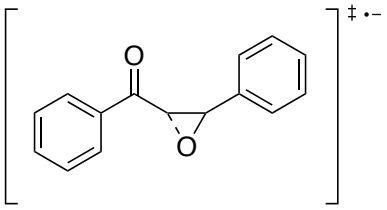

$\mathbf{1}^{\bullet-}_{\mathbf{C—O\ TS}}$

ROBHandH-LYP/6-31+G* Geometry

C	-4.511651	-0.454802	-1.216061
C	-4.938212	0.810765	-0.833971
C	-4.178754	1.54681	0.067168
C	-2.998608	1.023552	0.578519
C	-2.561746	-0.241752	0.197072
C	-3.333904	-0.977235	-0.69842
C	-1.278467	-0.811063	0.720943
O	-0.77236	-0.27109	1.904669
C	-0.001882	-0.196238	0.373537
C	1.211976	-0.931636	0.19321
O	1.226275	-2.206988	0.249873
C	2.46731	-0.195439	-0.039736
H	-0.041689	0.845721	0.114027
H	-1.276259	-1.896255	0.692974
H	-3.012796	-1.965904	-0.990753
H	-2.41232	1.589825	1.283615
H	-4.506993	2.527755	0.373439
H	-5.097952	-1.036976	-1.909443
H	-5.855385	1.216902	-1.23008
C	3.601497	-0.908128	-0.459719
C	4.807361	-0.269974	-0.701869
C	4.927624	1.10417	-0.526755
C	3.818351	1.82599	-0.098009
C	2.611667	1.19011	0.14562
H	3.513211	-1.972619	-0.595139
H	5.658693	-0.847316	-1.029073
H	5.866197	1.601545	-0.712721
H	3.895784	2.891114	0.057514
H	1.782812	1.780052	0.500122

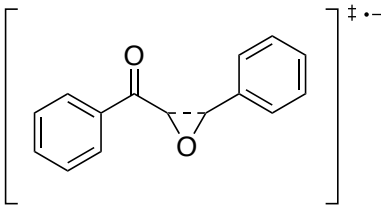

$1^{\bullet-}_{C—C\ TS}$

ROB3-LYP/6-31+G* Geometry

C	-4.404241	-0.992966	1.181185
C	-4.904447	-1.276067	-0.103105
C	-4.247502	-0.735802	-1.219293
C	-3.118577	0.066949	-1.069237
C	-2.598838	0.362845	0.223885
C	-3.278561	-0.194863	1.346421
C	-1.43044	1.157568	0.413837
O	-0.829291	1.818339	-0.662022
C	0.197089	0.859855	-0.541415
C	1.458478	1.216823	-0.017348
O	1.720669	2.379724	0.459163
C	2.526166	0.165803	-0.014712
H	0.028306	-0.046861	-1.112702
H	-1.138037	1.51365	1.398465
H	-2.906051	0.015139	2.34754
H	-2.623661	0.480082	-1.943627
H	-4.623585	-0.942892	-2.219437
H	-4.90328	-1.400489	2.058141
H	-5.784832	-1.900917	-0.227559
C	3.874392	0.568731	0.079926
C	4.912125	-0.365432	0.082459
C	4.631965	-1.735068	0.002246
C	3.297434	-2.154302	-0.075471
C	2.260005	-1.219613	-0.081072
H	4.091845	1.630409	0.148017
H	5.943245	-0.024602	0.148195
H	5.438165	-2.464375	0.009526
H	3.062484	-3.215487	-0.119904
H	1.234096	-1.574939	-0.113615

$1^{\bullet-}_{C—C\ TS}$ 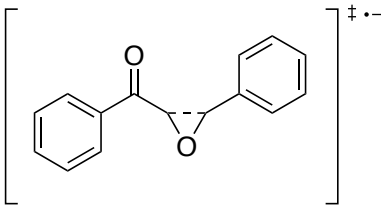

ROBHandH-LYP/6-31+G* Geometry

C	-4.317701	-0.995791	1.190148
C	-4.814775	-1.295097	-0.079557
C	-4.177618	-0.756771	-1.193459
C	-3.068878	0.061417	-1.054989
C	-2.55433	0.370956	0.221793
C	-3.212442	-0.182903	1.342512
C	-1.394918	1.17787	0.396341
O	-0.828279	1.83021	-0.683548
C	0.175604	0.872298	-0.562039
C	1.424399	1.214009	-0.031218
O	1.687146	2.356154	0.457588
C	2.47996	0.162296	-0.020013
H	0.011102	-0.020107	-1.139762
H	-1.123097	1.565742	1.36448
H	-2.842202	0.039214	2.332316
H	-2.590187	0.474034	-1.927978
H	-4.55163	-0.975563	-2.182248
H	-4.801924	-1.401283	2.065456
H	-5.678181	-1.93043	-0.194175
C	3.814964	0.557315	0.111842
C	4.842751	-0.373574	0.121571
C	4.561823	-1.729987	0.010908
C	3.238508	-2.140532	-0.104243
C	2.211384	-1.208998	-0.116263
H	4.03132	1.60827	0.203118
H	5.864738	-0.040538	0.216867
H	5.358949	-2.45626	0.022974
H	3.003839	-3.191343	-0.173753
H	1.193951	-1.557705	-0.179622

$1^{\bullet -}$ C—O ring-opened

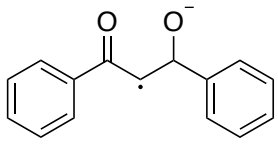

ROB3-LYP/6-31+G* Geometry

C	4.096217	0.023099	-1.669744
C	4.735568	-1.028673	-1.001747
C	4.271985	-1.426059	0.257244
C	3.176386	-0.779802	0.841586
C	2.523989	0.268659	0.178522
C	3.00296	0.665253	-1.080321
C	1.307917	0.957995	0.795303
O	1.205697	0.863515	2.176549
C	0.009926	0.285611	0.462182
C	-1.197267	0.98467	0.196284
O	-1.262386	2.244192	0.07458
C	-2.458929	0.181099	-0.016535
H	-0.001433	-0.794666	0.563866
H	1.289015	2.002376	0.436541
H	2.515036	1.486977	-1.6029
H	2.820315	-1.0764	1.824326
H	4.76646	-2.237782	0.786654
H	4.453711	0.346496	-2.644862
H	5.589013	-1.527324	-1.454909
C	-3.470147	0.713641	-0.835812
C	-4.658441	0.014813	-1.056842
C	-4.866511	-1.228226	-0.447145
C	-3.874959	-1.763467	0.381925
C	-2.680531	-1.068003	0.590999
H	-3.308985	1.682581	-1.299075
H	-5.42318	0.439055	-1.703067
H	-5.793355	-1.771627	-0.612822
H	-4.032291	-2.721567	0.871273
H	-1.929768	-1.493439	1.250539

$1^{\bullet-}$ C—O ring-opened

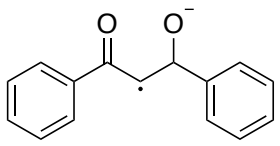

ROBHandH-LYP/6-31+G* Geometry

C	4.066986	0.004033	-1.664807
C	4.723757	-1.01032	-0.977252
C	4.277244	-1.378524	0.285098
C	3.181074	-0.740222	0.854358
C	2.512464	0.270442	0.172188
C	2.973799	0.638102	-1.09062
C	1.295712	0.949214	0.776045
O	1.18951	0.856958	2.139624
C	0.016449	0.271878	0.426816
C	-1.194389	0.967881	0.183209
O	-1.25651	2.20774	0.080489
C	-2.451893	0.17342	-0.01878
H	0.008939	-0.800497	0.516209
H	1.27686	1.982723	0.414634
H	2.472592	1.430298	-1.628057
H	2.838438	-1.013219	1.838871
H	4.784728	-2.160643	0.828692
H	4.410686	0.304131	-2.642632
H	5.576267	-1.502403	-1.418501
C	-3.469911	0.723789	-0.797183
C	-4.65402	0.034942	-1.008799
C	-4.846533	-1.21369	-0.429636
C	-3.846222	-1.765772	0.358849
C	-2.655866	-1.079897	0.558709
H	-3.319253	1.695885	-1.235684
H	-5.42652	0.470678	-1.622454
H	-5.769064	-1.749113	-0.588345
H	-3.992328	-2.7286	0.822113
H	-1.89725	-1.51848	1.185084

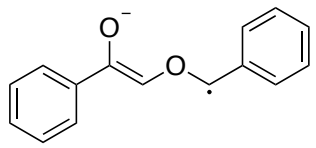

$1^{\bullet-}$ C—C ring-opened

ROB3-LYP/6-31+G* Geometry

C	5.470927	-1.0355	0.149446
C	5.856566	0.311925	0.027757
C	4.859777	1.294618	-0.081627
C	3.510166	0.955444	-0.071098
C	3.100972	-0.407597	0.051696
C	4.129046	-1.393135	0.162029
C	1.745097	-0.8026	0.068461
O	0.772471	0.119452	-0.044016
C	-0.560094	-0.27544	0.023699
C	-1.549285	0.67051	-0.153721
O	-1.347211	1.931506	-0.357488
C	-2.97661	0.181533	-0.061701
H	-0.721101	-1.321649	0.253113
H	1.439969	-1.841244	0.169259
H	3.848768	-2.440435	0.257129
H	2.753759	1.729924	-0.155834
H	5.142819	2.341163	-0.176073
H	6.229965	-1.810262	0.235163
H	6.90773	0.587	0.018542
C	-3.978008	1.097633	0.310119
C	-5.315935	0.707823	0.417771
C	-5.691146	-0.611935	0.142993
C	-4.710231	-1.532395	-0.246546
C	-3.373306	-1.139606	-0.351286
H	-3.687154	2.123697	0.514396
H	-6.067321	1.43612	0.715586
H	-6.731962	-0.91683	0.219687
H	-4.988483	-2.557195	-0.482533
H	-2.636674	-1.86563	-0.684347

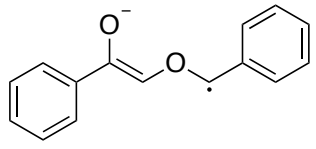

$1^{\bullet-}$ C—C ring-opened

ROBHandH-LYP/6-31+G* Geometry

C	-5.41658	-1.054192	-0.069983

C	-5.812036	0.283081	-0.083294
C	-4.836765	1.276007	-0.0741
C	-3.491759	0.952652	-0.05213
C	-3.076921	-0.39673	-0.03744
C	-4.078544	-1.392857	-0.04755
C	-1.714264	-0.768313	-0.012653
O	-0.772515	0.171237	0.013417
C	0.558456	-0.223635	-0.068589
C	1.539616	0.670546	0.229965
O	1.36355	1.889759	0.587939
C	2.954078	0.180544	0.083551
H	0.717415	-1.221754	-0.432974
H	-1.397694	-1.798607	-0.00327
H	-3.787653	-2.432389	-0.036957
H	-2.747944	1.731692	-0.046827
H	-5.129767	2.314637	-0.085096
H	-6.161162	-1.835113	-0.077211
H	-6.857948	0.543484	-0.100649
C	3.944395	1.0927	-0.284143
C	5.265132	0.695967	-0.440055
C	5.630079	-0.62591	-0.216973
C	4.658686	-1.541944	0.16726
C	3.338086	-1.141831	0.31919
H	3.663907	2.119864	-0.447556
H	6.010302	1.419077	-0.733879
H	6.656933	-0.935677	-0.330699
H	4.93083	-2.567751	0.361982
H	2.604544	-1.861938	0.643941

5

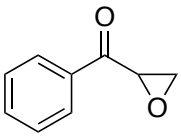

B3-LYP/6-31+G* Geometry

C	0.51492	0.200996	-0.047104
C	-0.922703	0.588236	-0.06646
C	-1.945692	-0.485765	-0.36249
C	-2.951834	-0.838717	0.66548
O	-3.303979	-0.045911	-0.475698
O	-1.290477	1.739213	0.156866
H	-1.665856	-1.249877	-1.089672
H	-2.950616	-0.297968	1.612043
H	-3.359158	-1.849395	0.679647

C	1.48883	1.216746	-0.000679
C	2.843732	0.893305	0.035566
C	3.243626	-0.449993	0.03809
C	2.283634	-1.466702	0.000163
C	0.925091	-1.14552	-0.048742
H	1.171139	2.257305	0.00072
H	3.59067	1.686058	0.062598
H	4.303367	-0.702771	0.069455
H	2.591474	-2.511683	0.007231
H	0.197003	-1.953601	-0.074309

5

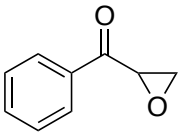

BHandH-LYP/6-31+G* Geometry

C	0.509757	0.202541	-0.051437
C	-0.919727	0.591645	-0.078401
C	-1.936383	-0.47359	-0.37353
C	-2.903407	-0.849105	0.663393
O	-3.278144	-0.042843	-0.436853
O	-1.27966	1.728919	0.139891
H	-1.669486	-1.21054	-1.119643
H	-2.879862	-0.334297	1.613397
H	-3.307249	-1.851005	0.666057
C	1.476225	1.208693	0.006724
C	2.820783	0.884076	0.048376
C	3.213398	-0.45077	0.043093
C	2.258795	-1.457674	-0.007539
C	0.910737	-1.134119	-0.060433
H	1.163105	2.241393	0.014309
H	3.563849	1.667719	0.085855
H	4.263636	-0.704469	0.078398
H	2.561789	-2.494763	-0.007273
H	0.18559	-1.932827	-0.096879

5$^{\bullet-}$ 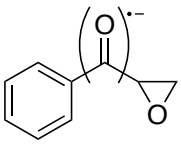

ROB3-LYP/6-31+G* Geometry

C	-0.490749	0.171684	-0.040639
C	0.914975	0.528524	-0.068602
C	1.938428	-0.535988	-0.252409
C	3.358912	-0.228937	-0.469603
O	2.9742	-0.709408	0.830804
O	1.309151	1.756307	0.059663
H	1.602361	-1.508978	-0.605027
H	3.662407	0.816763	-0.491938
H	3.978456	-0.916664	-1.048821
C	-1.475815	1.208248	0.013582
C	-2.838443	0.925336	0.037649
C	-3.304322	-0.400511	0.015798
C	-2.355542	-1.439713	-0.025011
C	-0.990772	-1.169583	-0.048997
H	-1.133731	2.239968	0.03168
H	-3.552911	1.749353	0.074552
H	-4.370905	-0.619342	0.037007
H	-2.68932	-2.478305	-0.030388
H	-0.303191	-2.012364	-0.061414

5$^{\bullet-}$ 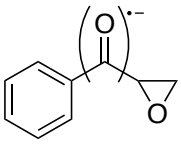

ROBHandH-LYP/6-31+G* Geometry

C	-0.489138	0.159365	-0.027933
C	0.907271	0.504315	-0.044594
C	1.930869	-0.559928	-0.192853
C	3.318868	-0.250708	-0.516073
O	2.988379	-0.625716	0.814253
O	1.30338	1.720899	0.053303
H	1.591102	-1.548513	-0.46008
H	3.600107	0.784775	-0.630537
H	3.920003	-0.970777	-1.055224
C	-1.456954	1.197421	0.007799
C	-2.812883	0.928948	0.021347

C	-3.28756	-0.381997	0.005125
C	-2.355388	-1.421413	-0.020538
C	-0.997393	-1.167545	-0.034704
H	-1.108858	2.217573	0.021409
H	-3.513817	1.753215	0.04521
H	-4.347591	-0.589151	0.017455
H	-2.696221	-2.448313	-0.024165
H	-0.324948	-2.011021	-0.039975

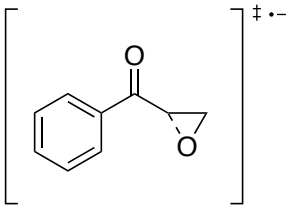

$5^{\bullet-}_{\text{C—O TS}}$

ROB3-LYP/6-31+G* Geometry

C	-0.503027	0.182461	-0.056619
C	0.916723	0.565369	-0.110168
C	1.914396	-0.455435	-0.384548
C	3.355557	-0.200074	-0.387962
O	3.010606	-0.831661	0.838381
O	1.271984	1.790575	0.09535
H	1.598613	-1.409534	-0.789984
H	3.679553	0.839573	-0.296651
H	3.991436	-0.791988	-1.055564
C	-1.490243	1.201572	0.018705
C	-2.850733	0.900389	0.059752
C	-3.291553	-0.430607	0.037215
C	-2.333383	-1.455163	-0.021319
C	-0.971955	-1.159802	-0.062048
H	-1.158031	2.234884	0.038015
H	-3.576349	1.710327	0.110978
H	-4.352359	-0.665478	0.072143
H	-2.651749	-2.495892	-0.024545
H	-0.266531	-1.985464	-0.082297

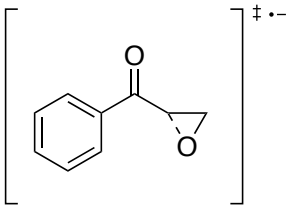

$5^{\bullet-}_{C—O\ TS}$

ROBHandH-LYP/6-31+G* Geometry

C	-0.506512	0.182098	-0.059342
C	0.912992	0.569403	-0.118572
C	1.896687	-0.428777	-0.416131
C	3.327904	-0.192248	-0.367914
O	3.002624	-0.849414	0.824801
O	1.250884	1.778517	0.117876
H	1.587458	-1.373879	-0.822251
H	3.651237	0.836213	-0.252465
H	3.96469	-0.753649	-1.047006
C	-1.481878	1.190302	0.012382
C	-2.833334	0.88811	0.057869
C	-3.263664	-0.434007	0.041537
C	-2.312487	-1.447931	-0.014524
C	-0.960474	-1.148802	-0.05895
H	-1.154361	2.21578	0.027285
H	-3.555928	1.688574	0.106948
H	-4.315154	-0.670382	0.078941
H	-2.625514	-2.480807	-0.013617
H	-0.255893	-1.963567	-0.077369

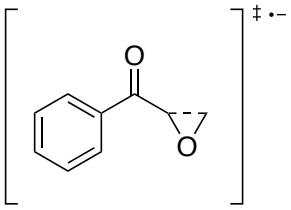

$5^{\bullet-}_{C—C\ TS}$

ROB3-LYP/6-31+G* Geometry

C	0.545003	0.169913	-0.018149
C	-0.902459	0.573621	-0.048282
C	-1.832492	-0.399	-0.44107
C	-3.480624	-0.782495	0.602527
O	-3.19813	-0.087697	-0.58324
O	-1.215792	1.779133	0.284039
H	-1.547406	-1.353296	-0.869981

H	-3.554554	-0.172297	1.500179
H	-4.086206	-1.682027	0.493754
C	1.528082	1.179605	-0.046593
C	2.89031	0.869939	-0.029273
C	3.311923	-0.46345	0.029235
C	2.34896	-1.480003	0.077138
C	0.98763	-1.168804	0.058057
H	1.199972	2.213937	-0.085398
H	3.625359	1.671575	-0.060172
H	4.37127	-0.707453	0.047584
H	2.65958	-2.520589	0.142156
H	0.265361	-1.977285	0.123949

5$^{\bullet-}_{\text{C—C TS}}$

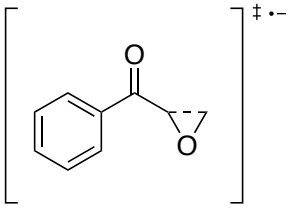

ROBHandH-LYP/6-31+G* Geometry

C	0.591183	0.155626	0.028329
C	-0.865437	0.541709	0.04568
C	-1.733352	-0.367054	-0.475406
C	-3.886725	-0.698005	0.360963
O	-3.106961	-0.085688	-0.567598
O	-1.161593	1.70097	0.511993
H	-1.444541	-1.310957	-0.903911
H	-4.240609	-0.100356	1.186303
H	-4.384271	-1.611923	0.074299
C	1.549283	1.152365	-0.161068
C	2.903868	0.852176	-0.189913
C	3.334139	-0.457619	-0.015485
C	2.393533	-1.4585	0.191307
C	1.038775	-1.153755	0.216095
H	1.216018	2.169402	-0.28514
H	3.624373	1.640218	-0.346214
H	4.386604	-0.693179	-0.030698
H	2.714175	-2.477213	0.345589
H	0.325077	-1.939912	0.401594

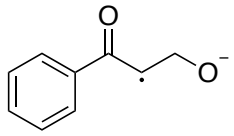

$5^{\bullet-}$ C—O ring-opened

ROB3-LYP/6-31+G* Geometry

C	0.581779	0.171739	0.011202
C	-0.878055	0.564316	0.007694
C	-1.824602	-0.350955	0.539006
C	-3.301963	-0.136598	0.494105
O	-3.569386	-0.8387	-0.681929
O	-1.183415	1.719017	-0.416942
H	-1.490957	-1.32997	0.867239
H	-3.557332	0.935071	0.432632
H	-3.809926	-0.560954	1.381142
C	1.555772	1.182855	0.091375
C	2.916984	0.871742	0.090032
C	3.333259	-0.461309	-0.008628
C	2.375521	-1.476479	-0.104575
C	1.013232	-1.163147	-0.090025
H	1.228882	2.216403	0.157912
H	3.653866	1.667932	0.164739
H	4.392529	-0.705672	-0.01578
H	2.687976	-2.51388	-0.196238
H	0.285812	-1.964459	-0.181805

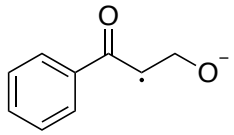

$5^{\bullet-}$ C—O ring-opened

ROBHandH3-LYP/6-31+G* Geometry

C	0.580366	0.170209	0.012071
C	-0.870039	0.559316	0.01367
C	-1.814673	-0.351882	0.548559
C	-3.281652	-0.139562	0.482793
O	-3.534543	-0.817263	-0.689175
O	-1.176043	1.691605	-0.406779
H	-1.482113	-1.322184	0.874111
H	-3.533129	0.92451	0.438691
H	-3.792747	-0.568409	1.354405
C	1.543218	1.176546	0.088167
C	2.894821	0.868444	0.084925

C	3.307242	-0.455256	-0.012042
C	2.35829	-1.464582	-0.103374
C	1.005262	-1.154573	-0.085728
H	1.218371	2.201521	0.153342
H	3.62594	1.658107	0.156266
H	4.358146	-0.696952	-0.020379
H	2.669489	-2.493297	-0.192039
H	0.283717	-1.949975	-0.171006

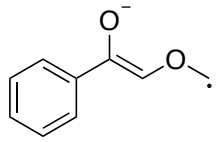

$5^{\bullet-}$ C—C ring-opened

ROB3-LYP/6-31+G* Geometry

C	1.601953	1.130791	0.248009
C	0.615615	0.180263	-0.076365
C	1.039048	-1.142163	-0.320193
C	2.385118	-1.502311	-0.214578
C	3.350335	-0.54707	0.127929
C	2.949161	0.774159	0.355311
C	-0.822677	0.634279	-0.170038
C	-1.788736	-0.320083	0.068394
O	-3.131759	0.033534	-0.005058
C	-4.074486	-0.906246	0.262061
O	-1.051393	1.883608	-0.429027
H	-1.59788	-1.353748	0.331841
H	-3.77578	-1.74711	0.887884
H	-5.067975	-0.481406	0.364434
H	0.31465	-1.895861	-0.616747
H	2.683014	-2.52946	-0.413915
H	4.39832	-0.826562	0.204322
H	3.687633	1.529581	0.615826
H	1.291245	2.1577	0.415852

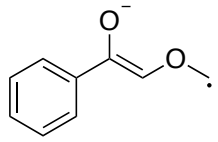

$5^{\bullet-}$ C—C ring-opened

ROBHandH-LYP/6-31+G* Geometry

C	1.54322	1.118477	0.315368

C	0.606678	0.172067	-0.104586
C	1.066839	-1.113497	-0.401346
C	2.406776	-1.446857	-0.255787
C	3.323176	-0.498437	0.180894
C	2.883076	0.788902	0.463389
C	-0.832062	0.590484	-0.234972
C	-1.767307	-0.370068	-0.00563
O	-3.116587	-0.068776	-0.157126
C	-3.990266	-0.819957	0.532145
O	-1.069884	1.820452	-0.520545
H	-1.557003	-1.392238	0.251509
H	-3.65077	-1.253259	1.461998
H	-5.010745	-0.493757	0.426083
H	0.378111	-1.856974	-0.76832
H	2.736847	-2.445376	-0.497371
H	4.365081	-0.75564	0.288683
H	3.584772	1.537584	0.7976
H	1.204691	2.119562	0.524338

6

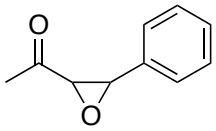

HF/6-311G* Geometry

H	4.627051	0.460854	-0.757829
C	3.689238	-0.072308	-0.812609
H	3.181352	0.174991	-1.737819
H	3.872556	-1.140633	-0.83164
C	2.850473	0.277152	0.391123
O	3.241692	0.964213	1.275839
C	1.458585	-0.289107	0.47336
C	0.465532	-0.060167	-0.582049
O	1.1069	-1.289552	-0.441765
H	1.104188	-0.433969	1.47856
H	0.777818	0.496678	-1.450291
C	-0.997797	0.005499	-0.289189
C	-3.716661	0.178339	0.261745
C	-1.681456	1.196243	-0.495752
C	-1.684944	-1.101318	0.186033

C	-3.039943	-1.012794	0.460238
C	-3.033744	1.284302	-0.218113
H	-1.157474	2.058151	-0.872079
H	-1.161889	-2.028031	0.328572
H	-3.56638	-1.876641	0.82469
H	-3.553222	2.211935	-0.378294
H	-4.768437	0.244336	0.474815

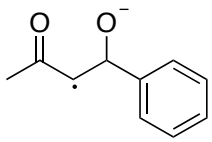

$6^{\bullet -}_{\text{ring-opened}}$

ROB3-LYP/6-31+G* Geometry

C	-3.703195	-0.283256	1.395369
C	-2.768804	-0.296064	0.190227
C	-1.477181	0.276616	0.336448
C	-0.477829	0.401167	-0.774258
O	-0.739299	1.719024	-1.136863
O	-3.179514	-0.840852	-0.87653
H	-3.243458	0.154522	2.287233
H	-4.022562	-1.307152	1.62637
H	-4.607385	0.289605	1.150483
H	-1.23031	0.785591	1.266847
H	-0.731641	-0.314731	-1.577322
C	0.957343	0.117901	-0.334012
C	1.525578	-1.149213	-0.541545
C	2.828524	-1.433472	-0.117598
C	3.589797	-0.445985	0.519703
C	3.036148	0.823875	0.724516
C	1.732197	1.101606	0.298394
H	0.940912	-1.92183	-1.044056
H	3.252327	-2.422821	-0.291716
H	4.606755	-0.661951	0.846817
H	3.623319	1.601315	1.214227
H	1.307087	2.09303	0.444803

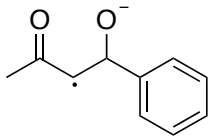

$6^{\bullet-}$ ring opened

ROBHandH-LYP/6-31+G* Geometry

C	-3.670352	-0.622245	1.266703
C	-2.743236	-0.328032	0.109636
C	-1.452267	0.201848	0.397202
C	-0.4727	0.648707	-0.637175
O	-0.68054	2.003636	-0.65049
O	-3.133242	-0.567261	-1.043706
H	-4.098035	-1.614684	1.148348
H	-4.493094	0.091677	1.253417
H	-3.174525	-0.556626	2.230182
H	-1.214755	0.447235	1.422579
H	-0.730697	0.172573	-1.591867
C	0.944483	0.210607	-0.29177
C	1.38376	-1.073835	-0.612324
C	2.664198	-1.495388	-0.280606
C	3.533491	-0.631955	0.378452
C	3.108179	0.651447	0.696524
C	1.82363	1.067147	0.361427
H	0.716231	-1.750344	-1.131031
H	2.987212	-2.494018	-0.540979
H	4.532518	-0.955632	0.634777
H	3.778221	1.332174	1.203815
H	1.492065	2.06683	0.5959

7

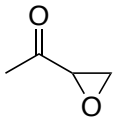

B3-LYP/6-31+G* Geometry

C	0.51492	0.200996	-0.047104
C	-0.922703	0.588236	-0.06646
C	-1.945692	-0.485765	-0.36249
C	-2.951834	-0.838717	0.66548
O	-3.303979	-0.045911	-0.475698
O	-1.290477	1.739213	0.156866
H	-1.665856	-1.249877	-1.089672
H	-2.950616	-0.297968	1.612043
H	-3.359158	-1.849395	0.679647
C	1.48883	1.216746	-0.000679
C	2.843732	0.893305	0.035566
C	3.243626	-0.449993	0.03809

$7^{\bullet-}$ ring-opened

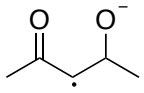

ROB3-LYP/6-31+G* Geometry

H	-2.931677	-0.303224	-0.552849
C	-2.160968	-0.669449	0.136912
H	-2.541351	-0.518041	1.155647
H	-2.02027	-1.742637	-0.027137
C	-0.877727	0.133856	-0.049369
O	-0.943246	1.393435	0.067924
C	0.31298	-0.566456	-0.378958
O	2.169321	-0.19169	0.764864
H	0.286166	-1.655126	-0.395032
C	1.655654	0.074282	-0.509427
H	1.562093	1.153866	-0.719081
H	2.256807	-0.382202	-1.318798

$7^{\bullet -}_{\text{ring-opened}}$ 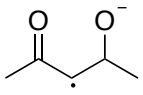

ROBHandH-LYP/6-31+G* Geometry

H	-3.002183	-0.171754	-0.345364
C	-2.167767	-0.671405	0.139402
H	-2.393723	-0.730387	1.203775
H	-2.077641	-1.682478	-0.245564
C	-0.907372	0.139785	-0.050385
O	-0.959802	1.370198	0.084141
C	0.299417	-0.548396	-0.383685
O	2.248827	-0.213718	0.720377
H	0.272703	-1.628791	-0.41488
C	1.63934	0.094713	-0.479255
H	1.523133	1.172928	-0.639887
H	2.183792	-0.299538	-1.350685

7 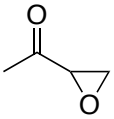

MP2/AUG-CC-PVTZ Geometry

C	2.035856	-0.650255	0.055609
C	0.779377	0.173114	-0.016744
O	0.771758	1.389901	0.017132
C	-0.502156	-0.606913	-0.110103
C	-1.654384	-0.130041	0.674828
O	-1.599785	0.062261	-0.736758
H	-0.427098	-1.664563	-0.336517
H	-1.521511	0.775094	1.254037
H	-2.389082	-0.847857	1.016268
H	2.893406	-0.007328	0.227807
H	2.163353	-1.198119	-0.879551
H	1.952991	-1.38995	0.853421

4-hydroxy-2-butanone

MP2/AUG-CC-PVTZ Geometry

C	0.880072	0.138227	0.058668
C	2.315072	-0.239826	-0.192526

O	0.553165	1.289616	0.313475
C	-0.141736	-0.973414	-0.020573
C	-1.533447	-0.518287	0.382002
O	-2.04613	0.462491	-0.505821
H	-1.47814	1.235027	-0.386466
H	-2.22402	-1.358845	0.344223
H	-1.513182	-0.141099	1.4085
H	-0.152506	-1.344006	-1.049751
H	0.197813	-1.803821	0.605842
H	2.400003	-0.783642	-1.133536
H	2.938238	0.64912	-0.213769
H	2.655757	-0.909788	0.598294

Acetate anion

CCSD/AUG-CC-PVTZ Geometry

C	0.042349	-1.342776	0
C	0	0.20697	0
O	-1.150962	0.703579	0
O	1.107363	0.792579	0
H	1.067572	-1.715736	0
H	-0.486438	-1.719344	0.87988
H	-0.486438	-1.719344	-0.87988

Acetoxyl radical

CCSD/AUG-CC-PVTZ Geometry

C	-1.338138	-0.152598	-0.000004
C	0.164518	-0.061303	-0.000015
O	0.563193	1.211866	0.000002
O	0.953223	-0.977448	0.000004
H	-1.639482	-0.708565	0.884527
H	-1.810669	0.826114	-0.000495
H	-1.639452	-0.709481	-0.883965

Chapter 5. Experimental data analysis

5.1 Reductions of α-epoxyketones

5.1.1 2,3-Epoxy-1,3-diphenyl-1-propanone (1)

5.1.1.1 Cyclic voltammetry of 1

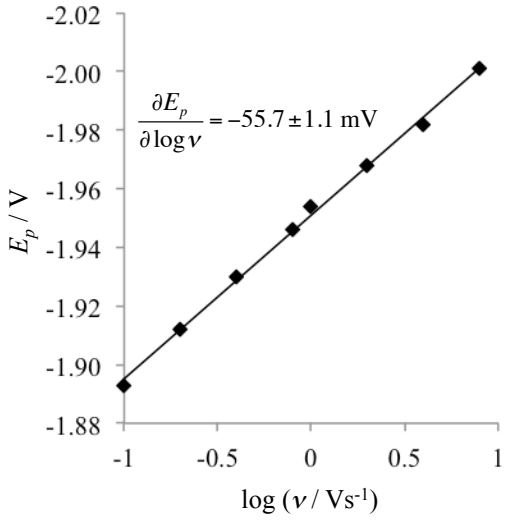

Figure 5.1: Variation of peak potential as a function of scan rate in DMF. C_1 = 0.003 M, 0.5 M supporting electrolyte (tetra-*n*-butylammonium perchlorate, TBAP), ν = 100, 200, 400, 800, 1000, 2000, 4000, 8000 mV/s

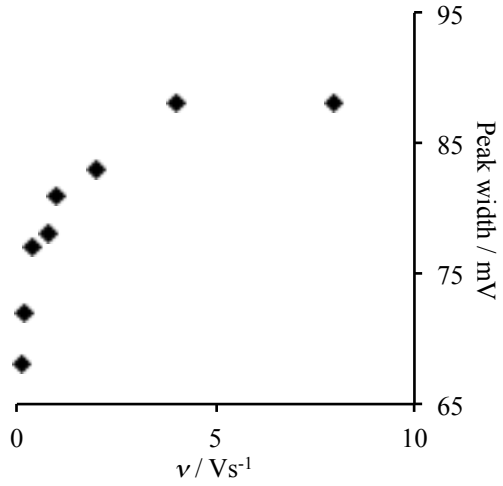

Figure 5.2: Variation of peak width as a function of scan rate in DMF. C_1 = 0.003 M, 0.5 M supporting electrolyte (TBAP), ν = 100, 200, 400, 800, 1000, 2000, 4000, 8000 mV/s

The cyclic voltammetry data indicates that the mechanism is mixed kinetic control (peak widths increase with sweep rate from ≈ 65 mV to ≈ 90 mV). Further analysis of the data is accomplished by fitting to published working curves[11] for this mixed kinetic control case to obtain the fitting parameters C_1 and C_2 (**Figure 5.3 – Figure 5.4**):

$$C_1 = \log\left(\frac{nF}{2RT}\frac{k_{cs}{D_A}^2}{{k_{het}}^4}\right) \qquad \textbf{Eq. 5.1}$$

$$C_2 = E^0_{A/A^{\cdot-}} + \left(\frac{RT}{nF}\ln 10\right)\log\left(\frac{k_{cs}D_A}{{k_{het}}^2}\right) \qquad \textbf{Eq. 5.2}$$

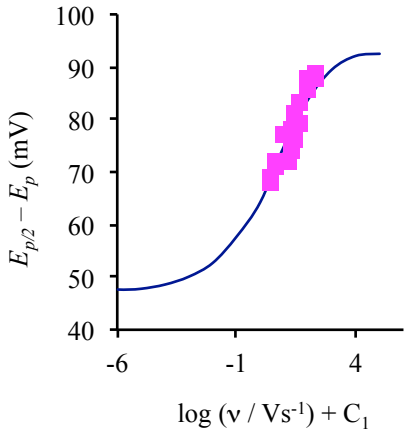

Figure 5.3: Determination of C_1 for **1**. Experimental peak widths are translated along the x-coordinate to obtain the fitting parameter C_1 = 1.38.

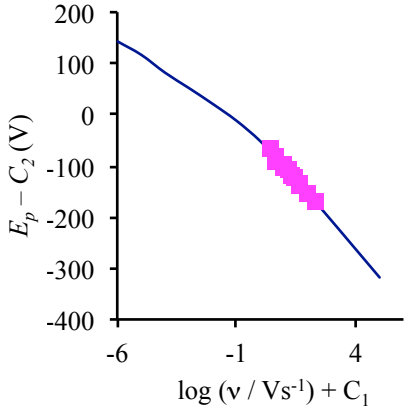

Figure 5.4 Determination of C_2 for **1**. Experimental peak widths are translated along the y-coordinate to obtain the fitting parameter C_2 = -1.83 V.

Combining **Eq. 5.1** and **Eq. 5.21** and the values of the fitting parameters gives:

$$E^0_{A/A^{\cdot-}} + \left(\frac{RT}{2nF}\ln 10\right)\log k_{cs} = -1.83\ \text{V} - \left(\frac{RT}{2nF}\ln 10\right)\left[1.38 - \log\left(\frac{nF}{2RT}\right)\right] \qquad \textbf{Eq. 5.3}$$

Determination of the ring-opening rate constant can then be made if the reduction potential of **1** can be obtained from another source.

5.1.1.2 Homogeneous redox catalysis of 1

Homogeneous redox catalysis experiments were performed with azobenzene, 9-fluorenone, and 4-nitro-*o*-xylene. Plots of $i_p/\gamma i_{pd}$ versus log $1/\nu$ and log C_{Med}/ν are presented in **Figure 2.11**. These plots are used to determine the rate-limiting step in the reaction. Catalysis shows a definite mediator dependency, therefore the electron transfer step is rate limiting.

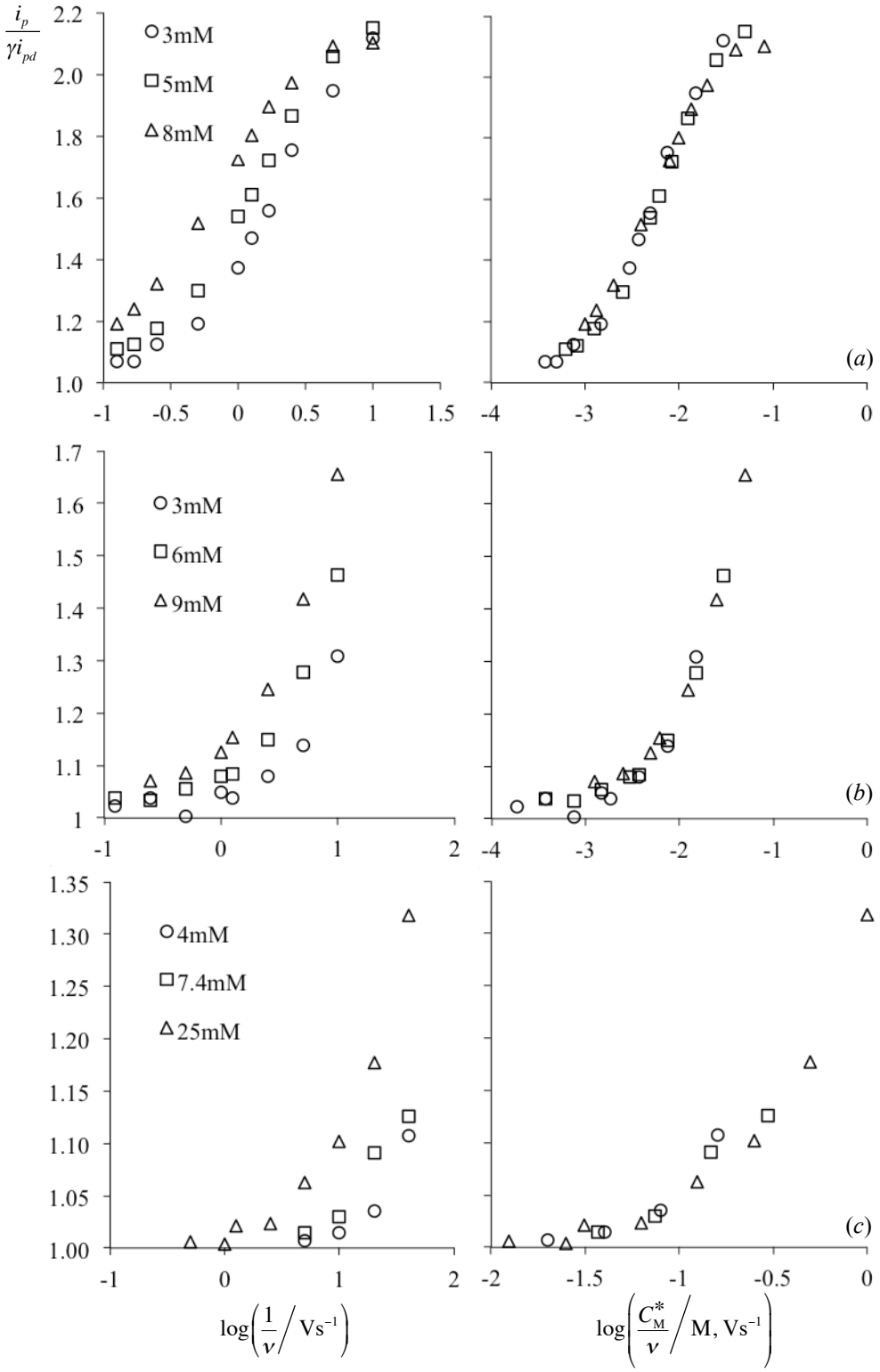

Figure 5.5: Variation of $i_p/\gamma i_{pd}$ as a function of sweep rate and mediator concentration for **1** clearly demonstrating electron transfer control in each case. (*a*) azobenzene, (*b*) 9-fluorenone, (*c*) 4-nitro-*o*-xylene

The data may then be fit to working curves generated by digital simulation. Catalysis depends only on the value of the dimensionless electron transfer rate constant $\lambda_{ET} = \left(\frac{RT}{nF}\right)\left(k_{ET}\frac{C_M^*}{\nu}\right)$. Then:

$$\log(\lambda_{et}) = \log\left\{\left(\frac{RT}{nF}\right)\left(k_{et}\frac{C_M^*}{\nu}\right)\right\} = \log\left(\frac{RT}{nF}k_{et}\right) + \log\left(\frac{C_M^*}{\nu}\right)$$

The data presented in **Figure 2.11** will be offset from the theoretical working curves by an amount equal to $\log\left(\frac{RT}{nF}k_{et}\right)$ and the homoegenous electron transfer rate constant may then be obtained. Plots of fits for all three mediators are presented in **Figure 5.6 – Figure 5.8**.

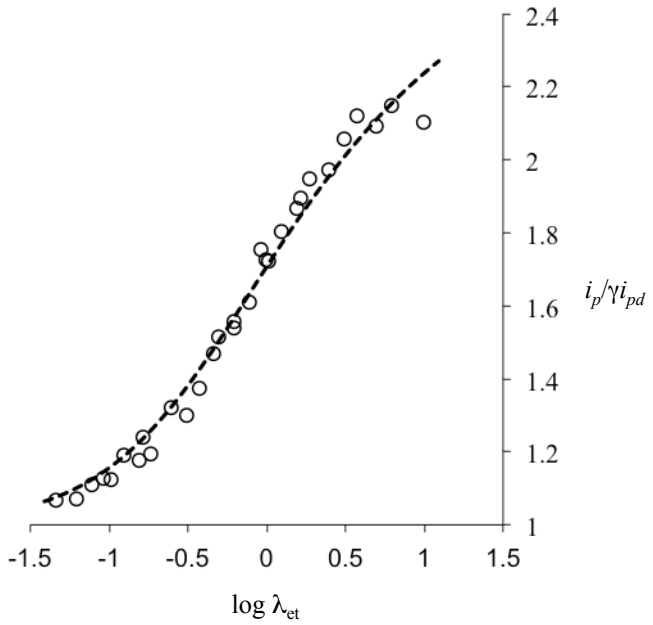

Figure 5.6: $i_p/\gamma i_{pd}$ data fit to dimensionless working curves for **1** (mediator = azobenzene). $\log\left(\frac{RT}{nF}k_{et}\right) = 2.092$, $k_{et} = (4.81 \pm 0.17)$ x 10^3 M^{-1} s^{-1}

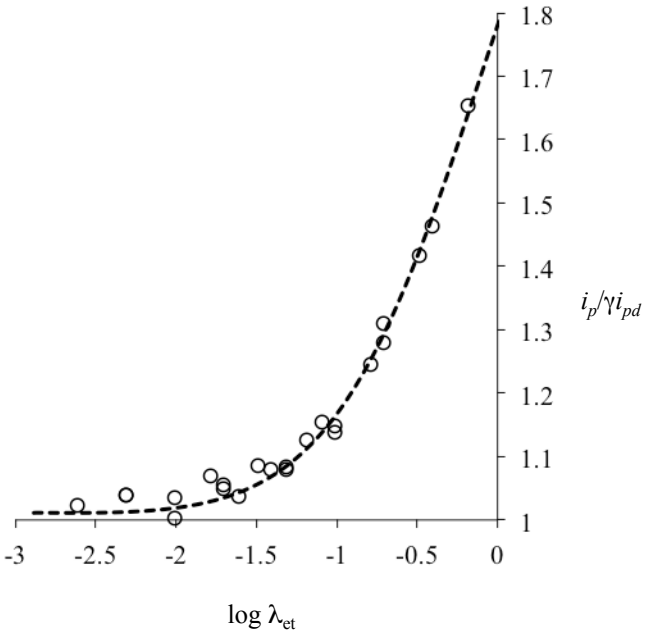

Figure 5.7: $i_p/\gamma i_{pd}$ data fit to dimensionless working curves for **1** (mediator = 9-fluorenone). $\log\left(\frac{RT}{nF}k_{et}\right) = 1.115$, $k_{et} = (5.07 \pm 0.15)$ x 10^2 M^{-1} s^{-1}

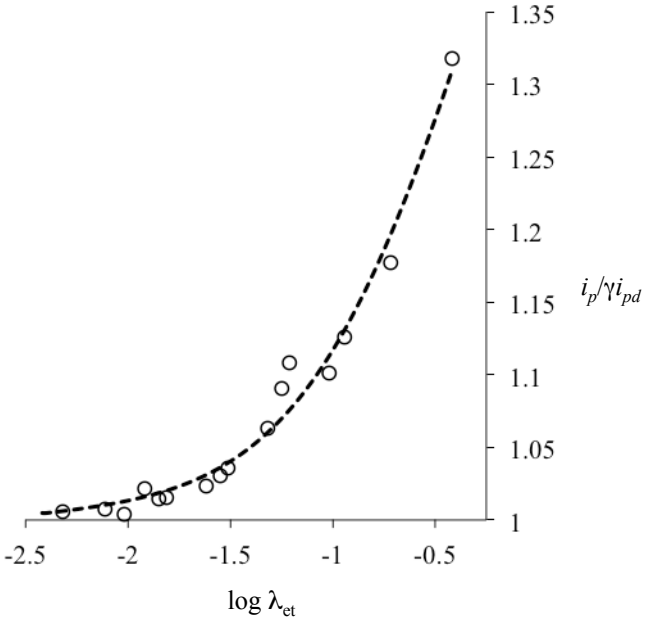

Figure 5.8: $i_p/\gamma i_{pd}$ data fit to dimensionless working curves for **1** (mediator = 4-nitro-*o*-xylene). $\log\left(\frac{RT}{nF}k_{et}\right) =$ –0.416, $k_{et} = (1.49 \pm 0.13)$ x 10^1 M^{-1} s^{-1}

From the rate constants a Marcus plot (see **2.3.1**) may be generated. The appropriate plot is given in **Figure 2.20**.

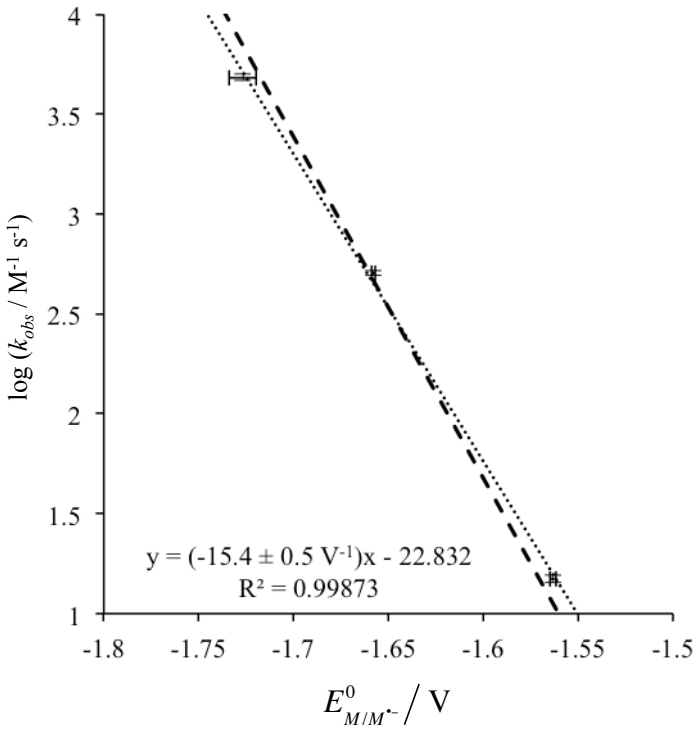

Figure 5.9: Marcus plots for **1**. Linear regression (dotted line) gives a slope, $m = -15.4 \pm 0.5$ V^{-1}. Extrapolation to the diffusion controlled rate constant using the theoretical slope (dashed line) yields the reduction potential, $E^o = -2.09 \pm 0.01$ V.

The slope of the trend line generated from the HRC data is -15.4 ± 0.5 V^{-1}, close to the theoretically correct value of -17.08 V^{-1}. Although the trend line generated by the data may be extrapolated back till it intersects the diffusion control rate limit to obtain the reduction potential of the substrate, in practice small errors in the data extrapolate out to large errors when projecting the trend line backwards, so the theoretically correct slope of -17.08 V^{-1} is used instead of the experimentally obtained slope. E^o of **1** is thus found to be -2.09 ± 0.01 V. **Equation 3** can then be solved to obtain the ring opening rate constant, $k_{cs} = (4 \pm 3) \times 10^8$ s^{-1}.

$$-2.06\ \text{V} + \left(\frac{RT}{2nF}\ln 10\right)\log k_{cs} = -1.83\ \text{V} - \left(\frac{RT}{2nF}\ln 10\right)\left[1.38 - \log\left(\frac{nF}{2RT}\right)\right]$$

5.1.2 2,3-Epoxy-propiophenone (2)

Epoxyketone **2** is identical in behavior with **1**. The relevant data is presented below. Following the same analysis the reduction potential E^o is determined to be -2.14 ± 0.01 V and the ring opening rate constant k_{cs} is found to be (8 ± 6) x 10^7 s^{-1}.

5.1.2.1 Cyclic voltammetry of 2

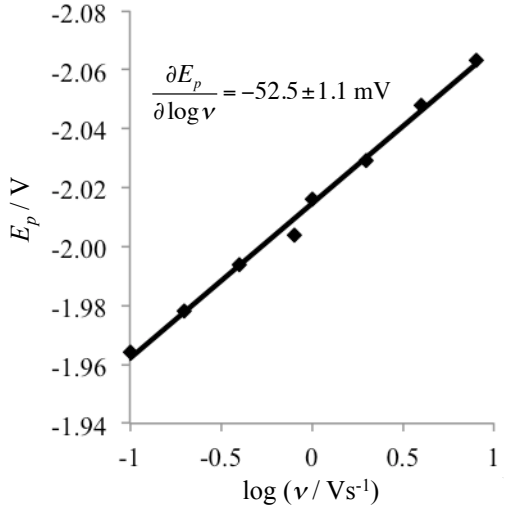

Figure 5.10: Variation of peak potential as a function of scan rate in DMF. C_2 = 0.003 M, 0.5 M supporting electrolyte (TBAP), ν = 100, 200, 400, 800, 1000, 2000, 4000, 8000 mV/s

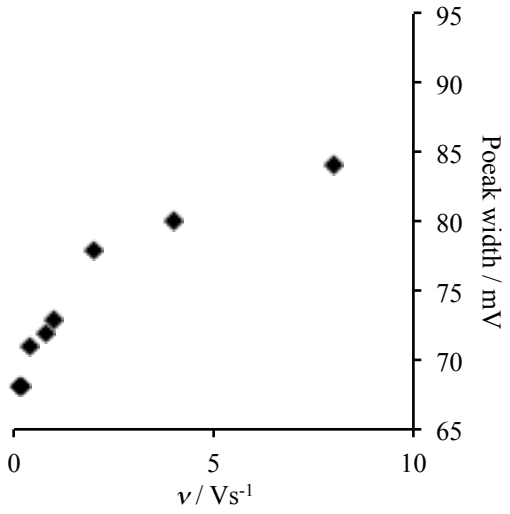

Figure 5.11: Variation of peak width as a function of scan rate in DMF. C_2 = 0.003 M, 0.5 M supporting electrolyte (TBAP), ν = 100, 200, 400, 800, 1000, 2000, 4000, 8000 mV/s

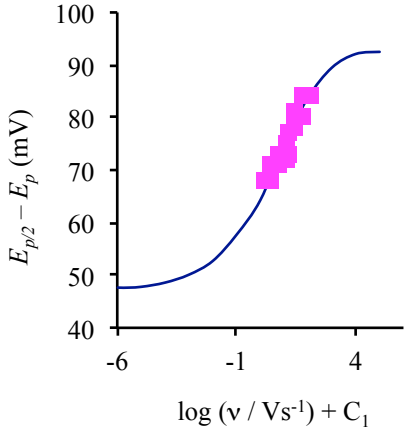

Figure 5.12: Determination of C_1 for **2**. Experimental peak widths are translated along the x-coordinate to obtain the fitting parameter C_1 = 1.14.

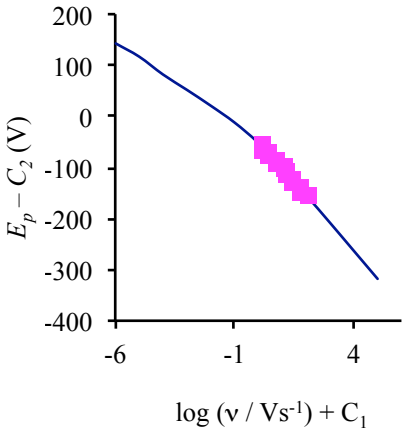

Figure 5.13 Determination of C_2 for **2**. Experimental peak widths are translated along the y-coordinate to obtain the fitting parameter C_2 = -1.90 V.

5.1.2.2 Homogeneous redox catalysis of 2

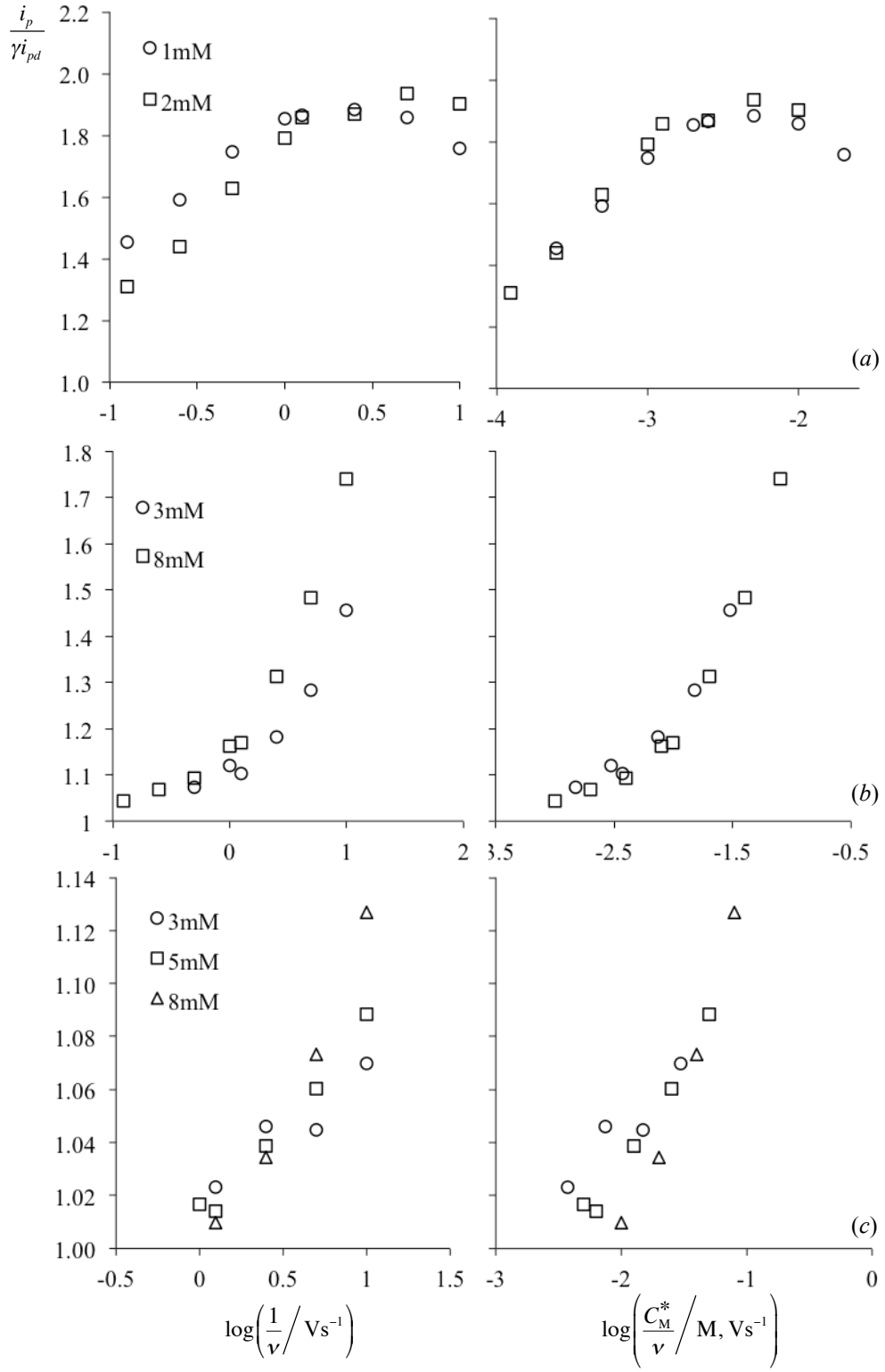

Figure 5.14: Variation of $i_p/\gamma i_{pd}$ as a function of sweep rate and mediator concentration for **2** clearly demonstrating electron transfer control in each case. (*a*) 1,4-diacetylbenzene, (*b*) azobenzene, (*c*) 9-fluorenone.

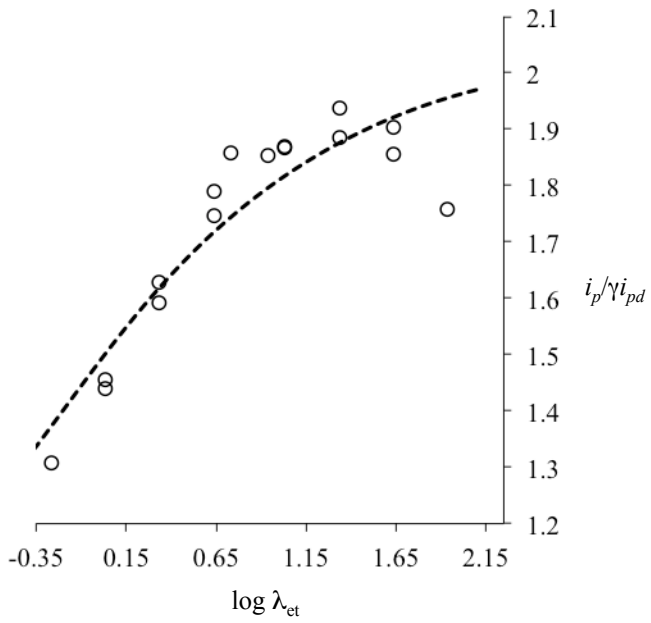

Figure 5.15: $i_p/\gamma i_{pd}$ data fit to dimensionless working curves for **2** (mediator = 1,4-diacetylbenzene). $\log\left(\frac{RT}{nF}k_{et}\right) = 3.64$, $k_{et} = (1.7 \pm 0.3)$ x 10^5 M^{-1} s^{-1}

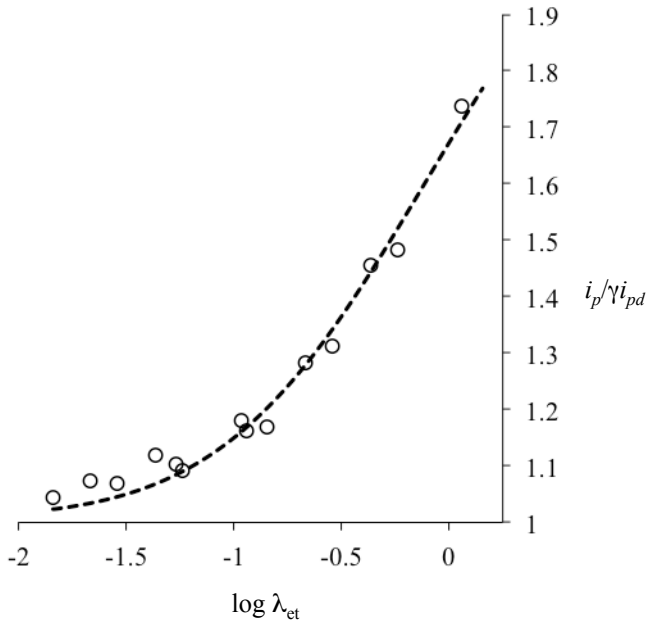

Figure 5.16: $i_p/\gamma i_{pd}$ data fit to dimensionless working curves for **2** (mediator = azobenzene). $\log\left(\frac{RT}{nF}k_{et}\right) = 1.156$, $k_{et} = (5.57 \pm 0.25)$ x 10^2 M^{-1} s^{-1}

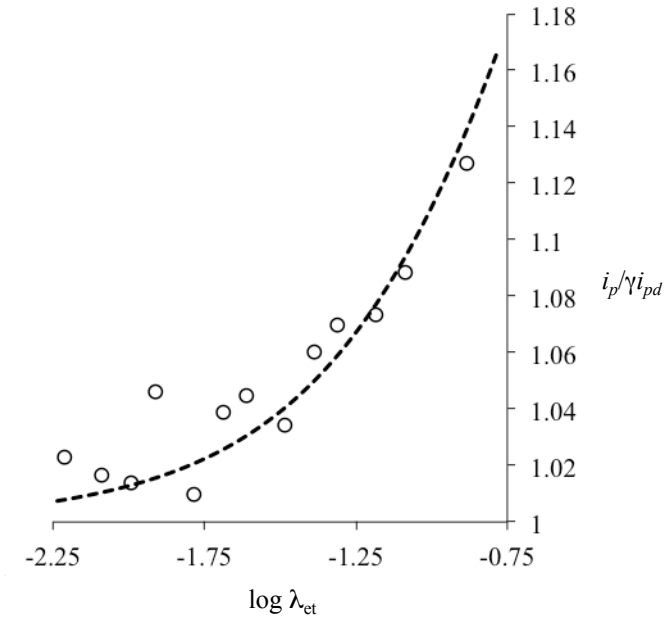

Figure 5.17: $i_p/\gamma i_{pd}$ data fit to dimensionless working curves for **2** (mediator = 9-fluorenone). $\log\left(\frac{RT}{nF}k_{et}\right) = 0.21$, $k_{et} = (6.4 \pm 0.5)$ x 10^1 M^{-1} s^{-1}

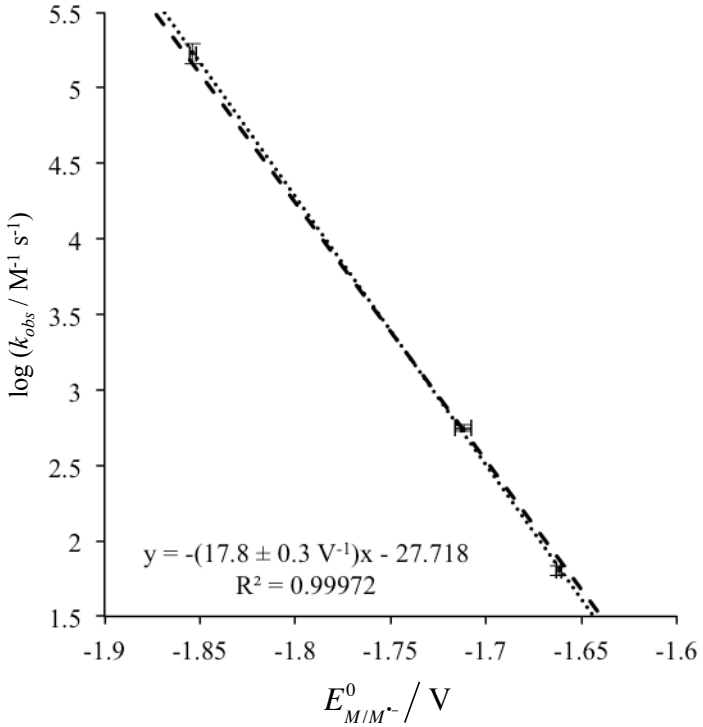

Figure 5.18: Marcus plots for **2**. Linear regression (dotted line) gives a slope, $m = -17.8 \pm 0.3$ V^{-1}. Extrapolation to the diffusion controlled rate constant using the theoretical slope (dashed line) yields the reduction potential, $E^o = -2.14 \pm 0.05$ V.

5.1.3 Cyclic voltammetry and convolution analysis of 2,2-dimethyl-1-(3-phenyloxiranyl)-1-propanone (3)

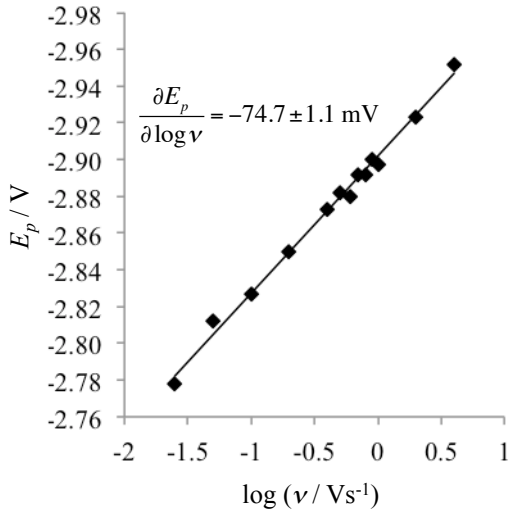

Figure 5.19: Variation of peak potential as a function of scan rate of **3** in DMF. C_3 = 0.0030 M, 0.5 M supporting electrolyte (TBAP), ν = 25, 50, 100, 200, 400, 500, 600, 700, 800, 900, 1000, 2000, 4000mV/s

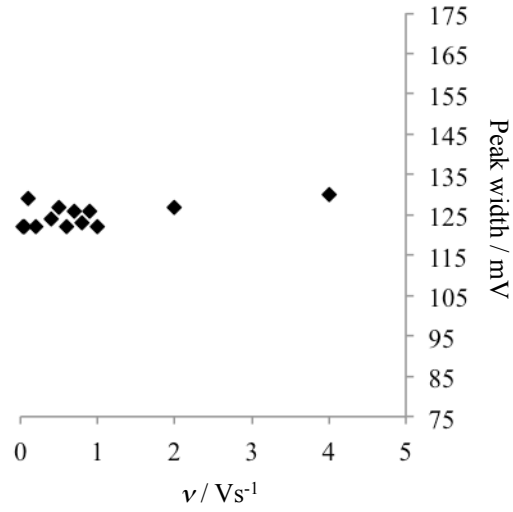

Figure 5.20: Variation of peak width as a function of scan rate of **3** in DMF. C_3 = 0.0030 M, 0.5 M supporting electrolyte (TBAP), ν = 25, 50, 100, 200, 400, 500, 600, 700, 800, 900, 1000, 2000, 4000mV/s

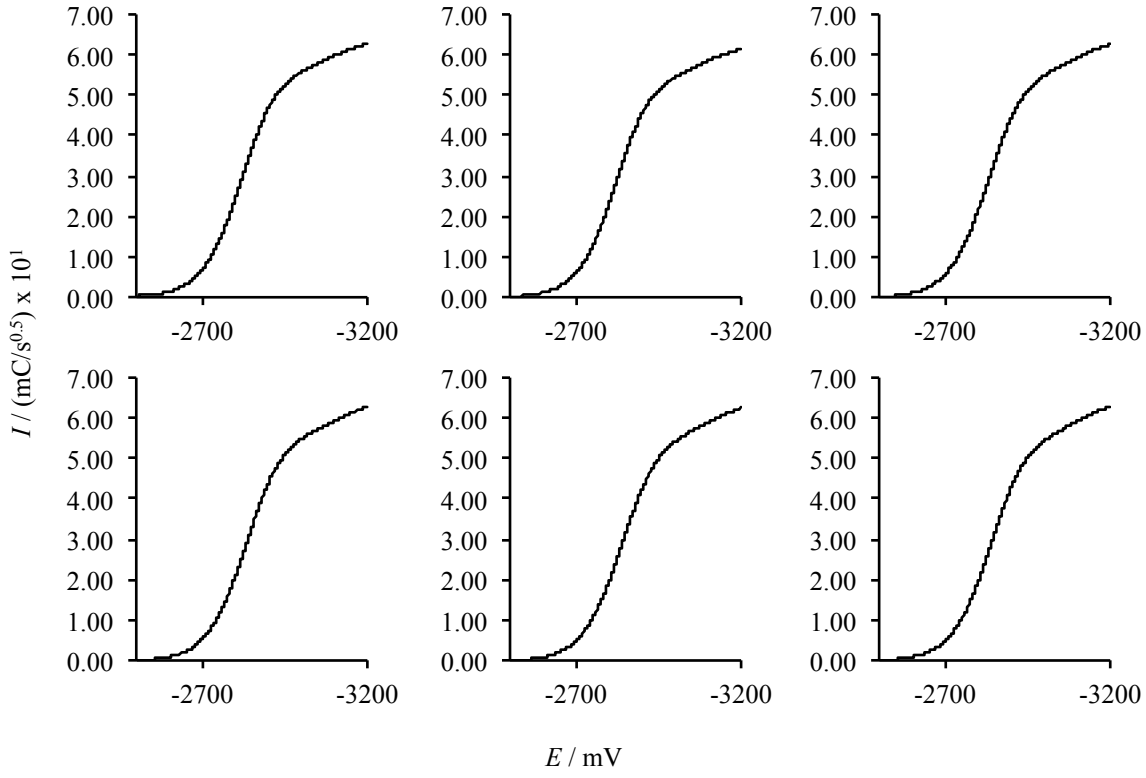

Figure 5.21: Convolution voltammograms of **3** in DMF. C_3 = 0.0030M, 0.5 M supporting electrolyte (TBAP), ν = 500 (upper left), 600, 700, 800, 900, 1000 (lower right) mV/s

The convolutions voltammograms give in **Figure 5.21** were obtained via convolution of the voltammograms with a BASIC program written in house. Each convolution voltammogram shows significant current from reduction of the solvent/electrolyte combination below ≈ 3V; to obtain the limiting current the limiting current the data was subjected to non-linear analysis with the regression analysis software TableCurve,[81] where all data collected below 3V was excluded

Table 5.1
Important potentials and currents obtained from cyclic voltammograms and convolution analysis for **3**

ν (V/s)	E_p (V)	$E_p - E_{p/2}$ (V)	i_p (mA)	I_{lim} (mC/s$^{1/2}$)
0.5	-2.882	-127	0.772	0.586176
0.6	-2.88	-122	0.831	0.574146
0.7	-2.892	-126	0.903	0.589182
0.8	-2.892	-123	0.971	0.589182
0.9	-2.900	-126	1.02	0.589182
1	-2.897	-122	1.08	0.589182

from the analysis (**Figure 5.22**). Important potentials (peak potential, peak width) and current (peak current, convolution current) obtained from the voltammograms are given in **Table 5.1**

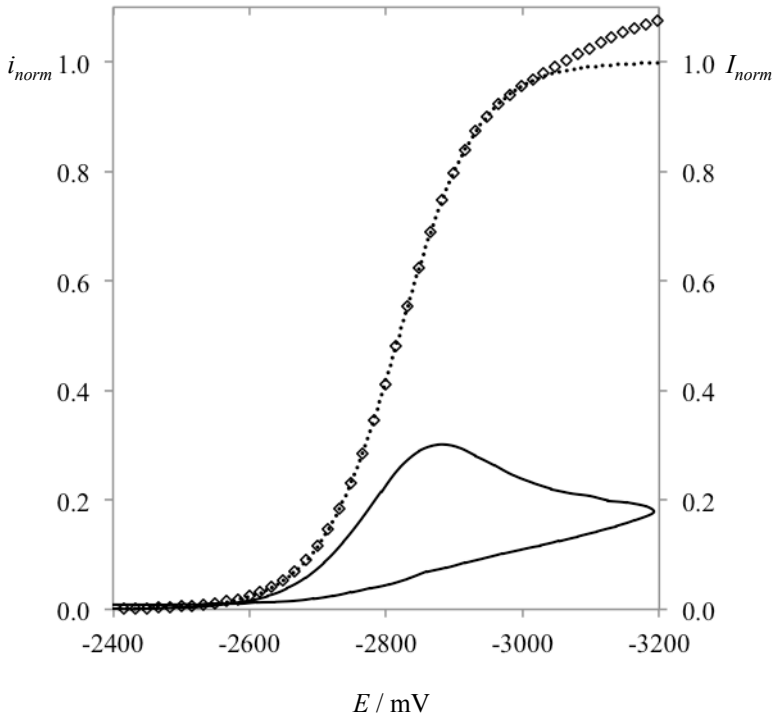

Figure 5.22: Cyclic voltammogram (___), convolution voltammogram (empty diamonds), and sigmoid function (•••) used to determine I_{lim}. Below 3V reduction of solvent/electrolyte causes an increase in both normal and convolutive current. Fitting the sigmoidal function to data above 3V (where most of the current is faradaic current from reduction of **3**) allows determination of I_{lim}. Voltammograms of **3** in DMF. C_3 = 0.003M, 0.5 M supporting electrolyte (TBAP), ν = 500 mV/s. $i_{norm} = \frac{i}{nFAD_3^{1/2}C_3(nF/RT)^{1/2}\nu^{1/2}}$, $I_{norm} = \frac{I}{I_{lim}}$

Each voltammogram was subjected to treatment according to the following equations:

$$E_{applied} = E^0_{A/A^{\cdot-}} - \frac{RT}{\alpha nF}\ln\left(\frac{D_A^{\frac{1}{2}}}{k_{het}}\right) + \frac{RT}{\alpha nF}\ln\left(\frac{I_{lim} - I_t}{i_t}\right) \qquad \textbf{Eq. 5.4}$$

$$\ln k_{het} = \ln D_A^{\frac{1}{2}} - \ln\left(\frac{I_{lim} - I_t}{i_t}\right) \qquad \textbf{Eq. 5.5}$$

$$\alpha = \frac{\partial \Delta G^{\neq}}{d\Delta G^0} = -\left(\frac{RT}{nF}\right)\frac{\partial \ln k_{het}}{\partial E} = \frac{nF\left(E - E^0_{A/A^{\cdot-}}\right)}{2\lambda} + \frac{1}{2} \qquad \textbf{Eq. 5.6}$$

Eq. 5.4 corresponds to a Butler-Volmer treatment of the data, assuming a constant value of α. **Eq. 5.5** allows determination of the heterogeneous rate constant as a function of potential (the current function, $\ln\left(\frac{I_{lim}-I_t}{i_t}\right)$, is potential dependent). **Eq. 5.6** gives the variation of the heterogeneous rate constant with potential. It is important to recognize that this current function is undefined in both extremes of current (as $I_t \rightarrow I_{lim}$ and as $i_t \rightarrow 0$) As such only the middle 60 – 80% of each voltammogram is used for the following analysis. TableCurve was used to fit the $-\left(\frac{RT}{nF}\right)\ln k_{het}$ versus E data to a generic form of the Marcus equation and then to generate values of α. Plots for each voltammogram are given in **Figure 5.23 – Figure 5.28**.

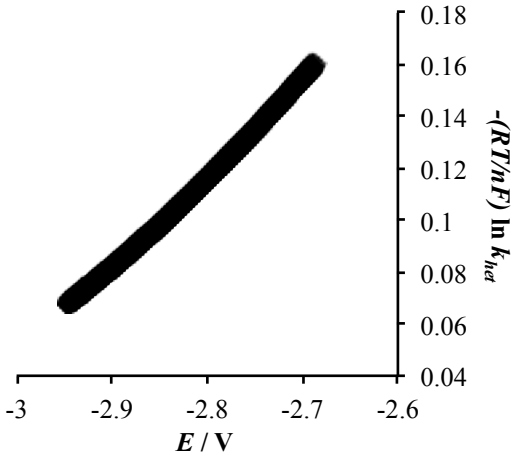

Figure 5.23: Compound **3**. $-\left(\frac{RT}{nF}\right)\ln k_{het}$ vs. *E*, ν = 500 mV/s, C_3 = 0.003 M in DMF, 0.5 M supporting electrolyte (TBAP)

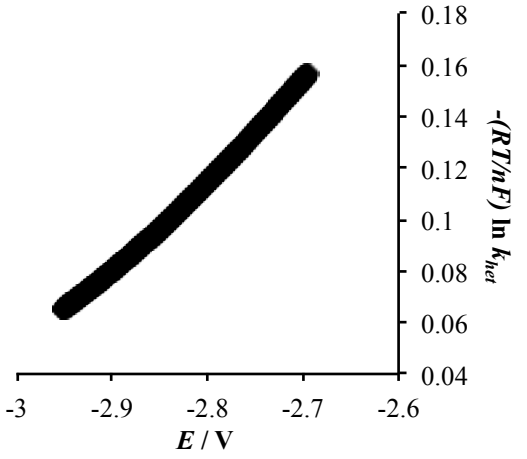

Figure 5.24: Compound **3**. $-\left(\frac{RT}{nF}\right)\ln k_{het}$ vs. *E*, ν = 600 mV/s, C_3 = 0.003 M in DMF, 0.5 M supporting electrolyte (TBAP)

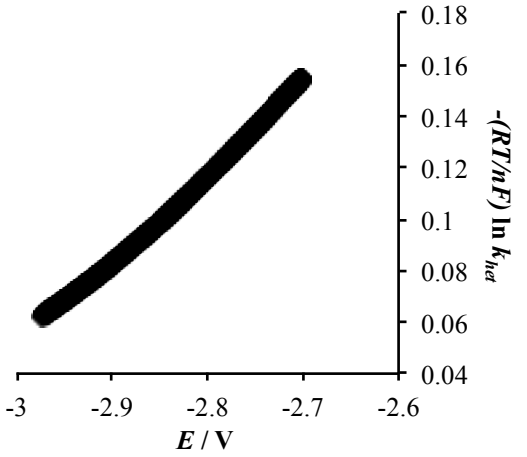

Figure 5.25: Compound **3**. $-\left(\frac{RT}{nF}\right)\ln k_{het}$ vs. *E*, ν = 700 mV/s, C_3 = 0.003 M in DMF, 0.5 M supporting electrolyte (TBAP)

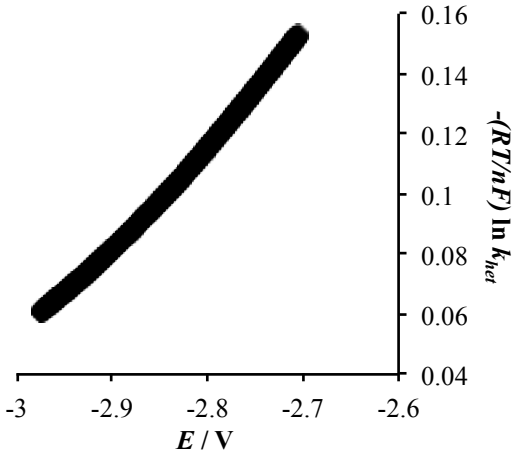

Figure 5.26: Compound **3**. $-\left(\frac{RT}{nF}\right)\ln k_{het}$ vs. *E*, ν = 800 mV/s, C_3 = 0.003 M in DMF, 0.5 M supporting electrolyte (TBAP)

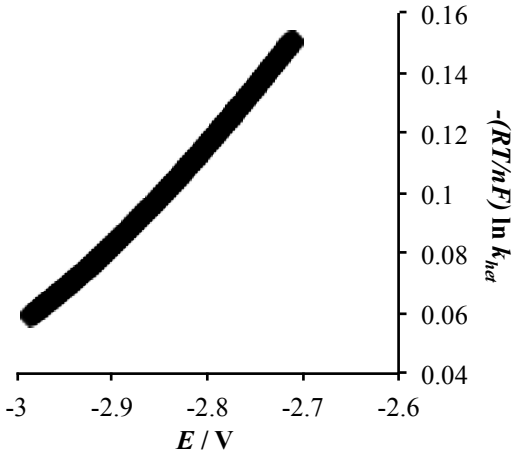

Figure 5.27: Compound **3**. $-\left(\frac{RT}{nF}\right)\ln k_{het}$ vs. *E*, ν = 900 mV/s, C_3 = 0.003 M in DMF, 0.5 M supporting electrolyte (TBAP)

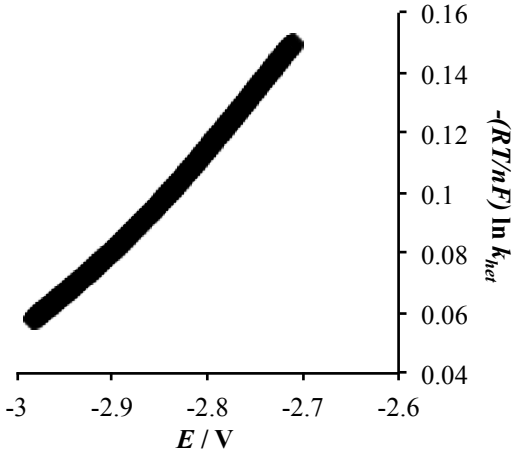

Figure 5.28: Compound **3**. $-\left(\frac{RT}{nF}\right)\ln k_{het}$ vs. *E*, ν = 1000 mV/s, C_3 = 0.003 M in DMF, 0.5 M supporting electrolyte (TBAP)

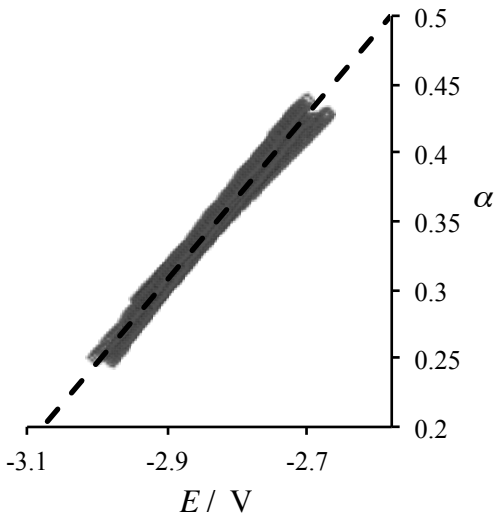

Figure 5.29: α as a function of potential. **3** in DMF, ν = 500-1000 mV/s. Extrapolation to $\alpha = 0.5$ gives the standard reduction potential of **3** in accordance with **Eq. 5.6**.

5.1.4 Cyclic voltammetry and convolution analysis of 1-[3-(1,1-dimethylethyl)-3-methyloxiranyl]-2,2-dimethyl-1-propanone (4)

NOTE: Cyclic voltammograms of **4** were treated in the exact same fashion as described for **3** above.

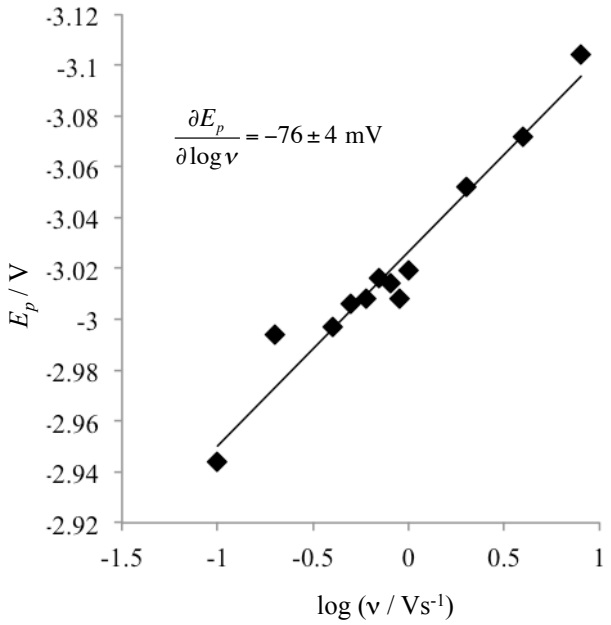

Figure 5.30: Variation of peak potential as a function of scan rate of **4** in DMF. C_4 = 0.0016 M, 0.5 M supporting electrolyte (TBAP), ν = 100, 200, 400, 500, 600, 700, 800, 900, 1000, 2000, 4000, 8000 mV/s

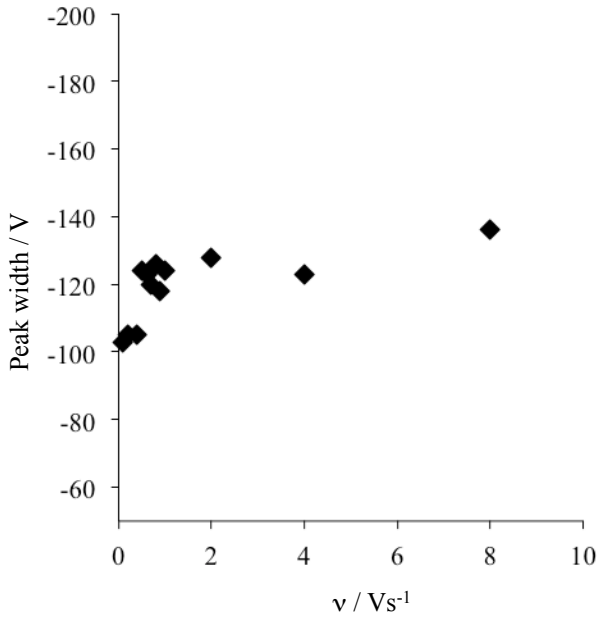

Figure 5.31: Variation of peak width as a function of scan rate of **4** in DMF. C_4 = 0.0016 M, 0.5 M supporting electrolyte (TBAP), ν = 100, 200, 400, 500, 600, 700, 800, 900, 1000, 2000, 4000, 8000 mV/s

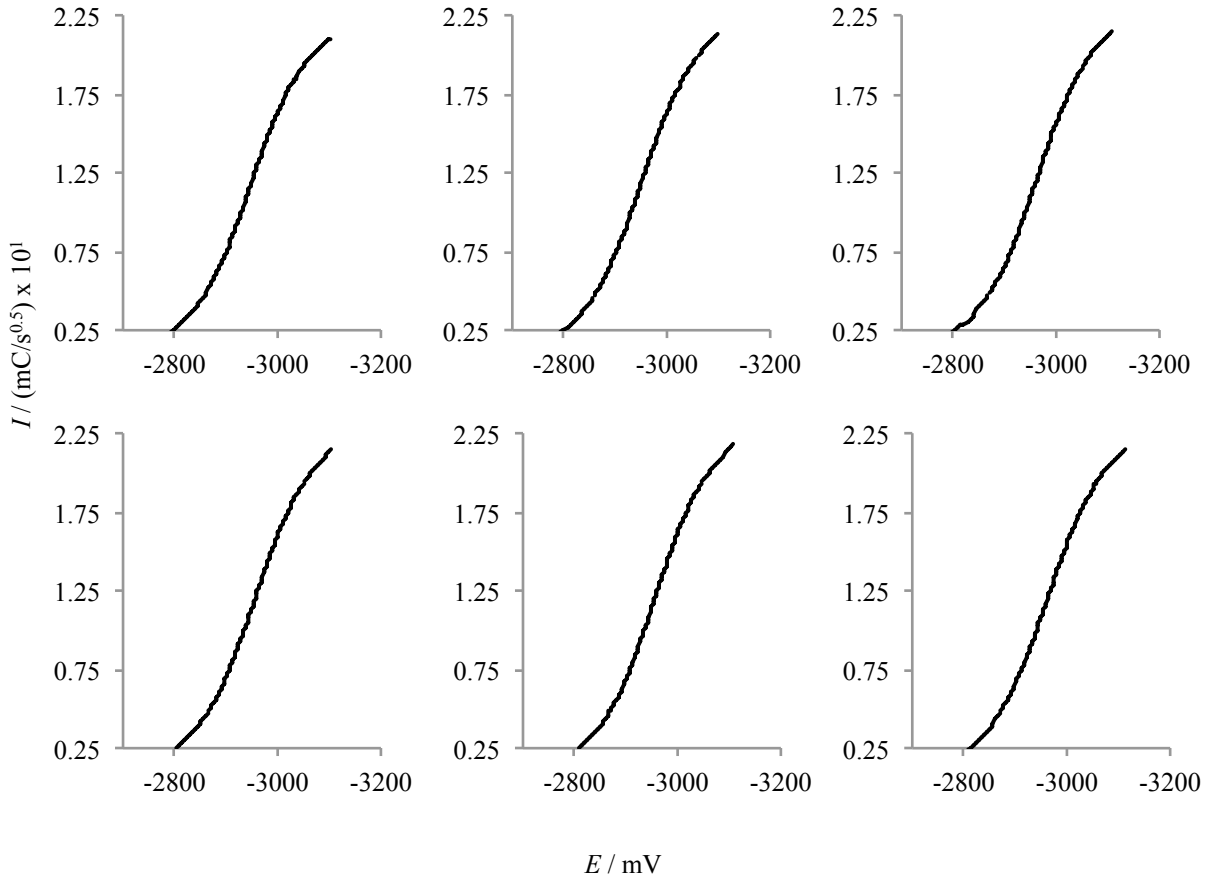

Figure 5.32: Convolution voltammograms of **4** in DMF. C_4 = 0.0016M, 0.5 M supporting electrolyte (TBAP), ν = 500 (upper left), 600, 700, 800, 900, 1000 (lower right) mV/s

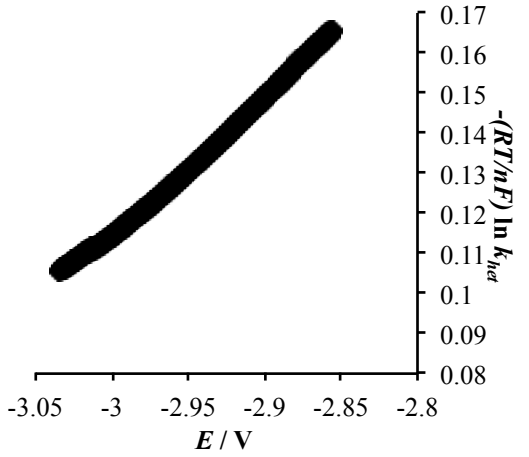

Figure 5.33: Compound **4**. $-\left(\frac{RT}{nF}\right)\ln k_{het}$ vs. *E*, ν = 500 mV/s, C_4 = 0.0016M in DMF, 0.5 M supporting electrolyte (TBAP)

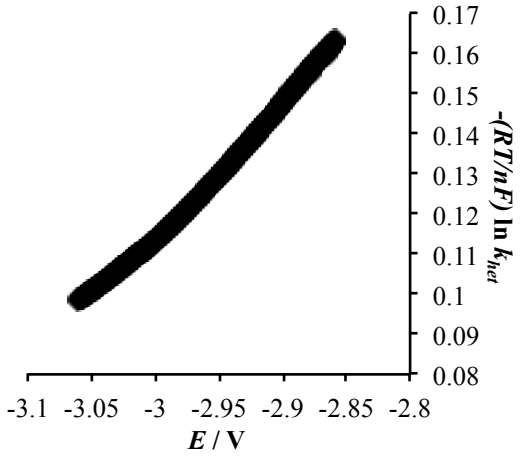

Figure 5.34: Compound **4**. $-\left(\frac{RT}{nF}\right)\ln k_{het}$ vs. *E*, ν = 600 mV/s, C_4 = 0.0016M in DMF, 0.5 M supporting electrolyte (TBAP)

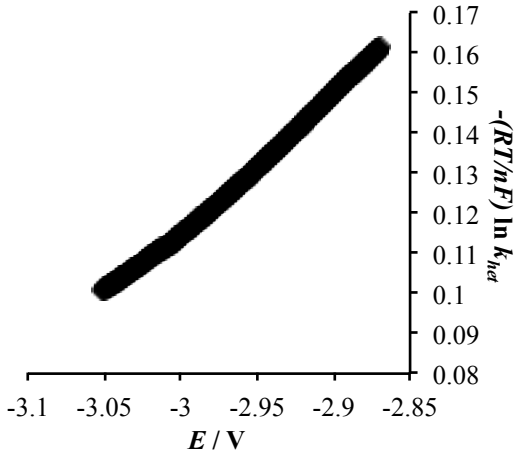

Figure 5.35: Compound **4**. $-\left(\frac{RT}{nF}\right)\ln k_{het}$ vs. *E*, ν = 700 mV/s, C_4 = 0.0016M in DMF, 0.5 M supporting electrolyte (TBAP)

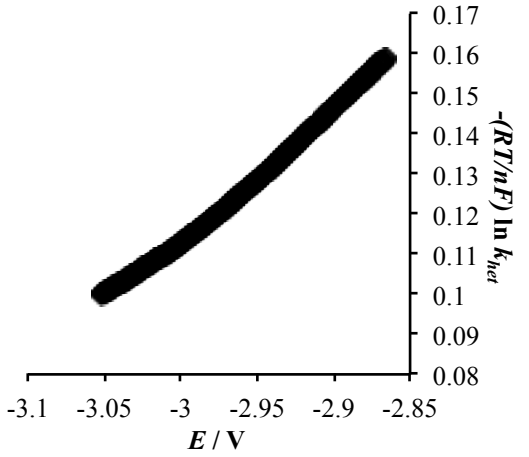

Figure 5.36: Compound **4**. $-\left(\frac{RT}{nF}\right)\ln k_{het}$ vs. *E*, ν = 800 mV/s, C_4 = 0.0016M in DMF, 0.5 M supporting electrolyte (TBAP)

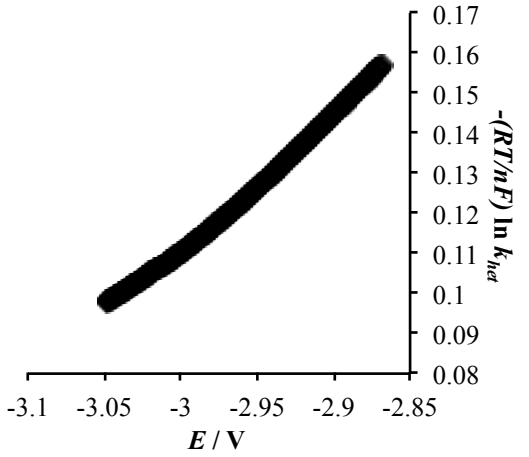

Figure 5.37: Compound **4**. $-\left(\frac{RT}{nF}\right)\ln k_{het}$ vs. *E*, ν = 900 mV/s, C_4 = 0.0016M in DMF, 0.5 M supporting electrolyte (TBAP)

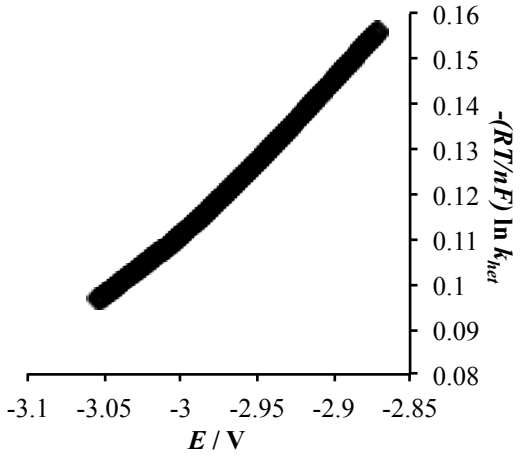

Figure 5.38: Compound **4**. $-\left(\frac{RT}{nF}\right)\ln k_{het}$ vs. *E*, ν = 1000 mV/s, C_4 = 0.0016M in DMF, 0.5 M supporting electrolyte (TBAP)

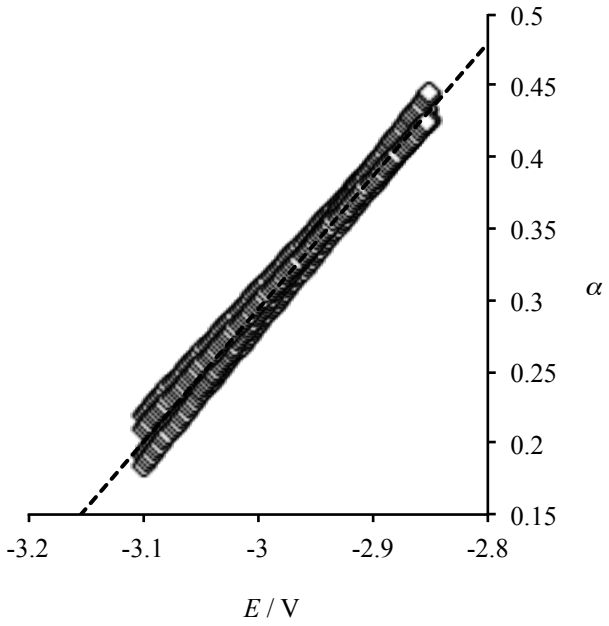

Figure 5.39: α as a function of potential. **4** in DMF, ν = 500-1000 mV/s. Extrapolation to $\alpha = 0.5$ gives the standard reduction potential of **4** in accordance with **Eq. 5.6**.

5.2 Oxidation of tetra-*n*-butylammonium acetate

5.2.1 Dry acetonitrile

5.2.1.1 Convolution voltammetry

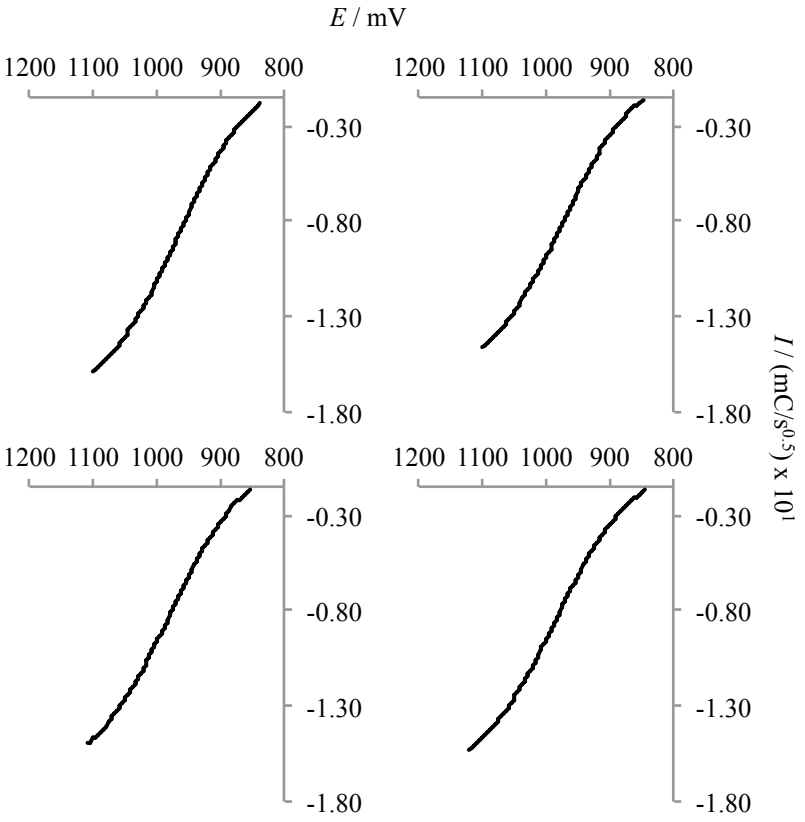

Figure 5.40: Convolution voltammograms of tetra-*n*-butylammonium acetate in dry acetonitrile. C_{AcO^-} = 0.003 M, 0.5 M supporting electrolyte (TBAP), ν = 100 (upper left), 200, 300, 400 (lower right) mV/s

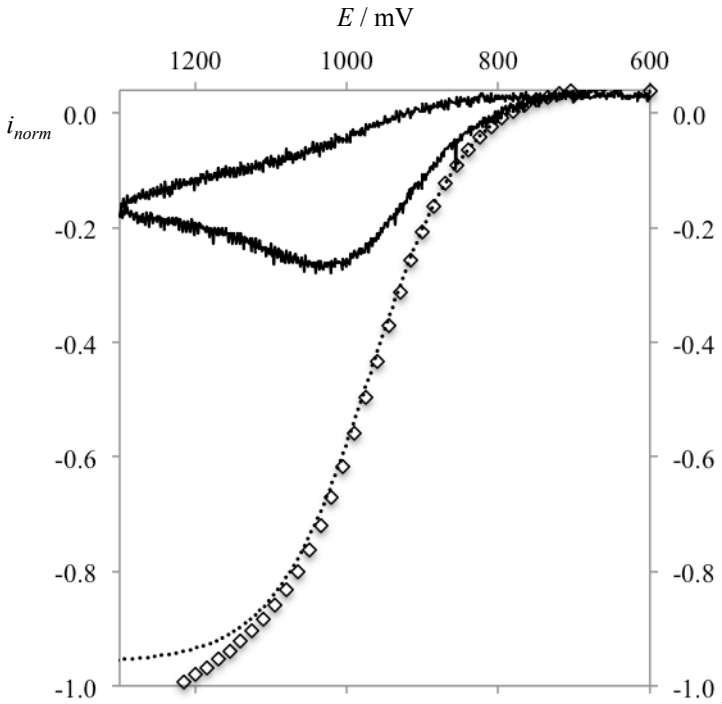

Figure 5.41: Cyclic voltammogram (___), convolution voltammogram (empty diamonds), and sigmoid function (•••) used to determine I_{lim}. Above 1.2 V reduction of solvent/electrolyte causes an increase in both normal and convolutive current. Fitting the sigmoidal function to data below 1.2 V (where most of the current is faradaic current from oxidation of acetate) allows determination of I_{lim}. Voltammograms of tetra-*n*-butylammonium acetate in DMF. C_{AcO^-} = 0.003 M, 0.5 M supporting electrolyte (TBAP), ν = 100 mV/s. $i_{norm} = \frac{i}{nFAD_3^{1/2}C_3(nF/RT)^{1/2}\nu^{1/2}}$, $I_{norm} = \frac{I}{I_{lim}}$

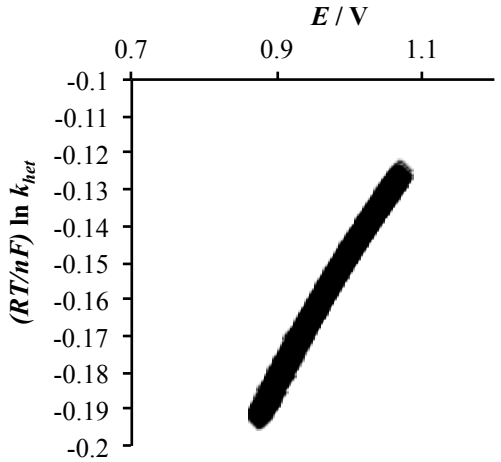

Figure 5.42: Tetra-*n*-butylammonium acetate in dry acetonitrile. $\left(\frac{RT}{nF}\right) \ln k_{het}$ vs. *E*, ν = 100 mV/s, C_{AcO^-} = 0.003 M in dry acetonitrile, 0.5 M supporting electrolyte (TBAP)

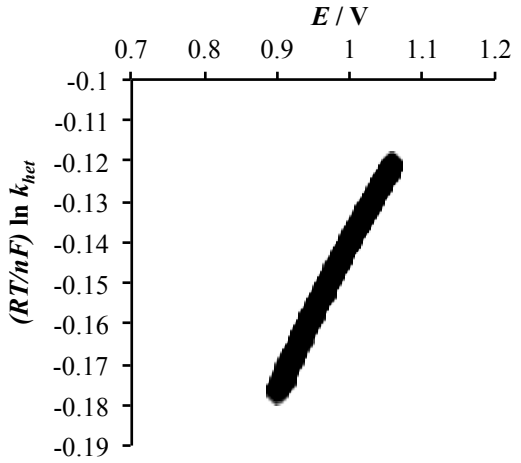

Figure 5.43: Tetra-*n*-butylammonium acetate in dry acetonitrile. $\left(\frac{RT}{nF}\right) \ln k_{het}$ vs. *E*, ν = 200 mV/s, C_{AcO^-} = 0.003 M in dry acetonitrile, 0.5 M supporting electrolyte (TBAP)

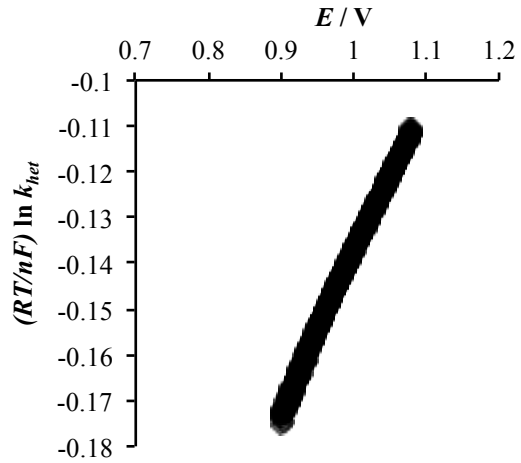

Figure 5.44: Tetra-*n*-butylammonium acetate in dry acetonitrile. $\left(\frac{RT}{nF}\right) \ln k_{het}$ vs. *E*, ν = 300 mV/s, C_{AcO^-} = 0.003 M in dry acetonitrile, 0.5 M supporting electrolyte (TBAP)

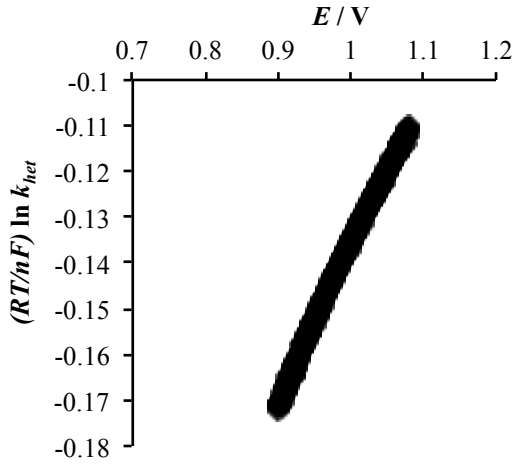

Figure 5.45: Tetra-*n*-butylammonium acetate in dry acetonitrile. $\left(\frac{RT}{nF}\right) \ln k_{het}$ vs. *E*, ν = 400 mV/s, $C_{\mathbf{AcO^-}}$ = 0.003 M in dry acetonitrile, 0.5 M supporting electrolyte (TBAP)

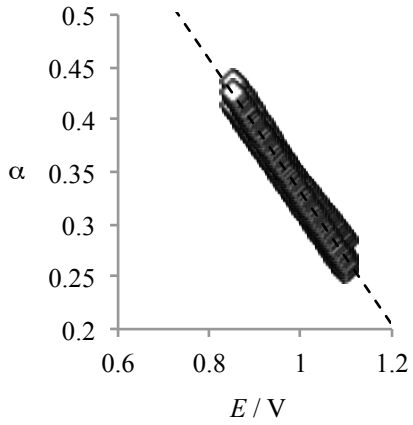

Figure 5.46: α as a function of potential. Tetra-*n*-butylammonium acetate in dry acetonitrile, ν = 100-400 mV/s. Extrapolation to α = 0.5 gives the standard oxidation potential of acetate in accordance with **Eq. 5.6**.

5.2.1.2 Homogeneous redox catalysis

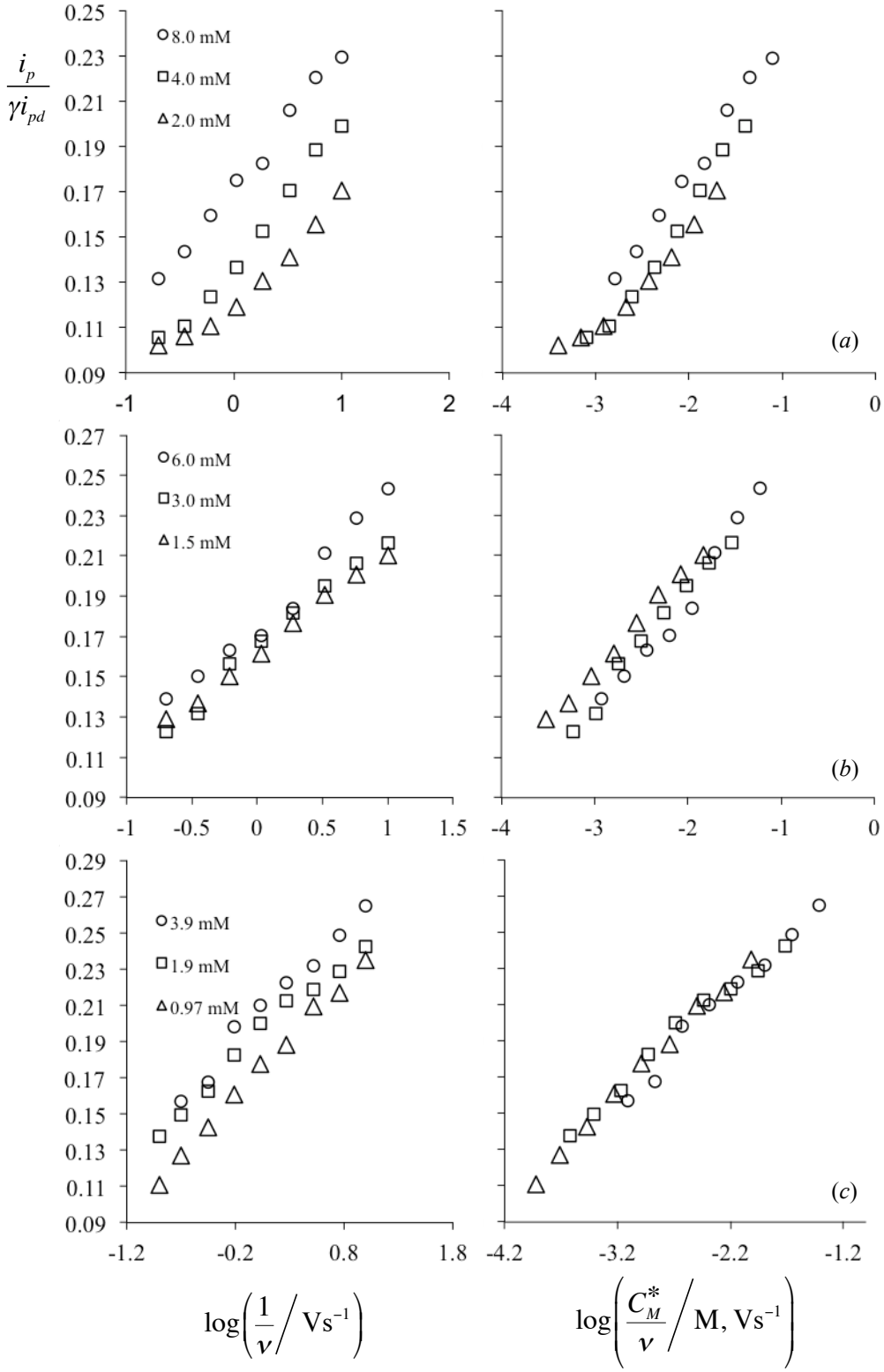

Figure 5.47: Variation of $i_p/\gamma i_{pd}$ as a function of sweep rate and mediator concentration for tetra-*n*-butylammonium acetate in anhydrous acetonitrile clearly demonstrating electron transfer control in each case. (*a*) ferrocene, (*b*) vinylferrocene, (*c*) *p*-bromophenylferrocene

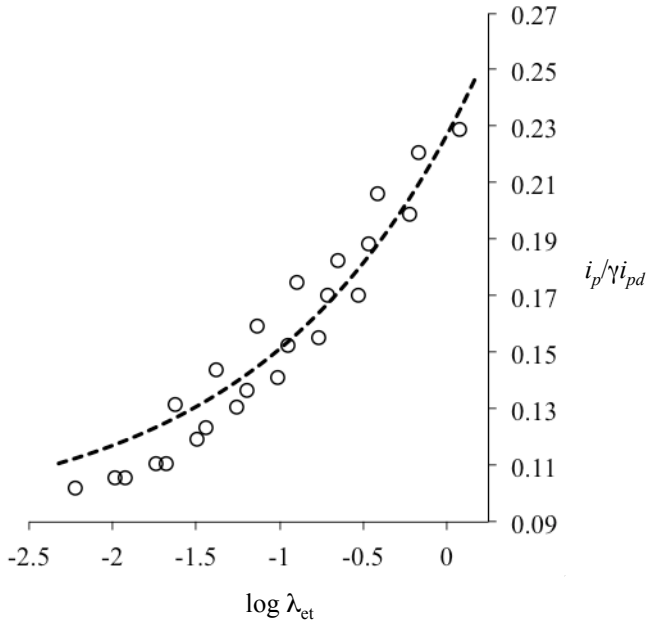

Figure 5.48: $i_p/\gamma i_{pd}$ data fit to dimensionless working curves for tetra-*n*-butylammonium acetate in dry acetonitrile (mediator = ferrocene). $\log\left(\frac{RT}{nF}k_{et}\right) = 1.17$, $k_{et} = (5.8 \pm 0.5)$ x 10^2 M^{-1} s^{-1}

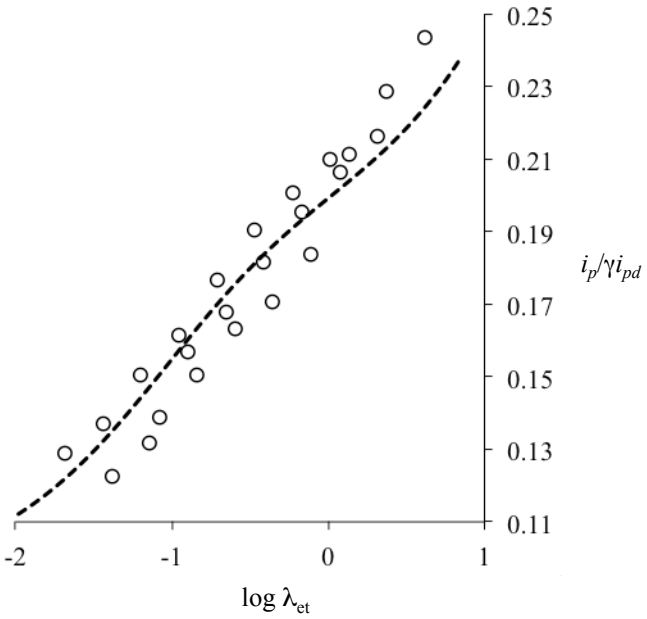

Figure 5.49: $i_p/\gamma i_{pd}$ data fit to dimensionless working curves for tetra-*n*-butylammonium acetate in dry acetonitrile (mediator = vinylferrocene). $\log\left(\frac{RT}{nF}k_{et}\right) = 1.84$, $k_{et} = (2.7 \pm 0.3)$ x 10^3 M^{-1} s^{-1}

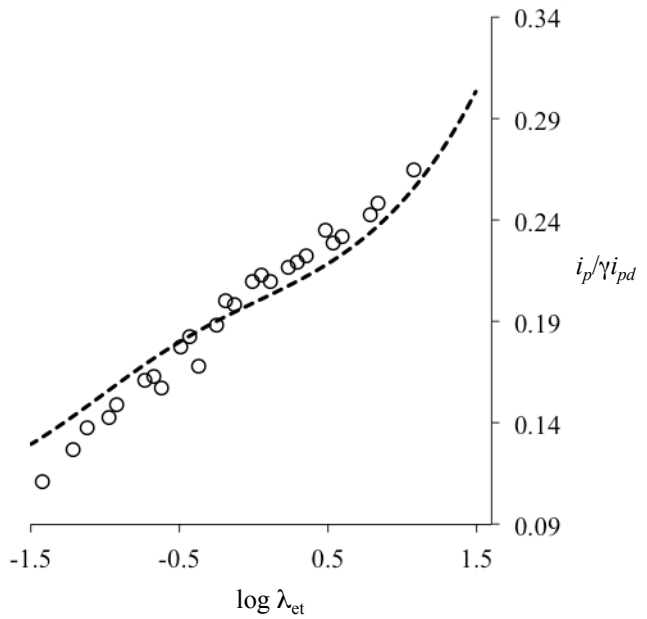

Figure 5.50: $i_p/\gamma i_{pd}$ data fit to dimensionless working curves for tetra-*n*-butylammonium acetate in dry acetonitrile (mediator = *p*-bromophenylferrocene). $\log\left(\frac{RT}{nF}k_{et}\right) = 2.494$, $k_{et} = (1.21 \pm 0.13)$ x 10^4 M^{-1} s^{-1}

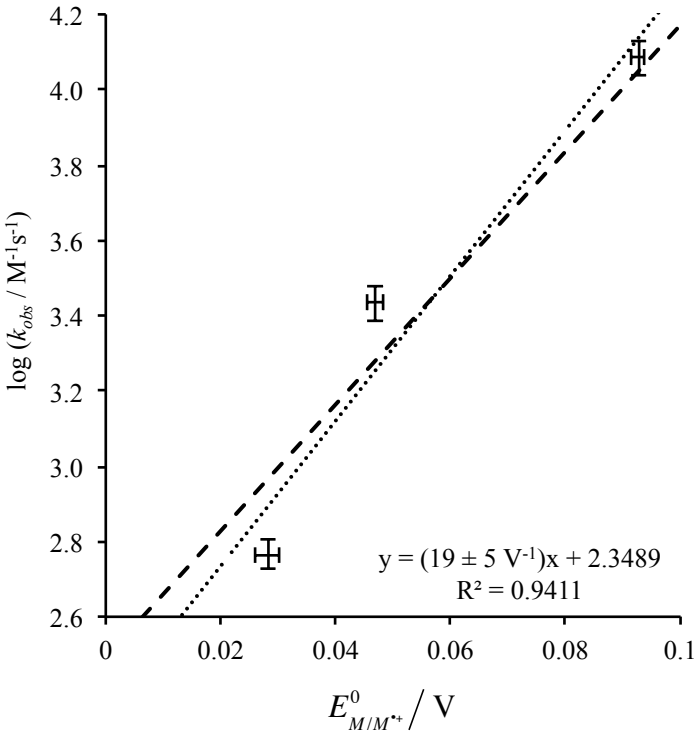

Figure 5.51: Marcus plots for tetra-*n*-butylammonium acetate. Linear regression (dotted line) gives a slope, $m = 19 \pm 5\ V^{-1}$. Extrapolation to the diffusion controlled rate constant using the theoretical slope (dashed line) yields the oxidation potential, $E^o = 0.43 \pm 0.08$ V.

5.2.2 0.5 M H_2O/acetonitrile

5.2.2.1 Convolution voltammetry

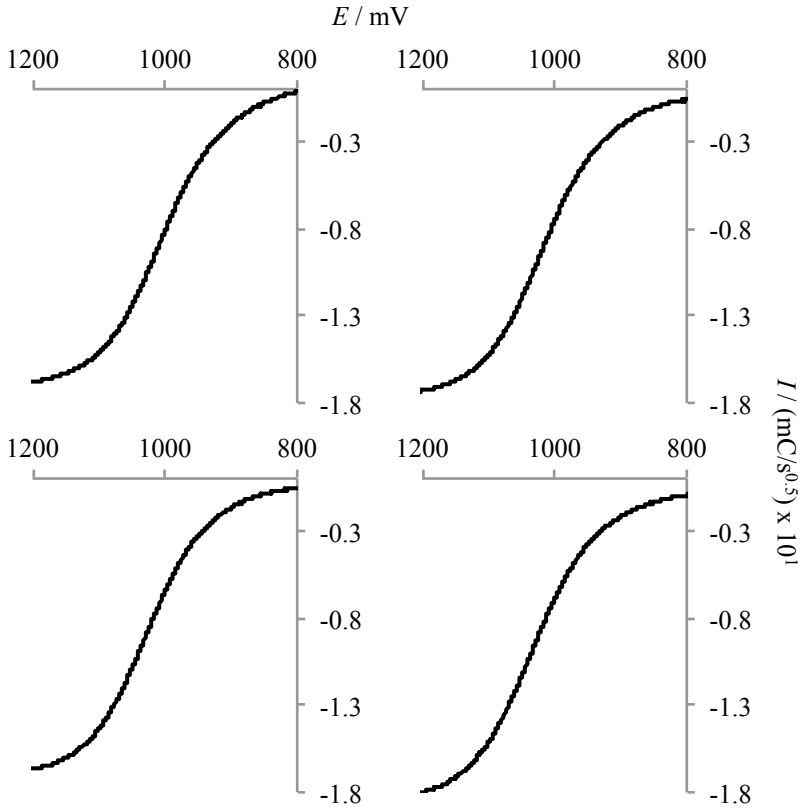

Figure 5.52: Convolution voltammograms of tetra-*n*-butylammonium acetate in 0.5 M H_2O/acetonitrile. C_{AcO^-} = 0.003 M, 0.5 M supporting electrolyte (TBAP), ν = 100 (upper left), 200, 300, 400 (lower right) mV/s

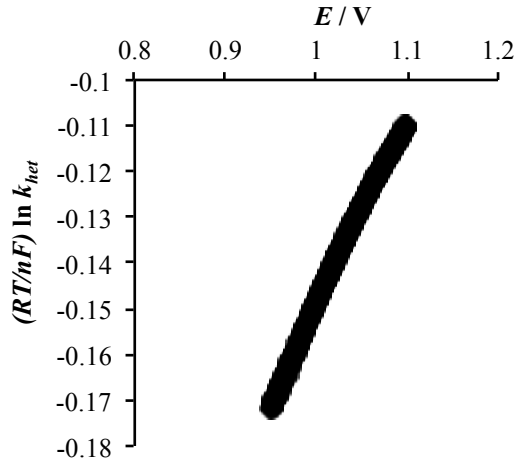

Figure 5.53: Tetra-*n*-butylammonium acetate in 0.5 M H_2O/acetonitrile. $\left(\frac{RT}{nF}\right) \ln k_{het}$ vs. *E*, ν = 100 mV/s, $C_{\mathbf{AcO^-}}$ = 0.003 M in 0.5 M H_2O/acetonitrile, 0.5 M supporting electrolyte (TBAP)

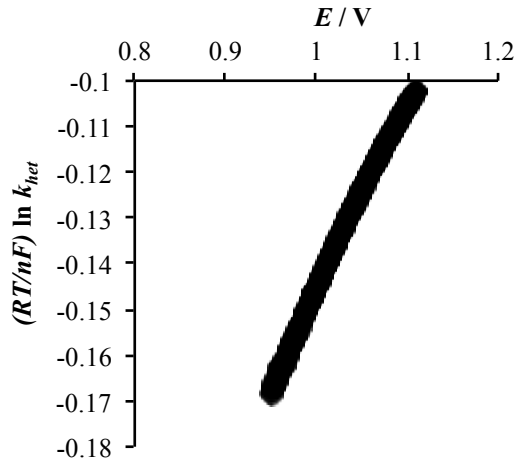

Figure 5.54: Tetra-*n*-butylammonium acetate in 0.5 M H_2O/acetonitrile. $\left(\frac{RT}{nF}\right) \ln k_{het}$ vs. *E*, ν = 200 mV/s, $C_{\mathbf{AcO^-}}$ = 0.003 M in 0.5 M H_2O/acetonitrile, 0.5 M supporting electrolyte (TBAP)

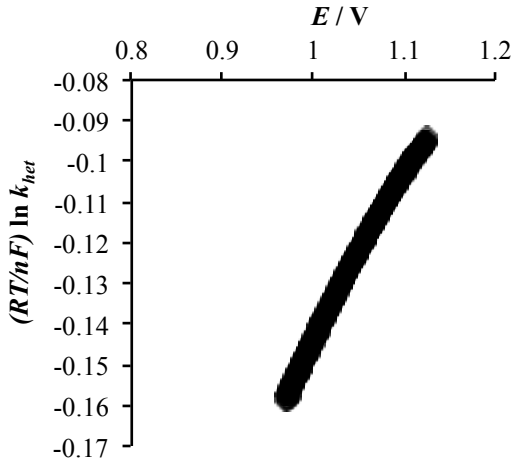

Figure 5.55: Tetra-*n*-butylammonium acetate in 0.5 M H_2O/acetonitrile. $\left(\frac{RT}{nF}\right) \ln k_{het}$ vs. *E*, ν = 300 mV/s, $C_{\mathbf{AcO^-}}$ = 0.003 M in 0.5 M H_2O/acetonitrile, 0.5 M supporting electrolyte (TBAP)

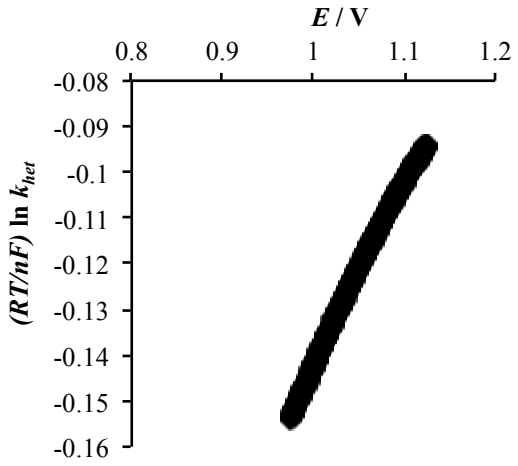

Figure 5.56: Tetra-*n*-butylammonium acetate in 0.5 M H_2O/acetonitrile. $\left(\frac{RT}{nF}\right) \ln k_{het}$ vs. *E*, ν = 400 mV/s, $C_{\mathbf{AcO^-}}$ = 0.003 M in 0.5 M H_2O/acetonitrile, 0.5 M supporting electrolyte (TBAP)

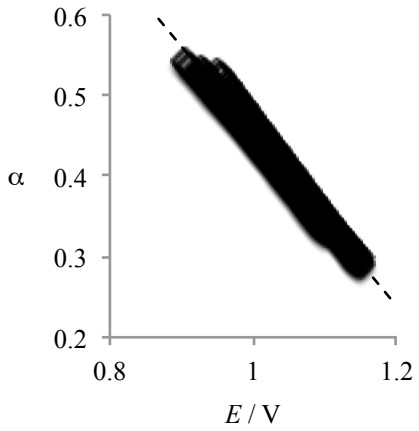

Figure 5.57: α as a function of potential. Tetra-*n*-butylammonium acetate in 0.5 M H_2O/acetonitrile, ν = 100-400 mV/s. Extrapolation to $\alpha = 0.5$ gives the standard oxidation potential of acetate in accordance with **Eq. 5.6**.

5.2.2.2 Homogeneous redox catalysis

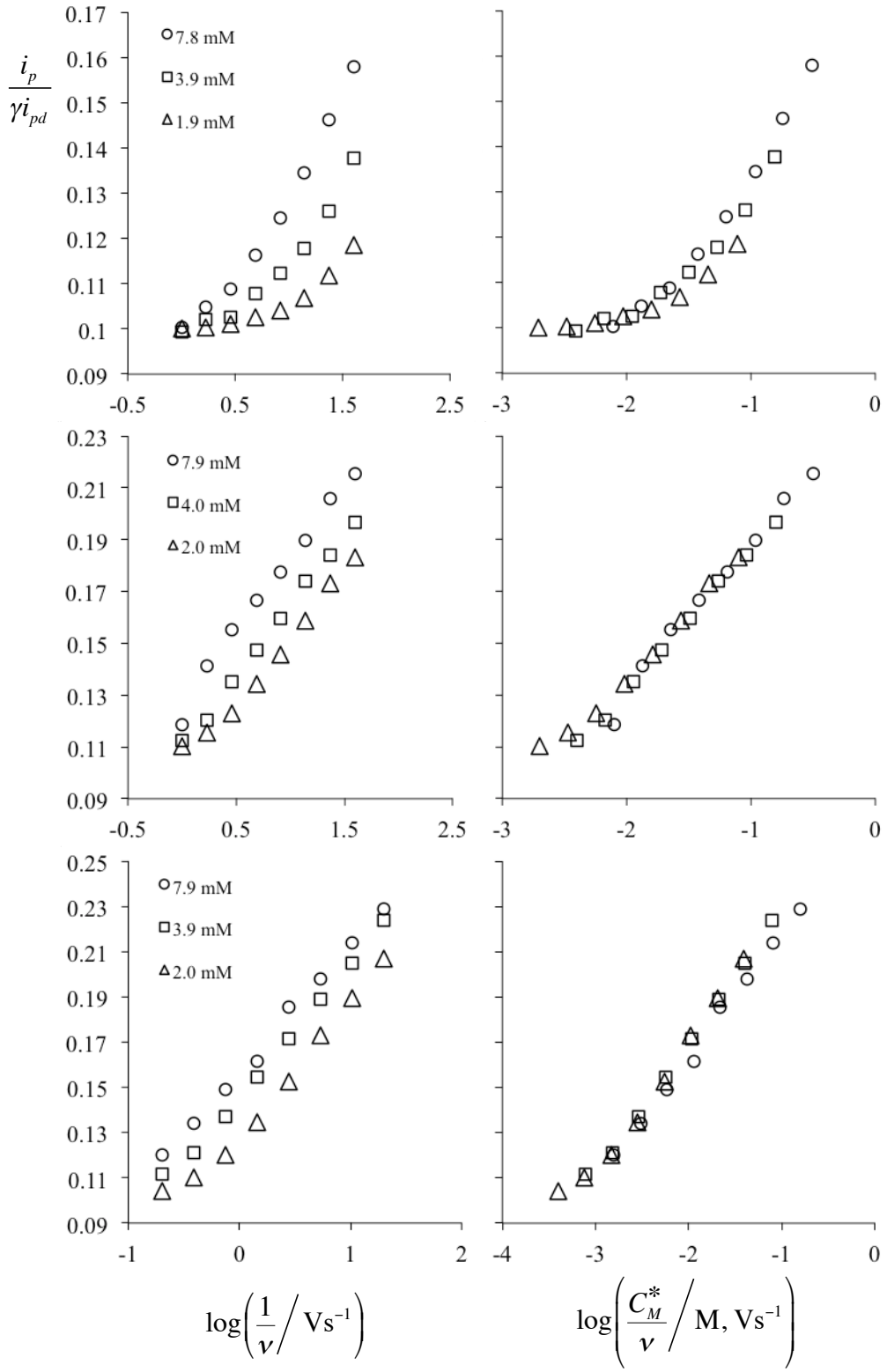

Figure 5.58: Variation of $i_p/\gamma i_{pd}$ as a function of sweep rate and mediator concentration for tetra-*n*-butylammonium acetate in 0.5 M H_2O/acetonitrile clearly demonstrating electron transfer control in each case. (*a*) ferrocene, (*b*) vinylferrocene, (*c*) *p*-bromophenylferrocene

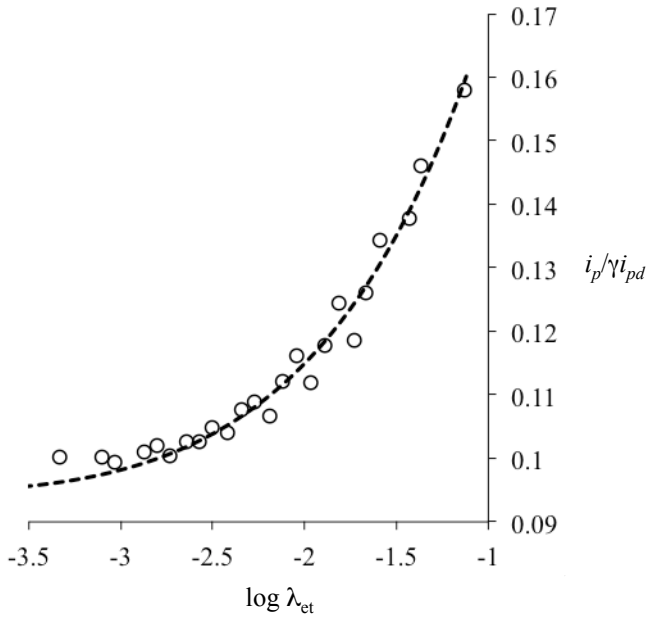

Figure 5.59: $i_p/\gamma i_{pd}$ data fit to dimensionless working curves for tetra-*n*-butylammonium acetate in 0.5 M H_2O/acetonitrile (mediator = ferrocene). $\log\left(\frac{RT}{nF}k_{et}\right) = -0.62$, $k_{et} = (9.3 \pm 0.9) \times 10^0$ M^{-1} s^{-1}

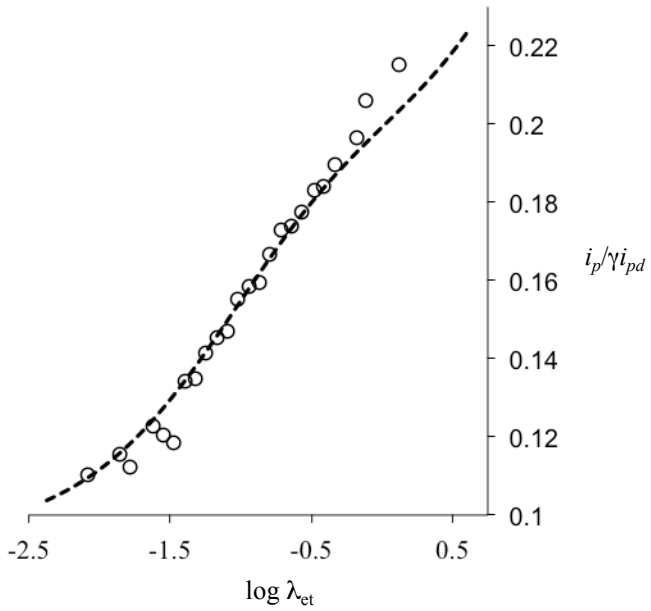

Figure 5.60: $i_p/\gamma i_{pd}$ data fit to dimensionless working curves for tetra-*n*-butylammonium acetate in dry acetonitrile (mediator = ferrocene). $\log\left(\frac{RT}{nF}k_{et}\right) = 0.623$, $k_{et} = (1.63 \pm 0.09)$ x 10^2 M^{-1} s^{-1}

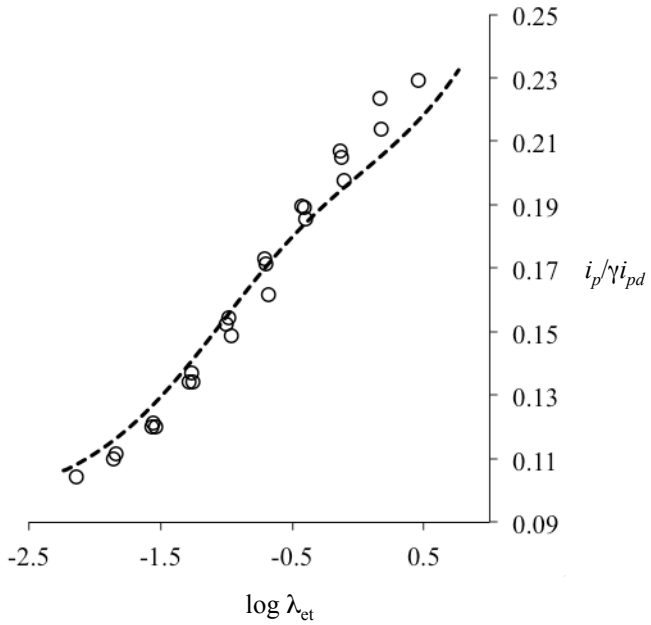

Figure 5.61: $i_p/\gamma i_{pd}$ data fit to dimensionless working curves for tetra-*n*-butylammonium acetate in dry acetonitrile (mediator = ferrocene). $\log\left(\frac{RT}{nF}k_{et}\right) = 1.26$, $k_{et} = (7.2 \pm 0.6)$ x 10^2 M^{-1} s^{-1}

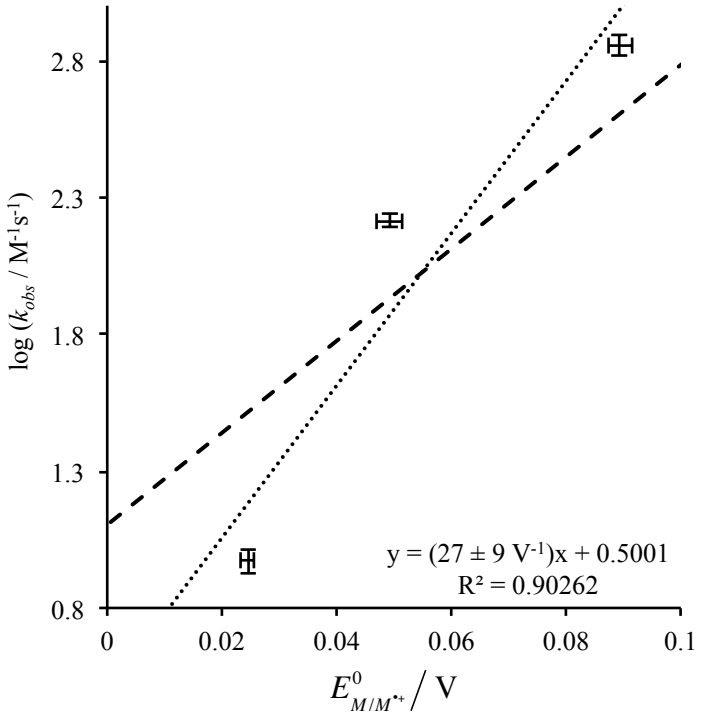

Figure 5.62: Marcus plots for tetra-*n*-butylammonium acetate. Linear regression (dotted line) gives a slope, $m = 27 \pm 9\ V^{-1}$. Extrapolation to the diffusion controlled rate constant using the theoretical slope (dashed line) yields the oxidation potential, $E^o = 0.51 \pm 0.09$ V.

Chapter 6. List of References

1. Marcus, R. A., On theory of electron-transfer reactions. 6. Unified treatment for homogeneous and electrode reactions. *J. Chem. Phys.* **1965,** *43* (2), 679-701.

2. Saveant, J. M., A Simple Model for the Kinetics of Dissociative Electron-Transfer in Polar Solvents - Application to the Homogeneous and Heterogeneous Reductions of Alkyl-Halides. *Journal of the American Chemical Society* **1987,** *109* (22), 6788-6795.

3. Andrieux, C. P.; Gallardo, I.; Saveant, J. M.; Su, K. B., Dissociative Electron-Transfer - Homogeneous and Heterogeneous Reductive Cleavage of the Carbon Halogen Bond in Simple Aliphatic Halides. *J. Am. Chem. Soc.* **1986,** *108* (4), 638-647.

4. Costentin, C.; Robert, M.; Saveant, J.-M., Concerted Proton-Electron Transfers: Electrochemical and Related Approaches. *Accounts of Chemical Research* **2010,** *43* (7), 1019-1029.

5. Migliore, A.; Polizzi, N. F.; Therien, M. J.; Beratan, D. N., Biochemistry and Theory of Proton-Coupled Electron Transfer. *Chemical Reviews* **2014,** *114* (7), 3381-3465.

6. Saveant, J.-M., Concerted Proton-Electron Transfers: Fundamentals and Recent Developments. In *Annual Review of Analytical Chemistry, Vol 7*, Cooks, R. G.; Pemberton, J. E., Eds. 2014; Vol. 7, pp 537-560.

7. Weinberg, D. R.; Gagliardi, C. J.; Hull, J. F.; Murphy, C. F.; Kent, C. A.; Westlake, B. C.; Paul, A.; Ess, D. H.; McCafferty, D. G.; Meyer, T. J., Proton-Coupled Electron Transfer. *Chemical Reviews* **2012,** *112* (7), 4016-4093.

8. Savéant, J. M., Electron Transfer, Bond Breaking and Bond Formation. In *Advances in Physical Organic Chemistry*, Gold, V., Ed. Academic Press: London, 2000; Vol. 35, pp 117 - 192.

9. Saveant, J. M., Dissociative Electron-Transfer - New Tests of the Theory in the Electrochemical and Homogeneous Reduction of Alkyl-Halides. *Journal of the American Chemical Society* **1992,** *114* (26), 10595-10602.

10. Andrieux, C. P.; Combellas, C.; Kanoufi, F.; Saveant, J. M.; Thiebault, A., Dynamics of bond breaking in ion radicals. Mechanisms and reactivity in the reductive cleavage of carbon-fluorine bonds of fluoromethylarenes. *Journal of the American Chemical Society* **1997,** *119* (40), 9527-9540.

11. Andrieux, C. P.; Saveant, J. M.; Tallec, A.; Tardivel, R.; Tardy, C., Concerted and stepwise dissociative electron transfers. Oxidability of the leaving group and strength of the breaking bond as mechanism and reactivity governing factors illustrated by the

electrochemical reduction of alpha-substituted acetophenones. *J. Am. Chem. Soc.* **1997,** *119* (10), 2420-2429.

12. Andrieux, C. P.; Robert, M.; Saeva, F. D.; Saveant, J. M., Passage from Concerted to Stepwise Dissociative Electron-Transfer as a Function of the Molecular-Structure and of the Energy of the Incoming Electron - Electrochemical Reduction of Aryldialkyl Sulfonium Cations. *J. Am. Chem. Soc.* **1994,** *116* (17), 7864-7871.

13. Antonello, S.; Musumeci, M.; Wayner, D. D. M.; Maran, F., Electroreduction of dialkyl peroxides. Activation-driving force relationships and bond dissociation free energies. *J. Am. Chem. Soc.* **1997,** *119* (40), 9541-9549.

14. Daasbjerg, K.; Jensen, H.; Benassi, R.; Taddei, F.; Antonello, S.; Gennaro, A.; Maran, F., Evidence for large inner reorganization energies in the reduction of diaryl disulfides: Toward a mechanistic link between concerted and stepwise dissociative electron transfers? *J. Am. Chem. Soc.* **1999,** *121* (8), 1750-1751.

15. Antonello, S.; Maran, F., The role and relevance of the transfer coefficient alpha in the study of dissociative electron transfers: Concepts and examples from the electroreduction of perbenzoates. *J. Am. Chem. Soc.* **1999,** *121* (41), 9668-9676.

16. Workentin, M. S.; Maran, F.; Wayner, D. D. M., Reduction of Di-Tert-Butyl Peroxide - Evidence for Nonadiabatic Dissociative Electron-Transfer. *J. Am. Chem. Soc.* **1995,** *117* (7), 2120-2121.

17. Donkers, R. L.; Maran, F.; Wayner, D. D. M.; Workentin, M. S., Kinetics of the reduction of dialkyl peroxides. New insights into the dynamics of dissociative electron transfer. *Journal of the American Chemical Society* **1999,** *121* (31), 7239-7248.

18. Pause, L.; Robert, M.; Savéant, J. M., Reductive Cleavage of Carbon Tetrachloride in a Polar Solvent. An Example of a Dissociative Electron Transfer with Significant Attractive Interaction between the Caged Product Fragments. *J. Am. Chem. Soc.* **2000,** *122* (40), 9829-9835.

19. Antonello, S.; Formaggio, F.; Moretto, A.; Toniolo, C.; Maran, F., Intramolecular, intermolecular, and heterogeneous nonadiabatic dissociative electron transfer to peresters. *Journal of the American Chemical Society* **2001,** *123* (39), 9577-9584.

20. Tanko, J. M.; Li, X. Z.; Chahma, M.; Jackson, W. F.; Spencer, J. N., Cyclopropyl conjugation and ketyl anions: When do things begin to fall apart? *Journal of the American Chemical Society* **2007,** *129* (14), 4181-4192.

21. Drumright, R. E.; Mas, R. H.; Merola, J. S.; Tanko, J. M., Interplay Between Conjugative and Steric Effects in Cyclopropylarenes. *J. Org. Chem.* **1990,** *55* (13), 4098-102.

22. Gillmore, J. G.; Tanko, J. M., Radical Ion Probes. 11. Reaction of 1,1-Dimethyl-5,7-di-t-butylspiro[2.5]octa-4,7-dien-6-one with 5-Hexenyl Magnesium Bromide. *Tetrahedron Lett.* **1998,** *39* (48), 8795-8798.

23. Phillips, J. P.; Gillmore, J. G.; Schwartz, P.; Brammer, L. E., Jr.; Berger, D. J.; Tanko, J. M., Radical Ion Probes. 8. Direct and Indirect Electrochemistry of 5,7-Di-tert-butylspiro[2.5]octa-4,7-dien-6-one and Derivatives. *J. Am. Chem. Soc.* **1998,** *120* (1), 195-202.

24. Tanko, J. M.; Brammer, L. E., Jr., Utilization of 1,1-Dimethyl-4,6-di-tert-butylspiro[2.5]octa-3,6-dien-5-one as a Hypersensitive Probe for Single Electron Transfer to Carbonyl Compounds. *J. Chem. Soc., Chem. Commun.* **1994,** (10), 1165-6.

25. Tanko, J. M.; Brammer, L. E., Jr.; Hervas, M.; Campos, K., Characterization of a Hypersensitive Probe for Single Electron Transfer to Carbonyl Compounds. *J. Chem. Soc., Perkin Trans. 2* **1994,** (7), 1407-9.

26. Tanko, J. M.; Drumright, R. E., Radical Ion Probes. I. Cyclopropyl-carbinyl Rearrangements of Aryl Cyclopropyl Ketyl Anions. *J. Am. Chem. Soc.* **1990,** *112* (13), 5362-3.

27. Tanko, J. M.; Drumright, R. E., Radical Ion Probes. 2. Evidence for the Reversible Ring Opening of Arylcyclopropylketyl Anions. Implications for Mechanistic Studies. *J. Am. Chem. Soc.* **1992,** *114* (5), 1844-54.

28. Tanko, J. M.; Drumright, R. E.; Suleman, N. K.; Brammer, L. E., Jr., Radical Ion Probes. 3. The Importance of Resonance vs. Strain Energy in the Design of SET Probes Based upon the Cyclopropylcarbinyl-to-Homoallyl Radical Rearrangement. *J. Am. Chem. Soc.* **1994,** *116* (5), 1785-91.

29. Wang, Y.; McLean, K. H.; Tanko, J. M., Radical Ion Probes. 9. The Chemistry of Radical Cations Derived from 9-Cyclopropylanthracene and 9-Bromo-10-cyclopropylanthracene. *J. Org. Chem.* **1998,** *63* (3), 628-635.

30. Wang, Y.; Tanko, J. M., Radical Ion Probes. 6. Origin of the High Intrinsic Barrier to Nucleophile-Induced Ring Opening of Arylcyclopropane Radical Cations. *J. Am. Chem. Soc.* **1997,** *119* (35), 8201-8208.

31. Chahma, M.; Li, X.; Phillips, P.; Schwartz, P.; Brammer, L. E.; Wang, Y.; Tanko, J. M., Activation/driving Force Relationships for Cyclopropylcarbinyl --> Homoallyl-Type Rearrangements of Radical Anions. *J. Phys. Chem. A* **2005,** *109*, 3372 - 3382.

32. Stevenson, J. P.; Jackson, W. F.; Tanko, J. M., Cyclopropylcarbinyl-Type Ring Openings. Reconciling the Chemistry of Neutral Radicals and Radical Anions. *J. Am. Chem. Soc.* **2002,** *124*, 4271 - 4281.

33. Hasegawa, E.; Yoneoka, A.; Suzuki, K.; Kato, T.; Kitazume, T.; Yanagi, K., Reductive Transformations of α, β-Epoxy Ketones and Other Compounds Promoted Through Photoinduced Electron Transfer Processes With 1,3-Dimethyl-2-phenylbenzimidazoline (DMPBI). *Tetrahedron* **1999,** *55*, 12957 - 12968.

34. Hasegawa, E.; Ishiyama, K.; Fujita, T.; Kato, T.; Abe, T., Electron-transfer reactions of aromatic alpha,beta-epoxy ketones: Factors that govern selective conversion to beta-diketones and beta-hydroxy ketones. *Journal of Organic Chemistry* **1997,** *62* (8), 2396-2400.

35. Hasegawa, E.; Ishiyama, K.; Horaguchi, T.; Shimizu, T., Exporatory Study on Photoinduced Single Electron-Transfer Reactions of Alpha,Beta-Epoxy Ketones with Amines. *Journal of Organic Chemistry* **1991,** *56* (4), 1631-1635.

36. Hasegawa, E.; Ishiyama, K.; Kashiwazaki, H.; Horaguchi, T.; Shimizu, T., Selective C-Beta-O Bond-Cleavage of Chalcone Epoxides Induced by Pyrylium Salt Sensitized Photoreactions and Dark Reactions with Cerium(IV) Salts. *Tetrahedron Letters* **1990,** *31* (28), 4045-4048.

37. Hasegawa, E.; Ishiyama, K.; Kato, T.; Horaguchi, T.; Shimizu, T.; Tanaka, S.; Yamashita, Y., Photochemically and Thermally Induced Free-Radical Reactions of Alpha,Beta-Epoxy Ketones with Tributyltin Hydride - Selective C-Alpha-O Bond-Cleavage of Oxiranylmethyl Radicals Derived from Alpha,Beta-Epoxy Ketones. *Journal of Organic Chemistry* **1992,** *57* (20), 5352-5359.

38. Kolbe, H., Untersuchungen über die Elektrolyse organischer Verbindungen. *Justus Liebigs Annalen der Chemie* **1849,** *69* (3), 257-294.

39. Vijh, A. K.; Conway, B. E., Electrode Kinetic Aspects of Kolbe Reaction. *Chemical Reviews* **1967,** *67* (6), 623-&.

40. Schäfer, H.-J., Recent contributions of kolbe electrolysis to organic synthesis. In *Electrochemistry IV*, Steckhan, E., Ed. Springer Berlin Heidelberg: Berlin, Heidelberg, 1990; pp 91-151.

41. Sperry, J. B.; Wright, D. L., The application of cathodic reductions and anodic oxidations in the synthesis of complex molecules. *Chem Soc Rev* **2006,** *35* (7), 605-621.

42. Eberson, L., Studies on Kolbe Electrolytic Synthesis .3. Electrolysis of Malonamic Acids as a Preparative Route to Succinic Amides. *Acta Chem Scand* **1963,** *17* (5), 1196-&.

43. Eberson, L., Studies on Kolbe Electrolytic Synthesis .4. A Theoretical Investigation of Mechanism by Standard Potential Calculations. *Acta Chem Scand* **1963,** *17* (7), 2004-&.

44. Eberson, L.; Granse, S.; Olofsson, B., Studies on Kolbe Electrolytic Synthesis .9. Comparison between Anodic and Peroxydisulfate Oxidation of Carboxylates - Kinetics of

Peroxydisulfate Decomposition in Presence of Acetate Ion. *Acta Chem Scand* **1968,** *22* (8), 2462-&.

45. Eberson, L., Studies on Kolbe Electrolytic Synthesis .1. Electrolysis of Some Alpha-Cyanocarboxylic Acids. *Journal of Organic Chemistry* **1962,** *27* (7), 2329-&.

46. Eberson, L.; Nilsson, S., Studies on Kolbe Electrolytic Synthesis .8. Further Investigations on Electrolysis of Alpha-Cyanocarboxylates. *Acta Chem Scand* **1968,** *22* (8), 2453-&.

47. Eberson, L.; Nyberg, K., Studies on Kolbe Electrolytic Synthesis .V. Electrochemical Analogue of Ritter Reaction. *Acta Chem Scand* **1964,** *18* (6), 1567-&.

48. Eberson, L.; Nyberg, K., Studies on Kolbe Electrolytic Synthesis .6. On Mechanism of Anodic Acetoxylation. *Acta Chem Scand* **1964,** *18* (6), 1568-&.

49. Eberson, L.; Sandberg, B., Studies on Kolbe Electrolytic Synthesis .7. Electrolysis of Some T-Alkylmalonic Half Esters. *Acta Chem Scand* **1966,** *20* (3), 739-&.

50. Andrieux, C. P.; Gonzalez, F.; Saveant, J. M., Homolytic and heterolytic radical cleavage in the Kolbe reaction - Electrochemical oxidation of arylmethyl carboxylate ions. *J Electroanal Chem* **2001,** *498* (1-2), 171-180.

51. Galicia, M.; Gonzalez, F. J., Electrochemical oxidation of tetrabutylammonium salts of aliphatic carboxylic acids in acetonitrile. *J Electrochem Soc* **2002,** *149* (3), D46-D50.

52. Astudillo, P. D.; Galano, A.; Gonzalez, F. J., Radical grafting of carbon surfaces with alkylic groups by mediated oxidation of carboxylates. *J Electroanal Chem* **2007,** *610* (2), 137-146.

53. Maslak, P.; Chapman, W. H.; Vallombroso, T. M.; Watson, B. A., Mesolytic scission of C-C bonds in radical cations of amino derivatives: Steric and solvent effects. *Journal of the American Chemical Society* **1995,** *117* (50), 12380-12389.

54. Wang, Y. S.; Luttrull, D. K.; Dinnocenzo, J. P.; Goodman, J. L.; Farid, S.; Gould, I. R., Associative return electron transfer. A bond-coupled electron transfer in the photoreactions of cyclopropylamines. *Photoch Photobio Sci* **2003,** *2* (11), 1169-1176.

55. Grimm, M. L.; Allen, W. J.; Finn, M.; Castagnoli, N.; Tanko, J. M., Reaction of benzophenone triplet with aliphatic amines. What a potent neurotoxin can tell us about the reaction mechanism. *Bioorgan Med Chem* **2011,** *19* (4), 1458-1463.

56. Grimm, M. L., Development of New N-Cyclopropyl Based Electron Transfer Probes for Cytochrome P-450 and Monoamine Oxidase Catalyzed Reactions. **2011**.

57. Li, X. Z.; Grimm, M. L.; Igarashi, K.; Castagnoli, N.; Tanko, J. M., The first calibration of an aminiumyl radical ion clock: why N-cyclopropylanilines may be poor mechanistic probes for single electron transfer. *Chem Commun* **2007,** (25), 2648-2650.

58. Brede, O.; Naumov, S., Free electron transfer-relations between molecule dynamics and reaction kinetics. *Chem Soc Rev* **2010,** *39* (8), 3057-3071.

59. McAlister, G. C.; Russell, J. D.; Rumachik, N. G.; Hebert, A. S.; Syka, J. E. P.; Geer, L. Y.; Westphall, M. S.; Pagliarini, D. J.; Coon, J. J., Analysis of the Acidic Proteome with Negative Electron-Transfer Dissociation Mass Spectrometry. *Anal Chem* **2012,** *84* (6), 2875-2882.

60. Dombrowski, G. W.; Dinnocenzo, J. P.; Zielinski, P. A.; Farid, S.; Wosinska, Z. M.; Gould, I. R., Efficient unimolecular deprotonation of aniline radical cations. *Journal of Organic Chemistry* **2005,** *70* (10), 3791-3800.

61. Parker, V. D.; Tilset, M., Facile Proton-Transfer Reactions of N,N-Dimethylaniline Cation Radicals. *Journal of the American Chemical Society* **1991,** *113* (23), 8778-8781.

62. Zhang, X. M.; Yeh, S. R.; Hong, S.; Freccero, M.; Albini, A.; Falvey, D. E.; Mariano, P. S., Dynamics of Alpha-Ch Deprotonation and Alpha-Desilylation Reactions of Tertiary Amine Cation Radicals. *Journal of the American Chemical Society* **1994,** *116* (10), 4211-4220.

63. Tanko, J. M.; Gillmore, J. G.; Friedline, R.; Chahma, M., Cyclopropylcarbinyl --> Homoallyl-Type Ring Opening of Ketyl Radical Anions. Structure/Reactivity Relationships and the Contribution of Solvent/Counterion Reorganization to the Intrinsic Barrier. *J. Org. Chem.* **2005,** *70*, 4170 - 4173.

64. Tanko, J. M.; Phillips, J. P., Rearrangements of Radical Ions: What it Means to be Both a Radical and an Ion. *J. Am. Chem. Soc.* **1999,** *121* (25), 6078-6079.

65. Andrieux, C. P.; Legorande, A.; Saveant, J. M., Electron-Transfer and Bond Breaking - Examples of Passage from a Sequential to a Concerted Mechanism in the Electrochemical Reductive Cleavage of Arylmethyl Halides. *J. Am. Chem. Soc.* **1992,** *114* (17), 6892-6904.

66. Hasegawa, E.; Arai, S.; Tayama, E.; Iwamoto, H., Metal-Free, One-Pot, Sequential Protocol for-Transforming alpha,beta-Epoxy Ketones to beta-Hydroxy Ketones and alpha-Methylene Ketones. *Journal of Organic Chemistry* **2015,** *80* (3), 1593-1600.

67. Okada, K.; Hasegawa, E.; Mukai, T., Organic-Photochemistry 62. Photosensetized Carbon-Oxygen Bond-Cleavage Reactions of Epoxides by 2,4,6-Triphenylpyrylium Tetrafluoroborate Salt. *Chemistry Letters* **1983,** (3), 305-308.

68. Hasegawa, E.; Kato, T.; Kitazume, T.; Yanagi, K.; Hasegawa, K.; Horaguchi, T., Photoinduced electron transfer reactions of alpha,beta-epoxy ketones with 2-phenyl-N,N-dimethylbenzimidazoline (PDMBI): Significant water effect on the reaction pathway. *Tetrahedron Letters* **1996,** *37* (39), 7079-7082.

69. Donck, S.; Baroudi, A.; Fensterbank, L.; Goddard, J. P.; Ollivier, C., Visible-Light Photocatalytic Reduction of Sulfonium Salts as a Source of Aryl Radicals. *Adv Synth Catal* **2013,** *355* (8), 1477-1482.

70. Larraufie, M. H.; Pellet, R.; Fensterbank, L.; Goddard, J. P.; Lacote, E.; Malacria, M.; Ollivier, C., Visible-Light-Induced Photoreductive Generation of Radicals from Epoxides and Aziridines. *Angew Chem Int Edit* **2011,** *50* (19), 4463-4466.

71. Nadjo, L.; Savéant, J. M., Linear Sweep Voltammetry: Kinetic Control by Charge Transfer and/or Secondary Chemical Reactions. *J. Electroanal. Chem.* **1973,** *48*, 113-145.

72. Oldham, K. B.; Spanier, J., Replacement of Ficks Laws by a Formulation Involving Semidifferentiation. *J Electroanal Chem* **1970,** *26* (2-3), 331-&.

73. Imbeaux, J. C.; Saveant, J. M., Convolutive Potential Sweep Voltammetry .1. Introduction. *J Electroanal Chem* **1973,** *44* (2), 169-187.

74. Bard, A. J.; Faulkner, L. R., *Electrochemical Methods. Fundementals and Applications*. John Wiley & Sons, Inc.: New York, 2001.

75. Andrieux, C. P.; Dumas-Bouchiat, J. M.; Savéant, J. M., Homogeneous Redox Catalysis of Electrochemical Reactions. Part I. Introduction. *J. Electroanal. Chem.* **1978,** *87*, 39 - 53.

76. Andrieux, C. P.; Dumas-Bouchiat, J. M.; Savéant, J. M., Homogeneous Redox Catalysis of Electrochemical Reactions. Part II. Rate Determining Electron Transfer. Evaluation of Rate and Equilibrium Parameters. *J. Electroanal. Chem.* **1978,** *87*, 55-65.

77. Andrieux, C. P.; Dumas-Bouchiat, J. M.; Savéant, J. M., Homogeneous Redox Catalysis of Electrochemical Reactions. Part III. Rate Determining Electron Transfer. Kinetic Characterization of Follow-up Chemical Reactions. *J. Electroanal. Chem.* **1978,** *88*, 43 - 48.

78. Andrieux, C. P.; Dumas-Bouchiat, J. M.; Savéant, J. M., Homogeneous Redox Catalysis of Electrochemical Reactions. Part IV. Kinetic Controls in the Homogenous Process as Characterized by Stationary and Quasi-Stationary Electrochemical Techniques. *J. Electroanal. Chem.* **1980,** *113*, 1 - 18.

79. Andrieux, C. P.; Blocman, C.; Dumas-Bouchiat, J. M.; M'Halla, F.; Savéant, J. M., Homogeneous Redox Catalysis of Electrochemical Reactions. Part V. Cyclic Voltammetry. *J. Electroanal. Chem.* **1980,** *113*, 19 - 40.

80. Savéant, J. M.; Su, K. B., Homogeneous Redox Catalysis of Electrochemical Reactions. Part VI. Zone Diagram Representation of the Kinetic Regimes. *J. Electroanal. Chem.* **1984,** *171*, 3341 - 349.

81. *TableCurve 2D*, Jandel Scientific Software: San Rafeal, CA.

82. Frisch, M. J.; Trucks, G. W.; Schlegel, H. B.; Scuseria, G. E.; Robb, M. A.; Cheeseman, J. R.; Scalmani, G.; Barone, V.; Mennucci, B.; Petersson, G. A.; Nakatsuji, H.; Caricato, M.; Li, X.; Hratchian, H. P.; Izmaylov, A. F.; Bloino, J.; Zheng, G.; Sonnenberg, J. L.; Hada, M.; Ehara, M.; Toyota, K.; Fukuda, R.; Hasegawa, J.; Ishida, M.; Nakajima, T.; Honda, Y.; Kitao, O.; Nakai, H.; Vreven, T.; Montgomery Jr., J. A.; Peralta, J. E.; Ogliaro, F.; Bearpark, M. J.; Heyd, J.; Brothers, E. N.; Kudin, K. N.; Staroverov, V. N.; Kobayashi, R.; Normand, J.; Raghavachari, K.; Rendell, A. P.; Burant, J. C.; Iyengar, S. S.; Tomasi, J.; Cossi, M.; Rega, N.; Millam, N. J.; Klene, M.; Knox, J. E.; Cross, J. B.; Bakken, V.; Adamo, C.; Jaramillo, J.; Gomperts, R.; Stratmann, R. E.; Yazyev, O.; Austin, A. J.; Cammi, R.; Pomelli, C.; Ochterski, J. W.; Martin, R. L.; Morokuma, K.; Zakrzewski, V. G.; Voth, G. A.; Salvador, P.; Dannenberg, J. J.; Dapprich, S.; Daniels, A. D.; Farkas, Ö.; Foresman, J. B.; Ortiz, J. V.; Cioslowski, J.; Fox, D. J. *Gaussian 09*, Gaussian, Inc.: Wallingford, CT, USA, 2009.

83. Becke, A. D., Density-Functional Thermochemistry .3. The Role of Exact Exchange. *J. Chem. Phys.* **1993,** *98* (7), 5648-5652.

84. Becke, A. D., A New Mixing of Hartree-Fock and Local Density-Functional Theories. *J. Chem. Phys.* **1993,** *98* (2), 1372-1377.

85. Cardinale, A.; Isse, A. A.; Gennaro, A.; Robert, M.; Saveant, J. M., Dissociative electron transfer to haloacetonitriles. An example of the dependency of in-cage ion-radical interactions upon the leaving group. *Journal of the American Chemical Society* **2002,** *124* (45), 13533-13539.

86. Čížek, J., On the Use of the Cluster Expansion and the Technique of Diagrams in Calculations of Correlation Effects in Atoms and Molecules. In *Advances in Chemical Physics*, John Wiley & Sons, Inc.: 1969; pp 35-89.

87. Purvis, G. D.; Bartlett, R. J., A Full Coupled-Cluster Singles and Doubles Model - the Inclusion of Disconnected Triples. *J. Chem. Phys.* **1982,** *76* (4), 1910-1918.

88. Scuseria, G. E.; Janssen, C. L.; Schaefer, H. F., An Efficient Reformulation of the Closed-Shell Coupled Cluster Single and Double Excitation (Ccsd) Equations. *J. Chem. Phys.* **1988,** *89* (12), 7382-7387.

89. Scuseria, G. E.; Schaefer, H. F., Is Coupled Cluster Singles and Doubles (Ccsd) More Computationally Intensive Than Quadratic Configuration-Interaction (Qcisd). *J. Chem. Phys.* **1989,** *90* (7), 3700-3703.

90. Andrieux, C. P.; Savéant, J. M.; Tallec, A.; Tardivel, R.; Tardy, C., Concerted and Stepwise Dissociative Electron Transfers. Oxidability of the Leaving Group and Strength of the Breaking Bond as the Mechanism and Reactivity Governing Factors Illustrated by the Electrochemical Reduction of a-Substituted Acetophenones. *J. Am. Chem. Soc.* **1997,** *119*, 2420 - 2429.

91. Andrieux, C. P.; Savéant, J. M., Homogeneous Redox Catalysis of Electrochemical Reactions. Electron Transfer Followed by a Very Fast Chemical Step. *J. Electroanal. Chem.* **1986,** *205*, 43-58.

92. Headgordon, M.; Pople, J. A.; Frisch, M. J., Mp2 Energy Evaluation by Direct Methods. *Chem Phys Lett* **1988,** *153* (6), 503-506.

93. Dunning, T. H., Gaussian-Basis Sets for Use in Correlated Molecular Calculations .1. The Atoms Boron through Neon and Hydrogen. *J. Chem. Phys.* **1989,** *90* (2), 1007-1023.

94. Haynes, W. M.; Lide, D. R., *CRC handbook of chemistry and physics : a ready-reference book of chemical and physical data*. 92nd ed. ed.; CRC Press: Boca Raton, Fla. :, 2011.

95. Auzmendi-Murua, I.; Bozzelli, J. W., Thermochemical Properties and Bond Dissociation Enthalpies of 3-to 5-Member Ring Cyclic Ether Hydroperoxides, Alcohols, and Peroxy Radicals: Cyclic Ether Radical + O-3(2) Reaction Thermochemistry. *J Phys Chem A* **2014,** *118* (17), 3147-3167.

96. Hancock, A. Radical Approaches to Synthesis and Mechanism. Dissertation, Virginia Polytechnic and State University, 2011.

97. Tanko, J. M., Virginia Polytechnic and State University: 2014.

98. Saveant, J. M., Molecular catalysis of electrochemical reactions. Mechanistic aspects. *Chemical Reviews* **2008,** *108* (7), 2348-2378.

99. Kollmar, C.; Kahn, O., Spin Polarization and Ferromagnetic Coupling in Metallocenium Charge-Transfer Complexes. *J. Chem. Phys.* **1992,** *96* (4), 2988-2997.

100. Abdel Latif, M.; Spencer, J.; Kidd, B.; Tanko, J. M., A concerted mechanism of electron transfer and oxidation potential for tetrabutylammonium acetate via conventional and convolution voltammetery under extreme anhydrous conditions. Virginia Polytechinic and State University: 2016.

101. *Spartan '04*, Wavefunction, Inc.: Irvine, CA.

102. Schmidt, J. R.; Polik, W. F. *WebMO Enterprise*, 14; WebMO LLC: Holland, MI, USA, 2016.

103. Schaftenaar, G.; Noordik, J. H., Molden: a pre- and post-processing program for molecular and electronic structures. *J. Comput.-Aided Mol. Design* **2000,** *14*, 123-134.

104. House, H. O.; Feng, E.; Peet, N. P., Comparison of Various Tetraalkylammonium Salts as Supporting Electrolytes in Organic Electrochemical Reactions. *Journal of Organic Chemistry* **1971,** *36* (16), 2371-&.

105. Lattanzi, A., Enantioselective epoxidation of alpha,beta-enones promoted by alpha,alpha-diphenyl-L-prolinol as bifunctional organocatalyst. *Org Lett* **2005,** *7* (13), 2579-2582.

106. Daikai, K.; Hayano, T.; Kino, R.; Furuno, H.; Kagawa, T.; Inanaga, J., Asymmetric catalysis with self-organized chiral lanthanum complexes: Practical and highly enantioselective epoxidation of alpha,beta-unsaturated ketones. *Chirality* **2003,** *15* (1), 83-88.

107. Carlson, R.; Hansson, L.; Lundstedt, T., Optimization in Organic-Synthesis - Strategies When the Desired Reaction Is Accompanied by Parasitic Side Reactions - an Example with Enamine Synthesis. *Acta Chem Scand B* **1986,** *40* (6), 444-452.

108. Pirkle, W. H.; Hoover, D. J., Stereospecific Alkylation of 3,5,5-Trisubstituted-4-Hydroxy-1-Para-Tosyl-2-Pyrazolines by Trimethylaluminum - an Efficient Synthesis of 3,3,5,5-Tetrasubstituted-1-Pyrazolin-4-Ones. *Journal of Organic Chemistry* **1980,** *45* (17), 3407-3413.

109. University of Rochester. Department of Chemistry: Not VooDoo X. http://chem.rochester.edu/~nvd/documents/Efficient_extraction_of_highly_polar_solvents_from_reaction_mixtures.doc (accessed March 2, 2016).